Loughborough University

This item was submitted to Loughborough's Research Repository by the author.
Items in Figshare are protected by copyright, with all rights reserved, unless otherwise indicated.

Effect of link geometry on properties of chains

PLEASE CITE THE PUBLISHED VERSION

PUBLISHER

© Ebrahim Abolfathi-Balaneji

PUBLISHER STATEMENT

This work is made available according to the conditions of the Creative Commons Attribution-NonCommercial-NoDerivatives 4.0 International (CC BY-NC-ND 4.0) licence. Full details of this licence are available at: https://creativecommons.org/licenses/by-nc-nd/4.0/

LICENCE

CC BY-NC-ND 4.0

REPOSITORY RECORD

Abolfathi-Balaneji, Ebrahim. 2019. “Effect of Link Geometry on Properties of Chains”. figshare. https://hdl.handle.net/2134/33208.

BLDSC no:- DX88959

LOUGHBOROUGH
UNIVERSITY OF TECHNOLOGY
LIBRARY

AUTHOR/FILING TITLE

ABOLFATHI-BALENJI, E

ACCESSION/COPY NO.

040013181

VOL. NO. | CLASS MARK

LOAN COPY

~~8 DEC 1989~~

~~- 3 JUL 1992~~

~~- 9 OCT 1992~~

20 FEB 1996

040013181 1

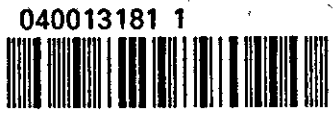

EFFECT OF LINK GEOMETRY ON PROPERTIES OF CHAINS

by

EBRAHIM ABOLFATHI–BALANEJI

A Doctoral Thesis
submitted in partial fulfilment of the requirements
for the award of

Doctor of Philosophy

of the Loughborough University of Technology

Department of Manufacturing Engineering

June 1989

by Ebrahim Abolfathi–Balaneji, 1989

Loughborough University
of Technology Library
Date Nw 89
Class
Acc No 040013187

To my family for their love and support

SUMMARY

The present work has arisen from a continuing need to improve the performance of round-steel lifting (hoist) and mining chains, and the hypothesis that this might be done by modification of the link geometry. The finite element (FE) method has been used to analyse the stresses in the chain links. The effects of link length and the bend radius in the crown were considered. The effect of maintaining link length constant and departing from the conventional straight sided (standard) geometry by changing the link shape from eight shape (pinched), through straight sided, to elliptical has been examined. Mining chains made from non-circular section rod have also been investigated. The finite element work has been supported by practical investigations using through-yield strain gauges.

The fatigue properties of the round-steel lifting chains have been investigated. Chains are often calibrated by application of manufacturing test force as one of the last manufacturing processes, to raise the load to which the chain will behave elastically in service. As a result, residual stresses are introduced, which improve the fatigue performance. The distribution of residual stresses has been examined by the finite element method and is compared with experimental results obtained by neutron diffraction, x-ray diffraction and strain gauge techniques. The best quantitative agreement between the FE predictions and experimental was obtained in the case of neutron diffraction.

In terms of the peak stresses for a given applied load, which result from combination of the residual stresses with the elastic stresses caused by loading, the conventional straight-sided link appears to be the optimum for a given rod diameter and pitch, although some benefit would result from a reduction in overall width.

ACKNOWLEDGEMENTS

I would like to record my appreciation of the advice offered to me at various stages of this work by my colleagues at Loughborough University of Technology, Wheway Becker (CM) Ltd., Science and Engineering Research Council, Institute Laue-Langevin (ILL), Grenoble, France, British Steels Swindon Laboratories.

Particular thanks are entitled to the following individuals:-

Dr. G.F. Modlen	Research supervisor, Senior lecturer (LUT)
Dr. R.A. Stark	Lecturer (LUT), collaboration and discussion during research period
Mr. J. Ascough	Lecturer (LUT), advice on FE work
Dr. A. Clegg	Research Director (LUT)
Dr. K. Kormi	Senior lecturer, Leeds Polytechnic, Advice on FE work
Dr. S. Potts	Managing Director Wheway Becker (CM) Ltd.
Mr. C. Middleton	British Steel Swindon Laboratories (x-ray work)
Dr. G. Swallowe	Lecturer (LUT) (neutron diffraction)
Dr. P. Webster	Senior lecturer, Salford Univ. (neutron diffraction)
Mr. R. Abery	Laboratory Technician (LUT)
Mr. J.T.W. Smith	" " "
Mr. R.I. Temple	" " "
Mr D. Houghton	" " "

CONTENT

Title

Certificate of originality

Summary

Acknowledgement

Chapter 1 INTRODUCTION

1.1 Introduction 1

1.2 Round link steel chains 2

1.2.1 General 2

1.2.2 Tensile strength of chains 2

1.2.3 Material 3

1.2.4 Stress 3

1.3 British Standards for round link steel chains 4

1.4 Fatigue 7

1.4.1 General 7

1.4.2 Prediction of fatigue life 7

1.5 Residual stresses 10

1.5.1 General 10

1.5.2 Effect of residual stresses 11

1.5.3 Determination of residual stresses 11

1.6 Finite element method 13

1.6.1 Finite element systems 13

1.6.2 Finite element analysis of chains 14

1.7 Objectives and layout of thesis 16

Chapter 2 MANUFACTURE OF ROUND STEEL LINK CHAINS

2.1 Introduction 19

2.2 Initial examination and raw material selection 20

2.2.1 Initial examination of raw material 20

2.2.2 Raw material selection 21

2.2.3 Steel types in chain manufacture 22

2.3	Forming	24
2.4	Welding (butt and butt flash)	25
	2.4.1 Bent link shape for butt and butt flash welding	26
	2.4.2 Butt welding process	26
	2.4.3 Flash butt welding process	27
2.5	Heat treatment of chains	28
2.6	Calibration	31
2.7	Mechanical testings	32
2.8	Surface protection	33
Chapter 3	FATIGUE TESTING OF 7 mm LIFTING CHAINS	
3.1	Introduction	35
3.2	Fatigue testing procedure	38
3.3	Fatigue testing results	39
	3.3.1 Statistical presentation of results	40
	3.3.2 S-N Curves	41
3.4	Analysis of fatigue failures	42
3.5	Mechanical testing of chain material	44
	3.5.1 Tensile tests	45
	3.5.2 Hardness tests	45
	3.5.3 Metallography	46
3.6	Effect of mean stress on fatigue	47
Chapter 4	RESIDUAL STRESS MEASUREMENT USING X-RAY AND NEUTRON DIFFRACTION METHODS	
4.1	Introduction	49
4.2	X-ray diffraction (camera method)	50
	4.2.1 Back reflection method	51
	4.2.2 Experimental procedure	52
4.3	X-ray diffractometer	53
	4.3.1 X-ray diffraction method	53

	4.3.2 Experimental procedure	54
4.4	Field diffractometer (Strainflex)	57
	4.4.1 Strainflex (Rigaku)	57
	4.4.2 Experimental procedure	59
4.5	Neutron diffraction	61
	4.5.1 Neutron diffraction method	62
	4.5.2 Experimental procedure	63
	4.5.3 Results and calculations	63
Chapter 5	RESIDUAL STRESS MEASUREMENT USING STRAIN GAUGE METHOD	
5.1	Introduction	67
5.2	Principle of residual stress determination and Bauschinger effect	69
5.3	Forming of eight shape and elliptical chain links	70
5.4	Heat treatment of chain links and preparation of material test specimens	70
5.5	Strain gauge selection and mounting	71
	5.5.1 Strain gauge selection	71
	5.5.2 Strain gauge mounting	73
5.6	Experimental procedure	74
5.7	Results and calibration of residual stresses	75
	5.7.1 Stress-strain curve of chain material	75
	5.7.2 Results and residual stress calculations relating to the x-ray work	76
	5.7.3 Results and residual stress calculations of different link geometries	77
Chapter 6	FINITE ELEMENT BEAM ANALYSIS OF CHAINS (1-D)	
6.1	Introduction	80
6.2	Loading assumption	82
6.3	19 mm Mining chain	83

6.3.1 Elastic analysis 84

6.3.2 Plastic analysis 85

6.3.2.1 Total stresses 85

6.3.2.2 Residual stresses 87

6.4 7 mm Lifting chain 88

Chapter 7 FINITE ELEMENT CONTACT ANALYSIS OF CHAINS (2-D)

7.1 Introduction 90

7.2 Pressure between two links in contact 92

7.3 Plane stress/strain analysis 94

7.4 Interface elements for stress analysis 95

7.5 19 mm Mining chains 97

7.5.1 Total stresses 98

7.5.2 Contact pressure and area 99

7.5.3 Residual stresses 100

7.6 7 mm Lifting chain 101

Chapter 8 FINITE ELEMENT STRESS ANALYSIS OF CHAINS (3-D)

8.1 Introduction 103

8.2 Contact pressure assumption 105

8.3 Mining chains 106

8.3.1 19 mm Mining chains 107

8.3.1.1 Mesh refinement 109

8.3.1.2 Elastic stresses 109

8.3.1.3 Total stresses 110

8.3.1.4 Residual stresess 111

8.3.1.5 Behaviour of strain gauges no. 3 and 10 112

8.3.2 22 mm Mining chains (oval-link and equivalent circular cross-section link) 113

8.3.2.1 Elastic stresses 113

8.3.2.2 Total stresses 114

8.3.2.3 Residual stresses 115

8.4 7 mm Lifting chain 116

8.5 Other aspects of chain link geometry 117

8.5.1 Internal radius at the crown 117

8.5.2 Barrel length (pitch) 118

Chapter 9 GENERAL DISCUSSIONS

9.1 Introduction 119

9.2 7 mm Lifting chain 119

9.3 19 mm Mining chain 120

9.4 Further discussions 123

Chapter 10 CONCLUSIONS AND SUGGESTIONS FOR FURTHER WORK

10.1 Conclusions 126

10.2 Suggestions for further work 129

REFERENCES 131

FIGURES AND TABLES 140

APPENDICES

Appendix A Energy absorption factor 306

CHAPTER 1

INTRODUCTION

1.1 INTRODUCTION

Chains manufactured from high-tensile steel are used in many applications, such as hoists, cranes, and in mining, where it is vital that their load-carrying capacity should be assured. The details of the manufacture of such chains may vary slightly but the following steps are generaly involved: cropping a length from bar-stock; forming the length to produce the next link on a continuous run of chain; butt or flash butt welding of the adjacent cropped ends of the link; and heat treatment of the welded chain by quenching and tempering. The temperatures used in heat-treatment (for the formation of γ Fe and the partial decomposition of martensite formed by quenching) depend on the steel used and the tensile strength required of the chain. Traditionally the final step is the application of a manufacturing test load, known as calibration in the trade, which is sufficient to deform the chain plastically and thus imparts the final dimensions to each link. It is now recognised that the residual stresses introduced by this process substantially affect the chain's mechanical properties and particularly its resistance to fracture under the effect of repeated tensile loads. However, there is no detailed knowledge of the magnitude or distribution of these residual stresses.

In this chapter, a brief background study is given regarding steel chains, their fatigue properties, the effect of residual stresses on fatigue properties, and the application of finite element analysis to chains. Objectives and the layout of the thesis are also given here.

1.2 ROUND LINK STEEL CHAINS

1.2.1 GENERAL

The chain is one of the most familiar as well as one of the most useful mechanical devices. Chains are mechanically strong, statistically reliable, and economical, and are used in many important components in hoists, slings, towing devices and conveyors.

Evidence of the manufacture of chains goes back to ancient times. The first chains were forged and fire-welded. At the end of the nineteenth century, finish-forming of the links using a die was introduced to improve accuracy. The turn of the twentieth century saw the first chain bending and chain welding machines (resistance welding method).

Increasing requirements with regard to quality, reliability and working life led to the development first of the heat-treated chains and finally to high-tensile chains. The development of corresponding welding methods ran in parallel. Apart from the previously mentioned resistance welding method, the so-called flash butt welding must also be mentioned because it permits welding not only of large nominal diameters but also highly alloyed steel.

1.2.2 TENSILE STRENGTH OF CHAINS

The tensile strength of chains is determined mainly by the material, the shape, and the surface conditions of use. Wear resistant materials with a high breaking strength combined with a high ductility, high notch impact strength and a high degree of surface

hardness are preferred for round steel chains. Chains must comply with the strain values specified in the appropriate standards; these can be obtained by stretching the chain. In BS3114 a specified minimum ratio of extension to length at a stated load is required in order to assume adequate energy absorption properties, Appendix A. Occasional overloads in operations should not lead to fracture, but merely to plastic changes in length. Wellinger [1] reported that the static strength of chains is approximately 60 - 70 % of the tensile strength of the material. The elongation decreases with increasing ratio (t:d) where t is inside length of chain and d, the diameter of the wire or rod from which the link is made.

1.2.3 MATERIAL

Depending on their application, chains are made of either plain carbon or high-tensile alloy steel. Manufacture of high tensile chains calls for a steel which can provide a tensile strength of 1200 to 1400 MPa after tempering, depending on quality grade, and in addition has adequate ductility (minimum elongation 14 %) and a high degree of notch impact strength as well as being weldable and having a high fatigue strength.

1.2.4 STRESS

It is essential to know operational stresses and their change, frequency and sequence with respect to time in order to evaluate safe working conditions and service life of a chain. The effect of chain shape on the tensile strength of the chain is illustrated by the stress charateristic of the short link chains shown in Fig. 1.1 [2,3]. The stresses in chain links with parallel side members (Fig.

1.1c) are lower than in those of a barrelled shape (Fig. 1.1a) and slightly higher than those in a link with a centre web (Fig. 1.1b). Wellinger [1] reported that for stressing below the elastic limit, for short link chains the region of highest tensile stress is the inside of the flank at the junction of the intrados with the straight sides (transition): for long link chains it is the outside of the crown. Maximum tensile stress was almost four times the nominal stress.

Hawkes et al [4] have reported that for short link chains at loads up to and just beyond elastic limit the position of the maximum stress occurs at the transition. Beyond the elastic limit, however, changes in link geometry cause the position of the maximum stress to move to the link crown as shown by use of the photoelastic-coating technique. On the other hand, theory predicts that the position of maximum stress in short link chains loaded elastically in tension is the crown [5]. This anomaly is due to the fact that the theoretical work assumed point loading between adjacent links and took no account of "bedding down" of the links.

The change in the pitch of a circular cross-section chain link has been investigated by employing the method of complementary work with plastic material properties [6]. The results of the work may be used in solving a number of practical problems connected with the determination of the change in pitch and load-bearing capacity of a different cross-sectional shapes. The results are particularly applicable to the standard link geometry and are not based on the detailed deformation of the chains.

1.3 BRITISH STANDARDS FOR ROUND LINK STEEL CHAINS

British Standards for lifting gear were first discussed some forty years ago. Various standards have since been drawn up which specify the dimensions of components, the material from which they must be made, the tests they must undergo before they can be given a certificate and all other information necessary to make them as safe as possible. A continual watch is kept by the relevant British Standards Institution committeeson improvements in design, material and manufacturing technique and on changes in requirements. When necessary, modifications to the standards are made.

From the early standards, a formula was developed at NPL which, given the link dimensions and design stress, determined the design load [7,8]. The formula has stood the test of the time and has, by an increase in the design stress, been the basis for the design of links made of the new, stronger, alloy steels. The formula is applicable to all chain links [9].

Anthony et al [7] proposed two empirical formulae for the diameter D_2 (Fig. 1.3) required for a link to have a particular working load limit W:

$$D_2 = .2\ A\ B\ [\ 6.7 + A - B/L\ ]$$

$$D_2 = B\ [\ .1 + A\ (1+A) - .12\ L/B\ ]$$

where L is the internal length of the link.
B is the breadth of the link.
A = [W/fB]
W being the working load limit of the link.
f being the maximum nominal extreme fibre stress in the link under the working load limit.

The two values predicted for D_2 seldom differ by more than almost 1.5 %, the larger of the two being selected in practice.

BS 4942 [10,11,12,13,14,15],'Short link chain for lifting purposes',

specifies the general conditions of acceptance for electrically welded round steel short link chain for lifting purposes. It includes non-calibrated (see Section 1.1) chain use in cranes, in chain slings and for general lifting purposes and calibrated chain for use with chain hoists and other lifting appliances: they will be referred as lifting chain in what follows.

BS 6521 [16],'Proper use and maintenance of calibrated round steel link lifting chain', specifies the principles for the use, inspection, in-service testing and maintenance of calibrated round steel link chains operating over chain wheels. The principal applications include manual and power driven hoists.

'Hoist designers handbook' [17] and 'a guide to Safety practices for chain sling' [18] may also be consulted in relation to the BS 6521.

BS 2969 [19],'High-tensile steel chains (round link) for chain conveyors and coal plough', specifies the requirements for a range of high grade special purpose calibrated, high-tensile electrically welded, steel chains for use with machines and equipment in mining and they will be referred as mining chain in what follows.

BS 6405 [20],'Non-calibrated short link steel chain (grade 30) for the general engineering purposes: class 1 and 2' (mean stress at specified minimum breaking load is 300 MPa). This standard deals with non-calibrated short link steel chain of grade 30 for general engineering purposes and provides for two qualities, class 1 quality chain for arduous duties such as lashing or load binding and class 2 quality chain for general duties.

1.4 FATIGUE

1.4.1 GENERAL

Fatigue is the progressive localised permanent structural change that occurs in a material subjected to repeated or fluctuating strains at stresses having a maximum value less than the tensile strength of the material. Fatigue may culminate in cracks or fracture after a sufficient number of fluctuations.

Fatigue fractures are caused by the simultaneous action of cyclic stress, tensile stress and plastic strain. If any one of these three is not present, fatigue cracking will not initiate and propagate. The cyclic stress starts the crack; the tensile stress produces crack growth (propagation). Although compressive stress will not cause fatigue, compression loads may do so, because of tensile stress induced in some parts of a structure.

The process of fatigue may be considered as consisting of three stages:

1) Initial fatigue damage leading to crack initiation.
2) Crack propagation until the remaining uncracked cross-section of a part becomes too weak to carry the loads imposed.
3) Final, sudden fracture of the remaining cross-section.

Stage (1) may be absent in components containing crack-like defects.

1.4.2 PREDICTION OF FATIGUE LIFE

In practice, prediction of the fatigue life of a material is

complicated because, except for a few relatively brittle materials, the fatigue life of a material is very sensitive to small changes in loading conditions, local stresses and local characteristics of the material. Because it is difficult to account for these minor changes in either the dynamic stress prediction techniques or in fatigue failure criteria, there is a large uncertainty inherent in analytical prediction of fatigue life. Thus the designer also is required to rely on experience with similar parts and eventually on qualification testing of prototype or production parts. Although laboratory fatigue tests performed on small specimens are not sufficient for precisely establishing the fatigue life of a part, it is useful to examine these data because laboratory tests (a) are the major source of fatigue failure criteria, (b) are useful in rating materials in terms of their relative resistance to fatigue, and (c) can be used to establish the relative importance of such items as fabrication method, surface finish, heat treatment, assembly technique and environment on the fatigue life.

In general, fatigue life can be expected to depend on the following parameters [21]:

1) Type of loading (uniaxial, bending, torsional)
2) Shape of loading curve
3) Frequency of load cycling
4) Loading pattern (periodic loading at constant or variable amplitude, programmed loading or random loading)
5) Magnitude of stresses
6) Part size
7) Fabrication method and surface roughness
8) Operating temperature
9) Operating atmosphere.

Traditionally, fatigue life has been expressed as the total number of stress cycles required for a fatigue crack to be initiated and then to grow large enough to produce catastrophic failure. Fatigue data also can be expressed in terms of crack growth rate. After the advent of better methods for crack detection, it was discovered that the cracks develop early in the fatigue life of the material and grow continuously until catastrophic failure occurs. This discovery has led to the use of crack-growth rates for prediction of fatigue life, the subject of Fracture Mechanics.

In operation, lifting chains used for hoisting and conveying, are usually subjected to variations with different loading values. Under these conditions, the fracture may occur at one or rarely two of the following positions: crown, transitions or weld.

Some of the parameters mentioned above such as loading frequency, loading pattern and surface roughness were investigated by Metz [22] using high-tensile lifting chain (A 7X21) complying with DIN 5684 [23], confirming their effect on the fatigue strength of chains. Furthermore, he reported that the effect of mean stress is irrelevant in the region of high stress range but as the stress ranges narrow, any change of mean stress has a more distinct effect on the fatigue life. The effect of mean stress was, however, far less than that caused by a comparable change in stress range. In his tests 99 % of the fractures occurred directly adjacent the welding seams, the remainder occurring in the transition zone.

Long link chains possess higher fatigue strength than those of short link chains; by contrast, an increase in link width decreases fatigue strength [1].

Although it has been reported (Bahke [3], quoting Wellinger [1]) that an increase in the tensile strength of a C-Mn steel chain by heat treatment caused an increase in the life at high stresses without a corresponding increase in fatigue limit (or possibly even a decrease), the chains compared had slightly different link shapes. Under these circumstances, one can regard this as only an isolated and rather ambiguous piece of information. Wellinger's results did, however, generally indicate that the fatigue strength of chains was fairly insensitive to the material's tensile strength. The chains were not calibrated.

Finally, some marked improvements in fatigue strength of short link chains can be produced either by dry rumbling or surface grinding, i.e. improving surface finish [24,25].

1.5 RESIDUAL STRESSES

1.5.1 GENERAL

Residual stresses are defined as stresses, which can exist in an elastic body, when it is free from external forces. They are sometimes referred to as internal or locked-in stresses. They are caused by mis-match between parts of the body that have been forced either by heat, transformation or mechanical working to expand or contract in a different way from the rest of the body and, in order to keep all these parts in a continuous whole, forces are needed between the various parts, and these constitute the internal stresses.

Residual stresses can be divided into two types, macroscopic and microscopic stresses. Microscopic stresses act over dimensions as

small as several unit cells, although their effect may extend through most of a grain: they are caused by structural inhomogeneties, which can also give rise to internal stresses even under macroscopically uniform deformation, or changes in temperature. Macroscopic stresses, on the other hand, vary continuously through the volume of the body and act over regions which are large compared with atomic dimensions. They can result from mechanical and thermal operations performed on the body. The macroscopic stresses, which originate directly from non-uniform plastic flow, as in the calibration of chains, have been a principal area of investigation in the present work.

1.5.2 EFFECT OF RESIDUAL STRESSES

Residual stresses may have a beneficial as well as a deleterious effect. When the residual stresses are of an unfavourable type (tensile at surface) they result in lowered yield and tensile strengths and lowered fatigue strength. Residual stresses are also responsible for warping during machining, quench cracks, season cracks and grinding cracks.

On the other hand, when the stresses are favourably distributed, i.e. compressive at the surface, they increase the fatigue strength of the materials, and are therefore intentionally produced by, for example, extrusion, forging operations, calibration of chains etc. This gives the possibility of using residual stresses to produce components with improved properties.

1.5.3 DETERMINATION OF RESIDUAL STRESSES

In view of their importance, it is not surprising that there has been

a continuing interest in developing methods for measuring residual stresses [26,27,28,29]. Since research effort first became directed at residual stress distributions, virtually every conceivable method of monitoring displacements has been employed.These can be classified into the following groups:

a) Mechanical: by necessity all mechanical techniques involve some degree of destruction; most experimental techniques have been based on the monitoring displacement over a defined gauge length, while physically relieving the locked-in stresses around the gauge by saw cutting, slicing, drilling or trepanning. The hole boring method [30] is also a mechanical technique.

The strains resulting from the relief of the locked-in stresses are usually measured by resistance gauges. The theory of elasticity is then used to relate the measured strains to the pre-existing residual stresses.

Moire' fringe-methods or holography have also been proposed for strain measurement in place of resistance gauges.

b) X-ray and neutron diffraction (Chapter 4): have been applied to the task of measuring stresses in crystalline materials for some considerable time. The x-ray method is capable of measuring only surface stresses while neutrons because of their greater penetrations, can be used to measure residual stresses within a component. Both methods are nondestructive.

c) Ultrasonic [26,31,32]: several approaches have been attempted, all relying on the anisotropy created by a change in stress state. The

method is nondestructive but has not yet been developed as a reliable routine method.

e) Magneto-elastic [26,33]: utilises the dependence of magnetic flux density in ferromagnetic materials on the applied stress state. The obvious advantage is nondestructive nature and apparent simplicity.

f) Analytical (computational) [26,34,35,36]: one,two, and three dimensional programmes have been developed (finite element method), and some experimental verification has been attempted (Chapters 6, 7, and 8).

1.6 FINITE ELEMENT METHOD

1.6.1 FINITE ELEMENT SYSTEMS

Development and application of digital computers have accelerated the development of numerical techniques, finite element, finite difference and boundary element. Finite Element Method (FEM) being firmly established as a general numerical method for the solution of partial differential equation system, subjected to known boundary and initial conditions, is the most powerful numerical technique. In essence, the method by a process of discretisation describes the overall behaviour of a continuum by a number of subregions or elements. Each element is connected to its neighbours by nodal points, Fig. 1.2. The behaviour and characteristics of individual elements are derived independently of each other in terms of certain parameters at the nodal points of each element. Complications due to specifications of arbitary loading, geometry, and boundary conditions disappear and different and possibly complex constitutive relationships for each element are

easily allocated.

Over the past decade or so, finite element analysis has evolved from a technique for large structural analysis to a tool available and familiar, to some extent, to most engineers. Software and hardware developments have reduced costs and finite element analysis is now viable even for small jobs. Nowadays, a large number of finite element systems (packages or codes) exist. At one extreme are large general purpose packages such as NASTRAN, ABAQUS, PAFEC and ASAS, each with its own strength and weaknesses, and at the other extreme, are micro-based packages such as SESAM for off-shore applications and BERSAFE for pressure vessels. The details of specific packages are outside the scope of this work and can be referred to the Finite Element Systems Handbook [37].

For the finite element analysis part of this research, ABAQUS finite element (FE) software at the Manchester Regional Computing Centre was used. ABAQUS is one of the most powerful nonlinear packages available and its capability and method of use are contained in the updated manuals of the package [38,39,40]. In the initial stages of the research PAFEC [41,42] was used, but all the results in this thesis were obtained by using ABAQUS.

1.6.2 FINITE ELEMENT ANALYSIS OF CHAINS

The finite element method was first applied into chains by SDRC [43] to study design modifications to the 14 mm diameter wheel chain links. They considered two alternative geometries to that of the standard chain links, namely; pinched at the centre; shaved, that is with material removed from the outside of the barrel, and flattened leg

(oval cross-section), Fig. 1.3. The objective of their design study was to determine if such changes in the standard link geometry would reduce the high tensile stress in the shoulder where fatigue failures generally occured. Elastic beam analysis of the link geometries was carried out following three-dimensional stress analysis. The load was applied by a point load at the crown and the overall conclusions were:

1) The standard link configuration is the optimum geoemtry to minimize the inner surface tensile stresses at the shoulder.
2) The pinched (eight shape) design is stiffer than the standard link design.
3) The shaved design does not appear to offer a significant advantage over the standard design. In addition, a point will be reached where the stresses in the barrel will exceed those in the shoulder as more material is removed from the cross-section.
4) The flattened leg (oval cross-section) provides a desirable means to reduce the shoulder stress without dramatically increasing the stress level in the leg.

Metz also reported stress distribution in the chain link using the finite element method [22], Fig. 1.4.

Further three-dimensional elastic finite element analysis of chains were taken up by Modlen [44,45,46] to investigate the effect of link geometry on strength of chains. Alternative link shapes were pinched and elliptical. The following conclusions were drawn. A change in the link geometry from pinched to elliptical causes a systematic change in the magnitude of the stresses under load. The most tensile principal stress always appears on the inside of the chain links, but its location moves away from the mid-plane towards the crown. At the same time, the overall extension of the chain under load increases;

i.e. the chain modulus increases. The results refer to links of a specific overall length made from wire rod of one diameter.

Modlen [45] also investigated the effect of link length (length of straight section) on the stress pattern at the exterior and interior of the chain links. It was reported that the tensile stress on the interior of the link decreases as link length increased but the stresses around the crown increase and the crown becomes the location of the largest tensile stresses.

In 1986, Mattheck et al [47,48] investigated the effect of wear between chain links on the stress concentration in chains using the finite element method and came up with a patented chain link.

The loading between chain links so far was assumed to be a point load. This assumption is only true at the onset of loading for chain links having perfect surfaces. As the loading increases the chain links deform elastically and then plastically at the crown and the loading is no longer a point load. Ideally, a three-dimensional contact analysis of the chain links needs to be carried out to determine the contact area and contact pressure envelope. At the present, there does not appear to be a finite element code able to achieve this task and to develop one capable of this analysis was outside the scope of this research. Hence, an approximate contact area and contact pressure envelope was sought in the present work to give the required nominal stress at the cross-section due to the loading.

1.7 OBJECTIVES AND LAYOUT OF THE THESIS

The main objectives of this study are:

1) To investigate the effect of link geometry on the total and residual stress patterns in mining and lifting chains using FEM.
2) To evaluate the changes in residual stresses due to increase in calibration loads for mining and lifting chains using FEM.
3) To verify the total and residual stresses obtained in (1) and (2) using the strain gauge, x-ray and neutron diffraction techniques.
4) To demonstrate the effect of calibration on fatigue strength of lifting chains.

Manufacture of round steel chain for lifting and mining purposes will be described in Chapter 2 with all the required testing procedures according to the British Standards. Fatigue testing of 7mm lifting chains will be covered in Chapter 3 with the statistical interpretation of the results. The effect of increase in calibration load in the fatigue strength of this grade of chains are also illustrated with S-N curves and cumulative curves for the probability of fracture. The rest of the experimental work involves the measurement of the total and residual stresses in the 19 mm mining and 7 mm lifting chains. The x-ray and neutron diffraction techniques were used for both grades of chains under various calibration loads and the experimental procedure and results will be presented in Chapter 4. The strain gauge method of total and residual stress measurement was used only for the mining chains (due to size limits) with various geometries, namely, oval cross-section, eight shape (pinched), standard and elliptical chain links under various calibration loads. The procedure and results will be given in Chapter 5.

The effect of link geometry on the total and residual stresses was

investigated in mining and lifting chains using the finite element method in one, two and three dimensions. An elasto-plastic material model will be used with work hardening. As the chains undergo a large deformations under loading a complete geometrically nonlinear analysis will be carried out with required material model (elastic or elasto-plastic) in one, two, and three-dimensional analysis of chains (Chapters 6, 7 and 8).

The residual stresses in chains as a result of pre-loading (calibration) will be found by taking the finite element models of chains through a loading-unloading cycle.

Beam analysis (one dimensional) of the chains will be introduced in Chapter 6. The load will be applied over one element at the crown to produce an elliptical pressure envelope and to avoid numerical difficulties at the crown (Chapter 6).

The two-dimensional contact stress analysis of the chains will be carried out in Chapter 7. The contact area and contact pressure envelope obtained from this analysis was incorporated in the three dimensional assumption of the contact pressure envelope.

A complete three dimensional stress analysis of the chains was carried out and the results will be discussed in Chapter 8. Finally, discussions, conclusions and suggestions for further work will be given in Chapter 9 and 10 respectively.

CHAPTER 2

MANUFACTURE OF ROUND-STEEL LINK CHAINS

2.1 INTRODUCTION

Round steel link chains have extremely wide ranging applications and only hoist (lifting) and mining chains will be considered here. The manufacturing processes used for these chains are quite similar.

The strength of chains remained fairly constant based upon mean stresses of 200 - 300 MPa up to the mid - 1940's. They were manufactured from wrought iron or mild steel. The period 1950 - 1970 saw the introduction of carbon steel and later, alloy steel chains with increasing strength levels up to 800 MPa, which is the present day norm. There is also grade D quality mining chain operating at 1000 MPa [49].

The art of chain manufacture is to produce the finished link dimensions and mechanical properties specified by the customer while ensuring that the resulting chain will perform satisfactorily in service. It has been found that the selection of raw material and its heat treatment play a vital role in obtaining such a chain (Sections 2.2 and 2.5). Hence, a balance must be struck between heat treatment and calibration which will minimize the problems in service (Section 2.6). Once the degree of calibration is established the various intermediate link shapes can be deduced. This deduction cannot be based purely on calibration since, in addition to the predicted geometrical changes, the finished link is always longer and narrower than the welded link, which in turn is shorter than the formed link due to upsetting during welding. The formed link dimensions having been established, the kingpost around which each link is formed can be machined. All this information together with details of raw material, manufacturing tolerances and mechanical properties are tabulated in a

basic chain sheet, Fig. 2.1. Quality and operational reliability of the round link steel chains depend above all on the preciseness of each separate operation such as the reliability of the systems of testing, heat treatment, inspection, etc. In this chapter these separate operations will be discussed in details.

2.2 INITIAL EXAMINATION AND RAW MATERIAL SELECTION

The selection of the material for round link chain is made according to the works directive and appropriate British Standards. Traditionally alloy steels of the Ni, Cr, Mo type have been used for high strength chains. Mining chain specifications leave the choice of steel to the manufacturer, applying certain provisos related to the content of sulphur, phosphorus and aluminium and to the grain size. The material having been selected, the initial examinations ought to be carried out before starting other manufacturing processes.

2.2.1 INITIAL EXAMINATION OF THE RAW MATERIAL

In order to ensure efficient chain manufacture and prevent any confusion or mistakes in the material supplied, chain manufacturers increasingly carry out spot tests despite the availability of the works test certificate. The starting material (cold drawn, hot rolled or annealed) is chemically and physically analysed, its tensile strength, elongation, carbon content and hardness values are determined, and where necessary, its heat treatment characteristic are investigated. In some circumstances a cold bending test is also applied.

Prior to forming, surface condition and dimensional accuracy must also

be checked and, where necessary, the steel surface must be cleaned off all non-metallic material in particular of the oxides (FeO, Fe_3O_4, Fe_2O_3). Descaling can be achieved by various methods, like pickling with sulphuric acid [50] and drawing through a die to straighten the coiled material (Fig. 2.2).

2.2.2 RAW MATERIAL SELECTION

High tensile steel chains are produced almost exclusively from electric steel. They are made of low alloy manganese, chromium manganese or boron steel. When considering steel composition to be used several factors must be considered:

a) Response to heat treatment - the required mechanical properties such as hardenability, ductility and toughness must be achieved for the chain size after the hardening and tempering to the desired strength level.

b) Weldability - for the steel selected, the requirement of good weldability places a restriction upon the total alloying addition to be made, and particularly on the carbon content.

c) Formability - larger link sizes are normally hot formed at a temperature close to 800° C, where the steel will be highly ductile and inherent formability of the material is unimportant. Smaller link sizes are, however, formed at room temperature and the material must be sufficiently ductile to allow this. For this reason drawn and annealed wire or rod must be used

d) Grain size - material in the finished link must have fine grain

size to achieve optimum combination of strength and toughness. This is usually ensured by the use of aluminium killed steels.

e) Steel cleanness - inclusion content of steel must be kept to minimum. The inclusions in the weld region become transversely aligned and can exert significant stress-raising effects.

2.2.3 STEEL TYPES IN CHAIN MANUFACTURE

Steels used in round link high tensile chain manufacture are :

alloy (low and high) and boron steel and a brief description is given below for each type.

a) Alloy steel - low alloy and case hardening steels are used almost exclusively in the manufacture of high tensile chains. Because of the larger contents of Mn ($\geq$.6) and Si ($\geq$.1) and partly because of the presence of alloying constituents such as Cr and Ni, the properties of the material such as tensile strength, yield point, elongation, wear resistance, notch impact strength, etc. are greatly modified. It should be pointed out that in practice a whole series of materials is used of different composition in accordance with the desired properties of the finished product. Plumbridge et al[51] investigated one of these materials, which is similar in chemical composition to the material used in this research.

The chemical composition of the steel used for manufacture of the 19 mm mining chain is : carbon .2-.25 %, silicon .2-.35 %, sulphur .015 % max., phosphorus .015 % max., manganese 1.2-1.5 %, nickel .95-1.3 %, chromium .45-.65 %, molybdenum .5-.6 %, aluminium .02-.05 % and copper .25 % max.

Mining chains are used in flight bar assembly, Fig. 2.3, to convey the coal from the mine face.

b) Boron steel - there are numerous technical papers [52,53,54,55,...] concerning the application of boron as an additive to commercial steels together with the 'rules' that researchers have revealed. The fact that hardenability of steel is enhanced by the addition of boron makes it a potential candidate in chain manufacture. Here, a review of the some of the properties of the boron-treated steel as a chain material for use as a grade T (80) (mean stress at specified minimum breaking load is 800 MPa) lifting chain [14] is given in comparison with low alloy steel (SAE 8622).

I) Chemical composition - boron is becoming an increasingly popular addition for fine grained low and medium carbon alloy steels to increase their hardenabilities. The mechanism of this effect is generally agreed to be the segregation of elemental boron at prior austenite grain bounderies, which causes the suppression of the ferrite, transformation and thus improves the hardenability. In order to ensure that this mechanism occurs the boron must be in a soluble form and, therefore, be protected with aluminium deoxidation. The amount of boron must be about .001 % and .004 % maximum.

The chemical composition of the steel used in manufacture of the 7 mm lifting chain used in this research is : carbon .18-.23 %, silicon .15-.35 %, sulphur .025 % max., phosphorus .025 % max., manganese .70-1.0 %, chromium .15-.3 %, nickel .40-.60 %, aluminium .02-.05 %, copper .25 % max. and boron .001- .003 %.

II) Hardenability - in the research carried out by Potts and Metha

[55,56], it was shown that the boron-treated steel has greater hardenability than the low alloy steel (SAE 8622) and equivalent hardenability to DIN 1.6542 (German specifications).

III) Temper resistance - boron-treated steel has significantly better toughness characteristics than the SAE 8622 material [55]. The work by King et al [57] and British Steel [58] also show good toughness and strength throughout the tempering temperature range up to 400° C.

IV) Low temperature impact properties - the results of the low temperature Charpy impact properties [55] show that, over the range -20° to 20° C, the boron-treated steel exhibits superior toughness properties compared with those of SAE 8622.

V) Chain tests - analysis of production quality tests indicate that at the required strength level, elongations are in excess of 20 % [59] and improvements on the previous SAE 8622 production which gave typically 17 % (BS4942).

On the whole, the boron-treated alloy steel exhibits excellent properties, generally superior to those of the low alloy steel SAE 8622.

Lifting chains of different sizes are used in various lifting tackles shown in Fig. 2.4.

2.3 FORMING

Pre-bending of the individual links may be either hot or cold. It depends upon the material diameter and its strength. The material is

cold formed up to about 20 mm diameter in size and pre-heated for larger diameters, Fig. 2.5. The material to be bent is sometimes lubricated with cutting oil in order to avoid damage to the material during bending and eliminate marks on the bent chain link while minimising wear between tool and material in order to prolong the working life of the tool.

The forming of the links prior to welding is carried out either mechanically or hydraulically. The simplex and duplex bending methods [50] are the two main mechanical bending methods. In simplex method, the wire is cut and formed around the kingpost at the operating station, while in the duplex method, the forming is carried out in two (pre-bending and finished bending) operating stations. The duplex bending method is therefore approximately 50 % more efficient.

The exact bending is very important for all the following production steps, because it provides the basis for the dimensional and mechanical properties of the finished chain. The definitive form, the final dimensions and the calibration force necessary to pull the chain to the final dimensions, are established mainly in this process.

2.4 WELDING (BUTT AND BUTT FLASH)

Either the butt or flush butt welding process is used, depending on the wire diameter and quality required. The important features of both methods are given in a table, Fig. 2.6 [60,61].

Butt welding offers shorter weld times; it is very clean with low material consumption and tighter bending tolerances to obtain a better weld. Its application range extends up to 20 mm wire diameter. Flash

butt welding requires longer weld times, produces undesirable welding splashes and consumes more material in upsetting and flashes, but less stringent bending tolerances and wire quality are needed. It is economical from about 13 mm diameters upwards.

2.4.1 BENT LINK SHAPE FOR BUTT AND BUTT FLASH WELDING

For butt welding, the chain links are bent cold and the welding gap is chiplessly formed by notching before the link lengths are cropped. Bending tolerances must be very close to ensure high quality chains in demand nowadays. Hence drawn and annealed stock is mainly used, which also gives clean contact surfaces for the electrodes, Fig.2.7a. For flash butt welding, the chain links are bent cold or, for higher tensile grades, hot from about 22 mm diameter up. The heating of the stock blanks for bending is done by resistance or induction heating, Fig. 2.5. The flat cut end is sufficient for the welding gap. Rolled material of appropriate tolerance and finish is normaly adequate for flash butt welding, as wider chain bending tolerances are acceptable for this process, Fig 2.7b.

2.4.2 BUTT WELDING PROCESS

The situation at the start of the butt welding is shown in Fig. 2.8a. The upsetting tools, which apply the necessary pressure during welding, press against the chain links bows. The saddle supports the back of the links while the two electrode pairs are clamped on the chain link legs to be welded. The upsetting tools advance to make a contact at the weld joint the current is switched on, which is divided into the shuntback and the proper weld current. The necessary weld pressure is applied by the upsetting tools. The advance is controlled

mechanically by a cam, so that a relatively simple welding is obtained.

The butt welding is three times as fast as flash butt welding, requiring high currents. The electrode contact surface is strictly limited by the chain geometry, a situation which becomes highly unfavourable with larger diameters.

2.4.3 FLASH BUTT WELDING PROCESS

The situation at the start of the flash butt weld is shown in Fig. 2.8b. The total tool system is very similar to that for butt welding, the difference lies in the flat ends of the weld joint, which is open at the start. The upsetting pressure is provided by the upsetting tool. The flash butt welding process is controlled by regulating system developed by the advances in hydraulics and electronic. It can be divided into three stages:

a) Reversal for pre-heating the weld joint - the regulating systems controls the current, the amount of contact pressure and the time to heat the open ends to achieve the required temperature.

b) Flashing - starts after the completion of the reversal phase with the open ends approaching each other slowly while the welding gap is open and the current is on.

c) Upsetting - after flashing, the upsetting is initiated by increasing the tool approach speed, the current being switched off during the upsetting and the welding is complete.

Butt welding machines are controlled mechanically by cam with additional elements, such as springs and pneumatics used for upsetting tools and electrodes. After welding, the weld flash is removed by trimming cutters working in directions opposed to each other. Fig. 2.9 shows the work station with electrodes, saddle and retracted flash trimming blade. The machines cope with chains of up to 2 - 20 mm diameter.

Flash butt welding machines handle all grades of chain in the range from 13 - 40 mm diameter. The machine operation is fully hydraulic. In the same work station, having been once clamped the chain links are welded and fully deburred. The working station is fully open to avoid problems from flashing slag, Fig. 2.10.

2.5 HEAT TREATMENT OF CHAINS

The heat treatment of chains is not laid down in the British Standards ,and only reference to mechanical properties are made, but how these are obtained is left to the manufacturer.

There are standard furnaces for heat treatment of round steel chains. These include furnaces with fuel firing, electric heating (resistance), combined heating, gas/electricity or oil/electricity and specially designed induction furnaces.

a) Standard furnaces with fuel firing - these furnaces have been used for decades, Fig 2.11 [62], and there are four types according to the chain steel diameter and throughput, mainly for austenizing processes. In these furnaces, the continuous chains are surrounded by burner flames, avoiding direct flame contact,and are heated by radiation and

convection. After achieving required temperature, the chains , singular or multi-stranded according to the diameter, are quenched and conveyed by the reeling device to the outside and left to cool in the open.

The design of the furnace is set by the requirements of the hardening process. There are two important factors to be considered here: heating time and throughput speed - a lower throughput speeds results in incorrect quenching, i.e. the chain cools above the quenching tank.

b) Standard furnaces with electrical heating - this furnace has the advantage of good temperature uniformity and is mainly used for the hardening process. Similar varieties in size as in fuel firing furnaces exist with the advantage of no over pressure. The heating in these furnaces is provided by the filaments in the form of rings, arranged along the whole height of the furnace. They are often more costly than the fuel firing furnaces [62]. Finally, they have cleaner environment - no possibility of pollution as in the case of fuel firing furnaces.

c) Standard furnaces with combined heating, gas/electricity or oil/electricity - these furnaces have been developed to combine the low energy cost of fuel firing furnaces with better temperature uniformity of electric furnaces. The main energy requirements is covered by the fuel firing part and electrically heated discharge part provides for the desired temperature uniformity needed in the heat treatment of high strength chains.

d) Induction furnaces - electrical induction heating has simplified many heat-treating operations. Small parts can be through-heated and hardened as in other type of furnaces. Local or selective hardening, as well as surface hardening, is possible at a very rapid production rate. Furthermore, a standard induction unit can be adapted to a wide variety of products by simply changing the induction coil and adjusting the equipment settings. Continuous induction hardening has been in use since 1960, and has progressively replaced gas-fired hardening to the point where induction is now used exclusively. Until recently, however, tempering has been a batch operation, with a floor to floor time of about 10.5 hours for total heat treatment. For heat treatment of chains Wheway Becker Ltd. [63,64] have developed a plant which enables as-welded chains to be continuously hardened and tempered, Fig. 2. 12a and 2. 12b. It consists of three coils in line:

Coil A - the chain is hardened by passing it through a solenoidal wound induction heating coil. The heating of the chain above the Curie Point of 768° C ensures an even heat distribution around the link and on quenching from 900° C into water, a uniform hardness of 500 BHN is achieved around each link.

Coil B - The chain is then passed through an homogenising coil. A series of coils wound in a unique manner result in a uniform tempering of the chains. The actual hardness achieved can be controlled by the power input and may be varied accordingly to the service application.

Coil C - the third coil is again solenoidal but of a different design for the hardening coil. This coil tempers the parallel sides of the link whilst leaving the crowns of the link at higher hardness level.

Again the power input can be varied to control the hardness of the side barrels according to the operational requirements.

The net effect of heat treatment plant is therefore to produce a chain with a high crown hardness, giving improved wear resistance, greater toughness, greater resistance to stress corrosion cracking, greater breaking load, lower residual stress levels in the link, larger service life, greater reliability and finally competitive price [63]. The chains used in this research had uniform properties.

e) Tempering furnaces - in most cases chains are tempered in shaft circulating furnaces. The chains are hung onto a rack which is then inserted into the furnaces. Chains can also be tempered using continuous process, i.e. the ascending and descending channels are heated. The built in ventilators provide the necessary circulation speed and gives an optimal temperature uniformity.

2.6 CALIBRATION

During manufacture each heat treated round steel chain link is loaded with the prescribed test force, so that the weld is tested. During this process every chainlink is deformed plastically: the single links are adjusted to the measurements in the standard specifications. This process is called 'calibration'. For this purpose fully automated calibrating machines are used. Calibration load can be adjusted precisely and each calibrating stroke can be shown on a measuring tape or digitally. Afterwards, the chain will subsequently behave elastically up to the calibration load: that is , the yield is raised. This increase in yield results in introduction of residual stresses into the chain improving its fatigue properties (Chapter 3).

If fracture occurs at or below the specified test force, the chain must be rejected. After having been successfully calibrated, chains must be inspected on all sides visually link for link for imperfect welds, burnt spots or cracks. Fluorescent dye-penetrant and magnetic testing are also used for crack detection [65]. Faulty links are replaced with standard quality chain links, then heat treated and tested again. If the number of faulty links exceeds 3 %, the chain must be rejected.

2.7 MECHANICAL TESTINGS

All requirements such as dimensional accuracy, elongation at the test force, breaking force, elongation at fracture, deflection, notch toughness and the numbers of cycles to failure under a standard fatigue cycle of the sample are ascertained during the final control according to the appropriate British Standards. The dimensional and tensile tests are obligatory and other tests can be done in accordance to the customer's requirements. The chain characteristic curve is also determined to show the relationship between effective force and extension. The chains which pass the the required tests in all the production stages, have to be finally approved by the works inspector. Following final inspection, samples are taken from each production batch of chain and are subjected to mechanical testings as below:

a) Hardness testing - is carried out onto flat ground onto the surface of a single link from each batch of chains to confirm the heat treatment has been carried out correctly.

b) Bend test - individual links are bent in a shock force manner transversely across the weld and must withstand a miminum deflection

without failure or appearance of surface flaws, Fig. 2.13. The deflection is usually measured with the bending force applied.

c) Notch-impact Charpy test - this test is intended for use in the investigation of the steel used for chain making and assesses the properties of steel using samples machined from the core of the straight legs of each sample link. The test is Charpy U notch and carried out at room temperature.

d) Tensile test - a sample of five or seven links is tested in a certified testing machine, Fig. 2.14a and 2.14b. The failure is pure "shear" failure [66].

e) Fatigue test - a sample of chain is subjected to cyclic loading between lower and upper tensile force limits and its fatigue life is found. This process will be covered in full details in Chapter 3.

2.8 SURFACE PROTECTION

In most cases steel chains are used in nature-black condition: for some application bright type is usual. After a short time the atmospheric influences cause the formation of a rust on the surface. By suitable protective coatings this rust formation can be prevented for a longer period of time.

As a protection during transport and as a preservative for longer storage various corrosion preventives proved effective. Coats of varnish and plastic-laminates form sufficient protection for a limited time, as long as the protective covering is not partially destroyed by external mechanical actions.

Chains with a bright surface are best protected by electroplated zinc, brass, copper, nickel, or chromium coatings. Often an intensive oiling or lubrication of the chain would be efficient. Hot galvanising forms a good protection against corrosion for thicker chains [67].

CHAPTER 3

FATIGUE TESTING OF 7 mm LIFTING CHAINS

3.1 INTRODUCTION

Fatigue usually starts by the formation of a crack at the surface and anything which makes crack initiation easier - e.g. decarburization, surface roughness, etc. will reduce fatigue life. Heat treated ferrous materials often have lower fatigue strength than expected because of inferior surface properties or poor surface finish. They can however be improved by removing the surface layer. For example, Foley et al succeeded in improving the fatigue strength of short link mining chains by dry rumbling and wet grinding [24]. Batson and Bradley ([68], quoted in [24]), significantly improved the performance of steel springs by the grinding surface. The reduction in fatigue strength was attributed by these workers to decarburization. The surface decarburization process was investigated and three distict features were postulated:

a) A reduction in the carbon content of the surface layer produces an inherently weaker material which would fail under lower cyclic stresses.

b) Surface roughness accompanying decarburisation contributes to the lowering of the fatigue strength.

c) Grain boundary oxidation in the surface layer acts in a similar manner to notches and is often the principal factor in the reduction of the fatigue strength of decarburized steel.

Once the grain boundary oxidation has occurred, nothing short of re-melting will remedy the situation fully. Some improvement in fatigue strength under tensile loading can be obtained, however, by

introducing residual compressive stresses into the decarburized layer, by surface hardening, nitriding, case hardening and shot peening. These techniques are described more fully by [29,69]. Surface hardening was recommended by Minuth et al [70] for the mining chains failing in fatigue (corrosion cracking) under surface frictions.

It is suggested that the hardness of the core of a specimen has a lesser effect upon fatigue strength than does the hardness of the decarburized layer. The effect of the depth of the decarburized layer on the fatigue strength of steels has also been investigated by several researchers and the results are quite varied; a continual decrease in fatigue strength with increase in decarburized depth has been reported with notch specimens, on the other hand, the depth of the decarburized layer was found to have no significant effect whatsoever, but the reduction in fatigue strength depended on the microstructure of the material before carburization [24]. The reduction in the fatigue limit was found to be 30 %, 40 % and 50 % for pearlite, tempered martensite, and martensite respectively [24].

Overstressing of pressure vessels has long been applied as an inspection tool to detect any leakage in the wall and to demonstrate the fitness for purpose of the vessel. It was found that overstressing improves the fatigue life by delaying crack growth [71]. The study on notched aluminium alloy sheets showed that the overloading of specimens produced similar beneficial effects by delaying the crack growth [72,73]. Preloading - generally known as proof or calibration loading - also improves the fatigue strength of stud links up to some extent [74] and short link chains significantly [75]. This will be thoroughly investigated in this chapter.

Most of the fatigue data in the literature have been determined for condition of completely reversed cycles of stress (zero mean stress). However, conditions are frequently met in engineering practice where the stress situation consists of an alternating stress and a superimposed mean stress. There are several possible methods of determining S-N curve for a situation where the mean stress is not equal to zero [76]. Early contributions to this problem were made by Goodman, so that the curves which show the dependence of limiting range of stresses on mean stresses are frequently called Goodman diagrams. Fig. 3.1 shows one common type of Goodman diagram [76,77] which can be constructed by a series of tests for a given material. Basically, the diagram shows the variation of the limiting range of stress, $(\sigma_{max} - \sigma_{min})$, with mean stress, σ_m. The test data usually lie somewhat above and below the σ_{max} and σ_{min} lines respectively. Very few test data exist for the condition where the mean stress is compressive. Data [78] for SAE 4340 (quoted in [76]) steel tested in axial fatigue indicate that the allowable stress range increases with increasing compressive mean stress and decreases with increasing tensile mean stress up to the yield stress (σ_y). This is an agreement with the fact that compressive residual stresses increase the fatigue limit.

In this chapter, the fatigue testing procedure with its results will be discussed for various calibration loads and two different batches of chains, Section 3.2 and 3.3. The failure analysis of fatigue tests will be described with the use of electron scanning microscopy in Section 3.4. Other mechanical testing of the chains such as, hardness testing with metallography will be presented in Section 3.5. Finally, the effect of mean stress on fatigue strength of chains will be elaborated using a Goodman diagram approach.

3.2 FATIGUE TESTING PROCEDURE

The short link chains used in this investigation are made from 7 mm diameter bars (R_1 = 5.55, R_2 = 3.45, L = 5.45 mm, Fig. 1.3) manufactured from boron steel with the chemical composition given in Chapter 2 and are used for lifting purposes, BS3243:4:1

The chain was in the hardened and tempered condition with no proof loading before testing.

Fatigue tests were carried out on a 250 kN Mayes servohydraulic machine that is capable of generating the required sinusoidal signal with an appropriate number of cycles per minute (rate of testing), Fig. 3.2. For all the tests, 500 cycles per minute was chosen to eliminate any possible effect due to rate of testing. Foly et al [24,25,75], Celander et al [74] and Stanford [79] used 2000, 850 and 200 cycles per minute in their work respectively. Meanwhile for the mining chains, the frequency ought to be in the range of 200 to 1000 cycles per minute, BS2969. The chain links were tested in three-link sets released from a continuous batch of a chain supplied by Wheway Becker Ltd. [80]. The sample was held in the machine by specially designed grips, shown in Fig. 3.3, with a pair of chain crowns cut and filed to simulate the real contact situation between the links rather than a pin through the links chosen by some researchers.

It is not possible to test under conditions of zero mean load, as is the norm with fatigue testing, since the links would go slack during the nominally compression part of each cycle. Furthermore, it was found that it was extremely difficult to set the machine to test under

conditions of zero minimum load. Hence, all the tests were conducted with a minimum load of 2 kN, the maximum load being varied for the test condition required, 12 - 24 kN.

The links were either tested to failure or until they reached two million cycles, at which stage the test was terminated and the links were considered to have survived. The fatigue lives of the specimens failing under two million cycles were recorded by the use of fracture trip facility on the testing machine.

To calibrate the specimens, they were first positioned in the machine and the load was raised up to the required level and sustained for a few seconds before unloading.

3.3 FATIGUE TESTING RESULTS

The fatigue tests were carried out with load ranges from 2 -24 kN down to 2 - 12 kN (the working load limit for this grade of chains is 16 kN) to study the scatter of results at various load levels and different calibration loads. The results are given in Table 3.1 showing the location of failure as well as end or centre link failure for a given batch.

A considerable amount of interest has been shown in the statistical analysis of fatigue data and in the reasons for the variability in fatigue test results. Since fatigue life and fatigue limit are statistical quantities, it must be realised that considerable deviation from an average curve determined with only a few specimens is to be expected. This will be thoroughly investigated in the next section using cumulative probability curves.

The basic method of presenting engineering fatigue data is by means of the S-N curves, a plot of stress against the number of cycles to failure N. A log scale is almost always used for N especially in the case of $N \geq 10^4$. This method will be used later to explain the fatigue test results of 7 mm lifting chains.

3.3.1 STATISTICAL PRESENTATION OF RESULTS

There are various statistical distribution functions which describe the distributuion of fatigue life at constant stress, such as: Weibull and Gaussian or normal distribution [81,82,83]. The normal distribution was used here because of simplicity and its common use in fatigue life analysis of chains (BS2969).

In this distribution, the fatigue results are plotted on a diagram with:

a) On one scale - the number of cycles to fracture (endurance) of the individual samples (logarithmic scale), i.e. log N :

b) On the other scale - the probability of fracture of the sample, i.e., the percentage of samples having an endurance less than log N (Gaussian cumulative).

- the number of cycles is ranked and plotted on the ordinate
- the probability of the fracture on the abscissa using the formula $i/(n + 1)$;

where i = the ranked value of the sample

n = the total number of tests

n was 10 except for load level of 16 kN when the calibration load was zero (n=20). The samples which survived the test will not be included in the plots. The best line is fitted to these points, Fig. 3.4 to

3.9. The shape of the line is a measure of the dispersion of the results, a horizontal line indicating zero dispersion. The fact that a good straight line is obtained indicates that the assumption that log N is normally distributed is consistent with the experimental results.

From these plots it can be seen that the new batch has a much lower fatigue life. This will be elaborated in the next section. In all the graphs as the calibration load increases, the fatigue life also increases, confirming the effect of increased calibration load on fatigue life of chains. In Fig. 3.8, the logarithms of the means of the lives of the uncalibrated and calibrated (20 kN) chains are not significantly different. Application of the 't' test [84] showed that the chance of getting a difference of the size or bigger is greater than 30 %, that is, there is no significant difference between the results for the uncalibrated chain and the chain calibrated at 20 kN.

3.3.2 S-N CURVES

The stress values used in the S-N curves are nominal stresses with no adjustment made for stress concentration. Under general loading condition, the stresses on a gross scale are elastic, but some parts of chain may deform plastically in a highly localized way, specially under loads around 30 kN and over. Hence, the fatigue testing is high-cycle ($N > 10^5$) fatigue and the S-N curves can be appropriately used to illustrate the fatigue results.

L_5, L_{20}, L_{50}, L_{80}, and L_{95} (L_5 being the average life at which 5 % of the samples will have fractured) were tabulated for all the fatigue test results in Section 3.3 and are then

plotted in the linear-log scale (S-N curve), Fig. 3.10 to 3.14. A smooth curve is drawn through the points, terminating at two million cycles due to the convention adopted earlier. Hence fatigue limit determination which is subject to considerable variation will not be attempted. It can be seen from the S-N curves that the increase in calibration load results in increase in fatigue life of 7 mm lifting chains. This effect is evident in all the S-N curves at the various probabilities of failure (5 - 95 %). It can be concluded that calibration of chains introduces compressive residual stresses (acting as mean stresses) which are deducted from the applied tensile stresses resulting in lower service stresses; consequently a significant improvement in fatigue life of chains is achieved.

3.4 ANALYSIS OF FATIGUE FAILURES

Fatigue fractures were examined by optical microscopy, which did not reveal any appreciable differences among the specimens. The eight specimens were then examined using electron scanning microscopy.

Fatigue cracks and fractures exhibit several features which can aid this recognition. Not all these features are present in any particular fracture but, in any individual case, consideration of these aspects can normally distinguish fatigue from other mechanism of failures [85,86]. These features are as follows:

general appearance
location of fracture
beach markings
rachet markings
fatigue striations

A typical chain fatigue fracture is given in Fig. 3.15, showing the final ductile fracture (rough zone) and a smooth appearance in the fatigue zone.

Fatigue failures often occur at regions of localized stress concentration, e.g. weld toes, changes in sections, an existing crack etc. Stress concentration zones in the chain link are at the crown (outside and inside surface) and the transition zone (inside surface) according to the elastic and elasto-plastic stress analysis (Chapters 6, 7 and 8). All the cracks initiated from the zones of largest stress concentration, except for some samples fracturing at the weld. In case of two samples, the cracks started from an existing dent, Fig. 3.16; Fig. 3.17 at the weld; and Fig 3.18 and 3.19 at the transition zone.

As the links were heat treated after the welding processes, the Heat Affected Zone (HAZ) was removed and the whole link has a uniform microstructure, Fig. 3.20 (a and b). The more reliable reason for fracture in the weld is most likely to be either because of stress concentration caused by the shape there. The steel being very clean the inclusions were unlikely to cause any stress concentration (Fig. 3.20a).

Fig. 3.21 shows the different location of fatigue failure, and Fig. 3.22 the locations of the fractures due to the tensile test and fatigue test.

Beach markings were observed, Fig. 3.16, Fig. 3.18 and Fig 3.19 which indicate that fatigue did not propagate continuously but in steps with intermediate pauses. Ratchet markings are shown in Fig. 3.17 which indicates that multiple crack initiation occurred.

There are a few other factors which may influence the fatigue fracture location such as:

effect of calibration load
load levels
different batches
whether the link was at the centre or the end of the three tested links

To investigate this a statistical software Minitab [87] was used. The fatigue results in Section 3.3 are presented in tabular and graphical forms, Table 3.1 to 3.3 and Fig. 3.23 and 3.24. Fig. 3.23 indicates that the percentage of fracture failures at weld zone does not change significantly with increase in calibration load, whereas, the percentage of fractures at the crown and transition zones changes considerably in the opposite direction (failures at the crown zone increases and the transition zone decreases). Fracture appears to be equally likely at centre and at end links. A similar pattern of behaviour occurs with an increase in load level except that there is a slight increase in the percentage of fracture occurring in the centre link, Fig. 3.24.

Different batches of chain seem to have a great deal of influence in the centre and end link failures, Fig. 3.25. It also affected the fracture location significantly - 76 % of the samples failed at the weld in the second batch (Fig. 3.25). In the earlier section, it was mentioned that the second batch of chains had shorter fatigue lives. This was combined with a higher rate of fracture at the weld. The probable explanation is that the welds of the second batch were not trimmed off totally as in the first batch. This may have caused local stress concentration at the weld zone higher than the above mentioned zones. Finally, the effect of centre or end links on the fracture position is shown in Fig. 3.26, showing that there is only a small difference in the percentages of the different fracture positions between centre and end links.

3.5 MECHANICAL TESTING OF CHAIN MATERIAL

The tensile testing, hardness testing and metallography of the chain material was carried out on the as-received condition and the results are discussed below:

3.5.1 TENSILE TESTS

Tensile testing was carried out for two sets of specimens, namely welded and plain, prepared from the chain link material. Testing was carried out on a Hounsfield tensometer using specimen no. 12 (nominal cross- section, 1/40 in^2. [16.29 mm^2]; nominal gauge length, .632 in. [16.053 mm]). In addition to the ultimate tensile stress, reduction in area and percentage elongation, the yield point was approximated from the end of the initial elastic loading line.

The results indicate that the weld material has ductility as good as the parent material. There are indications from the few tests carried out that the welded specimens had slightly lower values of tensile and yield stresses. The average tensile and yield stresses for plain and welded specimens are 1394, 1191 and 1285,1104 MPa respectively, Table 3.4.

A tensile test on a five-link specimen was carried out on a Mayes machine and the load-extension curve is given in Fig. 3.27. The ultimate load (68.4 kN) is slightly higher than the manufacturer's value of 64.1 kN and the elongation percentage is 29.5 %. The load-extension curve departs from a straight line at about 30 kN and breaks off at an extension of 32.3 mm.

3.5.2 HARDNESS TESTS

The hardness of chain link at three cross-sections (crown, mid-section and transition) and one section through the weld along the side of the link, was found using a Vickers pyramid hardness machine. Specially prepared specimens used for metallography were used on this test and the corresponding readings were tabulated, Table 3.5. Only two sets of readings are given here due to the fact that the other readings were very similar.

The Rockwell hardness test was also carried out on the prepared specimens to confirm the hardnesses given by the manufacture and Vickers hardness machine. The following readings were obtained for two specimens: 37, 37 and 39 (average 38): and 30, 43 and 42 (average 38). The Rockwell hardness number is equivalent to 363 Brinell hardness number, which is in the range (360 - 400) of the values given by the manufacturer.

There was not any difference in hardness corresponding to the apparent difference in ultimate tensile stress between plain and welded tensile specimens.

3.5.3 METALLOGRAPHY

Metallography was carried out to evaluate any microstructural defects in the chain link under investigation.

Four specimens were selected: one from the crown, one from the transition , one from the weld, and lastly one from the leg containing the weld to check for the heat affected zone and signs of 'directionality'. All these specimens were prepared and viewed under the microscope with no significant difference between them. A typical

tempered martensitic crystal structure with rectangular and cuboid inclusions can be seen, Fig. 3.20 (a,b). Appreciable grain-boundary thickening is evident at the edge of the cross-section, Fig. 3.20 b. The heat affected zone around the weld could not be distinguished, because the chain was quenched and tempered after the welding processes (weld going horizontally through Fig. 3.20 a). It was scarcely possible to distiguish any features of the structure that would indicate the location of the weld.

3.6 EFFECT OF MEAN STRESS ON FATIGUE

The effect of mean stress on fatigue strength of various metals specially that of steels has been very well established. This effect can be produced in chains by the introduction of residual stresses as a result of calibration of the links. To confirm the effect axial loading fatigue tests were carried out on the chain material (7mm lifting).

There are not any standards in the design of pull and push fatigue specimens, hence they had to be designed to avoid such effects as: stress concentration and fretting. The largest possible cross-sectional areas were chosen at the centre and both ends of the specimens to avoid high stress concentration zones as well as making use of the existing specimen holder. The details of the fatigue specimen are given in Fig. 3.28.

The as-received material (bent bars) was first cut to size and straightened up before machining the centre part. The specimens were then hardened at 925° C in air for about 11 minutes and water quenched vertically to minimize the amount of distortion. They were

finally tempered at 345° C for 6 hours in air circulating furnace (identical heat treatment as for 7 mm lifting chain), before machining was finished off. At the centre of the specimens the distortion varied from 0.25 to 0.43 mm (off centre line).

Three dimensional finite element elastic stress analysis of the 7 mm lifting chain was carried out to obtain stresses at the inside transition under 2 and 16 kN (working load limit) loads (fatigue testing load limit). The stresses are 121 and 971 MPa with 546 MPa as the mean stress. To achieve the same nominal stresses in the fatigue specimens, the loads must be 2.38 and 19.07 kN (as lower and upper limits) with amplitude of a = 8.35 kN. Four specimens were tested at five different mean stress levels and the results are given in Table 3.6. It can be seen that the reduction in mean stress (tensile) and increase in compressive mean stress improve the fatigue lives of the specimens significantly. It is certainly consistent with the fact that calibration of chains, introduces compressive residual stresses at the surface of chains acting as mean stress, improves the fatigue properties.

All the specimens were polished prior to any heat treatment giving a much smoother surface finish similar to that of 7 mm lifting chains. On the other hand, the as-machined specimens similarly heat treated had very rough surface finish resulting in shorter fatigue lives. This was confirmed both by Talysurf investigation of the specimen surfaces and fatigue testing of the as-machined specimens, Table 3.7.

CHAPTER 4

RESIDUAL STRESS MEASUREMENT USING X-RAY AND NEUTRON DIFFRACTION METHODS

4.1 INTRODUCTION

X-ray methods of measuring residual stress in crystalline materials have been tested and compared to other methods, and are in use throughout the world. Manuals have been written for their use in the United States and Japan [88,89], quoted in [90].

Usually the measurements are made manually on a conventional powder x-ray diffractometer or with a special ,unit. But there are other units that can make measurements in seconds (in the field) with reasonable precision. Both methods of measurement will be discussed later in this chapter.

The basis of the technique is straight forward and was first used by Aborn at the U.S. Steel Co. [91], quoted in [90]. When a polycrystalline piece of metal is deformed elastically in such a manner that the strain is uniform over relatively large distance, the lattice plane spacing in the constituent grains change from their stress-free value to some new value corresponding to the magnitude of the applied stress. This uniform macrostress causes a shift of the diffraction lines to new 2θ position. On the other hand, if the metal is deformed plastically, the lattice planes usually become distorted in such a way that the spacing of any particular (hkl) set varies from one grain to another and within each grain. This uniform microstrain causes a broadening of the corresponding diffraction line. Actually, both kinds of strain are usually superimposed in plastically deformed metals, and diffraction lines are both shifted and broadened, because not only do the plane spacings vary from grain to grain but their mean value differs from that of the undeformed metal.

From the line shift due to uniform strain, the strain may be calculated and, knowing the strain, we can determine the stresses present, either by using the mechanically measured elastic constants of the material, or by a calibration procedure involving measurement of the strain produced by known stress. X-ray diffraction can therefore be used as a method of "stress" measurement [90,92,93,94,95].

The fact that x-rays penetrate only a shallow depth is in fact useful, because in many cases there are steep gradients in the macrostress near the surface. By using neutrons, which can penetrate 2 - 3 cm of steel, the macrostresses are averaged over the volume from which the reflection is obtained (usually 2 X 2 X 2 mm). The stresses can be measured within the specimen volume by using appropriate slits. . The resolution in this case is the order of 1 - 2 mm, depending on the neutron intensity. This method of residual stress measurement will be discussed at the end of this chapter.

In this chapter an attempt to measure residual stresses in 19 mm mining and 7 mm lifting chains, using a laboratory diffractometer is described. They were then measured in the British Steel Laboratories using the Rigaku Strainflex equipment. Finally, the internal residual stresses at the centre of the 19 mm mining chain were measured at the Institut Laue-Langevin, Grenoble by neutron diffraction.

4.2 X-RAY DIFFRACTION (CAMERA METHOD)

This method of residual stress measurement is carried out using a back-reflection camera with the basic principle of x-ray diffraction. The method and the experimental procedure is given below.

4.2.1 BACK-REFLECTION METHOD

X-rays from the tube are collimated to pass through a cassette containing a film, and are reflected back from the specimen, mounted on a specimen holder, thus exposing the film, Fig. 4.1. This is a part of laboratory x-ray diffractometer. Both the normal and inclined photographs may be registered on one film by using an opaque metal film cover which has two openings diametrically opposite. After one exposure is made, the film holder is rotated 90° in its own plane with respect to the cover and the other exposure is made.

The stress, σ_{ϕ} , at any angle, ϕ , can be calculated from this equation [93].

$$\sigma_{\phi} = E(S_i - S_n)/2D(1+\nu)\mathrm{Sec}^2 2\theta \ \mathrm{Tan}\theta \ \mathrm{Sin}^2\psi$$

where σ_{ϕ} is the normal stress parallel to the specimen surface, its line of action being in the plane containing the incident beam and the normal to the surface; ψ , the angle at which the incident beam is inclined to the normal to the surface. D is the distance of the film from the specimen. S_i and S_n are the radii of the rings with the incident beam inclined and normal respectively and are measured from the developed film. The accuracy of the method can be evaluated.

Correct specimen surface preparation is extremely important [96]. If dirt and scale are present, they may be ground off, the grinding must be followed by deep etching to remove the surface layer left in compression by the grinding. Then the surface is lightly polished

with fine emery paper, to remove the roughness caused by deep etching, and slightly re-etched. Depth of x-ray penetration is dependent on the absorption coefficient of the material for a given beam and the beam dimension on the experimental surface, which are defined by the slits and the geometry of the experiment. The effective depth of penetration may be calculated using appropriate formulae [97]. The effective depth of penetration of Cr radiation into steel for the (211) plane ($2\theta = 154^{o}$) is approximately 5.4E-6 m.

Diffraction angle, θ , for iron may be calculated. The lattice spacing (d) for a cubic crystal is given by [98]:

$$d = a/(h^2 + k^2 + l^2)^{1/2}$$

where a, the lattice parameter of iron is .28664 nm, giving d = .11702 nm; From Bragg's Law : $n\lambda = 2d \sin\theta$ and taking n=1, λ = .154178 nm for K_{α} radiation of copper, we find the diffraction angle $2\theta = 82.412^{o}$. λ = .229092 nm for K_{α} radiation of chromium, the diffraction angle $2\theta = 156.394^{o}$.

4.2.2 EXPERIMENTAL PROCEDURE

A set-up as in Fig. 4.2 was used to measure the residual stresses with an elaborate specimen holder (goniometer) which has three rotation axis and sliding capability. Instant Kodak film cassette or standard type film holder may be used to achieve exposures. Chromium radiation of 40 kV and 20 mA (.8 kW) was selected to carry out the experiment. The surface of the 7 mm lifting chain link was prepared as mentioned in Section 4.2.1 and mounted on the goniometer using a fluorescent disc, Fig. 4.3, for correct positioning. For a fixed

specimen to the film distance two exposures were made and the film was developed in usual manner, Fig. 4.4. The rings were very diffuse and the ring radii could not be satisfactorily measured using two different kinds of densitometer. Different size (medium and narrow) collimators were used with no significant improvement as well as longer exposure time (3 - 12 hours) and faster film. The standard x-ray film type was replaced by instant Kodak film resulting no change in quality of the rings, even with a flatter chain-link material.

The chain link was tempered at 600° C in a salt bath for one hour with another link annealed at 900° C for 3 hours and 1 hour, to sharpen up the rings. The whole process was repeated with sharper rings, but still the radii of the rings could not be measured satisfactorily.

4.3 X-RAY DIFFRACTOMETER

The diffractometer may also be used for stress measurement. The only instrumental changes necessary are the addition of a specimen holder which will allow independent rotation of the specimen about the diffractometer axis and a change in the position of the receiving slit. In this section the laboratory diffractometer, the principles of stress measurement and experimental procedure will be discussed.

4.3.1 X-RAY DIFFRACTION METHOD

Fig. 4.5 illustrates the angular relationship involved in a laboratory diffractometer. Radiation divergent from the source S is diffracted to a focus at F′ on the focussing circle and F on the diffractometer circle. The specimen is turned through an angle ψ

for the inclined position. Different slit arrangements can be used at F and F′ to achieve both intensity and resolution, but a compromise can be made by placing narrow slits at some point between F and F′ to obtain satisfactory results. Choice of slits, collimators and monochromators are thoroughly covered in the literature [90,92,99] and its discussion will be avoided here.

The stress equation can be written in terms of angular position 2θ rather than plane spacing as in back-reflection [100].

$$\sigma_\phi = E \cot \theta (2\theta_n - 2\theta_i)/2(1 + \nu)\sin^2\psi$$

where $2\theta_n$ is the observed value of the diffraction angle in the "normal" measurement ($\psi=0$) and $2\theta_i$ its value at the inclined measurement ($\psi=\psi$). The quantity measured in the diffractometer method is $\Delta 2\theta$, $(2\theta_n - 2\theta_i)$ which is essentially the shift in the diffraction line due to stress as the angle ψ is changed.

4.3.2 EXPERIMENTAL PROCEDURE

The x-ray diffractometer with its accessories to measure the residual stresses on the 7 mm lifting chain is shown in Fig. 4.6. The intensity of the diffracted x-rays can be either plotted or printed out for a given scanning step.

Prior to the residual stress measurement, the diffractometer alignment had to be checked using a standard silicon sample (Fig. 4.3). The intensity, counts per second (cps) was plotted, Fig. 4.7, giving the

peak position (2θ) at 56.09° (compared with 56.12° expected for the standard).

The commercially heat-treated and calibrated link was mounted on specially made holders which were then placed in the chamber to carry out the measurement at $\psi = 0^{\circ}$ and $\pm 45^{\circ}$. For a given scan, the intensity was first plotted to locate roughly the peak diffraction angle, Fig. 4.8, then the scanning step (.01°, .02° ,.05°...) was refined at the region of peak position to determine the peak diffraction angle accurately by plotting the intensity printed out, Fig. 4.9. The diffraction peak was not shifted equally on either side (± 45) to the normal direction, Fig. 4.9. To find the minimum scanning time needed to define the peaks, intensity versus diffraction angle plots were produced at scanning times of 1/4, 1/2, 1, 2, 3 and 4 minutes, Fig. 4.10. Shorter scanning times seem to have produced fluctuating patterns and therefore scanning time of 2 minutes was chosen.

Two 7 mm lifting chains were tempered at 600° C for 3 and 2 hours in salt bath. The normal calibration load was reduced by a factor equal to the fractional reduction in hardness caused by the additional tempering (original hardness: 345 HV30; hardness after additional tempering: 263 HV30; normal calibration load: 38.5 kN; reduced calibration load 23.28 kN). Three positions on the surface of each link were considered, centre of the non-welded leg and 5 mm at either side of it (to left and right). The diffraction angle at these locations at $\phi = 0^{\circ}$ and $\pm 45^{\circ}$ were measured and tabulated, Table 4.1. The links were electro-polished instead of grinding the surface preparation process suggested by some workers. A solution of 94 % acetic acid and 6 % of perchloric acid was used with a D.C.

supply for 30 seconds.

The residual stresses corresponding to the Table 4.1 readings are given in Table4.2 and were calculated as below:

$$\sigma_\phi = -[E\cot\theta_o . \pi/2(1+\nu).180].(\Delta 2\theta/\Delta \sin^2\psi)$$

where, E= 207 GPa, ν =.29 , $2\theta = 136.95^o$ at $\psi = 0^o$ and θ_o is the diffraction angle for stress free material (usally replaced by θ).

$$\sigma_\phi = -6.2E7 \; . \; \Delta 2\theta/\Delta \sin^2\psi \qquad (\Delta 2\theta \text{ in degrees})$$

The stresses in Table 4.2 are not consistent (the specimen rotates 45° to the right and left) and large residual stresses exist at the noncalibrated state which had very little or no residual stresses. The errors could not be caused by the misalignment of the diffractometer, which was checked earlier. Generally the diffraction peaks are fairly broad (Fig. 4.9) specially when the specimen was rotated and the shift in diffraction peak could not be satisfactorily measured from the plot. However, all the measured stresses are compressive at the centre of the 7 mm lifting chain under various conditions.

Other measurements on other positions (such as crown) on the 7 mm lifting and 19 mm mining chain links were not possible, because of the diffractometer chamber size. Measurements were then carried out on a diffractometer especially designed for residual stress determination.

4.4 FIELD DIFFRACTOMETER (STRAINFLEX)

Residual stresses are measured in various ways in real part, either in an ordinary x-ray laboratory (Section 4.2 and 4.3) to which such samples may be brought occasionally, in a factory where frequent inspection is required, or in the field, for example in oil rigs, at large construction sites, pipelines or power stations or for parts which are too large for a commercial diffractometer. There are several units available for such situations, for example PARS [90] and Strainflex (Rigaku) which was used to carry out residual measurements on the 7 mm lifting and 19 mm mining chain links. The Strainflex equipment and results of measurements are given in this section.

4.4.1 STRAINFLEX (RIGAKU)

It consists of a goniometer, shown in Fig. 4.11 [101,102], which carries the x-ray tube on one rack and a scintillation counter on another rack. This enables the incident angle of the x-ray beam to be varied from $\psi_o = 0^o$ to 45° (Fig. 4.12) at 5° intervals and the scanning to be undertaken over the angular range $2\theta = 170^o$ to 140°. Fig. 4.13 shows the central unit consisting of the heat exchanger, for cooling the anode of the x-ray tube, the x-ray generator for supplying 30 kV, 2 - 10 mA to the tube and the microprocessor-based control and data processing unit, which controls the functioning of the goniometer and produces a printout of some parameters used in the residual stress measurements and their values, Fig. 4.14. The diffraction peak profile can also be printed for reference. A camera attachment allows qualitative assessment of the grain size and texture of a material.

The $Sin^2\psi$, fixed ψ_o technique was used to determine the residual stresses. When a material is isotropic, then a linear relationship is obtained between the diffraction peak position, 2θ , and $Sin^2\psi$ for, say, four ψ - angles (ψ_o= 0°, 15°, 30°, and 45°). The gradient of the linear regression equation is substituted into the stress equation with elastic constants of the material and $Cot\theta$ at 30° to give the residual stress.

The use of an approximately parallel beam allows tolerances of ±2 mm on the specimen position. This is achieved using transmission and receiving Soller slits to give parallel beam geometry in order to simplify the alignment procedure. Irradiated area can be varied from 20 X 5, 10 X 5 to 5 X 5 mm by restricting the Soller slits (to give parallel beam) aperture and a minimum area of 2 X 2 mm can be obtained by suitable masking of the material surface.

The diffraction peak position can be offset from its true position by the effect of 'coarse grained' and textured material [101]. The residual stress can vary between grains, and large grains favourably oriented to diffract the incident x-ray beam can contribute most to the diffraction profile leading to an erroneous peak position. Scans with different adjustments can give different residual stress values because the contributions to the diffraction peaks may come from different grains. The accuracy of the measurement made on coarse grained materials can be improved by oscillating the incident x-ray beam to allow more grains to contribute to the diffraction profile. This facility is available on the Strainflex with selection of ±3, ±5 or ±7 degrees.

'Texture' present in a material can cause a shift from the true diffraction position because the number of grains contributing to diffraction varies with 2θ whereas for an isotropic material the number remains constant. Therefore, a higher concentration of grains can give diffracted beam of higher intensity than the grains more favourably oriented for diffraction. In order to overcome the problem, the Strainflex incorporates the fixed ψ technique. This differs from the fixed ψ_0 technique in which the incident x-ray beam angle is kept constant, in that the angle subtended by the surface normal and normal to reflecting planes is maintained constant during the scan. This means that the x-ray tube and counter are moved simultanously. Although this does not eliminate entirely the effects of texture, it makes a significant improvement to the analysis on textured material.

The x-ray technique is very sensitive to any surface preparation given to a material because the x-rays only penetrate into the surface approximately 10 μm. The electropolishing technique which is a stress-free process can be used to prepare the surfce and remove any undesirable stresses introduced by abrasive preparation. A solution of 14 % water, 45 % H_3PO_4 and 41 % H_2SO_4 was used with 15 V D.C. and .5 - 1.5 A, in order to electropolish the region to be examined [103].

4.4.2 EXPERIMENTAL PROCEDURE

The measurement of residual stresses on chains were carried out in two parts using the Strainflex:

a) 7 mm Lifting chain - a set of 7 mm lifting chain links calibrated

at various levels (equivalent to 30, 38.5 and 50 kN) and a noncalibrated link were prepared for the measurements. The links were all tempered at 600° C (to sharpen diffraction peaks) in a salt bath (to avoid surface oxidation) for one hour and air cooled prior to calibration. The positions (Fig. 4.15) at which the measurements are to be taken were electropolished and an area of 2 X 2 mm was masked off. The chromium tube with 1° divergence and receiving slits was used to radiate (211) planes. The stresses are given in Table 4.3 and were calculated using elastic constants of E = 207 GPa and ν=.29. The residual stresses at the outside of the 7 mm lifting chain are all compressive with the highest magnitude occurring at the crown. The residual stresses at the centre and crown increase with increase in calibration load. Certainly this can be seen from the results, but the final calibration load did not have the expected effect on the level of residual stresses.

A typical analyser output is given in Fig. 4.14 with appropriate parameters illustrated in Fig. 4.16.

b) 19 mm Mining chain - a set of 19 mm mining chain links was hardened at 970° C in salt bath for 10 minutes and water quenched and tempered at 600° C for one hour in a salt bath and water quenched/air cooled. The links were calibrated at various levels. In all measurements, an area of 5 X 5 mm at the required positions was masked off. The chromium tube with 1° divergence and receiving slits was used to radiate (211) planes (also in case (a)).

A light electropolish was carried out for the water quenched link on positions P1 and P5 to assess whether surface scale was present, although all the heat treatment was carried out in salt bath. It was

established, however, that there was no need for surface electropolish which did not have very significant effect on the measurements, Table 4.4

The residual stresses are given in Table 4.4 for water quenched links and Table 4.5 for the air cooled link, in which the measurements were made after consequent calibration. For the former case, they are all compressive and increase in calibration load did not have the expected effect on the residual stresses (at the centre and crown) which were initially quite high. This may imply that the links underwent a substantial amount of deformation as a result of water quenching, which consequently produced the compressive residual stresses. In the latter case (Table 4.5) calibration can be seen to introduce residual compressive stresses although the expected increase in these stresses on going from a calibration load of 260 to 320 kN is not observed at the crown.

4.5 NEUTRON DIFFRACTION

The x-ray method of residual stress measurement is nondestructive and can only be used for surface stresses. The hole drilling technique [30] and Sachs boring method [104] are both destructive but measure the stresses in the bulk of components. Recently a neutron diffraction procedure [90,105,106,107] has been developed which allows through-thickness residual stresses to be measured without the need for destroying the component. It does, however, require the sample to be transported to a high flux neutron source.

In this section, the neutron diffraction method will be briefly introduced and the results of the work carried out at the Institute

Laue-Langevin (ILL), Grenoble, France will be presented.

4.5.1 NEUTRON DIFFRACTION METHOD

Neutron diffraction and x-ray methods both measure components of strain directly from changes in the lattice spacings of the crystals. Residual stresses are then calculated from these strains. Neutrons can penetrate several centimeters into most materials so that bulk strains can be investigated.

The principles of the neutron diffraction technique are illustrated in Fig. 4.17. If d is the lattice spacing in the direction of $\underline{Q}$ and 2θ is the scattering angle, then the lattice strain ε, in the direction of the scattering vector is given explicitly as [106]:.

$$\varepsilon = \Delta d/d = -\Delta\theta \, \mathrm{Cot}\theta$$

To obtain the absolute strain the lattice spacing of the unstrained material d_o must be known.

The sensitivity of the method depends upon the angular resolution of the systems and upon the volume of material sampled. The sensitivity of the method may be improved by using multi-slit Soller collimators to produce parallel beam with minimum loss in intensity. The volume of the material sampled is defined by the incoming beam and may be limited by inserting a mask just in front of the sample as illustrated in Fig. 4.17.

A large volume will permit a rapid counting rate and speed recording, but will give average strains over the volume which may not be

satisfactory in the region of steeply changing residual stress. A compromise is therefore required by choosing a few cubic millimeters.

A Bragg reflection, from a region of constant strain, usually has a Gaussian intensity profile, the centre of which may be determined accurately by a peak fitting routine, Fig. 4.18.

4.5.2 EXPERIMENTAL PROCEDURE

The 19 mm mining chain link (calibrated at 350 kN) which was used in Section 4.4, was chosen to undertake the task of residual stress measurement, Fig. 4.19. The measurements were carried out using the high resolution powder diffractometer situated on a thermal neutron guide from the High Flux Beam Reactor at the ILL.

Measurements were made of (211) peak shifts and profile changes as a function of position and orientation in the chain link. The (211) reflection was chosen because it was expected that the (211) strains would be similar to the average engineering strains and, using a neutron wavelength of 0.19106 nm, the angle 2θ was close to 90° thus giving optimum spatial resolution. In the x and z directions a sampling volume of 2X2X2 mm was used with the link mounted horizontally. Measurements in the y direction a volume of 2X2X10 mm was used with link mounted vertically. Measurements were made in a region close to the centre of the long side of the link as indicated in Fig. 4.20.

The measurements can be both plotted, Fig. 4.18, and printed Table 4.6.

4.5.3 RESULTS AND CALCULATIONS

Peak centres and widths obtained by computer fitting single Gaussians to the data, are plotted, Fig. 4.21 and 4.22. The width of a peak, from a perfect unstrained crystalline powder at the angle of the (211) steel reflection, arising solely from instrumental factors, is about 0.3^{o}. However, it is found in most experiments on engineering steels that have been annealed and elastically strained, that peak widths are usually in the region of 0.35^{o} to 0.45^{o}. If the steel has been plastically strained or there are steep strain gradients additional peak broadening and sometimes changes in peak shapes occur.

In this experiment single Gaussians provide a satisfactory fit to all the peak profiles but the measured peak widths are mostly in the range $0.7^{o} \pm 0.1^{o}$. This is not exceptional and would suggest that there is extensive microstrain present in the chain link. At y = 6 mm and 13 mm the peak widths are 1.26^{o} and 0.88^{o} respectively for the z direction data but remain near 0.7^{o} for the x and y data. The measuring positions at which the z peaks are extra wide do,however, coincide with regions of very steep z strain and their extra widths, and decreased peak heights, are quantitatively as would be expected for the strain gradient observed and the size of sampling volume used.

Fig. 4.23 shows the strains and Fig. 4.24 the stresses calculated from the peak centre positions assuming x, y and z directions correspond to the principal stress directions. As no measurement of diffraction angle was taken on a stress-free material, it was found from the stressed state of the chain link. The diffraction angle

corresponding to equal lattice spacing in all three directions was obtained from the plots of lattice spacings in the x and y-directions versus z-direction, Fig. 4.25 (Table 4.7). Experience and balancing considerations would suggest that this point corresponds to position of minimum strain and stress, and hence it was used as the strain free zero for calculation purposes. From Bragg's Law, considering λ = .19106 nm and d = .11723 nm, the diffraction angle is calculated $2\theta_o = 109.154^o$. Having ($\Delta\theta = 2\theta - 2\theta_o$), the strains can be calculated from the following expression and given in Table 4.8, 4.9 and 4.10.

ε = -6.207E-3 $\Delta\theta$ ($\Delta\theta$ in degrees)

From these strains, stresses were calculated and are shown in Table 4.8 and 4.9.

The x and y strains are small and opposite in sign in comparison with the large z strains suggesting that they substantially arise as a Poisson's ratio effect. The corresponding x and y stresses are at all positions small, whereas the z stresses change rapidly from compression to tension and back to compression as a function of position y. There were very large strains observed around y = 5 mm.

All three stresses are plotted along the positions with the absolute maximum principal stresses from the finite element analysis (Table 4.11) Fig. 4.26. There is a good agreement between the neutron diffraction and finite element results. Stresses in the x and y-direction are very close and have opposite sign to σ_z. All stresses meet at zero stress position.

The errors from all the measurements were also determined ranging from ±19 to ±64 MPa. The largest errors occurred at the steepest stress gradient implying that the irradiated volume is too large and better results may be obtained by smaller volumes with further refinements. It is anticipated that the residual stresses can be measured by this technique to an accuracy of about 20 MPa. Furthermore, the accuracy may be possibly improved by a factor of 2 due to better statistics (better curve fitting techniques) at substantially reduced counting times [106].

CHAPTER 5

RESIDUAL STRESS MEASUREMENT USING STRAIN GAUGE METHOD

5.1 INTRODUCTION

The strain gauge method of stress measurement is the most widely used technique in industry today. It involves the fixing of one or more strain gauges (length of wire or foil of known resistance and suitable form cemented to a non-conductive backing) to the surface of the material whose strain is to be determined. It is essential that intimate contact between the material and the gauge is assured. The gauge will then faithfully record the true surface strain. Surface preparation is probably the most vital factor effecting the adhesion of the gauge to the surface, and special cleaning technique must be adopted.

Assuming that the gauge is correctly bonded to the surface, any strain in the material is then transmitted directly to the gauges, which therefore increases or decreases in length and cross-sectional area. These changes in dimension are accompanied by a change of resistance which can be related directly to strain by multiplying by a constant known as gauge factor. This is provided by the manufacturer and for most conventional gauges is of order of 2 to 2.2. In most strain gauge measurement instruments or bridges this step is done automatically and the strain is read directly from a dial. Strain gauges thus represent a relatively simple method of obtaining a surface strain values.

There are a number of specially developed gauges. These are self-adhesive, high sensivity semi-conductor, fatigue gauges and etc. [108,109,110,111,112,113,114].

There are hundreds of strain gauge types available, it is therefore

important that the potential strain gauge users be aware of the various factors which might influence their decision on the choice of a gauge for his particular application.

The advantages of strain gauges as an experimental stress analysis technique can be summarised as follows:

relatively simple and quick.
direct reading.
many different type of gauges to suit particularly every condition.
used particularly in any environment.
no component size limitation.
good accuracy.
repeatable technique.
applicable to static, dynamic and transient.
used in actual service condition.
reduced weight and size compared with convensional mechanical transducers.
temperature effect mostly eliminated.
remote reading possible.
sensitivity can be improved using various wire.
finally, excellent repeatability.

The Bauschinger effect - the change in the stress-strain curve of a metal following plastic deformation in the appropriate direction - is of interest in connection with residual stress determination using the strain gauge technique.

The determination of residual stresses in the surface of 19 mm mining chain using the strain gauge technique is discussed with reference to Bauschinger effect in the next section. Apart from the standard 19 mm mining chain link, elliptical and eight shape links were formed, Section 5.3, and will be considered in the stress measurement process with the 22 mm oval cross-sectional mining chain. The heat treatment and surface preparation for the strain gauge work, on the chain links and test specimens to determine material stress-strain curve are presented is Section 5.4. The strain gauge selection and mounting processes are given in the following sections. Finally, the experimental procedure and results with calculation of the total and

residual stresses are given in Sections 5.6 and 5.7 respectively.

5.2 PRINCIPLE OF RESIDUAL STRESS DETERMINATION AND BAUSCHINGER EFFECT

Let us assume that the strain is followed at a particular position on a chain link, where the strain is uniaxial. When the chain material is loaded over its yield point (B), on BC in the stress-strain diagram, Fig. 5.1, on unloading, various possibilities arise. Thus the material behaviour may be such that:

a) residual tensile stress is achieved, point D.

b) residual compressive stress is achieved, point F.

c) no residual stress is achieved, point E. If, by any means the strains at points C and D or E or F could be measured, the corresponding residual stress could be determined. Strain gauges were here used for this purpose.

If the material at the unloaded condition (E), is loaded in compression, it yields at σ_y, and follows EFG rather than EF'G' in tension ($\sigma_{y'} < \sigma_y$). This phenomenon was first reported by Bauschinger in 1881 and carries his name, i.e. Bauschinger effect [115,116,117]. One way of describing the amount of Bauschinger effect is by the Bauschinger strain (β). This is the difference in strain between tension and compression curves at a given stress. As shown in in Fig. 5.1 permanent softening may be measured when parallelism is attained between forward and reverse flow curves, and is function of forward strain (ε_c) [118]. The Bauschinger effect was not considered in the finite element determination of the residual stresses, hence the stress values ($\sigma_{F'}$) will be higher than the measured values (σ_F). Bauschinger charts can be evaluated and plotted from a limited number of tests using a computerised method for

the determination of the intensity of the Bauschinger effect of the metallic materials [119].

5.3 FORMING OF EIGHT SHAPE AND ELLIPTICAL CHAIN LINKS

The dimensions of the eight shape and elliptical chain links were worked out for $\theta = \pm 24^{o}$ (Fig. 5.2 a) with the same pitch and nominal diameter as the standard 19 mm mining chain link. To achieve the required geometries the standard link had to be either pinched or pushed out by 7.4 mm (3.7 mm each side) at the barrel centre. The as-received standard links were first had to be annealed at 600° C to ease the forming of the links. Fig. 5.3 (a,b,c and d) illustrates the forming processes used for eight shape and elliptical chain links.The rollers, pins and the punch had to be hardened after machining to prevent bedding in. In both cases a 60 tonne press was used applying about 5 and 25 tonnes of load to form the elliptical and eight shape links respectively. The finished links are given in Fig. 5.2 b with the 22 mm oval cross-sectional mining chain link shown at the bottom.

5.4 HEAT TREATMENT OF CHAIN LINKS AND PREPARATION OF MATERIAL TEST SPECIMENS

Three kinds of heat treatment were carried out on the chain links to correspond to the x-ray work (air cooled/water quenched after tempering) and the finite element work on the as-received condition:

a) Hardened at 970° C in a salt bath to avoid surface decarburization for 15 minutes and water quenched; tempered at 600° C (in the x-ray work to sharpen the peaks) in salt bath for one hour and water quenched (material 1).

b) As in (a) except air cooled after tempering (material 2).

c) As in (a) except the tempering temperature and time were 475° C and 4.5 hours (air cooled) respectively (manufacturer's heat treatment), (material 3).

The surfaces of the different links were polished prior to the marking off the strain gauges positions accurately using the divider head with appropriate packing plates machined for this purpose, Fig. 5.4.

Tensile test specimens, Fig 5.5, were machined from the legs of the chain link to obtain the stress-strain curves of the material corresponding to the above heat treatment conditions. The threaded ends were used in tensile and squared parallel ends in compression conditions. The specimens diameter for material 1 was 7.31 mm and material 2 and 3 was 7.92 mm.

5.5 STRAIN GAUGE SELECTION AND MOUNTING

A brief account of steps in selection of strain gauges out of a very large number of gauges will be given in this section with some cautions on the mounting procedure.

5.5.1 STRAIN GAUGE SELECTION

The initial step in preparing for any strain gauge installation is the selection of the appropriate gauges for the task. Careful, rational selection of gauge characteristics and parameters can be very important; optimizing the gauge performance for specified environmental and operating conditions, obtaining accurate and reliable strain measurements, contributing to the case of

installation.

The installation and operating characteristics of a strain gauge are affected by the following parameters, which are selectable in varying degree [109]:

strain-sensitive alloy
backing material
gauge length
gauge pattern
self-temperature compensation
grid resistance

There are some operating constraints which are generally expressed in the form of requirements such as :

accuracy
test duration
stability
cyclic endurance
maximum elongation
simplicity and ease of installation

Since the gauge was required to remain on the link as the link was plastically deformed, a "post-yield" gauge was selected. A "YF" post-yield gauge, consists of Cu - Ni foil with plastic backing, operating temperature - 20° to + 70° C with 10 - 20 % strain , supplied by TML [109], was chosen. The YF gauge has a gauge length of 2 mm , with 1.8 mm gauge width (the smallest available) and 7.4 X 4 mm base. Since the strain gauges tend to average the strain over the area covered by the grid and the average of any non-uniform strain distribution is always less than the maximum, a strain gauge which is noticeably larger than the maximum strain region will indicate a strain magnitude which is too low, hence 2 mm gauge was chosen to avoid or at least minimize this effect. Single grid strain gauges are sufficient for the measurement, because only the stresses in the longitudinal direction of the chain link were to be measured. There was no option to choose a gauge with 120 Ω (± .3) rather than higher resistance in reducing heat generation rate and decreasing lead

wire effect. The gauge factor is 2.11 for the YF strain gauges which are supplied in packs of 10. The CN strain gauge adhesive recommended by the TML for YF type gauges was chosen. The adhesive has the same operating temperature as the YF gauges.

5.5.2 STRAIN GAUGE MOUNTING

TML connecting terminals were chosen to provide convenient junction points to connect gauges to instrumentation leads. They are made up of .033 mm thick copper foil and an insulation laminated with glass-epoxy approximately .15 mm thick with operating temperature up to 180° C.

The following steps were taken in mounting the strain gauges:

a)

Surface preparation of specimens - an area of approximately 2 - 4 times of base length in diameter was ground using an abrasive paper, so as to remove irregularity, rust and coating. Centre line to the gauge position was marked off without the line crossing the area on which the sensing element is directly placed. Some solvent such as methanol was used to clean the surface.

b)

Bonding to metal - a small drop of CN adhesive was used on the reverse side of the strain gauge and the gauge was plastered on the prepared surface of the specimen. The plastered gauge was set at its proper position and then instantly covered with a polyethylene sheet and was vertically pressed with thumb fairly hard for over a minute and it was then possible to take measurements after 15 minutes. When the adhesive set, the polyethylene sheet was peeled off clearly. Similarly, the connecting terminals were bonded at convenient

positions.

c)

Coating and soldering - the gauges and lead wires were soldered to the terminals. The lead wires were then anchored to the specimens and links, to avoid damages occuring from pulling before and during the test, and can be seen in Fig. 5.6 and 5.7 (a and b). Also, the gauges were coated with silicon rubber for protection. The equipment used in mounting the strain gauges are shown in Fig. 5.8. Finally, the whole installation was checked for damage and malfunctioning.

5.6 EXPERIMENTAL PROCEDURE

Material test specimens and chain links were tested on different testing machines and the procedure for each case is given separately below:

a)

Material test specimens - these specimens were tested using a 100 kN Instron testing machine, Fig 5.7 (a and b) and the strain gauge data logger with its peripherals shown in Fig. 5.9. The strain gauges were first soldered into the connection box before setting up the data logger and energizing the strain gauges (1 volt). To obtain the material stress-strain curve, the specimens were loaded up to the required strain in tension before unloading takes place, scanning at various load levels, Fig. 5.7a. The specimens were then loaded in compression and unloaded to zero just before buckling (two strain gauges start to disagree by large amount) using the compression bed, Fig. 5.7 b. A typical load- extension curve of a specimen depicting the loading-unloading cycle in tension and compression is given in Fig. 5.10 (extension here measured by cross-head displacement).

b)

The chain links corresponding to the x-ray works were calibrated using the 40 tonnes Amsler testing machine with two partially surface ground chain link holders, Fig. 5.11, whereas , the second set of chain links (different geometries) were calibrated using a Losenhausen testing machine with 22 mm diameter holders. After soldering the lead wires to the connection box and energizing the strain gauges, the links were loaded and unloaded (up to 100 KN) a few times in steps of 20 kN to check the response of the strain gauges. Each link was loaded up to the required calibration load in steps of 20 kN, scanning at each step before unloading in similar manner. The scanning outputs were printed for all 12 strain gauges, numbered as in Fig. 5.12, from which the loaded and unloaded strains corresponding to the calibration load could be read.

5.7 RESULTS AND CALCULATION OF RESIDUAL STRESSES

The material test specimen results are given in this section with results and calculation of residual stresses obtained by the x-ray and the finite element method.

5.7.1 STRESS-STRAIN CURVE OF CHAIN MATERIAL

The stress-strain curves of all three different chain materials are plotted from the material test specimen results, Fig. 5.13, 5.14, and 5.15. The material properties of these materials can be read and were determined from these curves:

	σ_y(MPa)	ε_y(με)	Hardening parameter,H′
1)	890	4260	963
2)	890	4250	646
3)	1000	4780	531

Young modulus was found to be 209 GPa. The work hardening parameter is defined as the slope of plastic part of the material stress-strain curve.

A four link 19 mm mining chain of material 2 was pulled using the Amsler testing machine. The ultimate failure load was 348 kN (364 kN for single link), hence nominal stress is 614 MPa. The overall extension was 14.6 % (gauge length was 336 mm and elongation of 49 mm), and the test speed was 3.77 mm/min. (test period was 13 minutes).

5.7.2 RESULTS AND RESIDUAL STRESS CALCULATION RELATING TO THE X-RAY WORK

The strain readings from gauges in equivalent positions were found to be very similar, but the readings from non-equivalent positions were markedly different, Fig. 5.16 to Fig. 5.21 (gauge positions shown in Fig. 5.12). The gauges at 60° to the crown in most of the cases showed an unexpected increase in the strain while the link was unloaded, Fig 5.17. This kind of behaviour was reproduced at these positions using the finite element method, Chapter 8.

The extreme strains - when fully loaded at the calibration load and those in the unloaded condition, are tabulated from figures similar to Fig. 5.16, Table 5.1 and 5.2 for the links made up of material 1 and 2 respectively (two links of each). The residual stresses were then evaluated as described in Section 5.2, Table 5.3 and 5.4. The total stresses were also determined at the calibration levels, Tables 5.5 and 5.6. The average total and residual stresses for each case

(material 1 and 2) at various calibration levels are plotted, Fig. 5.22 and 5.23 at the outside surface of the 19 mm mining chain. It can be seen from the Fig. 5.22 that the links yielded at the crown and barrel at all calibration levels. An increase in the calibration load levels did not have any significant effect on the total stress levels at the yielded regions (crown and centre) neither did the material type as such, Fig. 5.22 and Table 5.7. The residual stresses, on the whole, are compressive at the outside and inside surface, and increase in calibration load increases the magnitude of the residual stresses in both cases, not so much at the inside as the outside, Fig. 5.23 and Table 5.7. The results obtained for material 2 calibrated at 350 kN are not reliable because of the fact that the calibration load was not achieved properly (being very close to the failure and unable to control).

Residual stresses obtained from the x-ray work (Chapter 4) for both the 19 mm mining and 7 mm lifting chains are given in Fig. 5.24 with the corresponding strain gauge work. The patterns of stresses are similar but big variation in magnitude exist at the centre of the 19 mm mining chain for material 1. On the other hand, the agreement between the two sets of stresses at the crown is good for both materials but not at the barrel, Fig. 5.25.

5.7.3 RESULTS AND RESIDUAL STRESS CALCULATIONS OF DIFFERENT LINK GEOMETRIES

Two samples of each geometry, standard, eight shape, elliptical and oval cross-sectional links with the installed gauges at appropriate positions were calibrated at three different load levels using the Losenhausen testing machine and the strains at the extreme load

(calibration load and unloaded) levels are tabulated, Tables 5.8 to 5.11. The residual stresses and total stresses for all the calibration loads were determined using the principle outlined in Section 5.2, Tables 5.12 to 5.19.

Total stresses in mining chains from the strain gauge work were compared to those determined by the finite element method (Chapter 8), under load before and after onset of plastic flow in the links, Fig. 5.26 and 5.27. The stresses are in good agreement indicating the validity of both methods.

The effect of link geometry on the total and residual stresses (average of two links) can be seen in Fig. 5.28 and 5.29 for the first calibration load, and effect of calibration load on the residual stresses for various link geometries are given in Fig. 5.30 to 5.33. The elliptical and oval cross-sectional links follow very similar pattern, (Fig. 5.32 and 5.33), the residual stresses becoming tensile at the outside transition, Fig. 5.29. The eight shape and straight side links behave similarly (Fig. 5.30 and 5.31),eight shape link starting with tensile at the centre,with a wider gap at the centre moving to the crown as the calibration load rises, resulting in larger stresses (in magnitude) for both links, Fig. 5.29. The residual stresses at the inside centre and transition are, on the whole compressive and increase (in magnitude) as the calibration load increase, Table 5.20. At the centre of the eight shape link (inside) there is very little residual stress whereas at the transition very high compressive residual stress exists, Fig. 5.31.

Once, the surface of the links has yielded, there is very little increase in the total stress, Tables 5.20 and Fig. 5.28, except for

the eight shape link, Table 5.17. Hence, as the calibration loads increase the yielding extends to the interior from the surfaces leaving the surface stresses unchanged. The total stresses for various link geometries are given in Fig. 5.28 at the first calibration load with no variation at the crown. It can be seen that the stress near the crown depends little on link shape.

On the whole, increase in calibration load increases the total and residual stresses significantly in all geometries at the outside surface and inside transition and centre regions.

CHAPTER 6

FINITE ELEMENT BEAM ANALYSIS OF CHAINS (1–D)

6.1 INTRODUCTION

Under fatigue conditions, the varying stress caused by the external loading is added to any existing residual stresses: the position and magnitude of the resulting stress is important in determining the fatigue life.There are various ways of calculating these stresses numerically,such as: finite element beam analysis,two and three dimensional stress analyses. The finite element beam analysis of chains is extremely cost-effective in evaluating a multitude of different link geometric configurations. The more costly two dimensional contact and three dimensional solid stress analysis will be the theme of the following chapters.

The selection of beam elements suitable for large rotations,small strain applications is of considerable interest, and many possible formulations exist. In some problems,warping of the cross-section is important; this is specially true for some open sections. Sometimes distortion of cross-section in the plane must be considered;the classical example of this is the pipe bend. There have been attempts to provide a library of elements broad enough to satisfy most needs for beam type modelling.

In the ABAQUS library,beams in plane and beams in space are included. Since in chains only planar deformation occurs, due to geometry and loading,it is wise to use plane beam elements. Beams (Timoshenko beam element) that allow transverse shear are considered here. In these beams (element B22), additional approximation (to that of classical Euler-Bernoulli) is invoked in that the response to this shear is purely elastic: thus only axial, bending and torsional strains are considered in the nonlinear constitutive modelling. It is also

assumed that the cross-section does not deform in its section; the transverse shear is not considered to produce warping in the section: rather it is treated as a small relative rotation between the normal to the plane of the cross-section and the beam axis. The basic formulation of these elements is given in [39,120].

Work carried out by the SDRC describes the study of design modifications to a (9/16") 14 mm nominal diameter wheel chain link [43]. The effect of link geometry (shaved,oval cross-section, eight shape,standard) given in Fig. 1.3 and 5.2a, on the position of highest elastic stresses at the shoulder has been mainly investigated. An elastic beam element with point load at the crown was used and it was concluded that :

1. The standard link configuration is the optimum geometry to minimize the inner surface tensile streses at the shoulder.
2. The shaved design does not appear to offer a significant advantage over the standard design.
3. The eight shape design results in higher stresses at the shoulder and lower at the leg.
4. The oval cross-section design provides a desirable means to reduce the shoulder stress without dramatically increasing the stress levels at the leg.

The purpose of this phase of the analysis is to evaluate the merits of two possible design modifications of alloy steel mining chain and compare them with the standard design configuration for such links in the light of the SDRC work. The basis for this is the 19 mm nominal diameter link design with semi-circular ends and the straight legs (standard). The general conceptual geometry for the two modified links is illustrated and given in Chapter 5.

The following is a description of the modified link geometries analysed,Chapter 4.

1. The wire cross-section remains constant while the line of centroids curves inwards towards the centreline of the link,eight shape (pinched).
2. The wire cross-section remains constant while the line of centroids curves outwards from the centreline of the link, elliptical.

In this chapter, the loading assumption used in the beam analysis of chains will be discussed. Later, the 19 mm mining chain is analysed elastically and elasto-plastically to evaluate residual stress distributions at various calibration levels. The stresses will also be given through thickness of the chains at different sections. Finally, a similar analysis will be carried out for the 7 mm lifting chains.

6.2 LOADING ASSUMPTIONS

The loading of the chains can be modified in many different ways. A point load at the crown used by the SDRC is very crude and causes a convergence problem locally in the elasto-plastic analysis. Ideally, contact analysis in three dimension would give the appropriate contact area and pressure envelope at the crown. In the beam analysis a compromise was made by assuming an elliptical pressure envelope at the crown. The extent of pressure was limited to one element at the crown only and the ratio of the loads at the nodal points are calculated as below: The general parabolic distribution of loads can be solved for the particular solution [42]:

$q = a + bx + cx^2$

where q is the pressure at any point x ($0<x<1$).

$A = a + b/2 + c/3$

where A is the area under the curve which is the total load.

$Q_1 = a/6 - c/6$

$Q_2 = 2a/3 + b/3 + c/5$

$Q_3 = a/6 + b/6 + 3c/20$

where Q_1, Q_2 and Q_3 are the loads at positions $x = 0$, .5 and 1.

General Case	Special Case	
Area under the curve is unity	$a + b/2 + c/3 = 1$	(1)
At $x = 0$, $dq/dx = 0$	$dq/dx = b + 2cx = 0$	(2)
Finally, $q = 0$ at $x = 1$	$a + b + c = 0$	(3)

Equation (2) $b = 0$

Equation (1) $a + c/3 = 1$ (4)

Equation (3) $a + c = 0$ $a = -c$ (5)

Substitute (5) into (4) $-c + c/3 = 1$ $c = -3/2$ and $a = 3/2$

Therefore

$Q_1 = 11/40$

$Q_2 = 28/40$

$Q_3 = 1/40$

Check $\Sigma Q = 11/40 + 28/40 + 1/40 = 40/40 = 1$

The ratios of the loads area 11/40, 28/40 and 1/40 from the crown.

6.3 19 mm MINING CHAIN

Beam modelling of chains is the simplest and cheapest of all the modelling and has been attempted here to obtain an understanding of the total and residual stress distributions in different geometries of

chains. Only one quarter of the 19 mm mining chain was chosen by making use of geometrical and loading symmetry. The quadratic beam element (B22) uses Timoshenko beam theory and includes shear deformation [39,120]. The finite element mesh consists of 15 B22 elements (3 noded, quadratic interpolation) of approximately equal lengths in all the geometries, Fig. 6.1. The model is constrained at the crown in the x-direction, at the centre in the y-direction and rotation about the z-direction at both ends. The cross- section of the model is specified easily using the standard section in the ABAQUS library. The program assigns integration points on the section and integrates the section numerically to obtain generalised force-moment/ strain-curvature relations. This in conjunction with numerical integration along the beam length, allows complete generality in material response (plasticity) , since each point of each section is individually considered by the constitutive routines. The default integration for the beam in a plane (B22) is 5 points and up to 9 points are permitted.

Geometrical nonlinearity was also considered with residual force and moment tolerances of .1% and 1.% respectively.

6.3.1 ELASTIC ANALYSIS

The model described in the previous section was analysed elastically with Young's modulus, E=205 GPa. The whole loading was applied in one increment and the results are presented below:

The stresses (largest absolute principal stresses) were plotted at the inside, centre and outside for all the geometries,Fig. 6.2. The loading was the manufacturer's calibration load for this grade of

chains. The stresses have similar pattern for all geometries at the inside,centre and outside, except at the leg region, where the elliptical link has higher and eight shape link lower stresses than that of the standard link. The position of the largest tensile stress at the inside of chain link is different for all the geometries: in the case of elliptical link it is at the centre of the leg rather than the transition zone for the other geometries. The standard link seems to be at the middle of two extreme geometries (elliptical and eight shape). The stresses at the outer and inner fibres of all the geometries have opposite sign. There is no variation of stress at the centroid of the links due to geometry, but the stress reduces to zero at the crown from a tensile value at the centre. It passes through the intersection of internal and external stress curves.

The stresses at the crown (3 integration points) were discarded: the method of load application and the approximation of the method give unrealistically large stresses. This will also apply to all the other beam analysis results.

6.3.2 PLASTIC ANALYSIS

To determine residual stresses the elastic beam model was used with material nonlinearity included. The elasto-plastic material model considered has the following properties: yield stress, σ_y = 1000 MPa and hardening parameter (H')=531 MPa (experimental values obtained in Chapter 5). The load increments may be applied automatically (to find the failure load) or manually (to determine residual stresses).

6.3.2.1 TOTAL STRESSES

Stresses at the calibration levels, 260,320,and 380 kN were computed for all three geometries and plotted at the inside, centre and outside the links, Fig. 6.3,6.4 and 6.5. At the yielded regions, the increase in calibration load does not have significant effect on the stresses, whereas in the elastic zones, it results in reduction of stresses for the eight shape link (Fig. 6.4 and 6.5). At all the calibration loads and for all the geometries the barrel and crown have yielded both at the inside and outside, leaving the shoulder elastic except for the eight shape link which has the central region of barrel still elastic. The elastic analysis gave some insight into the stress distribution before the elasto-plastic analysis, which is not very different.

All the geometries were tested to failure using automatic incrementation , i.e. the model was loaded up to a point, where the solution did not converge (very small load increment produces very large unrealistic displacements), hence the failure was achieved. The failure loads were 380, 380 and 324 kN for the standard, eight shape and elliptical links respectively. The load carrying capacity of the models are lower than the tested values: 24%, 24% and 35% respectively.

Stresses may be computed through thickness of the beam models at 9 points, and are given in Fig. 6.6,6.7 and 6.8, for all geometries at calibration load, (cl)=320 kN, at important positions such as central barrel, 30 and 60 degrees to the crown. There are not appreciable differences in total stresses at the sections 30 and 60 degrees to the crown between different link geometries but at the centre the standard link stresses lie between the elliptical and eight shape link stresses.

The displacements at the centre of barrel and crown are given in Table 6.1 for all the geometries at various calibration loads. The elliptical link has moved in the most, whereas the eight shape link appears to be the stiffest. The deformed meshes at cl=320 kN are given for all the geometries, Fig. 6.9. The whole mesh seems to pivot about a point 45 degrees to the crown.

6.3.2.2 RESIDUAL STRESSES

The chain models with elasto-plastic material properties were loaded up in 30 equal increments for all calibration levels and unloaded in 10 equal increment to obtain the residual stresses. The residual stresses for all cases were plotted, Fig. 6.10,6.11 and 6.12. The stresses at the crown are invalid due to the load application there.

The residual stresses are compressive at the inside of the barrel except for the eight shape link and tensile at around the crown. Higher calibration loads results in higher compressive stresses at the barrel and lower tensile residual stresses at the crown and nearby, Fig. 6.11.

The residual stresses at the centroid of the chain links are tensile in all cases, nearing zero at the crown. The eight shape link starts with zero residual stress at the centroid in the barrel and rises to maximum at the transition zone, and finally drops to zero before rising again at the crown, Fig. 6.12. As the calibration load increases, the tensile residual stresses decrease at the barrel and some parts of the shoulder in the case of the standard and the elliptical links.

The residual stresses are compressive at the outside in all cases. The standard link seems to have larger residual stresses than the other geometries. Higher calibration loads result in higher residual stresses in all cases, Fig. 6.10.

The residual stresses through the thickness of the chain models are also given in Fig. 6.13,6.14 and 6.15 at various important sections, such as centre, 30 and 60 degrees to the crown. The stresses are virtually all the same at 60 degrees and close at 30 degrees to the crown but vary significantly at the centre, where the standard link stresses have a very similar pattern to that of the results obtained using the neutron diffraction technique (Chapter 4), Fig. 6.13.

6.4 7 mm LIFTING CHAIN

7 mm Lifting chain which was used in fatigue testing in the experimental work (Chapter 3) was analysed here using the finite element method. The same strategy as in the 19 mm mining chain was taken in the elastic and elasto-plastic analysis for total and residual stress calculations. The mesh of 15 three noded beam (B22) elements was used. The material model is the same except for the yield stress (=1148 MPa). The elastic stresses at the inside, centre and outside are given in Fig. 6.16. The stresses at the inside of the barrel are twice that of the outside and the stresses at the centroid are virtually half way between the two outer fibres. All the stress curves meet at an angle about 47 degrees to the crown, at the calibration load of 38.5 kN (the manufacturer's calibration load for this grade of chain). The stresses from the elasto-plastic analysis have a similar pattern to that of the elastic analysis except for the centroids, where the stresses have shifted up, Fig. 6.17. The

stresses again all meet at an angle about 38 degrees to the crown. Higher calibration loads cause the stresses to rise at all locations; it can be seen that the stress patterns are similar to that of the mining chains (standard link).

Residual stresses are also computed and presented in Fig. 6.18. They are compressive at the outside, inside and tensile at the centroid fading away at the crown. Higher calibration loads result in higher residual stresses, Fig. 6.18. Deformations of the model at various load levels are given in Fig. 6.19.

Total and residual stresses are given in Fig. 6.20 and 6.21 for sections at the centre, transition, 30 and 60 degrees to the crown. The residual stresses at the centre and transition are equal and. the pattern is the same as the results obtained from the neutron diffraction technique. The residual stresses at two other sections are also equal (Fig. 6.21).

CHAPTER 7

FINITE ELEMENT CONTACT ANALYSIS OF CHAINS (2–D)

7.1 INTRODUCTION

In the finite element stress analysis of chains, the modelling of the applied load has paramount importance in the evaluation of total and residual stresses. This requires a full scale investigation of the contact between two links when loaded. Stress analysis of bodies in contact is an important class of structural mechanics problem. The extent of the contacting surfaces may depend on the level of applied loads, and the contact may be frictional or smooth. Such stress analysis problems are nonlinear and therefore quite complex solution methods.

A contact problem occurs when at least two of the bodies not mechanically joined touch each other without becoming rigidly attached. They can touch either at a point, along a line, over a surface or over a combination of these elements, defining a contact region. The transmission of forces from one body to another is done through this region by normal compressive stresses and by tangential or shear stresses if friction exists. While the initial state of contact is determined by the geometric features of the bodies, the extent of the contact generally changes when the bodies are deformed by the applied loads or other source of stress.

Exact solutions of contact problems exist for simple, idealised problems , requiring sophisticated mathematical analysis [121,122]. Such solutions are not feasible for contact problems involving more complicated geometries, such as chains, although an attempt was made to solve the contact between links elastically in the next section.

Chan and Tuba [123] presented an incremental procedure for frictional

and frictionless contact problems. An over-relaxation procedure was used to solve the set of nonlinear equations. The equilibrium equations are formulated for each body separately in terms of the displacements and the contact forces. Another condition is imposed, that the points in the contact bodies cannot interpenetrate. The nodal displacements can then be solved for and an iterative process carried out within the step to allow several points to come in contact. The process is repeated with higher loads to obtain new contact points until the external load is reached.

Fredriksson and Urzua et al [124,125,126] presented an incremental formulation of contact problems of frictional and frictionless contact at the same time. The equilibrium equations are formulated in terms of unknown nodal displacement increments and the interface tractions are computed from the stresses at the end of each step. These tractions are applied to the next step by computing an equivalent nodal load vector. At each step, the appropriate constraints are applied for nodes in contact. Due to finite increments, iterations are necessary within the increment. This procedure is very similar to the standard approach for elasto-plastic problems. A similar algorithm was coded up in ABAQUS (interface and gap elements) with two and three dimensional contact problems with material and geometrical nonlinearities.

The primary objective of this chapter is to evaluate the contact pressure and contact area for 19 mm mining and 7 mm lifting chains, in two dimension with no friction considered, and to investigate how the method of load application affects the total and residual stress patterns. The contact pressure and contact area between links will be investigated analytically for elastic conditions, and numerically

using interface elements for plane stress and plane strain conditions. Secondly, this may be used to model the contact pressure in three dimensional stress analysis rather than a full and costly three dimensional contact stress analysis (Chapter 8).

7.2 PRESSURE BETWEEN TWO LINKS IN CONTACT

The contact between two elastic links may be derived from the more general case of contact between two elastic bodies given by Timoshenko and Goodier [121]. The principal radii of curvature of one of the bodies are R1 and R'1, and of the other body, R2 and R'2; ψ the angle between normal planes containing the curvatures 1/R1 and 1/R2, then the constants A and B are determined from the equations

$$A + B = 1/2 \left(1/R1 + 1/R'1 + 1/R2 + 1/R'2 \right) \qquad (1)$$

$$B - A = 1/2 \left[\left(1/R1 - 1/R'1 \right)^2 + \left(1/R2 - 1/R'2 \right)^2 + 2 \left(1/R1 - 1/R'1 \right) \left(1/R2 - 1/R'2 \right) \cos 2\psi \right]^{1/2} \qquad (2)$$

In the case of two chain links R1 = R2 = R and R'1 = R'2 = R' and $\psi = 90$; (1) and (2) become

$$A + B = 1/R + 1/R' \qquad (3)$$

$$B - A = 0 \quad A = B \qquad (4)$$

The contact pressure between the links is semi-elliptical with the major (2a), minor (2b) axis and maximum contact pressure (q_0); where a and b are calculated from:

$$a = m \left[3 \pi P \left(K1 + K2 \right) / 4 \left(A + B \right) \right]^{1/3} \qquad (5)$$

$$b = n \left[3 \pi P \left(K1 + K2 \right) / 4 \left(A + B \right) \right]^{1/3} \qquad (6)$$

in which m and n are numbers depending on the ratio (B-A)/(A+B);

$\cos \theta = \left(B - A \right) / \left(A + B \right)$

For two links $\cos\theta = 0 \Rightarrow \theta = 90$; from the table [121] m=n=1

also $K1 = K2 = \left(1 - \nu \right) / \pi E$: where ν, Poisson's ratio, E , Young's modulus. P is the applied load in the links.

The maximun contact pressure, $q_0 = 3*P/2\pi a\ b$ (7)

There are two cases to be considered in contact pressure evaluation:

a) Mining chain

R1 = R2 = 9.5 mm

R'1 = R'2 = -12.75 mm

Substituting (3) and (4)

A + B = .0268

A = B

Hence, A = B=.0134

For E = 209 GPa and ν = .3 ; K1 = K2 = 1.386 E-6 ;

(5) , (6) and (7) become

$a = b = .06246\ (P)^{1/3}$

(contact area is a circle with radius a)

$q_o = 122.38\ (P)^{1/3}$

Contact angle is the internal angle subtending the contact region.

i.e. 12.75 α = a

Contact angle (α) is $\alpha = 4.4938\ a$ (in degrees)

b) Lifting chain

R1 = R2 = 3.45 mm

R'1 = R'2 = - 5.55 mm

Similarly

A + B = .1097

A = B

A = B = .0548

$a = b = .03905\ (P)^{1/3}$

$q_o = 313.14\ (P)^{1/3}$

Contact angle (α) is 10.3236 a (in degrees)

The values of a, q_0 and α are given in Table 7.1 for both cases.

The maximum contact pressures are so great that there must be plastic

flow.

7.3 PLANE STRESS/STRAIN ANALYSIS

Often in stress analysis, a full three dimensional treatment of a problem can be avoided by assuming the structure to be adequately represented if plane stress or plane strain conditions adopted. Historically, plane solutions were the first attempted by the finite element method. The basic definitions and applicable expressions can be found in many standard text books on the theory of elasticity (e.g. [127,128]) and only a brief outline of the assumed conditions is included here. A fully three dimensional situation reduces to a two dimensional problem if all quantities are independent of one of the coordinate directions, usually assumed be the z-axis. Furthermore, for a planar condition to exist, all body forces and surface forces acting on the solid must act in the xy plane (i.e. have no z component).

a) PLANE STRAIN

If, in addition to the above assumption, the normal strain in the z direction, ε_z , is zero then a plane strain condition is said to exist. In this case the only non-zero stress components are the in-plane components σ_x, σ_y, τ_{xy} and the through-thickness stress σ_z. All the equations of elasticity are satisfied and this is an exact theory within the framework of three dimensional elasticity. Conditions of plane strain usually occurs if the thickness of the solid (in the z-direction) is large in comparision with the representative x and y dimensions.

b) PLANE STRESS

On the other hand, it is assumed that the normal stress in the z-direction , σ_z, is zero, a plane stress condition exists. In this case the in-plane stress component, σ_z, σ_y, τ_{xy} are again non-zero together with the normal strain component, ε_z. This is an approximate theory since the limitations placed on the variation of the ε_z strain over the xy plane cannot generally be satisfied and τ_{xz} and τ_{yz} are non-zero. However it is assumed that they can be neglected for analysis. The body is thin (i.e. it is small in comparision with the representative x and y dimensions). Also there are no surface forces acting on the end faces ($z = \pm t/2$).

7.4 INTERFACE ELEMENTS FOR STRESS ANALYSIS

These elements are available for modelling surface interface conditions, principally the gap/friction interface. The elements are provided with an interpolation or shape function that is compatible with the various elements in the program,so that an appropriate choice can be made to match the element chosen for the modelling on each side of interfaces.

Typical elements are shown in Fig. 7.1 a. First a load system is constructed for reporting shear and pressure stresses between the surfaces (if they are in contact), as well as the relative displacements of corresponding points. It is assumed that the nodes on the opposite faces of the interface elements are matched in position and that this local system does not rotate during the motion. The local directions normal and tangential to the interface can be

specified directly [38] or calculated by the program. If the latter option is chosen the local system is based on the average interface surface, found by taking the average of the coordinates of corresponding nodes on the surfaces of the bodies A and B (Fig. 7.1 b):

$$x = 1/2 \; (\; x_{NA} + x_{NB} \;)$$

The 'average interface surface' is then constructed using the element's interpolation function and these positions. The normal is defined as the normal to this average interface surface, pointing from surface A to surface B. If the average normal direction does not give the correct definition of the normal direction, it ought to be specified using *NORMAL (a module in the software to specify the normal direction) option.

The program calculates the initial clearance between the surface at each calculation point from the coordinates specified for the surface nodes forming the interface elements. Thus, if the clearance is small, these coordinates should be given to sufficient accuracy. The stress calculation points are always between the corresponding node pairs of the two surfaces. Then at each such point, the program determines if the two bodies are touching or not, based on the relative positions of corresponding points of the nodes of the two surfaces, projected on the normal direction. If the bodies are not touching, no forces are transmitted at this point. If they are touching, the appropriate surface theory is applied to model the force transmission.

The surface theory presently implemented in the program is a classical Coulomb friction law: the surfaces slide when the shear stress

between them tries to exceed the coefficient of friction times the normal stress. The coefficient of friction is assumed to be constant. For perfect sliding , coefficient of friction $\mu = 0$; the surfaces lock in shear as soon as they touch when μ is very large (e.g. 1.E10).

7.5 19 mm MINING CHAINS

Plane stress/strain analysis of chains in contact is the second most economical analysis after the beam analysis (Chapter 6). To carry out this analysis it was necessary to model only a quarter of the 19mm mininig chain because of geometrical and loading symmetries. The mesh, Fig. 7.2, consists of 90 eight-noded quadratic isoparametric plane stress/strain elements with 16 three noded one dimensional interface elements. The mesh is very fine in the region of contact to be able to detect very closely, the effect of contact on the contact area, pressure, and deformations. The refinement was carried out using the facility called Multipoint Constraint (MPC) in the software, ABAQUS [38,39]. This allows the analyst to go from one element to two in two and three-dimensions by constraining the appropriate nodes [129]. It is a very efficient way of mesh refinement and details can be found in the ABAQUS User's Manual. The mesh is constrained at the centre of the barrel is the y-direction and at the crown in the x-direction. A uniform pressure was applied to the face of elements lying at the centre of the internal link in the y-direction. The magnitude of this pressure is twice the nominal stress at the centre of the barrel due to differential areas. This application of load is more realistic than a point load at the centre of internal link [44,45,46].

Geometrical nonlinearity was also considered with convergence tolerance ranging from .5 % and 1.% and automatic incrementation.

7.5.1 TOTAL STRESSES

The model described earlier was analysed elasto-plastically with the same material model as in Chapter 6. Plane stress and plane strain analysis were carried out at various calibration loads and up to failure. Fig. 7.3 shows the various stress contours (plane stress case) for cl= a)260 kN, b) 320 kN, c) 380 kN and failure load of 497 kN. As the calibration load increases, the stresses at the outside barrel increase and it falls as soon as the link starts failing. This is also indicative of yielding taking place as the calibration load increases. The stresses around the contact region increase with increase in calibration load. To obtain a clear picture at the boundaries (inside and outside), the stresses (largest absolute principal stresses) are plotted, Fig. 7.4 and 7.5 for both plane stress and plane strain.

At the outside, the stresses at the barrel are compressive and range from 500 to 1500 MPa depending on the calibration level; whereas stresses at the crown are tensile and range from 1000 to 2000 MPa. Plane stress and plane strain analysis both give similar stress pattern with plane strain stresses rather high, Fig. 7.4. At the inside, the opposite is true, i.e. stresses at the barrel are tensile and crown are compressive. Similar patterns exist for both analyses with plane strain resulting in rather high stresses, Fig. 7.5. The stresses resemble the results from the beam analysis (Chapter 6) at the outside and inside.

The deformation at various calibration levels and failure load are given in Fig. 7.6 for plane stress case. With increase in load, the links get pulled in at the barrel and extended out at the crown. Consequently, the contact and penetration between the links increases. This will be investigated in the next section.

7.5.2 CONTACT PRESSURE AND AREA

Implementation of interface elements in two dimensional plane stress/strain analysis of chain resulted in the evaluation of contact between the chain links. The contact starts with a point at the crown and as the load builds up, the contact points increase to 2, 3, and so on. The extent of contact pressure and area for both elastic and elasto-plastic materials are considered below:

A) Elastic material

The contact pressures at the surface of contact along the outer link are give in Fig. 7.7 at various load levels for plane stress and strain conditions. The pattern for both cases is the same and is that of approximately quarter of an ellipse, which is expected theoretically for two links in contact, as established earlier (Section 7.2). Similar variation in contact angle and pressure exist between them with somewhat higher values in the case of theory. The theoretical result does not take into account any deformation of the link as a whole, whereas in fact the load tends to reduce the radius of curvature of the link, increasing the area of contact and reducing the pressure. Plane strain analysis results are rather higher than plane stress case at various calibration loads.

B) Elasto-plastic material

Fig. 7.8 illustrates the results for this case. The contact pressure remains constant just over yield stress, and shoots up just before falling to zero (plane stress). Similarly, the plane strain behaves the same with a constant pressure of higher magnitude. With an increase in calibration load, the plane strain analysis gives higher contact pressures and correspondingly smaller contact areas than the plane stress analysis (Fig. 7.9). The contact ceases to exist between the links at about 53.45 degrees at the outer link, as the inner link starts to wedge into the outer link. The extent of contact area varies of course with load, Fig. 7.9.

7.5.3 RESIDUAL STRESSES

The chain model was loaded up to calibration loads automatically and unloaded to give the residual stresses. This was achieved in 28, 44 and 40 increments as the calibration load built up. The Von Mises residual stress contours are given in Fig. 7.10. At the first calibration load there is about 200 MPa residual stresses at the barrel and crown with larger variation at higher calibration loads.

In the region of the crown, on the inside, the residual stresses predicted for plane stress conditions are tensile, whereas for plane strain conditions they are largely compressive (Fig. 7.11). The stresses in the barrel for the plane stress condition are higher for lower calibration loads with no significant change at the largest calibration load, Fig. 7.12.

There is a significant variation in the residual stress distribution

at the inside of chain link with higher tensile stresses at the crown (for plane stress) than that of in plane strain. The stresses at the barrel are all compressive with lower values for the plane strain condition, Fig. 7.11.

Overall, the residual stresses at the boundaries of the chain link are compressive with larger magnitude at the inside of the shoulder and at the outside of the barrel except at the contact zone (tensile). They also increase with an increase with calibration load and resemble the results from the beam analysis (Chapter 6).

7.6 7 mm LIFTING CHAIN

The mesh with element numbering is given in Fig. 7.13 for the 7 mm lifting chain with elasto-plastic material properties as in Chapter 6, (Section 6.4). Similar analysis as the mining chain (previous section) was carried out in plane stress condition only and the results are presented below:

The Von Mises stress contours are given in Fig. 7.14 at various calibration loads, and stresses (largest absolute principal stresses) at the inner and outer surface are given in Fig. 7.15 and 7.16, and deformation at Fig. 7.17. Before the chain fails at 64 kN, the stresses drop dramatically at the inside barrel and outside crown. Otherwise, the stresses behave as expected - with higher calibration loads resulting in higher stresses.

The plastic contact pressure remains steady with lower pressure at failure stages, Fig. 7.18. The elastic contact pressure variation is also included in Fig. 7.18 (Comparing with Table 7.1), highlighting

the effect of considering plasticity. The contact angle versus nominal pressure at the central barrel is given in Fig. 7.19, indicating an almost a linear relationship.

The residual stresses are given in contour form (Von Mises Stresses) and plots at inner and outer boundaries of the chains, Fig. 7.20, 7.21 and 7.22. No significant residual stresses are introduced by the first calibration load except at the region of inside barrel and crown. But as the calibration loads increase, the residual stress distribution changes dramatically (b and c). Similar behaviour appears at the boundaries with a drop for the third calibration load at the outside barrel. Again the stresses at the boundaries are compressive except at the inner contact region and are comparable to those obtained using the beam analysis (Chapter 6).

CHAPTER 8

FINITE ELEMENT STRESS ANALYSIS OF CHAINS (3–D)

8.1 INTRODUCTION

Soon after the emergence of the finite element method for analysis of linear elastic structural problems,it was further developed to be used for nonlinear problems. Initially, in the mid-sixties, these developments were concerned with the implementation of nonlinear constitutive equations in finite element codes which had been designed for linear elastic analysis [130], quoted in [131]. Therefore, geometric nonlinearity was also included in the finite element analysis methods, and again the starting point for such nonlinear analysis was linear elastic finite element analysis [131].

The researchers who carried out these analyses generally thought of their nonlinear problems as modified linear problems, which resulted in a solution method called the initial stress (strain) method, nowadays known as modified Newton-Raphson method. Another type of method which emerged was to see nonlinear problems as a series of linear problems, to be solved sequentially. This is the so-called the tangent modulus method, nowadays recognised as the full Newton-Raphson method. Various other nonlinear solution methods have since been developed and are discussed elsewhere [127,132,133,...].

There are problems in which the above types of nonlinearity are combined. A paper by J.C.Negtegal [131] discusses this topic well in detail. There are two classes of combined nonlinear problems. One type of problem is the geometric instability problem with material nonlinearity. In this problem, the main nonlinearity is of a geometric nature and is supplemented by nonlinear material behaviour. A typical example of such a problem is a spherical cap with ring load. The second type of problem is characterised by large scale material

nonlinearity, which has as a consequence that geometric nonlinearity must also be taken into account. Typical areas in which this situation arises are the analysis of metal forming problems and the analysis of chain links under loads, such as to cause plastic yielding: the latter is the subject of this research work. The finite element formulation, constitutive equations, element selection and solution procedure are all given in the ABAQUS theory manual [39] as well as in some standard text books [127,134].

The following preliminary general considerations apply to the finite element analysis of chains:

a) Load incrementation - one of the difficulties encountered in any nonlinear incremental-iterative solution scheme is the choice of load increment. An improper choice of load increment may result in an expensive iteration or convergence may never be achieved. Thus from economical point of view, the automatic incrementation option should be used when the solution is not known (in the case of chain analysis to failure), and manual incrementation when the solution is either known or can be predicted (in the case of calibration of chains).

b) Convergence criterion - at the end of each iteration, the solution is checked to see whether it has converged or diverged within pre-set tolerances. A convergence tolerance that is too loose results in an inaccurate solution and one that is too tight results in needless accuracy. Hence, in this study, a realistic convergence tolerance was taken in the range of 0.3 % to 1.0 % for load and moment tolerances.

c) Analysis termination criterion - there are two criteria to end an incremental-iterative scheme. Firstly, the failure of a structure

takes place when no further loading can be sustained. This is provided for in ABAQUS when the load increment becomes smaller than 0.001 percent of the applied load (as is the case in all failure load determination). Secondly, the failure of a structure makes the convergence difficult to satisfy in a specified number of iterations. This is implemented in ABAQUS and 20 iterations were used throughout this chapter.

In this chapter a complete three dimensional analysis of chains will be carried out with a realistic pressure distribution due to contact (considering the observations in Chapter 7) between chain links. First, the contact pressure assumption will be disscused in detail, (Section 8.2). Then, the mining chains (19 mm circular and 22 mm oval cross-section) will be analysed to examine the effect of changes in link geometry on the stress pattern under elastic and elasto-plastic conditions during calibration and loading to failure (Section 8.3). Finally, the lifting chain will be considered under similar loading conditions to those of mining chains (Section 8.4).

8.2 CONTACT PRESSURE ASSUMPTION

In the three-dimensional finite element analysis of chains, the modelling of loading is as important as geometrical modelling which will be discussed in the next section. From the theory of two elastic bodies in contact ([121], Chapter 7) the contact pressure envelope is ellipsoidal. In the case of plasticity, this will not be the case, as was shown in Chapter 7 for the two-dimensional contact. The ideal envelope can be found by application of three-dimensional contact analysis, which was not possible in the course of this research. But a compromise was made in assuming a contact pressure envelope by

taking into account the elastic contact envelope and the two-dimensional contact analysis results. The assumed contact envelope is shown in Fig. 8.1 for chains of oval and circular cross-section. In both cases, the assumed envelope (with a pressure of some 3000 and 1000 MPa) is applied at the surface of elements refined at the inside of the link crown, shown in Fig. 8.2, where the contact occurs.

With the above envelope, the sizes of the elements in the refined zone were changed (by altering the angles ϕ and ψ). ϕ and ψ are the subtended angles of contact at the crown in the z and y-directions respectively, Fig. 8.2. In each case an elastic finite element analysis was carried out to determine the reactions at the centre of the link (in the y-direction) for evaluation of applied load. The angle ϕ was then plotted against the applied load. The results of similar analyses for all ϕ, considered in this research, are given graphically in Fig. 8.3. The size of the elements can be adjusted from this graph to achieve any particular load (by choosing appropriate values of ϕ and ψ). Table 8.1 shows the corresponding values of ϕ and ψ for all the grades of chains at various load levels. It also shows the contact angle for 19 mm mining and 7 mm lifting chain from the two-dimensional contact analysis (Chapter 7); at low loads the values are comparable with those assumed in the three-dimensional analysis but are somewhat larger at higher loads. The relationship between ϕ and ψ is given by:

$$R_1\psi = R_2\phi$$

(R_1 is the inner radius of the link at the crown and R_2 is the radius of cross-section of the link).

8.3 MINING CHAINS

High-tensile steel chains are used in mining equipment to transport coal from the mine face to the surface, hence the name "mining chain". Their size varies from 14 to 26 mm diameter. In this research, 19 mm diameter and 22 mm oval cross-section (oval-link) mining chains were investigated. The configuration of both types of chains are given in Chapter 5 (Fig. 5.2 a). Geometries (eight-shape and elliptical) different from that of standard chains will be disscused in Section 8.3.1 and the oval-link chains will be considered in Section 8.3.2.

8.3.1 19 mm MINING CHAINS

A full three-dimensional stress analysis of chains was undertaken to understand the state of stressing under both calibration and service loading as well as to determine the residual stress distribution resulting from the calibration processes. The finite element formulation of the problem was omitted but can be found in the ABAQUS theory manual [39] as well as in the standard text books on the subject [127].

It was necessary to model only an eigth of the chain link because of geometrical and loading symmetries. A suite of programs in the Pascal programming language was developed to generate the mesh by choosing appropriate values of the parameters (Fig. 8.2 and Fig. 5.2 a).

R1 - internal radius at the crown,

R2 - radius of the chain link,

L - half the barrel length,

M1 - number of segments in the barrel,

M2 - number of segments in the shoulder (exclusive of 6 segments in the refined zone),

θ - angle of straightness (=0,+24 and -24 for the standard, eight shape and elliptical),

ϕ - angle of refined zone at the section through the crown,

ψ - angle of contact.

Solid elements with 20 or 27 nodes with reduced integration were chosen: these use a lower order integration to form the element stiffness. This can usually provide improved accuracy and significantly reduces running time in three-dimensional analysis. The multipoint constraint (*MPC) facility was used to refine the mesh in the region of contact between chain links, as proposed in Section 8.2. Application of multipoint constraint (MPC) for three-dimensional elements can be found in the ABAQUS manual [38,39,40]. The formulation of the multipoint constraint is also covered by Ang et al [129]. *MPC enables mesh refinement to be produced by permitting two smaller elements to be in contact with one larger element on one face of the latter.

The mesh is constrained at the centre of the barrel in the y-direction, at the crown in the x-direction and at the midplane in the z-direction. The required loading may be applied using the procedure established in Section 8.2 (i.e. by generating a mesh with appropriate parameters).

Geometrical nonlinearity was also considered in all the analyses with convergence tolerances of 0.3 % to 1.0 % with either automatic or manual incrementation, depending on which was suitable. The same material model as in Chapter 7 was used with calibration loads of 260 kN, 320 kN and 380 kN.

8.3.1.1 MESH REFINEMENT

In finite element stress analysis, the solution depends on the mesh size, i.e., the finer the mesh the better the results are up to a point. But finer meshes result in longer running times, hence a compromise needs to be made. In this section, the effect of mesh refinement on the total and residual stresses was investigated with the intention of arriving at an optimum number of elements to achieve the best solution.

Two parameters (M1 and M2), the number of slices in the barrel and in the shoulder respectively, Fig. 8.2, were chosen as follows:

a) M1 = 1 and M2 = 1

b) M1 = 3 and M2 = 2

c) M1 = 6 and M2 = 4

Loading of 320 kN (its equivalent pressure) was applied in all three cases with the boundary conditions and material properties given in Section 8.3.1. The residual stresses were found by taking the model through a loading-unloading cycle. The total and residual stresses at the inside and outside of the model are plotted in Fig. 8.4 and 8.5 for all the mesh sizes. It can be seen that the residual stresses in case (a) are very different from those in cases (b) and (c), which are virtually the same. The total stresses also behave in a similar manner. Since the refined zone was kept unchanged, the total and residual stresses were the same in that region in all cases considered. Hence, case (b) is the optimum case giving a shorter run time than case (c) and results that are in agreement with the more precise results to be expected from the more refined mesh (c).

8.3.1.2 ELASTIC STRESSES

Elastic stress analysis was carried out for all geometries (standard, eight shape and elliptical) whose meshes are given in Fig. 8.6 (a,b and c). The elastic stresses are given in Fig. 8.7 for the outside and inside the links. The stress distribution is similar to that in which a point load was applied at the crown [45,46]. Overall, the eight shape link has the lowest stresses except at the inside transition (largest); the elliptical link has the largest stresses with the exception of inside transition; the standard link seems to have stresses intermediate between those of the other two geometries.

8.3.1.3 TOTAL STRESSES

The finite element elasto-plastic analysis of all the geometries was carried out for all the calibration levels and also to failure. The total stresses are plotted at the inside and outside for all the geometries and for all the load levels, Fig. 8.8 to 8.15.

The total stresses at the inside of the links are tensile in the barrel and some part of the shoulder, and increase with increasing calibration load, Fig. 8.15. The stresses at the inside crown are compressive with large magnitude resulting from the local pressure loading. The overall stress pattern is the same as the elastic stress pattern.

The total stresses at the outside of the links are compressive in the barrel and some part of the shoulder and tensile at the crown of the link, Fig. 8.14. As the calibration load increases, more yielding of the link takes place, and when the fracture load is reached, extensive yielding has taken place.

In agreement with experimental results, the numerical analysis indicates that the links with different geometries will fail at different loads (Table 8.2). The failure load of the elliptical link is very closely predicted by the finite element method, whereas the failure loads of the standard and eight shape links are underestimated by 6 % and 8 % respectively.

The mesh for the elliptical link under failure load was generated with a modified version of the mesh generating programe for the standard and eight shape links.

8.3.1.4 RESIDUAL STRESSES

The residual stresses were found by taking the models through a loading-unloading cycle. The loading was achieved by 15 equal increments ,and the unloading by 5. The inside and outside residual stress distributions are presented below:

The residual stresses at the inside are given in Fig. 8.16 to 8.19. They are compressive along the barrel except for the eight shape link which exhibits some tensile stress at the beginning of the barrel. The stresses at the refined area and nearby are tensile. The stress patterns appear to be the reverse of the total stresses (Section 8.3.1.3) Fig. 8.19.

The residual stresses at the outside are given in Fig. 8.20 to 8.23. They all are compressive with varying degree of magnitude and there is no variation in the stresses at the crown due to different geometries, Fig. 8.23. The residual stresses ,in general, increase as the calibration load increases, but some variation exists in some cases.

The total and residual stresses at the crown do not vary as a result of geometrical changes except at the inside zone (due to the application of pressure at this zone), Fig. 8.24. The variation due to geometry can be seen in Fig. 8.25 for the centre of the link. Residual stresses for the standard link geometry at the centre are in good agreement with the results obtained from the neutron diffraction work (Chapter 4), with appropriate material models and the pattern is the same as in Fig. 8.25. The stresses at the sections through the centre of the barrel and crown both correspond to the calibration load of 320 kN.

8.3.1.5 BEHAVIOUR OF STRAIN GAUGES NO. 3 AND 10

In the strain gauge work discussed in Chapter 5, it was found that the strain gauges numbered 3 and 10 ,positioned at 60 degrees to the crown, behaved very oddly. That is to say when the links were being unloaded, the strains at these gauges increased (in some cases) rather than decreasing as expected. This phenomenon was investigated using the finite element analysis of the all three geometries. The results of the analysis are plotted either for the same position as gauges 3 and 10 or positions on either side of the gauges. In Fig. 8.26, the strains in the y-direction are plotted for a loading-unloading cycle. Similar variations in strain are also observed in the x and z-directions. The anomaly occurred in three cases :

a) For the elliptical shape link
b) For the standard link if the gauge is slightly closer to the crown than its designed position.
c) For the eight-shape link if the gauge is slightly closer to the crown than its designed position.

A slight discrepancy in the gauge position is entirely possible, since the installation of the gauges exactly on the marked position is very difficult and also the marking of the position involves inaccuracies because of uneveness in the link caused in the manufacturing process. It may thus be concluded that the numerical analysis has reproduced, at least qualitatively the anomaly observed experimentally. The same conclusion may also be arrived at by considering the largest absolute principal stresses plot verses loading, Fig. 8.27.

8.3.2 22 mm MINING CHAINS (OVAL-LINK AND EQUIVALENT CIRCULAR CROSS-SECTION LINK)

The heavy-duty oval-link chain was designed to allow a stronger chain to be used in a panline of specified size (Fig. 2.3). For example, the 22 mm pan line originally designed to accommodate either 22 mm twin outboard or 26 mm twin inboard chain assemblies of the conventional type, will, with the development of the oval-link mining chain, now be capable of utilising 26 mm twin outboard and 30 mm twin inboard assemblies, creating obvious savings in pan line costs, weights and heights [135].

The oval-link and its equivalent circular cross-section link with the same inner radius at the crown and the same barrel length and cross-sectional area were analysed using the finite element method and the results are presented in the following sections. The mesh for the oval-link was generated using another Pascal program (Fig. 8.28), while the equivalent link was generated with the original program.

8.3.2.1 ELASTIC STRESSES

The mesh of Fig. 8.28 was loaded in two ways using either:

a) a point load at the crown

b) the contact pressure envelope established earlier (Section 8.2)

The elastic stresses corresponding to the first calibration load (393 kN) are given in Fig. 8.29 for the inside and outside the link. The stresses at the top layer and bottom layer (Fig. 8.28) of the oval-link are identical in both cases: hence, only the top layer stresses are given except in the region of contact, where the top layer experiences higher stresses under the immediate prescribed loading pressure. Higher stresses are experienced when the point load is applied, Fig. 8.30 and 8.31; stresses are ignored at the region of application of the load. Since the modelling is here unrealistic. Furthermore, the stresses of the equivalent link are higher than those of the oval-link when either a point load or a contact pressure. envelope was applied, Fig.29.

8.3.2.2 TOTAL STRESSES

The stresses at the inside and outside are shown in Fig. 8.32 given by a complete finite element analysis of the oval-link for two calibration loads, 393 kN and 489 kN,and for the failure load. The stresses generally increase with the increase in the applied load for both the inside and outside the link.

Similar results occurred in the case of equivalent link, Fig. 8.33. The total stresses for the equivalent link are given in Fig. 8.34. The link behaviour under calibration load of 489 kN is shown in Fig. 8.34 for elastic and elasto-plastic analysis. The barrel and outer crown yielded completely, whereas in the elastic state, the inside-barrel stresses are well below yield stress (Section 8.3.2.1).

The total stresses are given in Fig. 8.35 and 8.36 under the first calibration load and the failure load. The oval-link underwent smaller stresses than its equivalent under the first calibration load, Fig. 8.35, while at failure, the stresses in the oval-link are larger at the outside barrel and lower at the crown than those of the equivalent link, Fig. 8.36. The failure load of the oval-link was predicted to be 546 kN, 3.4 % lower than that of the equivalent link. The actual failure load of the oval-link was 606 kN, the numerically predicted figure being 10 % less.

8.3.2.3 RESIDUAL STRESSES

The residual stresses were found by taking the models through a loading-unloading cycle. They are plotted for the inside and outside of the links, Fig. 8.37 and Fig. 8.38 . With an increase in calibration load, the residual stresses also increase in the case of both links. This is very significant in the oval-link. The stress pattern remains the same for both links, although they have different cross-sections. For both links , the peak stresses are positioned just after the transition zone at the inside and are roughly equal to the largest stresses at the outside the link. Such higher compressive residual stresses at the transition zone are very desirable.

Fig. 8.39 illustrates the residual stresses caused by the calibration load of 393 kN for the two links. The equivalent circular cross-sectional link has larger stresses than those of the oval-link at the inside whereas the oval-link has larger stresses along the outside of the barrel.

The stresses in the refined zone and nearby are invalid because of

application of pressure and ought to be ignored.

The total and residual stresses are given through a section at the centre and crown for the two links under a calibration load of 489 kN, Fig. 8.40 and Fig 8.41. There is no difference between the two at the centre, but some difference at the crown, where the pressure was applied - at the start and end curve (invalid results because of load application).

8.4 7 mm LIFTING CHAIN

Three-dimensional stress analysis of 7 mm lifting chain was carried out with the material properties given in Chapter 7 and with the same boundary conditions as for the mining chains. A mesh with 3 and 2 slices at the barrel and shoulder of the link was considered with a refined zone for contact pressure implementation. First an elastic analysis was carried out with stresses shown in Fig. 8.42 at the inside an outside the barrel. The model was then loaded up to calibration loads elasto-plastically to compute the total stresses. It was also loaded up to failure load (64 kN) and the stresses are given in Fig. 8.43. Finally the unloading was completed to give the residual stresses, Fig. 8.44.

Total stresses increased with increase in calibration load. Similarly, the residual stresses increased, except for the third calibration load, in which case, the stresses do not appear to have changed significantly at the outside the barrel with increasing calibration load, Fig. 8.44.

Fig. 8.45 to 8.47 give the stresses through section at the centre,

transition and crown to help in interpreting the effect of calibration load on fatigue failure. The total and residual stresses have the same pattern at the transition and centre sections, differing at the crown. The effect of increase in calibration load is very significant at all three sections.

8.5 OTHER ASPECTS OF LINK GEOMETRY

So far during this research only cross-sectional and overall link geometries such as inward or outwardness of the links have been considered. Other aspects of the link geometry such as increase in barrel length (pitch) and internal radius at the crown have not been been investigated. In this section a thorough understanding of the above mentioned parameters will be attempted for the 19 mm standard mining chain.

8.5.1 INTERNAL RADIUS AT THE CROWN

Barrel length of the standard 19 mm mining chain was kept constant at 17 mm and only the internal radius at the crown was allowed to change (9.5, 12.7 and 16 mm). The model was loaded with the pressure distribution established earlier (Section 8.2). A complete elastic and elasto-plastic analysis of the link was carried out for all three cases and the stresses at the boundaries (outside and inside) were plotted, Fig. 8.48 and 8.49. The stresses were raised by the increase of internal radius as expected, but considerable rise was not achieved in the elasto-plastic analysis except at the tensile peak position at the inside of the link. Most importantly, the peak tensile stress position was moved towards the crown with the increase in internal radius. Residual stresses were also obtained by taking

the models through the loading-unloading cycle and are given in Fig. 8.50 and 8.51 at the outside and inside of the links for calibration load of 320 kN. The residual stresses decreased with increase in internal radius. The internal radius of 9.5 mm is the optimum radius as far as the total and residual stresses are concerned, but it is not practical because of the interlink configurations. Hence the second best radius (R1=12.7), given in the British Standards Specifications for this grade of chain is a satisfactory practical choice.

8.5.2 BARREL LENGTH (PITCH)

Three different barrel lengths were chosen for a fixed internal radius at the crown (12.7 mm): L= 10, 17 and 27 mm. From the elastic and elasto-plastic analysis of all three cases the stresses were plotted, Fig. 8.52 and 8.53. With increase in barrel length the total stresses were decreased in the elastic analysis and was unchanged in the elasto-plastic analysis. However the effect on the residual stresses are significant, Fig. 8.54 and 8.55. The barrel length of L=17 mm (given in the British Standards Specifications) is optimum as far as the total and residual stresses are concerned.

On the whole, the British Standards Specification for the 19 mm mining chains has the optimum dimensions as far as the total and residual stresses are concerned for given link diameter.

CHAPTER 9

GENERAL DISCUSSIONS

9.1 INTRODUCTION

In this work various experimental stress measurement techniques such as: x-ray, neutron diffraction and strain gauge methods were used to determine stresses in the 7 mm lifting chains, 19 mm mining chains and 22 mm oval-link mining chains. In addition to the experimental work, FE was also used to compute the corresponding stresses which were either total (under calibration loads) or residual (as a result of calibration). Lastly, an extensive amount of fatigue testing of 7 mm lifting chain was carried out with some related direct stress tests on chain material specimens to show the effect of mean stress on fatigue properties of the chain material. Some of the above results were discussed under relevant headings and only the important overall features will be included in this section with special emphasis on the potential benefits of differential heat treatment of chains.

9.2 7 mm LIFTING CHAIN

FE stress analysis of the 7 mm lifting chains gave the stresses under the calibration loads and the residual stresses as an end result of these loads. These stresses were obtained from various models, ranging from a simple beam analysis (1-D) through contact analysis (2-D) to three-dimentional (3-D) stress analysis. The stresses from all three different analyses confirmed the existence of residual stresses as a result of calibration, the predicted magnitudes of the residual stresses being similar. Discrepancies are, of coures, expected because of the different theoretical modelling of the link and its loading, but overall the results are consistent.

The x-ray measurements of the residual stresses also confirmed the

existence of the residual stresses, largely as expected from the FE work, as well as the effect of increased calibration loads on their magnitude. The stresses at the outer surface of the 7 mm lifting chain were all compressive with larger magnitudes in the middle region of the side and at the crown of the links.

The effect of residual stresses on the fatigue properties of this grade of chain was demonstrated by fatigue testing results (Chapter 3). Fatigue lives of the links were improved dramatically by calibration: up to tenfold depending on the degree of calibration. A calibration load of 20 kN (25 % over working load limit) did not have any significant effect on the fatigue lives since it was insufficient to cause plastic deformation. The effects were very much more apparent with calibration loads of 30, 38.5 and 50 kN. The upper bound for the calibration load for conformity with existing standards is 56 kN, which was calculated using the concept of energy absorption factor (Appendix A); in other words, the 50 kN calibration load chosen in the testing is permissible. Similar improvements were achieved in the testing of the chain material, in which the presence of residual stresses was simulated by a variation in mean stress. The results may be represented by reference to the concept of the Goodman diagram. The fact that the calibration of chains introduces residual compressive stresses at their surface produces a reduction in mean stress, which results in higher fatigue lives, in accordance with the Goodman diagram (and the experimental fatigue specimen results).

9.3 19 mm MINING CHAIN

A complete FE stress analysis was carried out on the 19 mm mining chain of different shapes (standard, eight shape and elliptical) and

22 mm oval-link mining chains. Experimental stress measurements on these links were carried out using x-ray, neutron diffraction and strain gauge techniques to establish confidence in the FE results.

The link, slowly cooled after tempering, did not appear to exhibit surface residual stresses. Water quenching after tempering gave rise, as expected, to surface residual compressive stresses. However, calibration (required to raise the load to which the chain behaves elastically) caused modification of these stresses so that the effect of water quenching was effectively lost.

The neutron diffraction technique also confirmed the existence of residual stresses within the the link, with compressive stresses in the outer layer and tensile in the central region. Satisfactory quantitative agreement with the FE work was obtained. Strain gauge work also confirmed the residual stress pattern obtained by the other methods and was in good agreement with the FE calculations during loading, both under initial elastic conditions and also after yielding.

The x-ray results clearly demonstrate the effect of increase in calibration load in increasing the magnitude of the residual stresses. The neutron diffraction work is particularly informative in that it provides quantitative confirmation of the FE results at positions within the body of the link. The results of the FE analysis of residual stresses might be made slightly more realistic by introducing the possibility of inelastic behaviour during unloading, which could not be modelled at the time this work was done.

In the study of the optimum link geometry, to examine the way in which

link shape affects the load before plastic deformation begins in the uncalibrated condition, the following alternatives were considered: different link shape (standard, eight shape and elliptical), link length, inside link diameter and oval cross-section (as opposed to the usual circular cross-section). In fact, the oval-link gave the highest value of nominal stress at yielding. As the service stresses are the summation of the residual and the stresses which would be produced if the links were loaded elastically, optimum link shape depends on whether a link is calibrated or uncalibrated. It also depends on the level of calibration and the applied load which may determine the fatigue fracture position (provided the link is not loaded beyond the calibration load). It is in fact found that the standard 19 mm mining chain link is the optimum shape as regard to the combination of the elastic stresses under load and the residual stresses; the oval-link geometry is advantageous in contrast to the circular cross-sectional link regarding elastic stresses only, whereas the situation is reversed considering residual stresses. Further general remarks will be made in the conclusions (Chapter 10) with respect to the link length and inside diameter.

Anomalous strain gauges results (strains rising as the links were unloaded, Fig. 8.26 and 8.27) were obtained in determining residual stresses (Chapter 5). Similar anomalies were produced using the FE method indicating that some area at the position of strain gauges placed at 60° to the crown is behaving in this manner for standard, eight shape and elliptical shapes. This position is very close to the point which the maximum absolute principal stresses change from compressive to tensile, Fig. 9.1. Elastic FE analysis in which geometric changes are ignored gave a slightly different change-over position from that given by large-deflection elastic

analysis - but in the latter case the position remained unchanged with load. It had been thought that the anomaly might be connected with movement of this point during unloading, so that a change from, say, tension to compression at the gauge as a result of movement of the change-over point, would mark the expected change in strain during unloading. The FE results do not appear to support this hypothesis, however, and the cause of the anomaly remains unclear. During loading, the gauges involved also show a change in sign of the strains when plastic deformation sets in. It may be that some local deformation is taking place to cause the anomaly.

9.4 FURTHER DISCUSSIONS

The general form of residual stresses distribution in the chain links is quite complex, but in the barrel of the chain links, it can roughly be understood as arising from plastic flow in tension and bending under load, Fig. 9.2 (a). Then the tension and some of the bending is removed during unloading (Fig. 9.2 (b)), but without refined analysis, the extent of bending cannot be evaluated. Hence the FE method plays an important role in establishing the residual stress distribution.

The total force and moment operating on any section cut through the chain link (or body) to produce two halves must be zero to satisfy the static equilibrium condition within the link [29]:

$$\int \sigma \, dA = 0$$

$$\int dM = 0$$

It is possible that there are more radical ways of affecting the properties of chains. If one considers load-carrying properties alone rather than, for example, fatigue strength, then one approach would be to make use of a higher tensile strength material by alteration of heat treatment or steel specification. This would, however, almost inevitably result in a reduction in the elongation of the chain at fracture and would not therefore be an acceptable solution. An approach that has been referred to (Chapter 2) is to make use of differential tempering so that the crowns are harder than the barrels. This is done by an additional tempering operation with a specially designed coil so that the eddy currents are produced principally in the barrels. During tensile elongation, the crowns remain resistant to plastic deformation so that the bending moment applied to the barrel is much reduced. The stress state in the barrel then approximates to uniform tension, and there is no region of compression as in the standard chain. The extension of the chain then comes mainly from the barrels: the load-carrying capacity is increased because the barrel material, being entirely in tension, is more effectively used.

Whilst differential heat treatment is undoubtedly an effective method of raising the chain's load-carrying capacity, calibration is still employed to raise the effective elastic limit. The question of the effect of differential tempering on the residual stress field and on subsequent fatigue behaviour is unclear.

A preforming stage to modify the chain shape has already been referred to, namely, the rolling of flats on the 22 mm round bar before forming "oval" links. One can, of course, envisage more extensive preforming, carried out with the objective of raising the resistance to bending in

the crown, in much the same was as in the use of differential heat treatment, or possibly giving the barrel section a reduced resistance to bending. Some work has indicated that this approach might be effective [43], but it is questionable whether the extra manufacturing costs could be justified by the consequent improvement in properties.

Although fatigue testing is specified for mining chain, it is not clear to what extent it is actually relevant, since most mining chain is withdrawn from service because of wear due to rubbing. For hoist chain fatigue properties are probably more relevant. However, if fatigue strength is important, and the chain is used with its surface unchanged from that produced by heat treatment in air, then the surface decarburization thereby produced means that the advantages of high tensile strength in improving fatigue strength are largely lost, In these circumstances, calibration remains the only way of making use of the higher tensile strength, since higher residual compressive stresses can be produced in the higher strength material. In addition, as shown by Foly et al [24,25], removal of the decarburized surface could additionally be used as a means of raising the fatigue strength.

CHAPTER 10

CONCLUSIONS AND SUGGESTIONS FOR FURTHER WORK

10.1 CONCLUSIONS

This work has dealt with the application of the finite element (FE) method to chains in order to determine the effect of the link shape on both the stress under load (total stresses) and residual stresses and to enable informed decisions to be made regarding the selection of link shape. The research was applied to 7 mm lifting chain and to 19 mm and 22 mm mining chain, the diameter referring to the diameter of the circular section rod from which the link is manufactured. In the case of the 19 mm links, three geometries were examined: straight sided, pinched (eight shape) and elliptical. The 22 mm rod had flats rolled on it before manufacture of the chain: it is referred to as oval-link. The FE work was supported by the following practical methods of stress determination: strain gauge (for stresses and under load and residual stresses): x-ray and neutron diffraction (residual stresses). Static tensile and fatigue testing (7 mm lifting chain) was also carried out.

1

Calibration of the 7 mm lifting chain significantly improved the fatigue performance. The improvement is ascribed to the presence of compressive residual stresses at the position of formation of fatigue cracks, which changes the mean stress in the fatigue cycle. The effect was reproduced with plain specimens, with a surface comparable to the chains', under direct stress loading. Statistical investigation showed that the fatigue fracture positions were affected by increase in calibration load and also by batch variation.

2

X-ray measurements of the residual stresses in 7 mm lifting chain and 19 mm mining chain after calibration revealed the presence of compressive residual stresses in the surface. Residual stresses

within the volume of the 19 mm mining chain were measured by neutron diffraction and found to be in good agreement with the FE results.

3

Strain gauge measurements of the strains in the 19 mm mining chain (3 link geometries) and the oval-link under load- both for the initial elastic strain and after yielding - were in good agreement with the FE work. The residual stresses measured by the strain gauges were predominantly compressive. There are two positions on the outside of the elliptical and oval-links where tensile residual stresses were indicated, in contradiction of the FE work. This has little bearing on the chain's fatigue performance, however, since the stresses under load at these locations are compressive.

4

Most of the FE work was carried out with three-dimensional elements. Comparable results could, however, be obtained with some reduction in computing time by the use of beam elements. Realistic representation of the loading is necessary: point loading between the links is inadequate.

5

Comparable results were obtained using two-dimensional contact analysis of the 19 mm standard mining and 7 mm lifting chains (Chapter 7). Furthermore, increase in calibration load improved the surface residual stresses, that is, they became more compressive. The information on the contact area and pressure envelope was used to model the contact in the three-dimensional stress analysis.

6

A full three-dimensional stress analysis of all the above mentioned various link geometries were carried out. Overall, the standard 19 mm mining chain link geoemtry is the optimum shape as far as the total and residual stresses are concerned (Chapter 8). The stresses (total

and residual) in this link geometry tend to lie between the eight shape and elliptical link geometries. The residual stresses are all compressive except for the eight shape link which has tensile stresses on the inside of the barrel centre, confirmed by the strain gauge work. For a given nominal cross-sectional area, the oval-link geometry is advantageous in contrast with the circular cross-sectional link geometry considering total stresses only, while considering residual stresses the situation is reversed (Section 8.3.2).

In the 19 mm standard chain link, a change in barrel length (pitch) and inside diameter (inside width) at the crown has a significant effect on the total and residual stresses at the chain link surfaces. For a given barrel length, the narrowest link is the optimum shape as long as the the inside diameter at the crown is larger than the chain link's own diameter with respect to both total and residual stresses. On the other hand, for a given inside radius at the crown, the total stresses are decreased by an increase in barrel length and, in the case of the residual stresses, the situation is not clear cut, that is, the compressive residual stresses are larger in some regions than the others.

Whether a link geometry is an optimum shape or not depends on the state of the service stresses (combination of total and residual stresses). This implies that for calibrated and non-calibrated chain links the optimum link shape would be different. All the stresses obtained from the FE work were validated by the use of strain gauge technique. Some discrepancy between the two sets of results is to be expected because elastic unloading was assumed in the FE work (that is, the Bauschinger effect was neglected). This should result in an over-estimate of the residual stresses.

10.2 SUGGESTIONS FOR FURTHER WORK

The study reported here has shown that using the finite element method in conjunction with the experimental total and residual stress measurement techniques can provide valuable information about the effect of link shape on chain performance [136,137,138]. The experimental techniques have demonstrated the validitiy of the results predicted by FE analysis. The research can be extended in a number of ways:

1

The fatigue limits of the 7 mm lifting chain may be determined at various calibration loads with further testing of different batches to examine the effect of batch variations in the fatigue testing results. Better knowledge of the fatigue life statistics is needed to be able to predict the effect of chain length (the number of links) on fatigue life.

2

Further x-ray measurements of residual stresses are required to clarify the effect of increasing calibration load on the residual stresses in both grades of chains. In the neutron diffraction work, finer sampling volumes should be taken in the regions of steep stress gradients to establish the residual stress pattern more accurately within the centre of the 19 mm mining chain as well as extending the measurement to other critical sections such as: transition and crown regions.

3

Further work is required to establish the residual stress pattern thoroughly by using extra sampling points in the strain gauge work and further testing of the chain material specimens to complete the

stress-strain curve. The forming of the non-standard links needs to be improved so that they conform more accurately to the assumed model.

4

A complete three-dimensional contact analysis of the chains should be carried out to achieve the best solution in conjunction with other complicated alternatve geometries [47,48] not considered here.

5

Finite element analysis in conjunction with fracture mechanics should be applied to estimate the flaw size that the inspection techniques applied to chains should be capable of detecting [139].

6

In service, chains can inevitably undergo impulsive or shock loading which can cause a sudden failure of the chain. This problem was approached in the appropriate standards by the introduction of energy absorption factor (Appendix A) which is an empirical method and a through understanding of the problem may be achieved by the use of FE.

7

More radical changes in link shape may be considered, such as: variable cross-sectional area at different parts of the link geometry (e.g., narrower at the centre and thicker at the crown) perhaps coupled with differential heat treatment which is already in use in the chain industry. The FE can be used to take up this task.

8

Further work is required to clarify the anomaly ocurring in the strain gauge work for determination of residual stresses in the standard, eight shape and elliptical geometries (at the outside transition). FE residual stress determination should be extended to cater for the Bauchinger effect on unloading.

REFERENCES

1 Wellinger, K., and Stanger, A.,"Properties of round-steel chains under static and alternating loading", VDI-Zeitschrift, 1959, P 1425-1431.

2 Bahke, E.,"Principles defining the strength of wire ropes and chains, Part I", Wire Vol 29 No. 2, 1980, P 54-61.

3 Bahke, E.,"Principles defining the strength of wire rope and chains, Part II", Wire Vol 30 No. 2 (1980), P 168-176.

4 Hawkes, I. and Foly, J.H., "Elastic-plastic strain distributions in short-link chains under load", J. of Strain Analysis, Vol 3, No. 1, 1968.

5 Squires, H.V. and Foly, J.H., "Fatigue testing of short-link chain under line-loading conditions", J. of Strain Analysis, Vol 5, No. 1, 1970.

6 Pankova, M.D., "Elasto-plastic change in the pitch of a chain link", IZV, Vyssch. Uchebn. Zavod, Machino-stroyenga,, 1975.

7 Anthony, G.T., Gorley, T.A.E. and Hayes, J.G.,"A simple new design formula for chain links", in "Industrial numerical analysis", (Elliot.,C.M., and McKee,S.), Oxford Univ. Press, P 25-52.

8 Gough, H.J., Cox, H.L. and Sopwith, D.G., "Design of crane hooks and other components of lifting gear", Proc. of Institute of Mechanical Engineers, Vol 128, 1934, P 253-360.

9 British Standards Institute,"Chain slings for welded construction :grades M(4), S(6), and T(8)", BS 6304, BSI, London, (1982).

10 British Standards Institute, "Short link chain for lifting purposes Part 1. Specification for general conditions of acceptance", BS 4942, BSI, London, (1981).

11 British Standards Institute, "Short link chain for lifting purposes Part 2. Specification for grade M(4) non-calibrated chain", BS 4942, BSI, London (1981).

12 British Standards Institute, "Short link chain for lifting purposes Part 3. Specification for grade M(4) calibrated chain", BS 4942, BSI, London (1981).

13 British Standards Institute, "Short link chain for lifting purposes Part 4. Specification for grade S(6) non-calibrated chain" BS 4942, BSI, London (1981).

14 British Standards Institute, "Short link chain for lifting purposes Part 5. Specification for grade T(8) non-calibrated chain", BS 4942, BSI, London (1981).

15 British Standards Institute, "Short link chain for lifting purposes Part 6. Specification for grade T(8) calibrated chain", BS 4942, BSI, London (1981).

16 British Standards Institute, "Proper use and maintenance of calibrated round steel link lifting chains", BS 6521, BSI, London (1984).

17 Behnke, E.R., "Hoist desigers' handbook and Hoistaloy load chain application guide", Columbus McKinnon Corporation, Tonawanda, New York State, U.S.A.

18 Feiser, C.F., "Guide to OSHA compliance - Safety practices for chain slings", Plant Engineering, Aug 9, 1973, P 67-71.

19 British Standards Institute, "High-tensile steel chains (round link) for chain conveyors and coal ploughs", BS 2969, BSI, London (1980).

20 British Standards Institute, "Non-calibrated short link steel chain (grade 30) for general engineering purposes: class 1 and 2", BS6405, BSI, London (1984).

21 Metals handbook, "Failure analysis and prevention", Vol 10, 8th ed., 1975, P 95-125.

22 Metz, H.,"Lifting chains", Wire, Vol 8, No. 5, 1979, P 214-222.

23 DIN 5684, "German Standards for lifting chains", May 1984.

24 Foley, J.H. and Hollan, B., "Fatigue strength of chains and the effect of surface condition", Safety in Mines Research Establishment, Sheffield, (1967).

25 Foley, J.H., "Fatigue strength of 18 mm conveyor chains", Safety in Mines Research Establishment, Sheffield, (1971).

26 Parlane, A.J.A., "The determination of residual stresses: a review of contemporary measurement techniques", Proc. Int. Conf. on Residual stresses in welded construction and their effects, London, 15-17 Nov 1977, Vol 1, P 63-78.

27 Stahlkopf,K., Egan, G.R. and Dau, G.,"Recent advances in residual stress measurement", Residual stresses in welded construction and their effects, Int. Conf., London, Nov 15-17 1977, Published by Welding Institute, Cambridge, 1978, P 321-335.

28 Denton, A.A.,"Determination of residual stresses", Metallurgical Reviews, Institute of Metals, Vol 11, 1966, P 1-23.

29 Treuting, R.G., Wishart, H.B., Lynch, J.J. and Richards, D.G., "Residual stress measurements", A series of four educational lectures on residual stress measurements, ASM, 33rd National Metals Congress and Exposition, Detroit, Oct 15-19, 1951.

30 Procter, E.,"Residual stresses and their effect", The Welding Institute, 1981, P 34-40.

31 Allen, D.R. and Sayers, C.M.,"The measurement of residual stress in textured steel using an ultrasonic velocity combinations technique", Ultrasonics, Vol 22, Jul 1984, P 179-188.

32 Fukuoka, H., Toda,H. and Naka, H.,"Nondestructive residual-stress measurement in a wide-flanged rolled beam by acoustoelasticity", Experimental Mechanics, Mar 1983, P 120-128.

33 Namkung, M. and Heyman, J.S., "Residual stress characterization with an ultrasonic/magnetic technique", Nondestructive Testing Communications, Vol 1, 1984, P 175-186.

34 Ravindran Nair, R., Natarajan, R. and Rao, U.R.K.,"Analysis of residual stresses due to quenching considering microstructural transformations", Int. J. Mach. Tool Des. Res., Vol 22, No. 4, 1982, P 309-319.

35 Chen, P.C.T. and Cheng, Y.F.,"Stress analysis of an overloaded breech ring", Reliability, stress analysis and failure prevention methods in mechanical design, Am. Soci. of Mech. Engineers, W.D. Milestone (ed.), 1980, P 175-180.

36 Schajer, G.S.,"Application of finite element calculation to residual stress measurements", J. of Engineering Materials and Technology, Vol 103, Apr 1981, P 157-163.

37 Brebbia, C.A., "Finite Element Systems", 2nd. ed., Computational Mechanics Centre (1982).

38 ABAQUS User's Manual, Vol 1-3, Hibbitt, Karlsson and Sorenson, Inc., 35 South Angell St., Providence, Rhode Island 02906.

39 ABAQUS Theory Manual, Hibbitt, Karlsson and Sorenson, Inc., 35 South Angell St., Providence, Rhode Island 02906.

40 ABAQUS Example Manual, Hibbitt, Karlsson and Sorenson, Inc., 35 South Angell St., Providence, Rhode Island 02906.

41 PAFEC Data Preparation Manual, Pafec Ltd., Strelley Hall, Nottingham (1978).

42 PAFEC 75 Theory, Results, Pafec Ltd., Strelley Hall, Nottingham (1978).

43 SDRC, "The study of design modification to the 9/16 inch nominal diameter wheel chain link", May 1978, Unpublished (Interim Report).

44 Modlen, G.F.and Stark, R.A., "Static and fatigue strength of chains", Proc. of the 2nd. Conf. of the Irish Durability and Fracture Committee, Limerik, (1984).

45 Modlen, G.F., "Effect of link geometry in the stresses in short links under load", Internal Report, (Loughborough Univ. of Tech., 1985) Unpublished.

46 Lee, C.N.,"Stress behaviour of chain links - finite element analysis of stress", Vol 1 and 2, B.Sc. Dissertation (Loughborough Univ. of Tech., 1985) Unpublished.

47 Mattheck, V.C. and Burkhardt, S.,"Structural failure analysis of a chain link for mining practice and proposal for chain link

design", Der Maschinenschaden 59 (1986) Heft 5.

48 Mattheck, V.C. and Burkhardt, S.,"Design and dynamic behaviour of a chain link having a better wear resistance", 3rd, Int. Conf. on Structural failures, Vienna, Jul 10-12, 1989.

49 Burdon, C., "Manufacture of mining and industrial chains", Mining Tech., Vol 66, No. 760, Feb 1984, P 59-66.

50 Neuhaus, R., "The manufacture of round-wire chains", Wire-Coburg, Germany Issue 95 Jun 1968, P 137-147.

51 Plumbridge, W.J. and Knee, N.,"Effect of tempering temprature on monotonic and cyclic properties of a high-strength low-alloy chain steel", Materials Science and Technology, Vol 1, Aug 1985, P 577-582.

52 Pakrasi, S., Just, E., Betzold, J. and Hollrigl-Rosta, F., "How boron affects the hardenability of low carbon alloy steels", Conf. Proc., Society of AIME Milwaukee, Sep 1979.

53 Llewellyn, D.T. and Cook, W.T., "Metallurgy of boron-treated low-alloy steels", Metals Technology, Vol 1, Part 12, Dec 1974, P 517-529.

54 Keown, S.R. and Pickering, F.B., "Some aspects of the occurance of boron in alloy steels, Metal Science, Vol 11, Jul 1977, P 225-233.

55 Potts, S.R., "Metallurgical evaluation of the suitability of MS7 boron-treated alloy steel for production ofgrade T (80) chain", Wheway Becker (CM) LTD, Green Lane, Walsall, West Midlands, Apr 1983, Unpublished.

56 Mehta, K.K, "Comparative brittle fracture studies on 18 mm high-tensile chain links manufactured from MnB 6 and 23 MnNiCrMo 6 4 steels", Thyssen Edelstahlwerke AG Research Laboratory, 5810 Witten, W. Germany, Nov 1982.

57 King, J.E. and Geary, W., "Embrittlement effects of fracture toughness and fatigue threshold behaviour in martensitic steels containing boron", Annual Report on SERC Grant No. GR/C/36285, Nottingham Univ., Apr 1984.

58 British Steel Corporation Research Organisation, "The effect of B additions on the stress corrosion properties of experimental chain steels", Sheffield Laboratories, Feb 1983.

59 Potts, S.R., "Boron-treated steels for making grade 80 chain", Wheway Becker (CM) Ltd., Green Lane, Walsall, West Midlands, Unpublished.

60 Wust, A., "Butt welding of wires with reference to chains - Part 1", Wire, Vol 35, No. 4, 1985, P 179-181.

61 Wust, A., "Butt welding of wires with reference to chains - part 2", Wire, Vol 35, No. 5, 1985, P 237-238.

62 Krause, R., "Thermal treatment of round steel chains", Wire

World Int., Vol 63, No. 4, Apr 1977, P 136-138.

63 Potts, S.R.,"Wheway Watson (CM) Ltd. heavey duty C+ mining chain", Wheway Becker (CM) Ltd., Green Lane, Walsall, West Midlands, 1987.

64 "The impossible is faster - by induction heating", Metals and Materials, Vol 4, No. 11, Nov 1988.

65 Becker-Prunte "The manufacture of round steel link chains and accessories", W. Germany.

66 Kurrein, M.,"Plasticity of metals", Griffin, London, 1964, P 263

67 Becker-Prunte "Production of the high tensile round steel chains", W. Germany.

68 Batson, R.G. and Bradley, J.,"Static and endurace tests of laminated springs made of carbon and alloy steels", D.S.I.R., Engineering Research Special Report No. 13, 1929.

69 Niku-Lari, A.,"Advances in surface treatments", Vol 4, Pergamon Press, 1987, P 73-113.

70 Minuth, E. and Hornbogen, E., "Metallographic investigation of a fractured chain link", Practical Metallography 13 (1976), P 584-598.

71 Novotny, L.G., "Overstressing of pressure vessels to increase service life", Int. Conf. on Fatigue of Engineering Materials and Structures, Proc. of the Inst. of Mech. E., Sheffield (1986), Vol 1 P 249-256.

72 Kumar, R. and Gary, S.B.L.,"Effect of instant and frequency of overloads on fatigue life", Int. Conf. on Fatigue of Engineering Materials and Structures, Proc. of the Inst. of Mech. E., Sheffield (1986), Vol 1, P 257-264.

73 Nawwar, A.M. and Shewchuk, J., "The effect of preload on fatigue strength of residually stressed specimens", Experimental mechanics, Vol 23, Dec 1983, P 409-413.

74 Celander, I., "Preload influence on fatigue characteristics of chain cable exposed to salt water and atmospheric conditions", 4th. Annual Offshore Tech. Conf., Houston (1972), P 645-648.

75 Foley, J.H., "The effect of proof loading of the fatigue strength of 1.5 % manganese steel short-link chain", Safety in Mines Research Establishment, Sheffield, (1973).

76 Dieter, G.E., "Mechanical metallurgy", 2nd. ed., McGraw-Hill, 1976, PP 403-450.

77 As in 21, P 103.

78 Ransom, J.T.,"Discussion" in Proc. Am. Soc. Test. Mater. Proc., Vol 54, 1954, P 847-848.

79 Stanford, K.,"Modern chain making", Metallurgia, Vol 45, No. 8,

Aug 1987, P 438-439.

80 Wheway Becker (CM) Ltd.,"9/32 inch Grade 'T' (Felco) calibrated load chain for pulley blocks", Green Lane, Walsall, West Midlands.

81 Tracy, P.G., Rich, T.P., Browser, R. and Tramontozzi, L.R., "On the statistical nature of fracture", Int. J. of Fracture, Vol 18, No. 4, Apr 1982, P 253-277.

82 ASTM,"A guide for fatigue testing and statistical analysis of fatigue data",(Supplement to Manual on Fatigue Testing, STP No. 91), Special Technical Publication No. 91-A (2nd ed.), 1963.

83 Kharahk, M.F.,"Analysis of results of tests on chains for strength and durability", Ind. Lab. (USSR), Vol 35, No. 10, (English Translation), P 1477-1483.

84 Modlen, G.F., Private communication.

85 Whalley, B.G., "The Analysis of service failures", The Metallurgist and Material Technologist, Vol 15, No 1, Jan 1983, P 21-25.

86 Abolfathi, E., "Residual stresses in chains", Apr 1986, (Loughborough Univ. of Tech.), Unpublished.

87 Minitab Reference Manual, 1985, Minitab, Inc., 3081 Enterprise Dr., State College, PA16801, USA.

88 Christenson, A.L., "The measurement of stress by x-rays", SAE (Society of Automotive Engineers), New York, Technical Report 182, 1960.

89 Committee on Mechanical Behaviour of Materials, "Standard method for x-ray stress measurement", The Society of Material Science, Japan, 1973.

90 Noyan, I.C. and Cohen, J.B.,"Residual stress measurement by diffraction and interpretation", MRE (Materials Research and Engineering), Springer-Verlag, 1987, P 211-229.

91 Lester, H.H. and Aborn, R.M., Army Ordnance 6, 120,200,283,364 (1925-26).

92 Cullity, B.D.,"Elements of X-ray diffraction", Addison-Wesley Publishing Company Inc., 1956, P 440.

93 Kirk, D.,"State of the art - theoretical aspects of residual stress measurements by x-ray diffractometry", Strain, Vol 6, No 2, Apr 1970, P 75-80

94 Maeder, G., Lebrun, J.L. and Sprauel, J.M.,"Present possibilities for the x-ray diffraction method of stress measurement", NDT Int., Vol 14, No. 5, Oct 1981, P 235-247.

95 Macherauch, E.,"X-ray stress analysis", Experimental Mechanics, Vol 6, Mar 1966, P 140-153.

96 As 92 P 444.

97 As 92 P 269

98 As 92 P 459

99 SAE,"Residual stress measurement by x-ray diffraction - SAE J784a", SAE (Society of Automotive Engineers), Handbook Supplement, Aug 1971.

100 As 92 P 446

101 British Steel Corporation (BSC), "X-ray stress analysis", Swindon Laboratories Resaerch Services, Moorgate, Rotherham, 1985.

102 Rigaku/Strainflex Series, "X-ray stress analyzers MSF-2M, PSF-2M", Rigaku Corporation, 3-9-12 Matsubara-cho, Akishima-Shi, Tokoyo, 196 Japan.

103 Instruction Manual for Electrolytic Polisher, Rigaku Cat. No. 2904, Manual No. ME210FD.

104 As in 69, P 165.

105 Young, W.B.,"Residual stress in design, process and materials selection", ASM's Conf. Proc. on Residual stress - in design, process and materials selection, Cincinnati, Ohio, USA, Apr 27-29, 1987, P 21-26.

106 Stacey, A., MacGillivary, H.J., Webster, G.A., Webster, P.J. and Ziebeck, K.R.A., "Measurement of residual stresses by neutron diffraction", J. of Strain Anal., Vol 20, No. 2, 1985.

107 Allen, A.J., Hutchings, M.T. and Windsor, C.G., "Neutron diffraction methods for the study of residual stress fields", Advances in Physics, Vol 34, No. 4, 1985, P 445-473.

108 Measurement Group,"Student manual for strain gage technology", Bulletine 309, 1983, Education Division, P.O. Box 27777, Raleigh, North Carolina 27611, USA.

109 TML, "Direction for use of TML strain gauges and adhesives", TML Pam E-105, Alexandra Buildings, 59 Alcester Rd, Studley, Warks.

110 Budynas, R.G.,"Advanced strength and applied stress analysis",, McGraw-Hill, 1977.

111 Hearn, E.J.,"Stress analysis", Design Engineering Guide, Published by Design Engineering Handbook, Products Journals Ltd.,Summit House, Glebe Way, West Wickham, Kent, at 716, P 21-28.

112 Vaughan, J.,"Application of B and K equipment to strain measurements", Oct 1975, Bruel and Kjaer, DK-2850 N/Erum, Denmark.

113 Micro-Measurements,"S/N Fatigue life gauge", Product Bulletin PB 103, 70 High St., Teddington, Middlesex.

114 Window, A.L. and Holister, G.S.,"Strain gauge techniques", Applied Science Publishers, 1982.

115 Uko, D.K.,"The Bauschinger effect and applications to the manufacture of high strength linepipe", Ph D Thesis (McMaster Univ., Apr 1978).

116 Jamieson, R.M. and Hood, J.E.,"Bauschinger effect in high-strength low-alloy steels", J. of the Iron and Steel Institute, Vol 209, No. 1, P 46-48.

117 Sowerby, R., Uko, D.K. and Tomita, Y.,"A review of certain aspects of the Bauschinger effect in metals", Materials Science and Engineering, Vol 41, 1979, P 43-58.

118 Abel, A.,"A new look at the Bauschinger effect", Metals Australia, Vol 4, No. 8, Sep 1972, P 267-271.

119 Bray, A., Cresto, P.C., Ferro-Milone, A. and Gabola, G.,"A computerized method for the evaluation of the Bauschinger effect - Application to different types of steel", Materialpruf 22, (1980), Nr. 6 Jun.

120 Hinton, E. and Owen, D.R.J.,"An introduction to finite element computation", 1979, Pineridge Press Ltd., P 140.

121 Timoshenko, S.P. and Goodier, J.N.,"Theory of elasticity", 3rd ed., McGraw-Hill, 1970, P 409-421.

122 Lipson, C. and Juvinall, R.C.,"Handbook of stress and strength - design and material application", Macmillan, 1963.

123 Chan, S.K. and Tuba, I.S., "A finite element method for contact problems of soild bodies - Part 1. Theory and validation", Int. J. Mech. Sci., Pergamon Press, Vol 13, 1977, P 615-625.

124 Fredriksson, B., "Finite element solution of linearly elastic contact problems with friction", Report LiTH-IPK-R-033. Linkoping Institute of Technology, Linkoping, May 1975.

125 Fredriksson, B., "Finite element solution of surface nonlinearities in structural mechanics with special emphasis to contact and fracture mechanics problems", Computers and Structures, Vol 6, Pergamon Press ,1976, P 281-290.

126 Urzua, J.L.,Pecknold, D.A., Lopez, L.A., Munse, W.H., "Analysis procedure for frictional contact problems using interface finite elements", Structural Research Series No. 438, Dept. Of Civil Eng., Univ. of Illinois, Urbana, Illinois, Mar 1977.

127 Zienkiewicz, O.C.,"The finite element method", 3rd ed., McGraw-Hill, 1967.

128 Hinton, E. and Owen, D.R.J.,"Finite element programming", 1977, Academic Press.

129 Ang, K.K. and Valliappan, S.,"Mesh grading technique using modified isoparametric shape functions and its application to

wave propagation problems", Int. J. for Numerical Methods in Engineering, Vol 23, No 2, 1986, P331-348.

130 Marcal, P.V. and King, I.P., "Elastic plastic analysis of two-dimensional stress systems by the finite element method", Int. J. Mech. Sci., 9, 1967, P 143-155.

131 Hinton, E., Owen, D.R.J. and Taylor, C.,"Recent advances in non-linear computational mechanics", 1982, Pineridge Press Ltd., P 87-113.

132 Argyris, J.H., "Continua and discontinua", Proc. Conf. Matrix method in structural mechanics, Air force Inst. Tech. Wright-Patterson A.F. Base, Ohio, Oct 1965.

133 Abolfathi, E., "Nonlinear solution techniques in structural Analysis", M.Sc. Thesis (Univ. College of Swansae, Apr 1985).

134 Owen, D.R.J. and Hinton, E.,"Finite elements in plasticity, theory and practice", 1980, Pineridge Press Ltd.

135 Wheway Becker (CM) Ltd., "Heavey duty oval link chain", Green Lane, Walsall, West Midlands.

136 Abolfathi,E., Modlen, G.F. and Stark, R.A.,"Effect of pre-loading on fatigue behaviour of hoist chains", Proc. of the 4th Irish Durability and Fracture Committee -IDFC4, The Queens's Univ., Belfast, UK, 24-26 Sep, 1986.

137 Abolfathi, E., Ascough, J., Stark, R.A. and Modlen, G.F.,"Residual stresses in high-tensile steel chains", 2nd Int. Conf. Fatigue and Stress of Engineering Materials and Components, Imperial College, London, UK., 21-22 Sep 1988.

138 Abolfathi, E., Modlen, G.F., Ascough, J., Swallowe, G., Webster, P.,"Residual stresses in chains: A comparison of neutron diffraction and finite element results", Journal of Strain Analysis, To be published.

139 Pahlevan, S.,"Fatigue and fracture of grade 30 chain", B.Sc. Dissertation (South Bank Polytechnic, 1988) Unpublished.

140 British Standards Institute, "Alloy steel chains grade 80 - ploished short link calibrated load chain for pulley blocks", BS3114, BSI, London (1959).

FIGURES AND TABLES

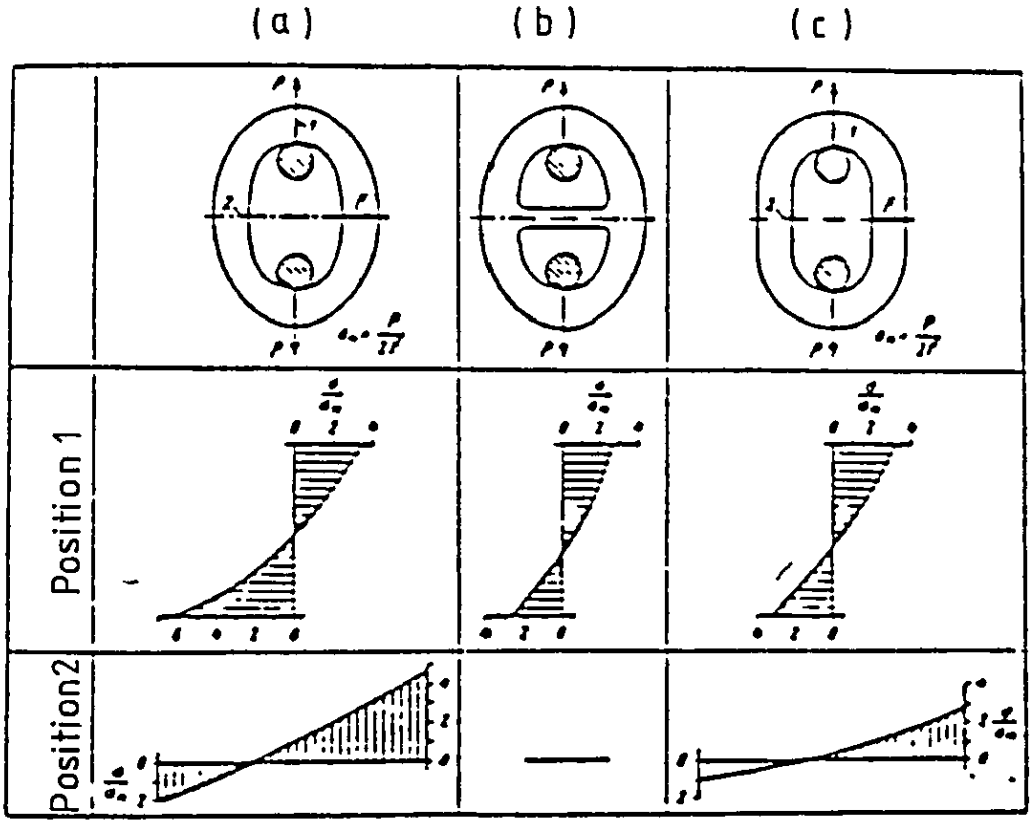

Fig. 1.1 Stress distribution of different chain links

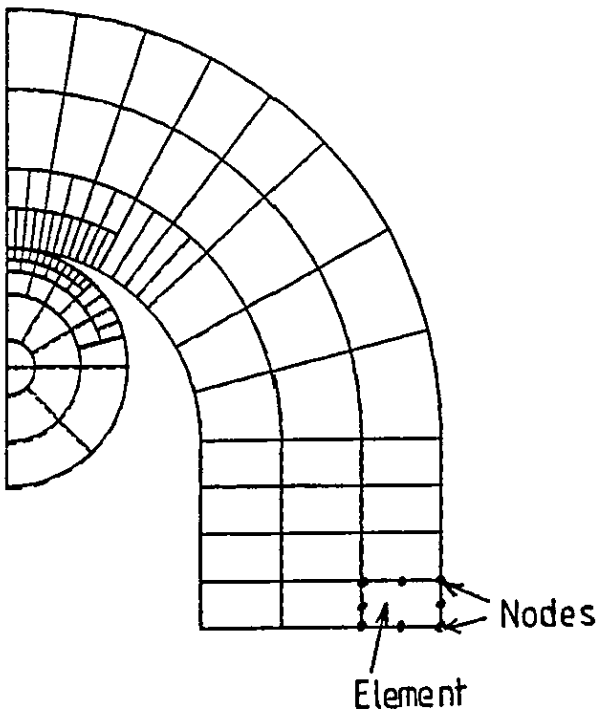

Fig. 1.2 Finite element mesh of the quarter of a chain link showing an eight-noded isoparametric element.

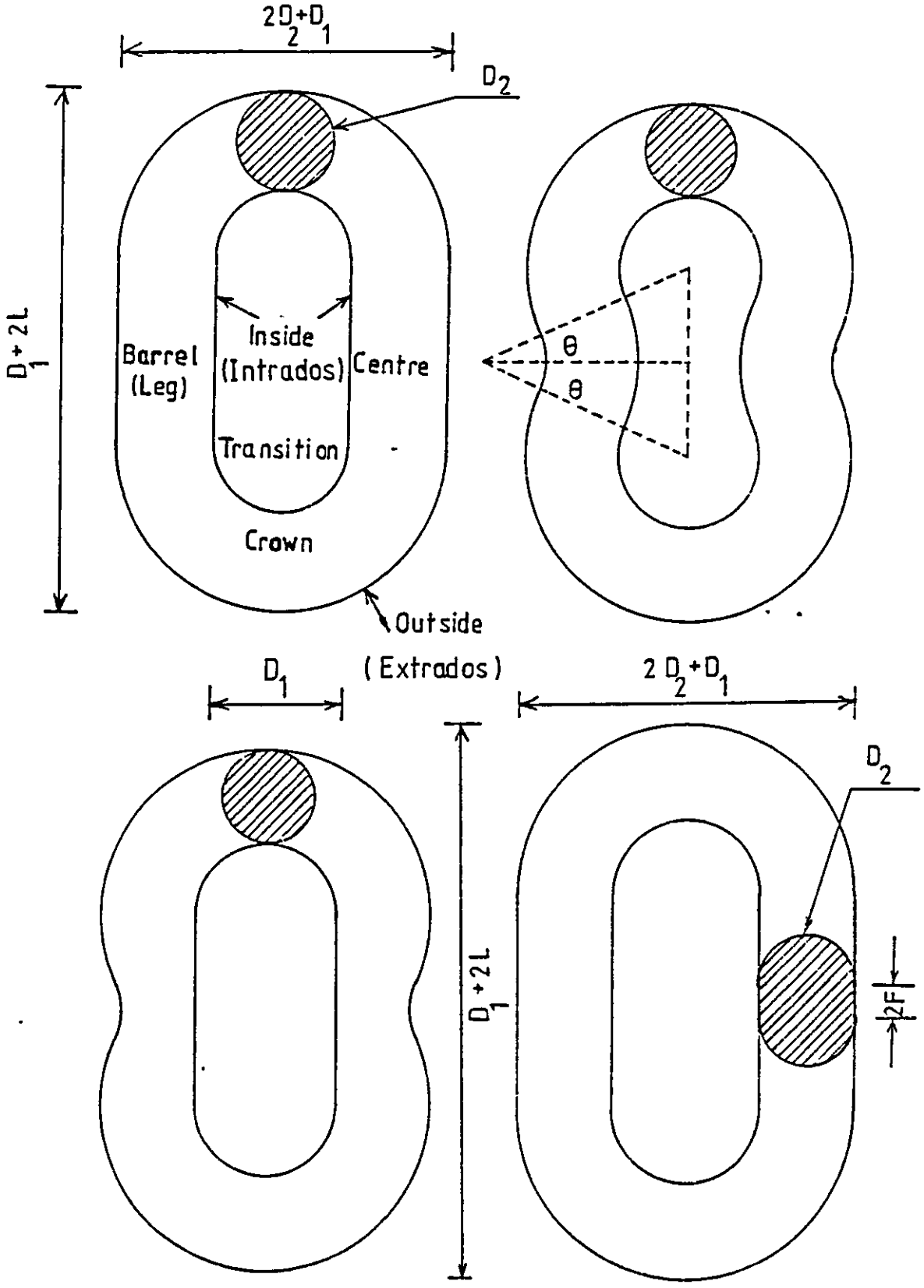

Fig. 1.3 Different chain link geometries (standard, eight shape, or pinched, shaved and oval-link) with relevent terminologies.

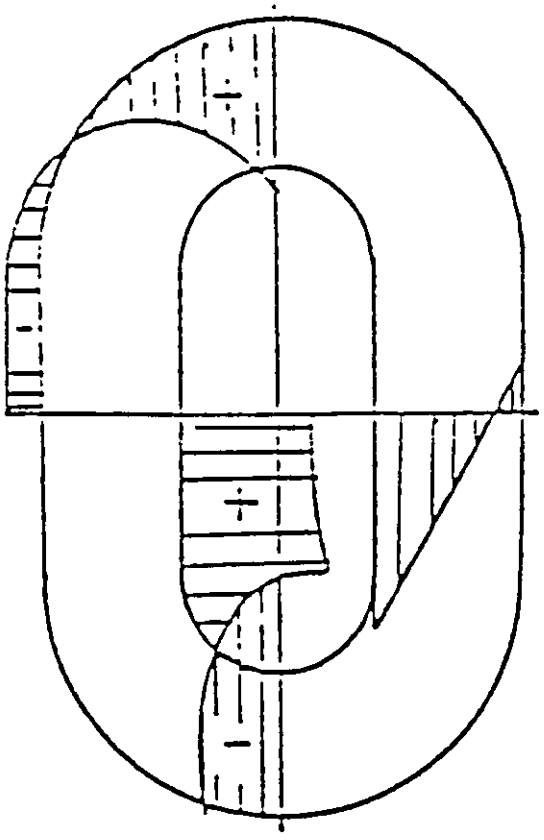

(a)

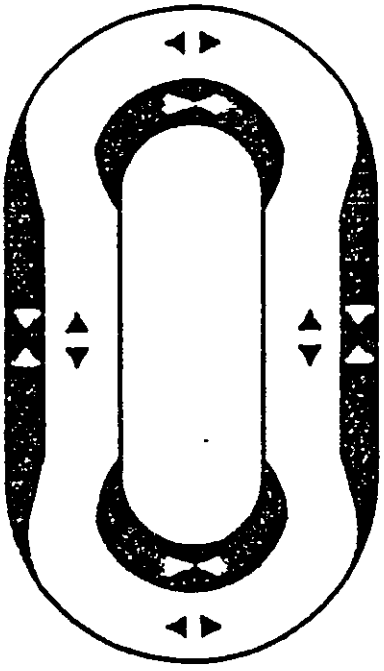

(b)

Fig. 1.4 Qualitattive stress distributuion in the chain link. a) at the outside and mid-surfaces. b) at all the regions.

Note: Compression Tension

```
=====================================================================
        [ BASIC  CHAIN  SHEET  WHEWAY  WATSON (CM)  LTD  ]
   [ ISSUE No :  15        ] For internal use only.          M.J.B
=====================================================================
  CHAIN            9/32 (7.1) FELCO LOAD GRD T          :Spec No. S 087B
-------- -                                               : Date   17:04:86
---------------------------------------------------------------------
  [ Material  :-  MS.11            [  Wire diameter min  6.93   max 7.2
---------:-------------------------:-----------------:-----------------
F        :    Pitch                :  22.7  +/-0.13  :
 O       : Inside width          :  :   9.5    "     :
  R      : Outside width A/peak   :  23.5           :
   M     : Blank length           :  76.06          :
    I    :   L.P.M                :  65             :
     N   :   Weight               :  .02388kg       :
      G  : Mandrel size           :  22.7 * 25.5    :
.........:.........................:.................:.................
W        :    Pitch                :  21.05 +/-0.13  :
 E       : Inside width           :  9.20    "      :
         : Outside width AC/weld  :  23.5    "      :
  J      :   Maximum weld         :   7.67          :
    I    :    Upset               :   1.43          :
     N   :    L.P.M               :                 :
      G  : Squeeze I.D mark       :  plain face     :
.........:.........................:.................:.................
E   C    :   Stamps               :   FH-T          :
 M   L   :   Spacing              : every 20 links  :
  B   I  :   Weld max             :   8.2           :
   O   P :    L.P.M               :                 :
     S   :   Stroke               :                 :
      S  :                        :                 :
.........:.........................:.................:.................
    P    :   Pitch                :  to mould       :
 C   A   : Inside width           :    "            :
  A   R  : Outside width AC/weld  :    "            :
   L   T :    L.P.M               :                 :
.........:.........................:.................:.................
H   T    : Harden temp Centigrade :      925        :
 F   R   : Tempering temp    "    :   340 - 350     :
      E  : Tempering time    "    :   6 hours       :
   T   A :                        :                 :
        T:                        :                 :
.........:.........................:.................:.................
T        : Calibration load final :   38.5 kN       :
  E      :     Test load          :                 :
   S     : Extension at test      :                 :
    T    : Break load  MIN        :   64.1 kN       :
  P      : Extension at break MIN : 10% on 36"length:
   E     :      E.A.F             :                 :
    O    :   Brinell hardness     :   360 - 400     :
     M   : Minimum bend test      :                 :
      T  :                        :                 :
.........:.........................:.................:.................
F        :   Pitch                :  21.29 - 21.59  :
 I   C   : Outside width AC/weld  :   23.57         :max weld adjacent
  N   A  :   "       "    AJ/weld :    "            :outside width.254
   A   L :   Inside width         :  8.91 min       :
    L    : Calibration load MIN   :   38.5 kN       :
         : Seat pin diameter cf   :   8.0           :
*********************************************************************
```

Fig. 2.1 Wheway Becker (CM) company's basic chain sheet.

Fig. 2.2 Chain steel (raw material) in form of rings or bars.

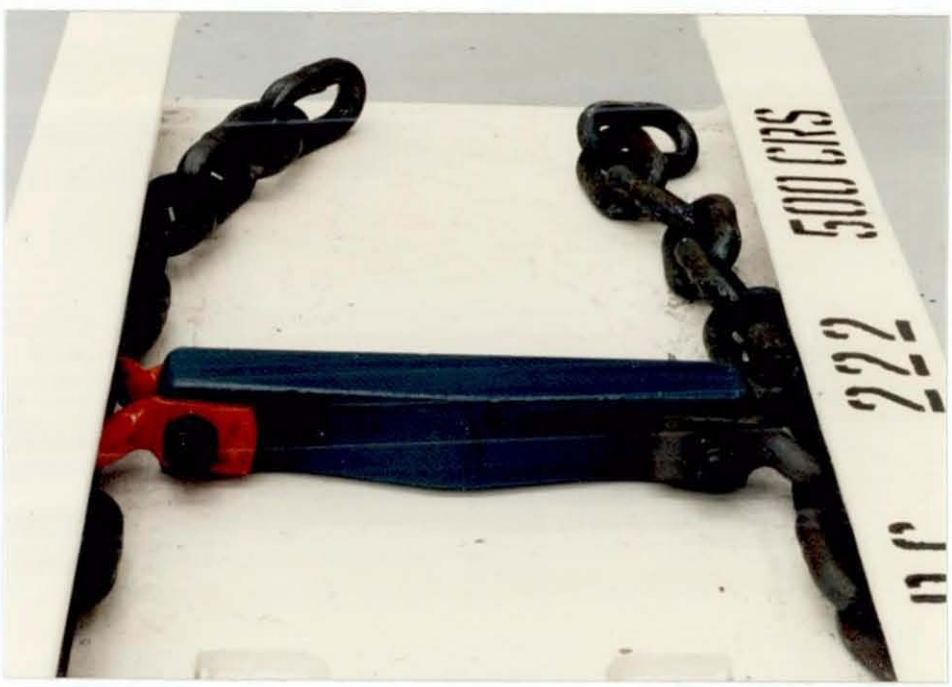

(a)

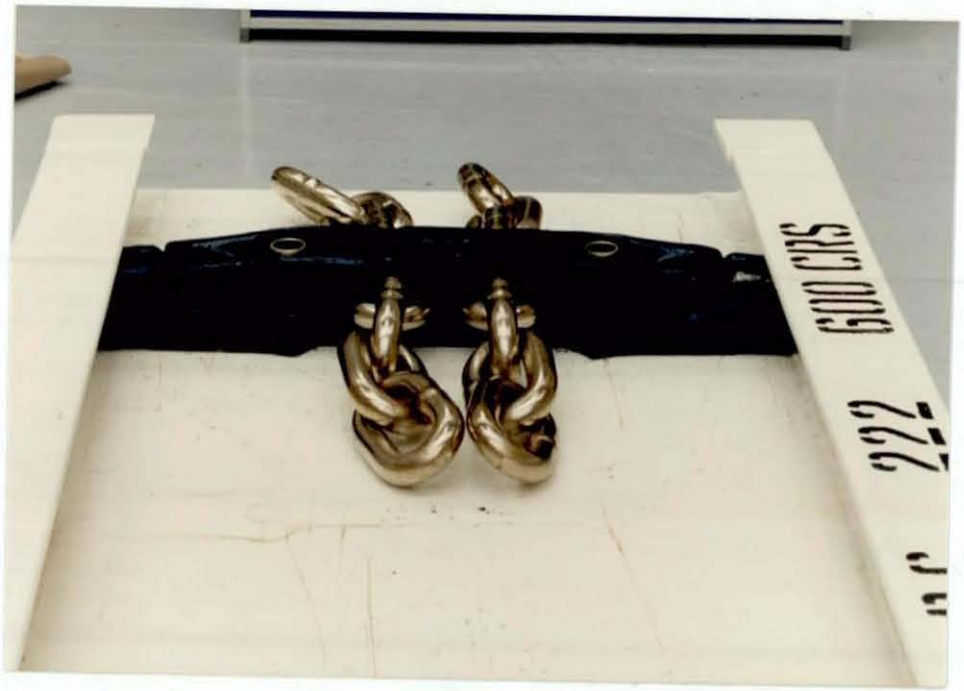

(b)

Fig. 2.3 J.J. Series flight bar assembly. a) Twin outboard. b) Twin inboard.

(a)

(b)

Fig. 2.4 Lifting chains. a) used in lifting tackles. b) different sizes.

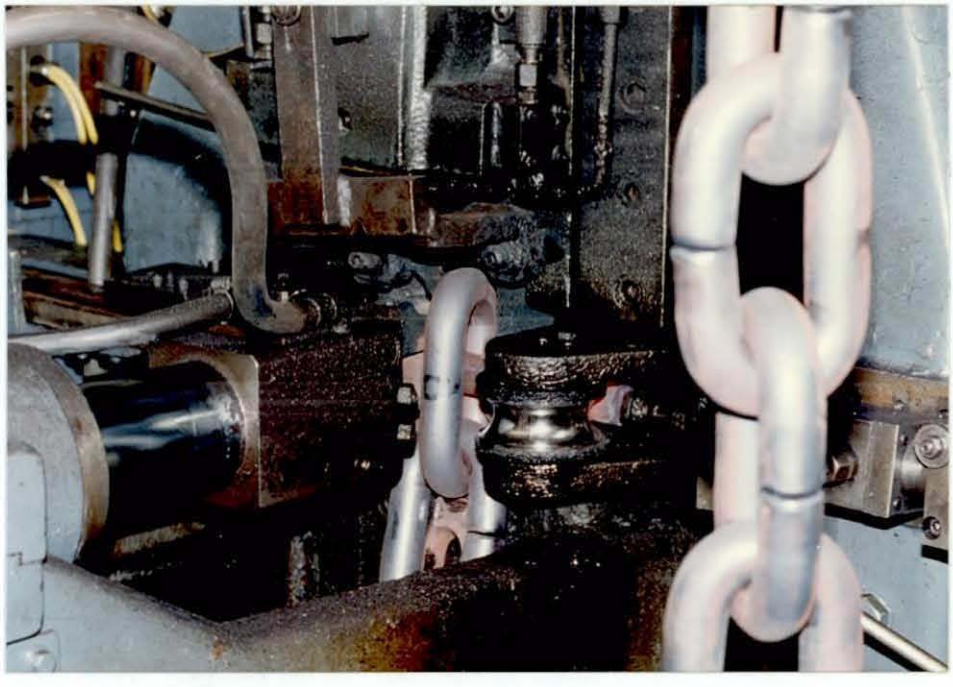

Fig. 2.5 Hot forming of chain links over 20 mm diameter.

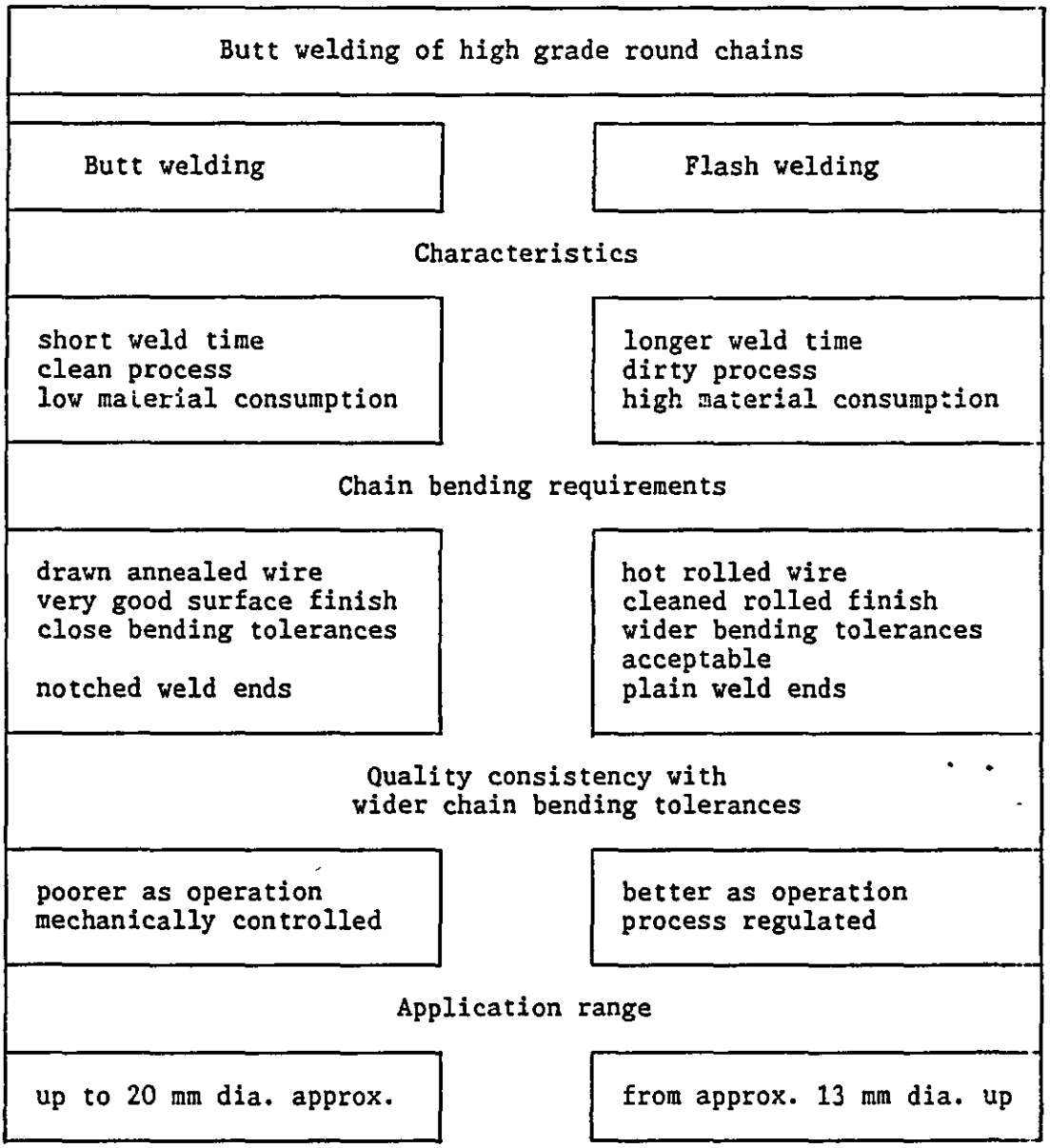

Fig. 2.6 Butt welding

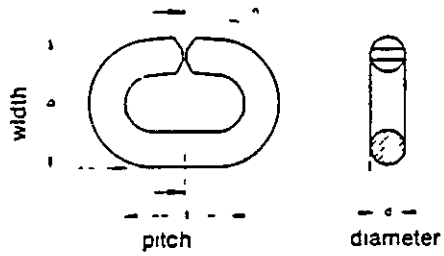

Fig. 7a Chain link for butt welding

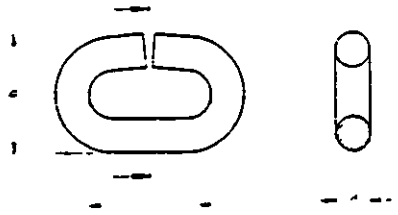

Fig. 7b Chain link for flash butt welding

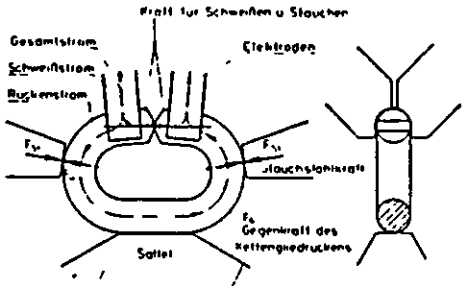

Fig 8a **At start of weld operation**

Kraft für ... = force for welding and upsetting; Gesamtstrom = total current, Schweißstrom = welding current, Rückenstrom = link back current, Elektroden = electrodes, Stauchstahlkraft = upsetting tool force, Gegenkraft . = chain link back reaction strength, Sattel = saddle --

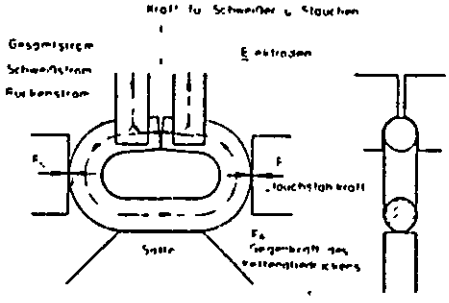

Fig 8b **At start of weld operation**

Kraft für . ¬ force for welding and upsetting, Gesamtstrom = total current, Schweißstrom = welding current, Ruckenstrom = link back current, Elektroden = electrodes, Stauchstahlkraft = upsetting tool force, Gegenkraft . = chain link back reaction strength Sattel ¬ saddle

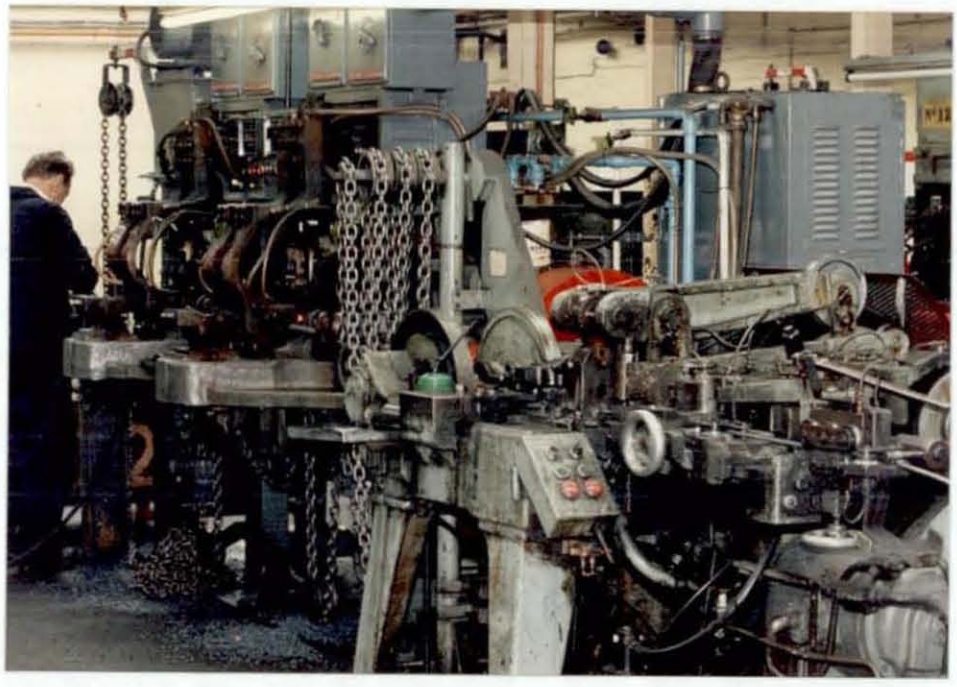

(a)

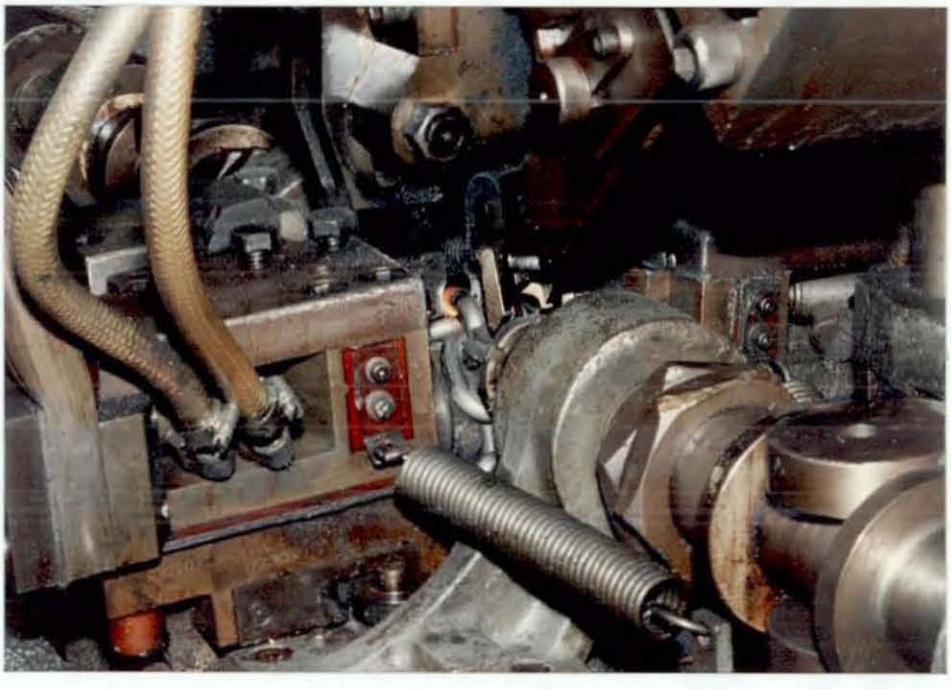

(b)

Fig. 2.9 a) Work station comprising of : wire drawing, forming, butt welding and trimming. b) Butt welding in one plane.

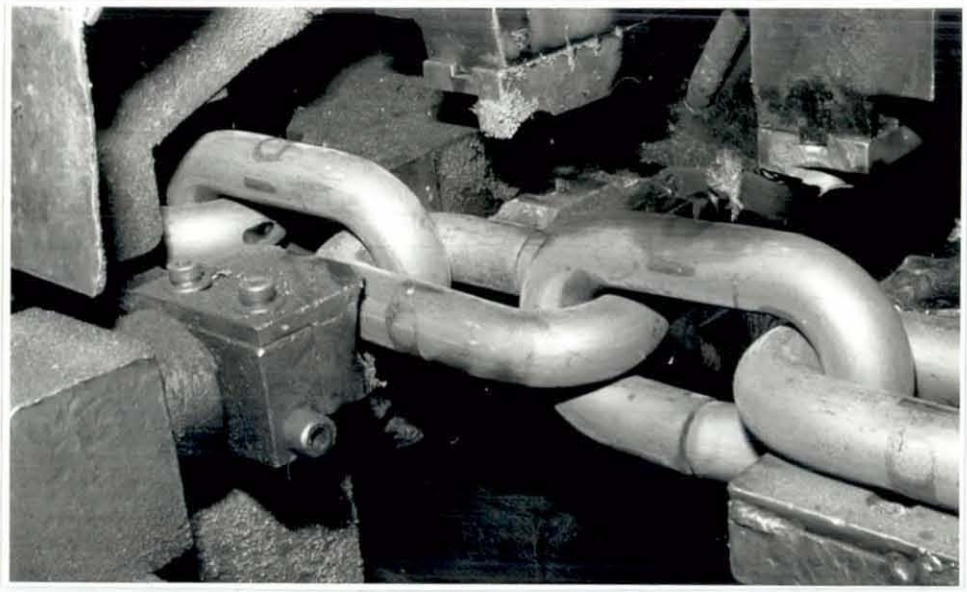

Fig. 2.10 Flash butt welding work station.

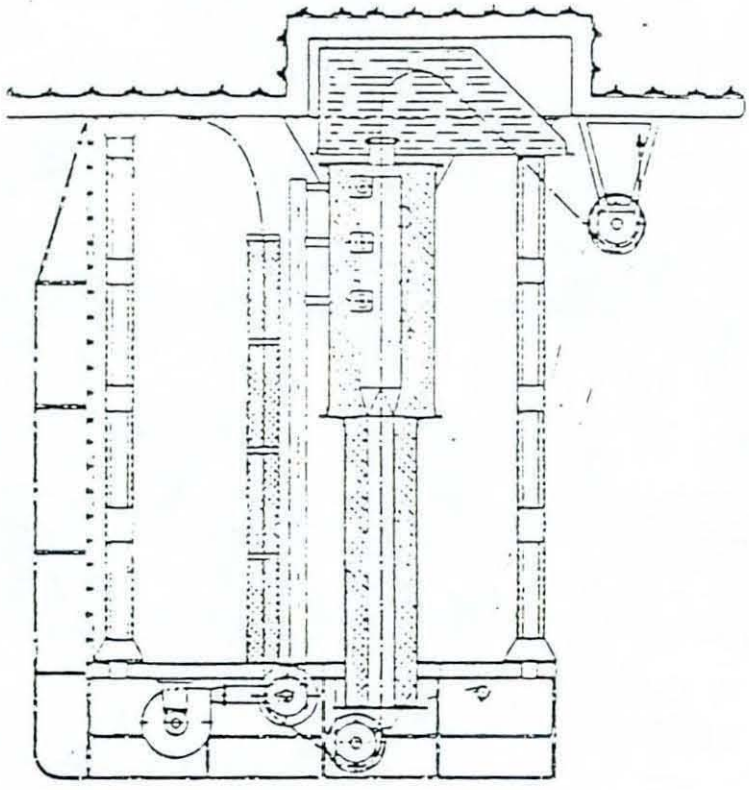

Fig. 2.11 Standard furnace with fuel heating.

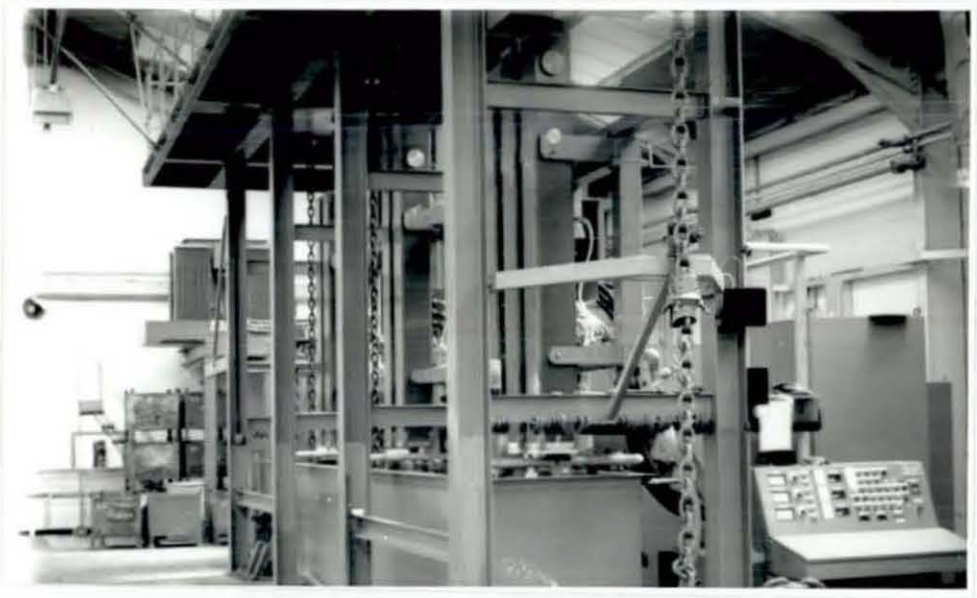

(a)

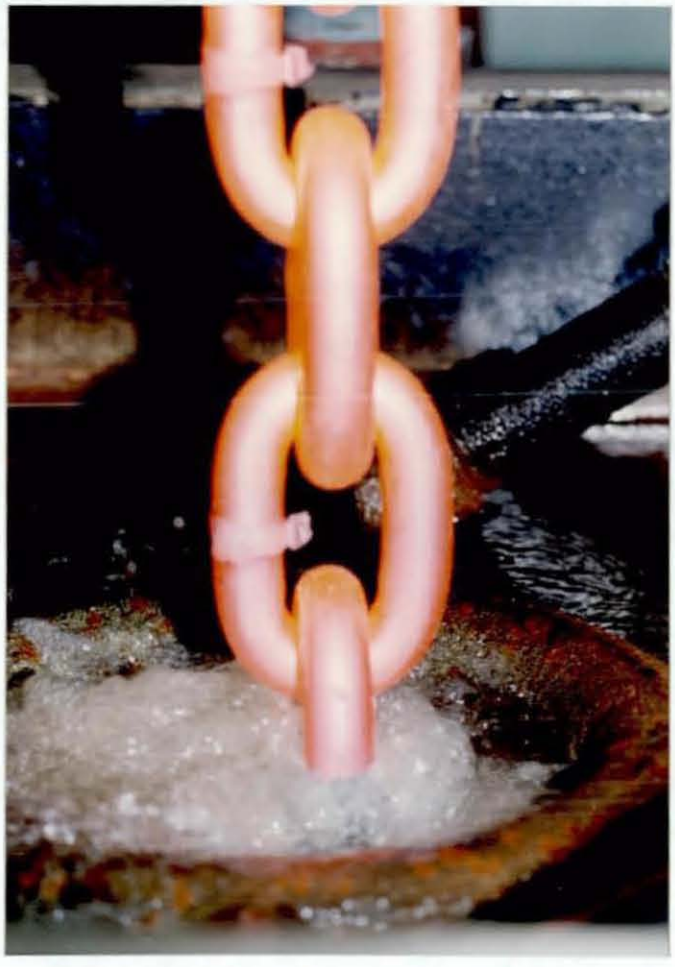

(b)

Fig. 2.12 a) Heat treatment centre (electrical induction) capable of continuous hardening and tempering of round link chains. b) Water quenching in the heat treatment centre at (a).

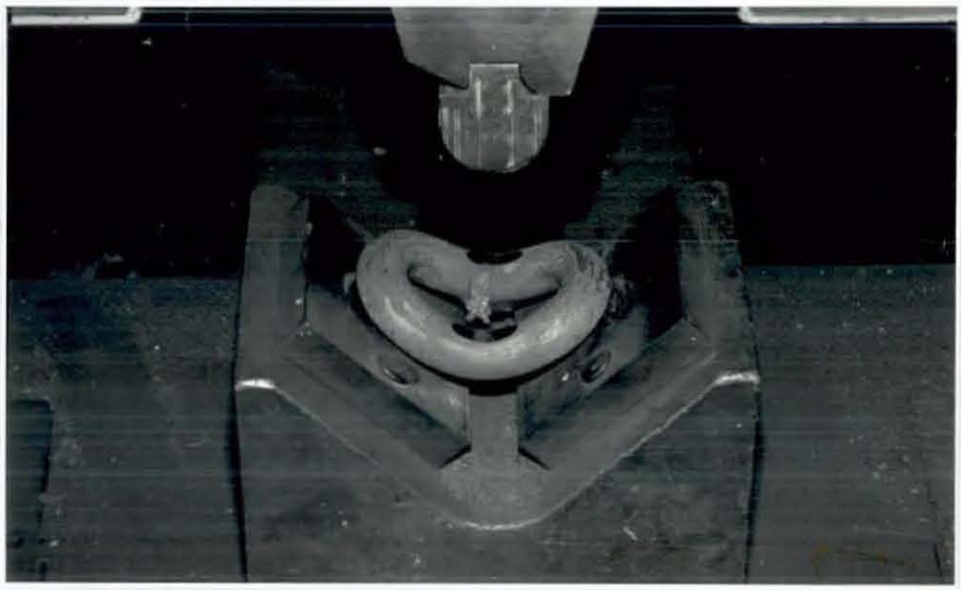

Fig. 2.13 Bend test of a single link.

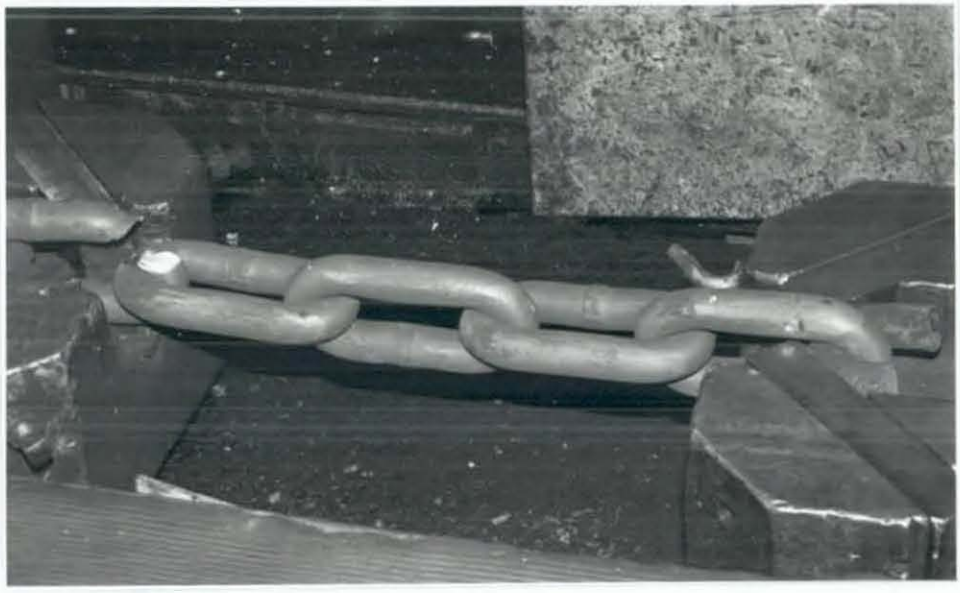

(a)

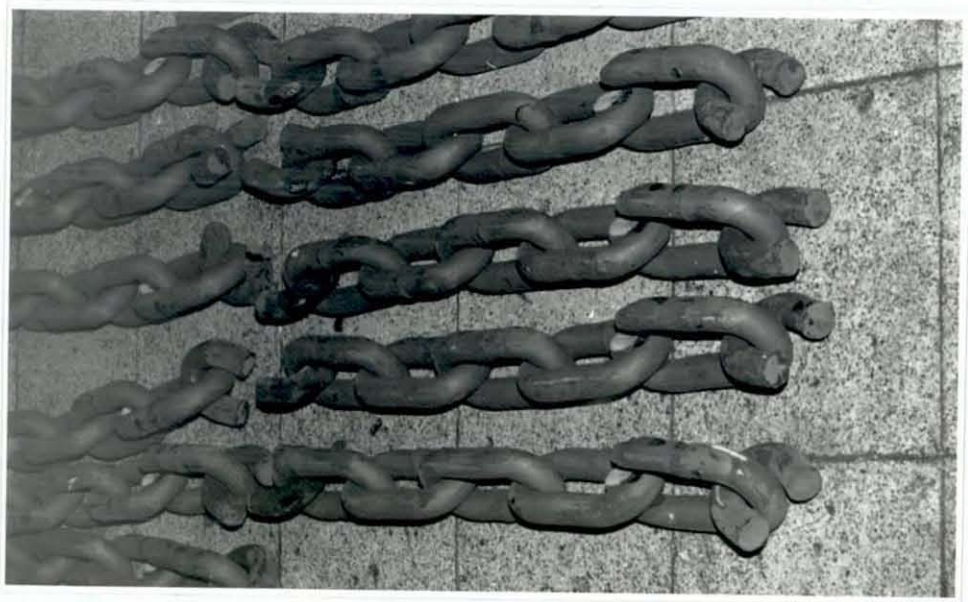

(b)

Fig. 2.14 a) Tensile testing of 5 links (100 tons Avery). b) "Pure" shear failure of chains under tensile loading.

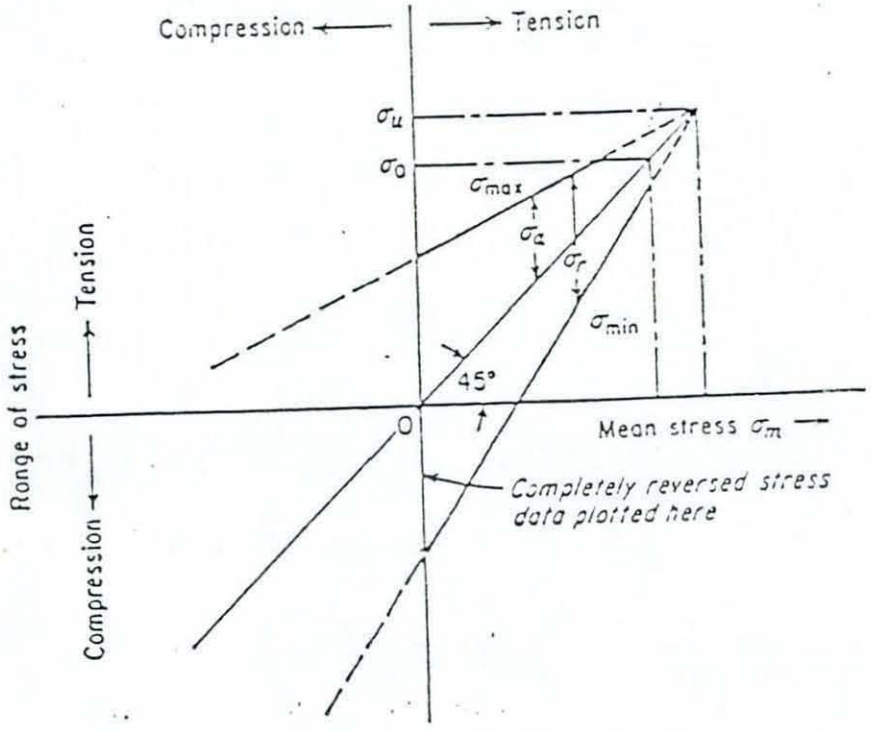

Fig. 3.1 Goodman diagram.

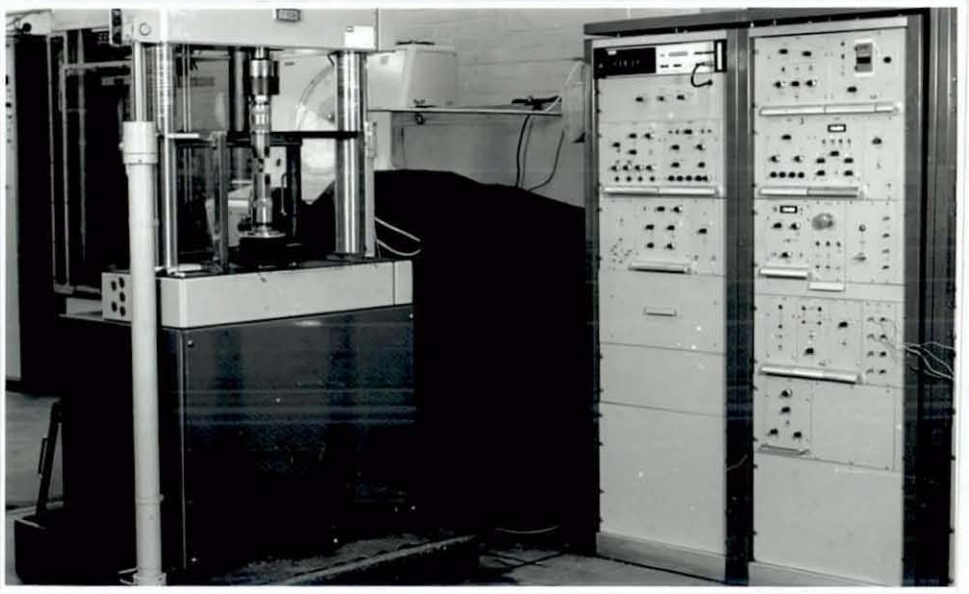

Fig. 3.2 Mayes machine, control and the signal generator.

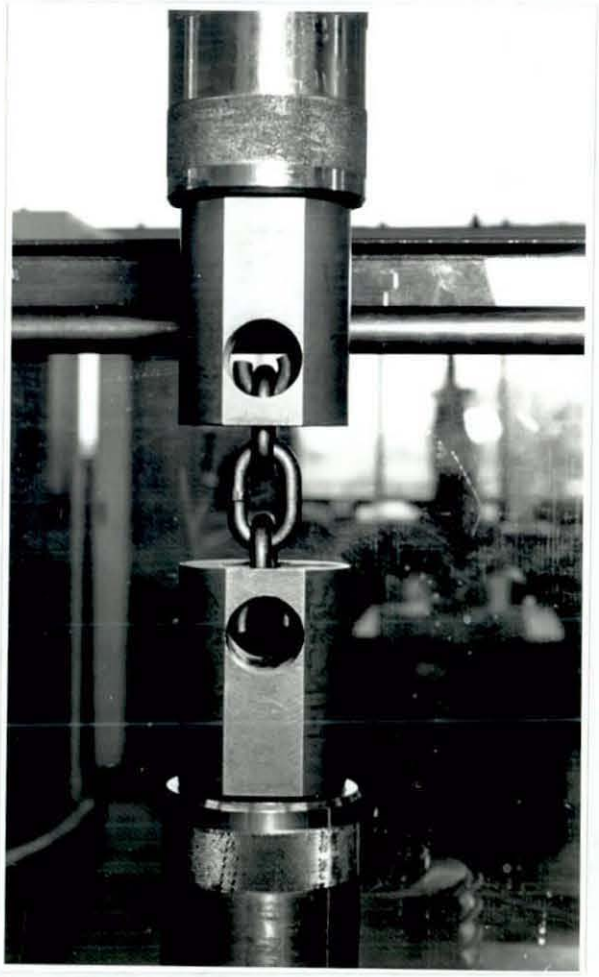

Fig. 3.3a Specially designed grips with crowns of chain link (holding arrangement).

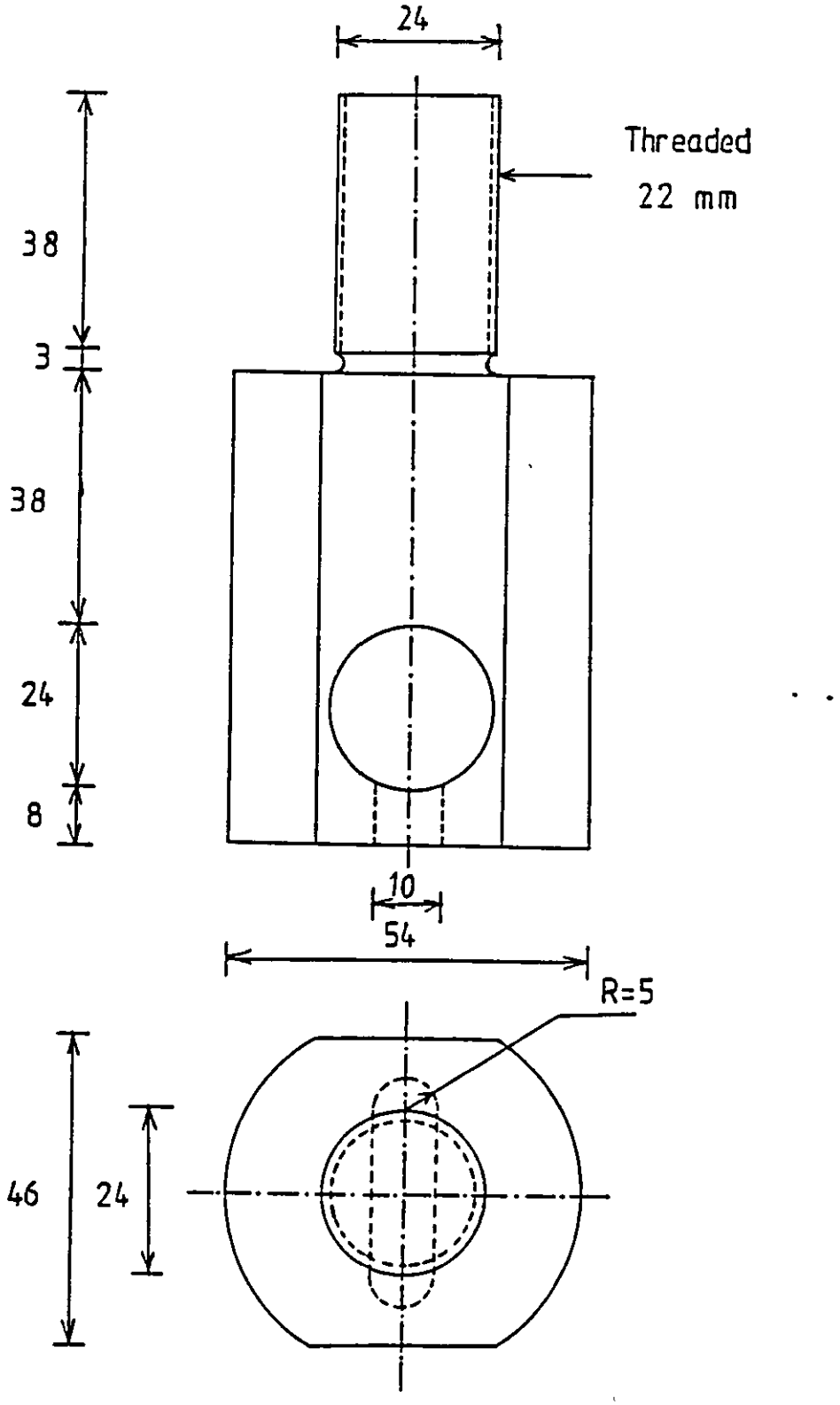

Fig. 3.3b Detail drawing of the grips (all dimensions in mm).

Batch	Centre or End	Location	Calibration load, kN					
			0	20	30	38.5	50	Total
1	Centre	Trans.	12	2	3	4	3	24
		Crown	2	0	8	7	1	18
		Weld	5	0	9	7	8	29
	End	Trans.	21	4	15	3	5	48
		Crown	3	0	4	8	10	25
		Weld	17	4	11	8	3	43
2	Centre	Trans.	0	0	0	1	2	3
		Crwon	0	0	0	0	1	1
		Weld	15	0	11	5	2	33
	End	Trans.	0	0	4	2	2	8
		Crown	0	0	0	0	7	7
		Weld	4	0	10	2	11	27
Total			79	10	75	47	55	266

Table 3.1 A Minitab output of the fatigue testing results of the 7 mm lifting chain showing the effect of calibration on number of fractures.

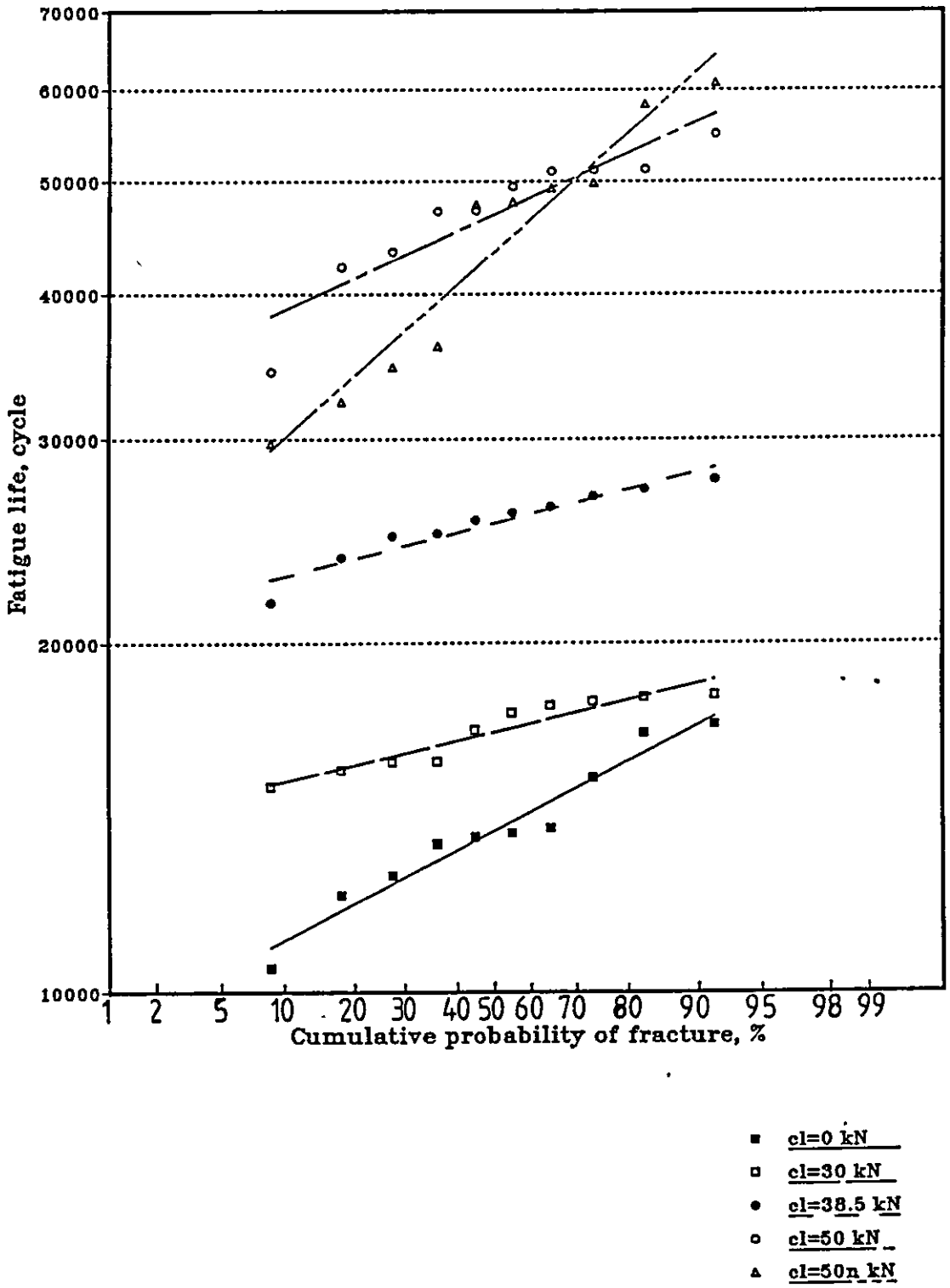

Fig. 3.4 Cumulative probability of failure at a load range of 2–24 kN (nominal stress.27–321 MPa) for various calibration loads,cl. n Implies that the sample is from the batch 2.

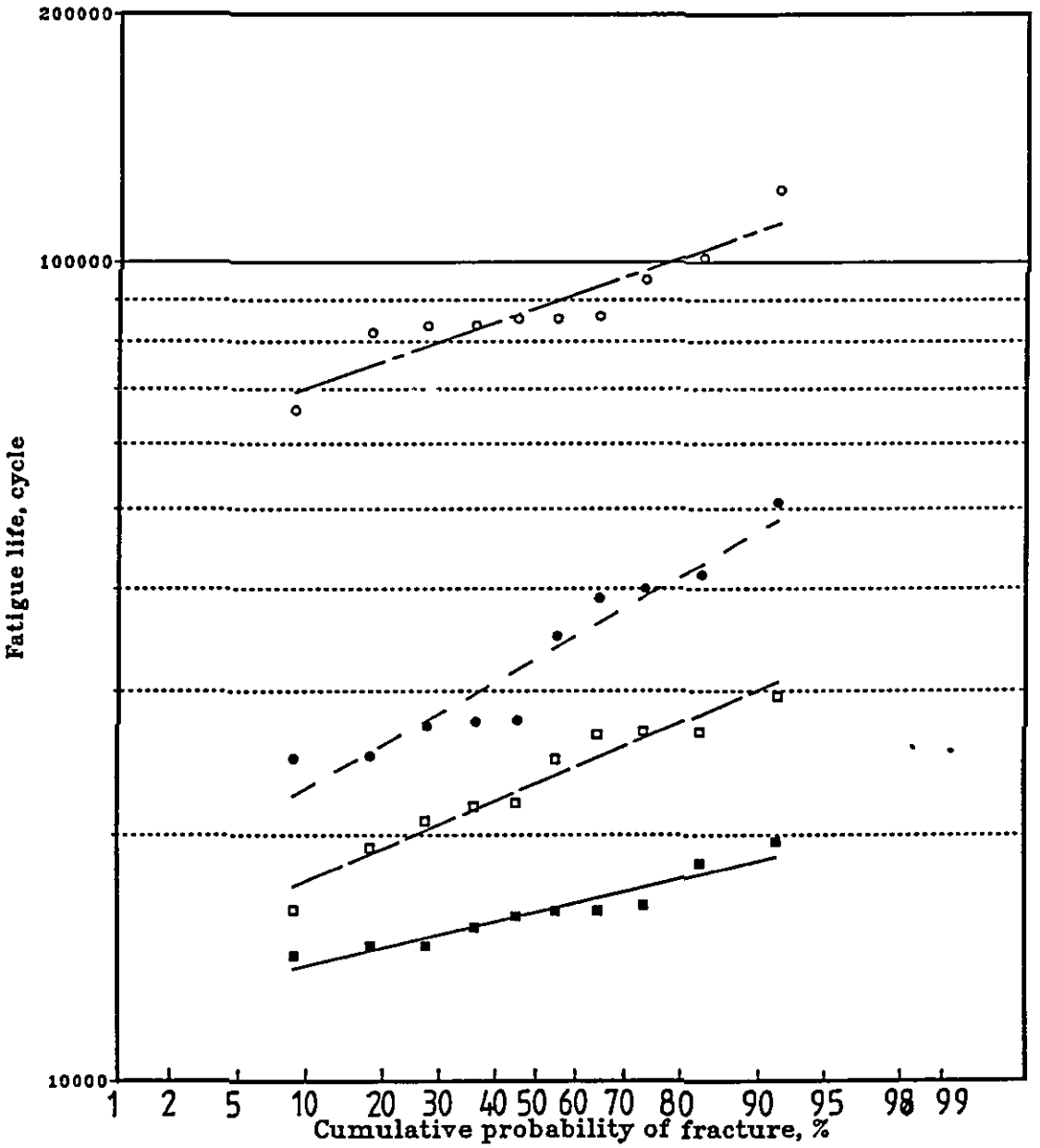

Fig. 3.5 Cumulative probability of failure at a load range of 2–22 kN (nominal stress, 27–294 MPa) for various calibration loads, cl.

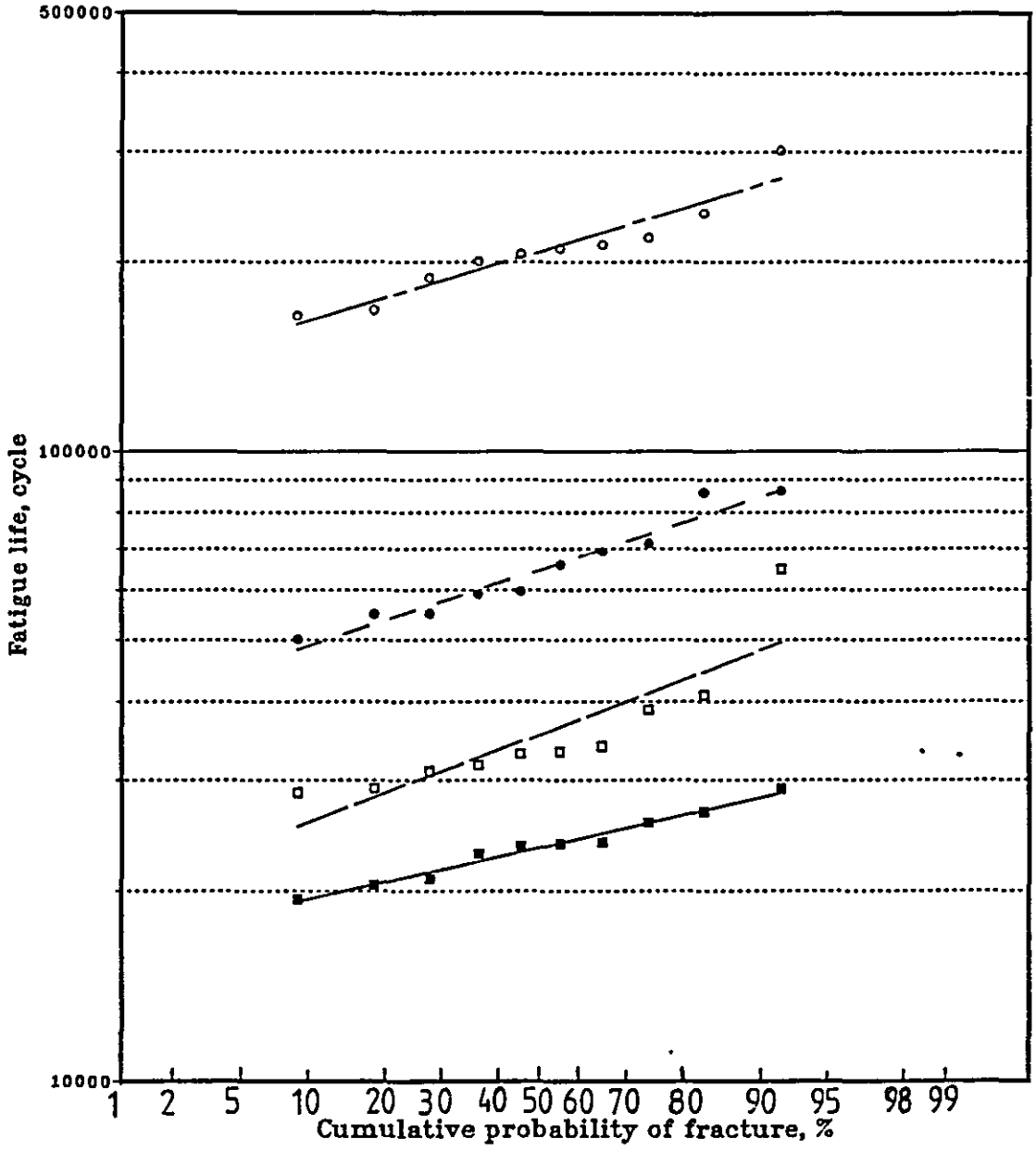

Fig. 3.6 Cumulative probability of failure at a load range of 2–20 kN (nominal stress.27–267 MPa) for various,calibration loads,cl. n implies that the sample is from the batch 2.

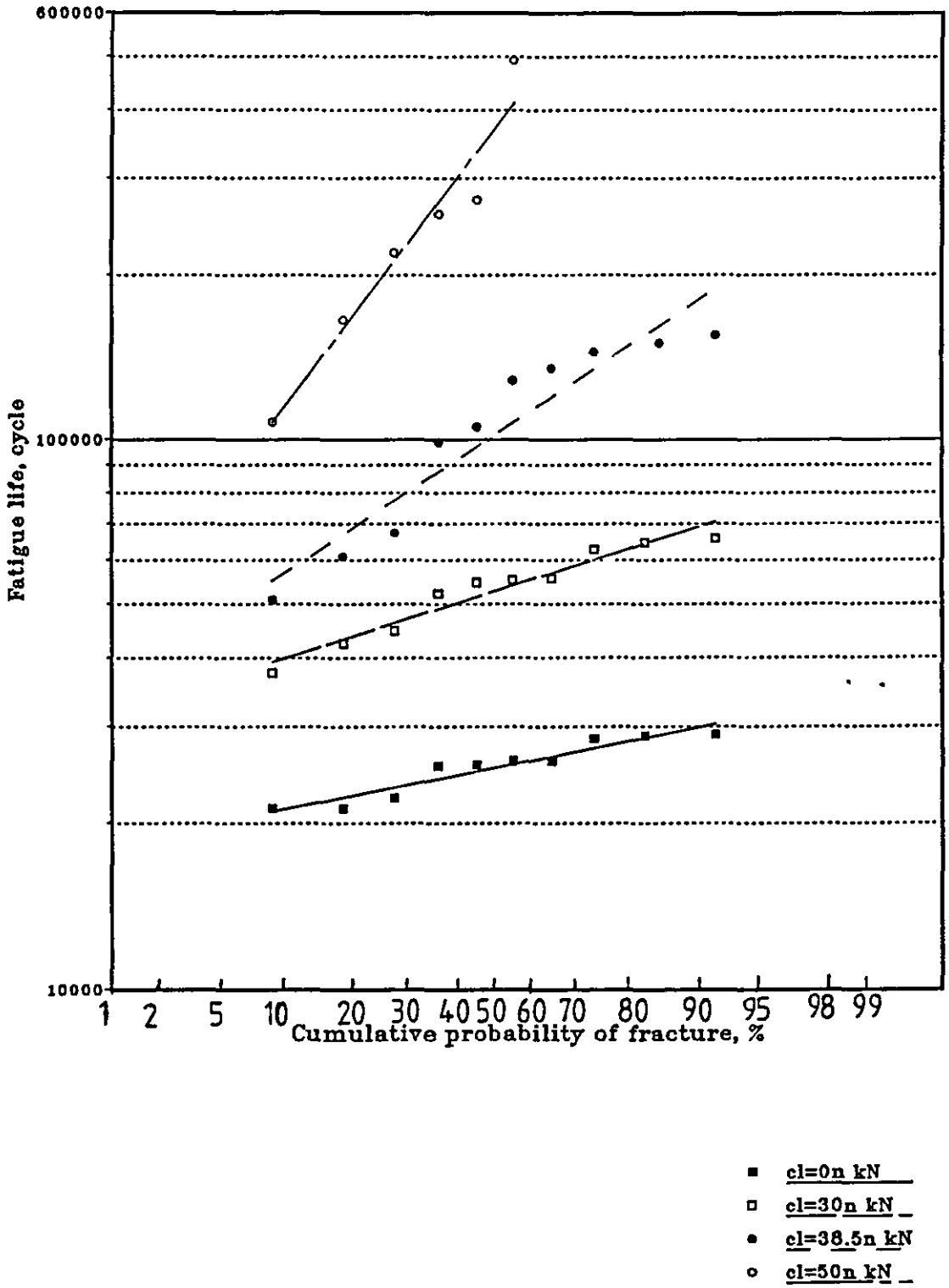

Fig. 3.7 Cumulative probability of failure at a load range of 2–18 kN (nominal stress, 27–241 MPa) for various calibration loads, cl. n implies that the sample is from the batch 2.

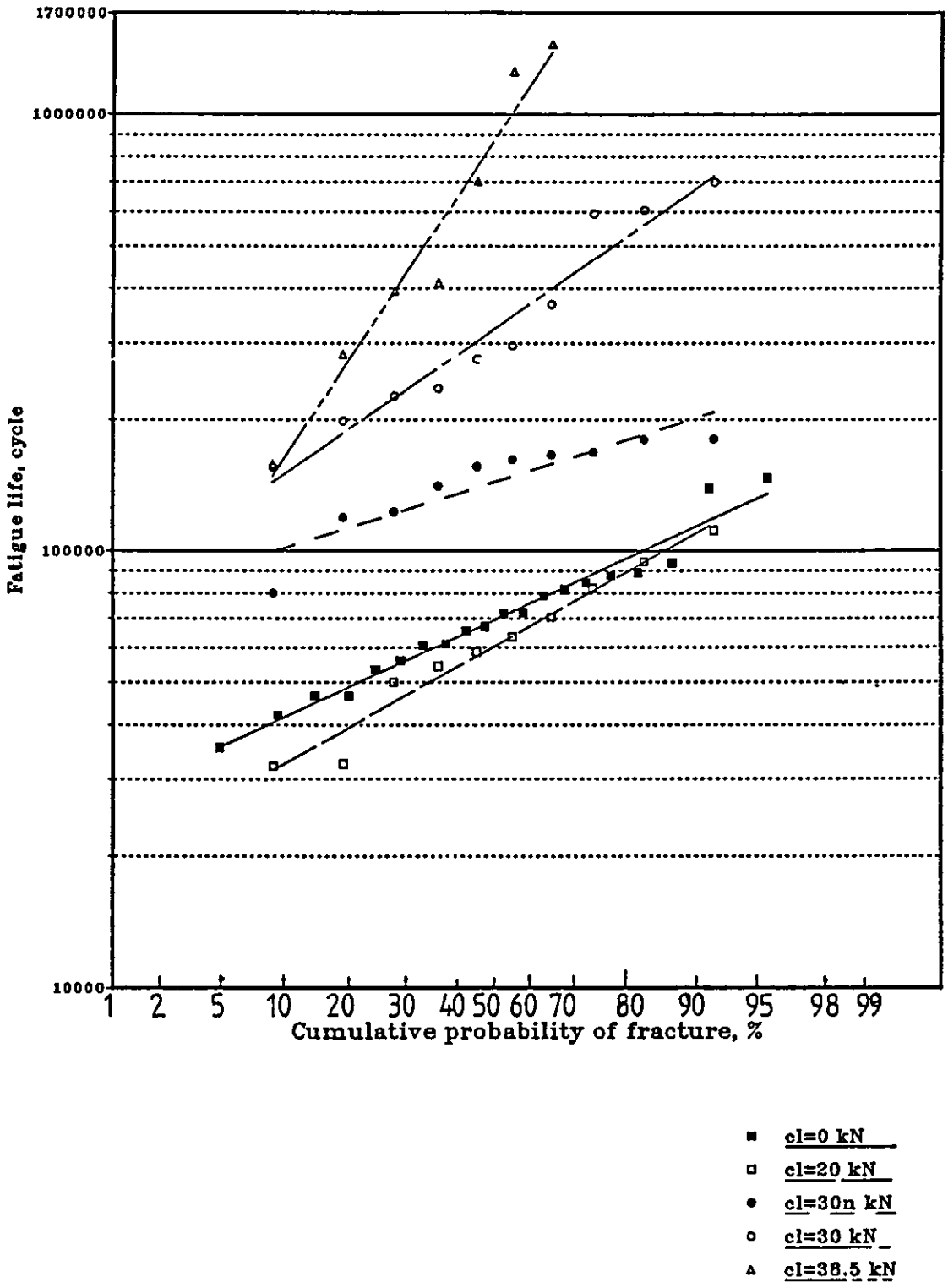

Fig. 3.8 Cumulative probability of failure at a load range of 2–16 kN (nominal stress, 27–214 MPa) for various calibration loads, cl. n implies that the sample is from the batch 2.

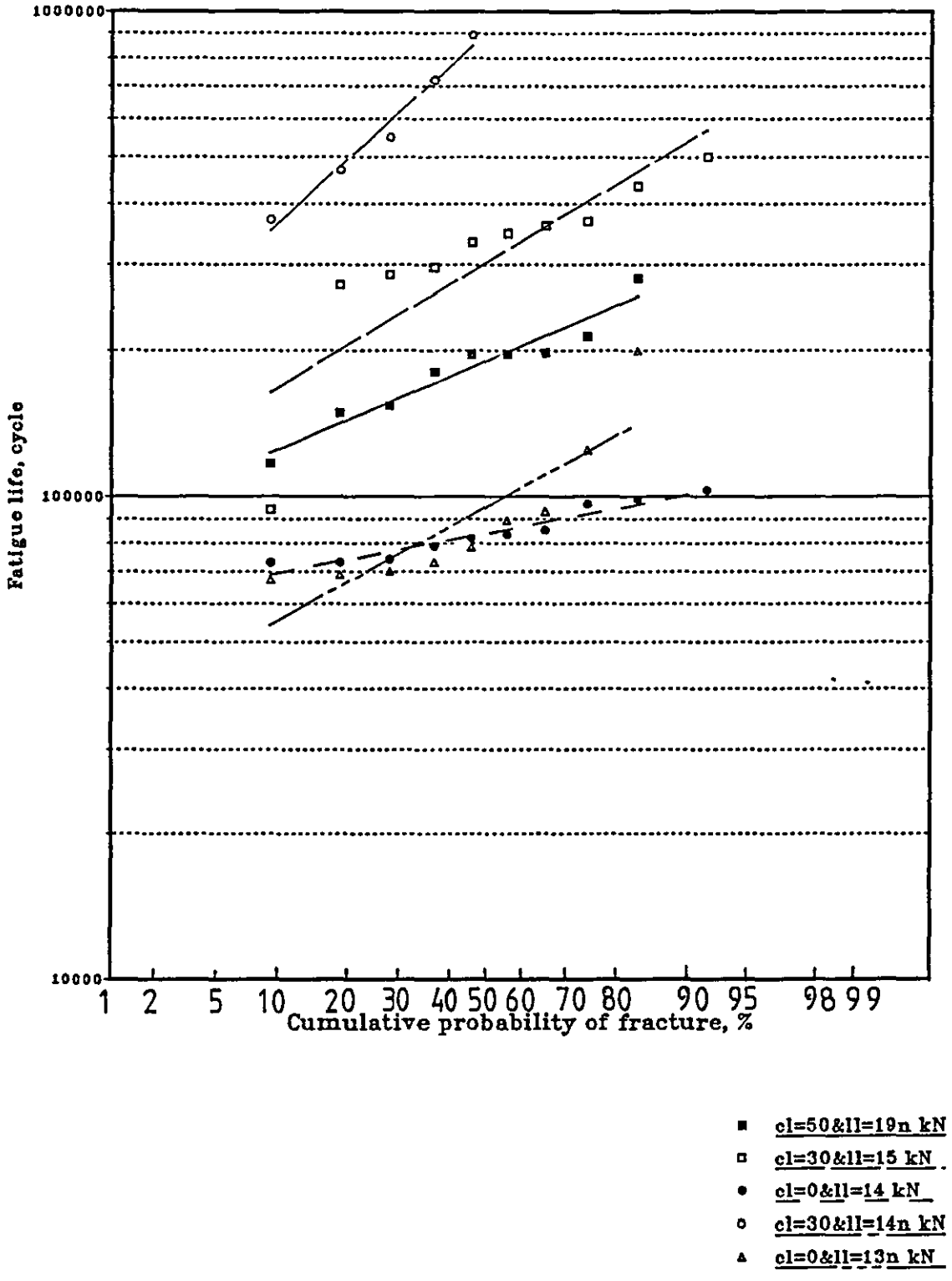

Fig. 3.9 Cumulative probability of failure at a load range of 2-19,15,14 ,13 kN (nominal stress, 27-254,201,187,174 MPa) for various calibration load, cl, kN. n Implies that the sample is from the batch 2.

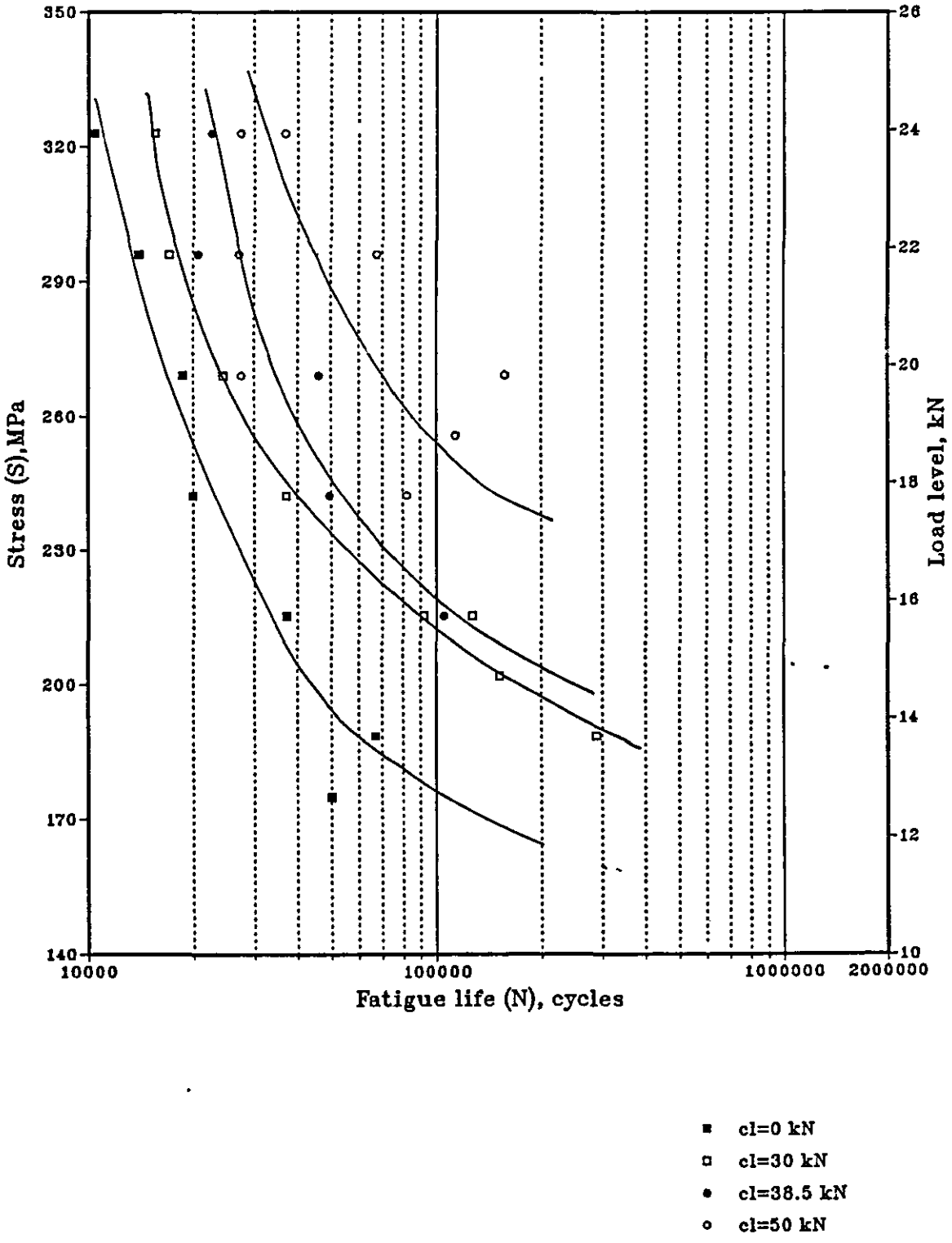

Fig. 3.10 S–N Curve for 5 % probability of failure for various calibration loads (cl). All specimens were unbroken after two million cycles at a loading of 2–12 kN.

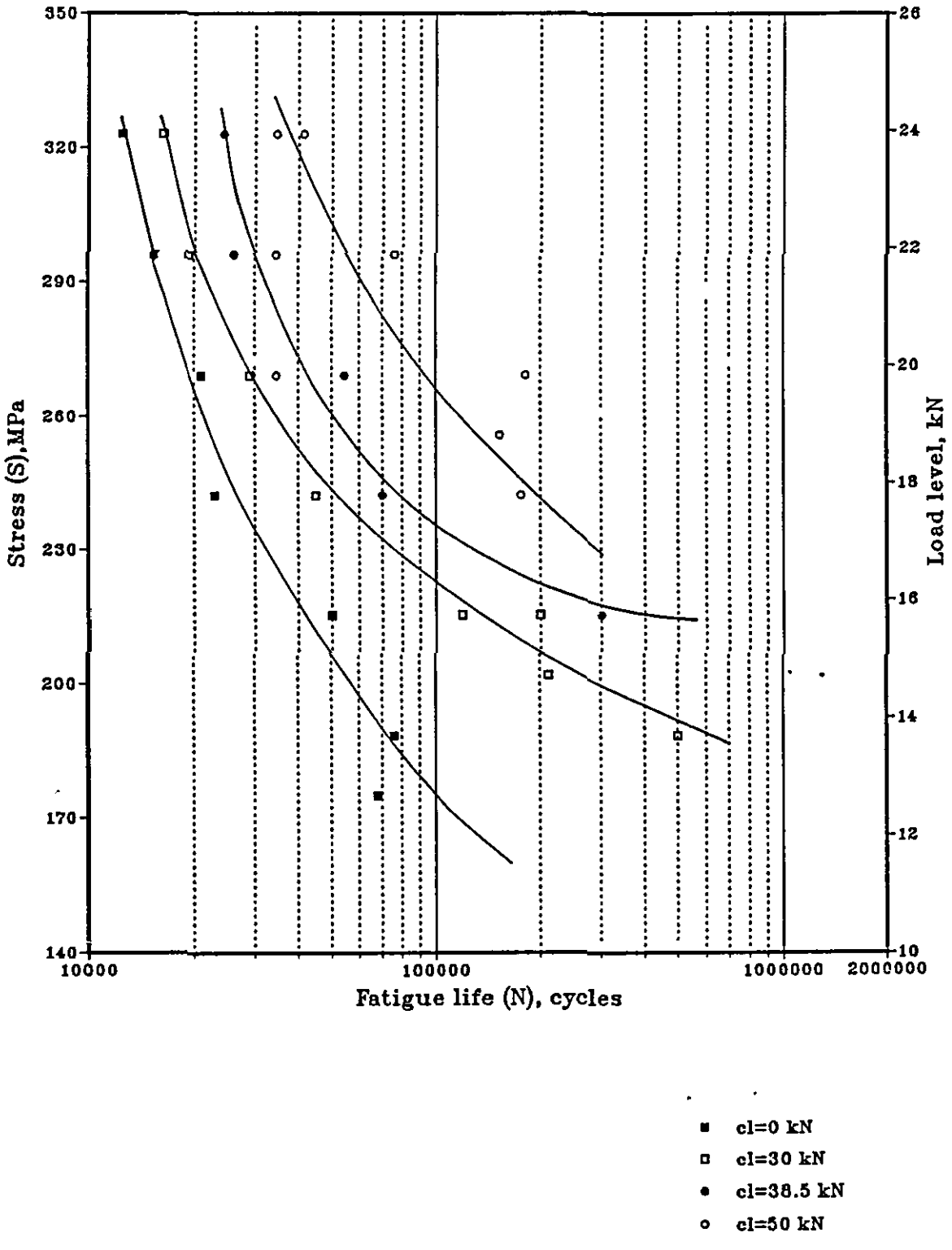

Fig. 3.11 S–N Curve for 20 % probability of failure for various calibration loads (cl). All specimens were unbroken after two million cycles at a loading of 2–12 kN.

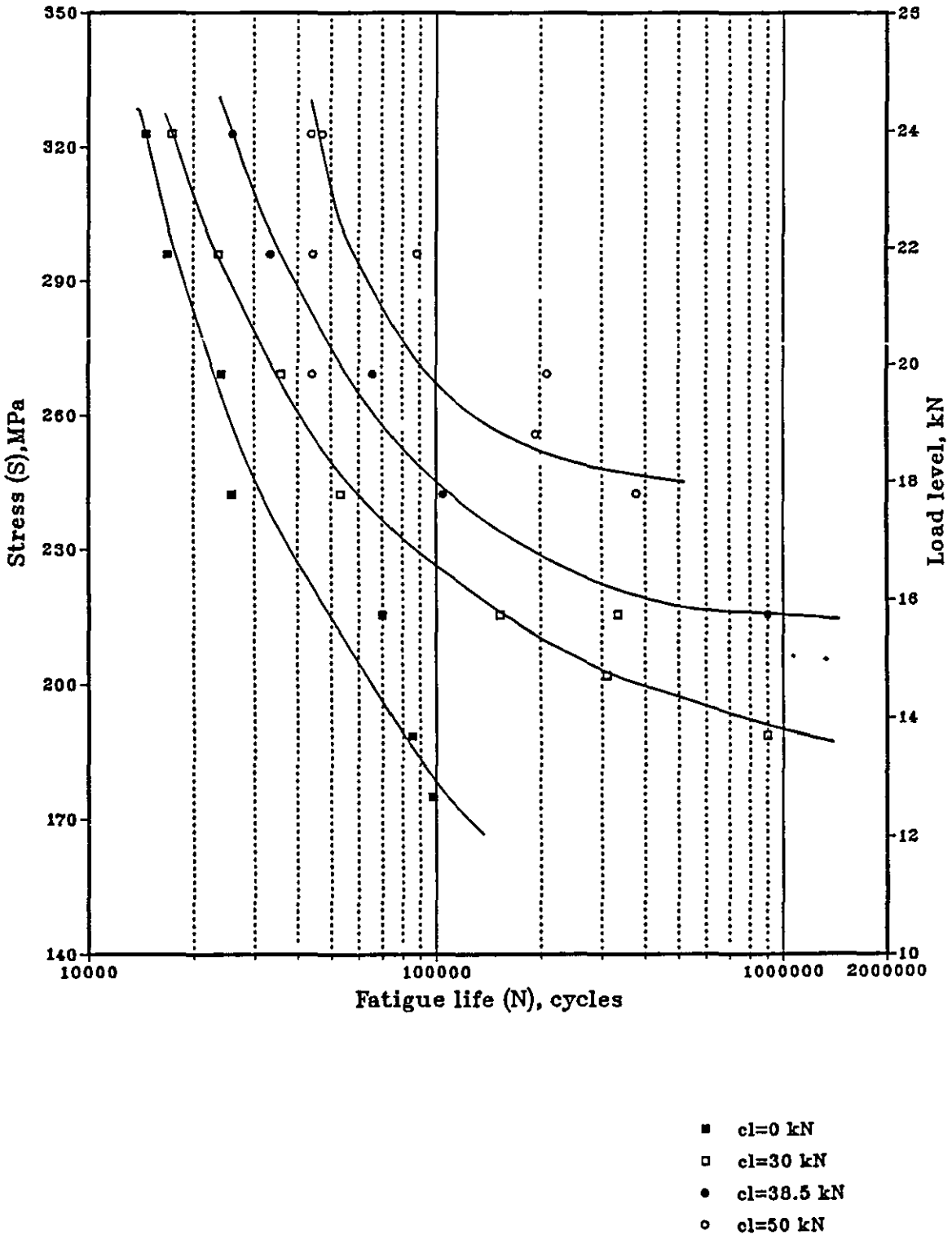

Fig. 3.12 S–N Curve for 50 % probability of failure for various calibration loads (cl). All specimens were unbroken after two million cycles at a loading of 2–12 kN.

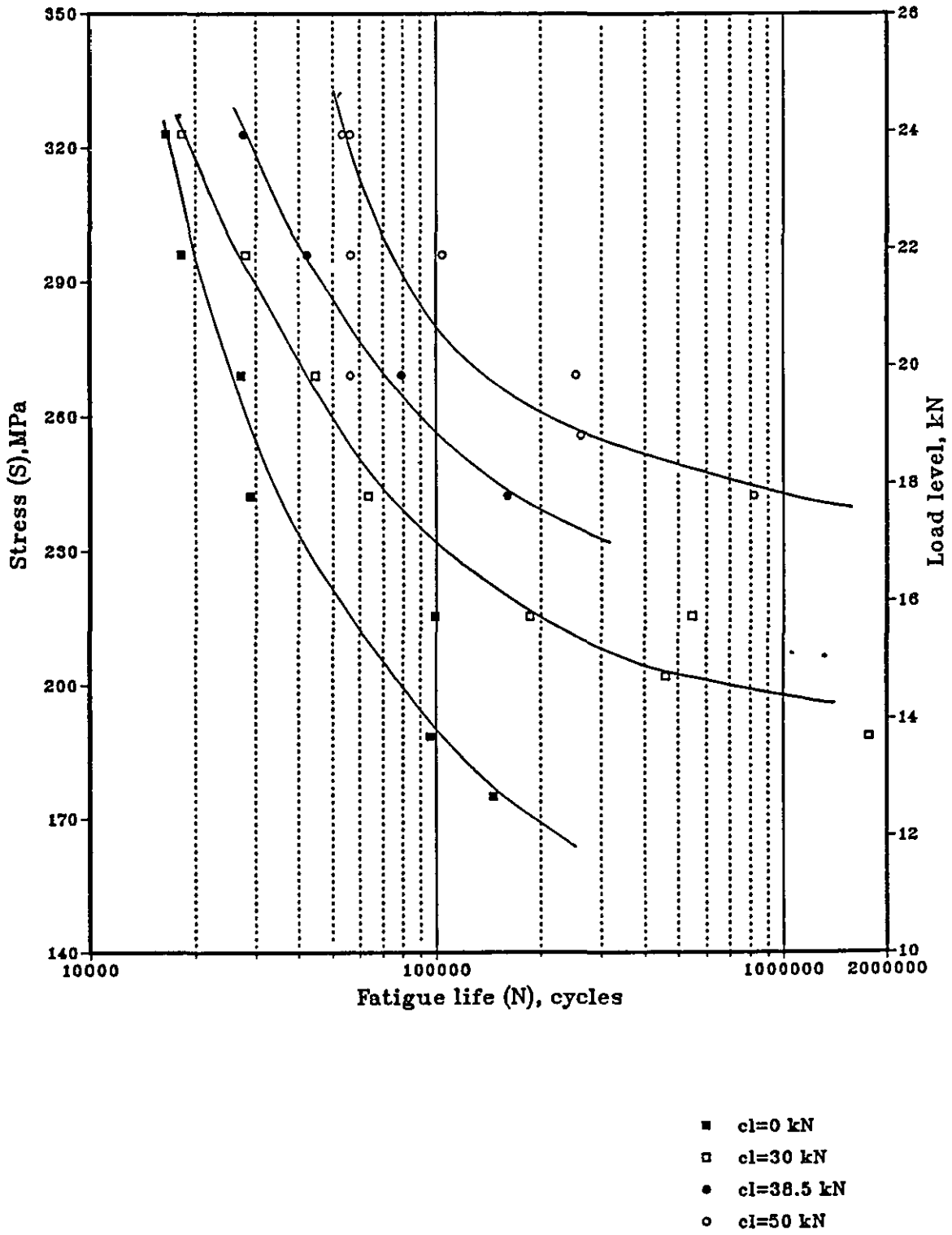

Fig. 3.13 S–N Curve for 80 % probability of failure for various calibration loads (cl). All specimens were unbroken after two million cycles at a loading of 2–12 kN.

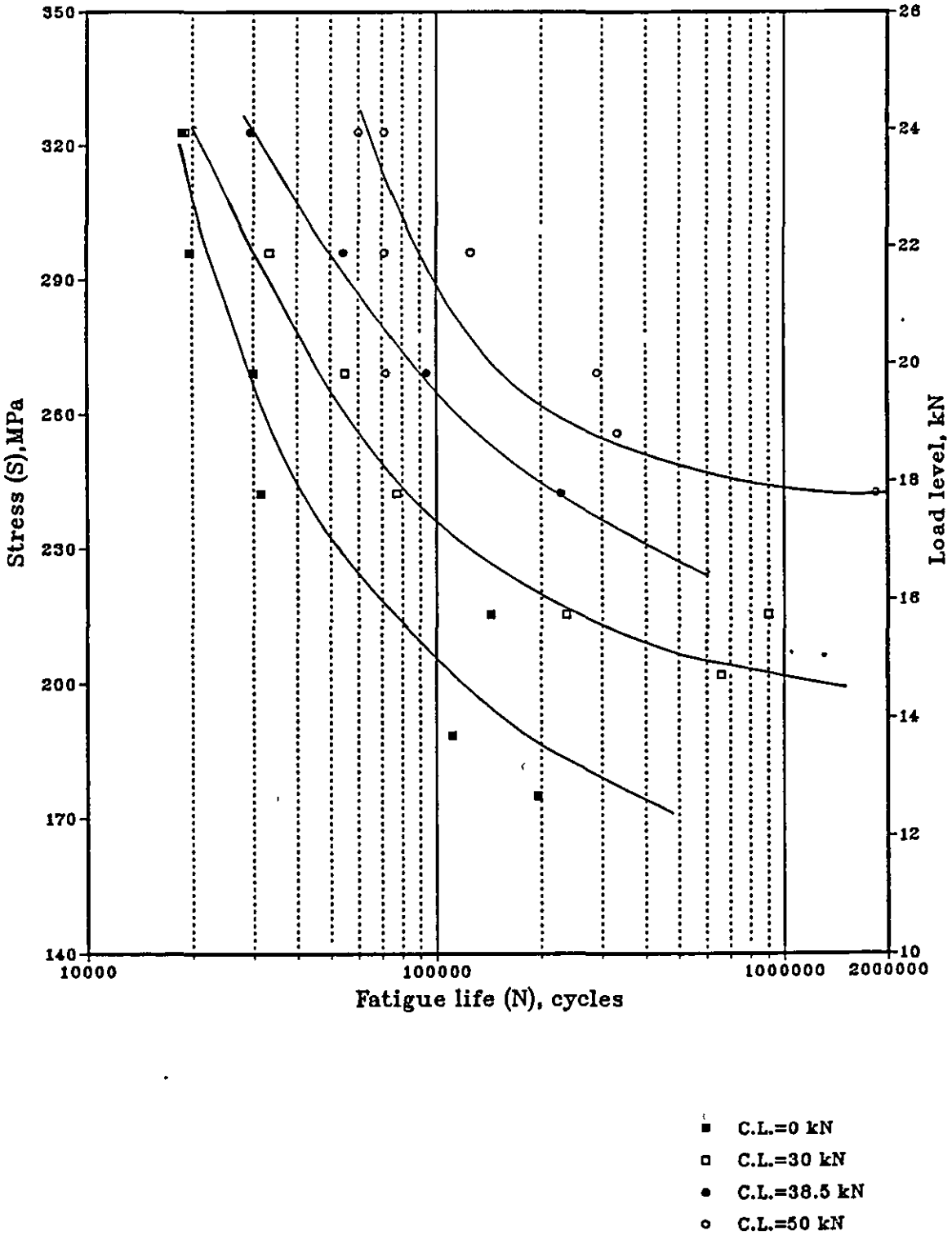

Fig. 3.14 S–N Curve for 95 % probability of failure for various calibration loads (cl). All specimens were unbroken after two million cycles at a loading of 2–12 kN.

Fig. 3.15 Typical chain fatigue fracture surface showing rough and smooth regions.

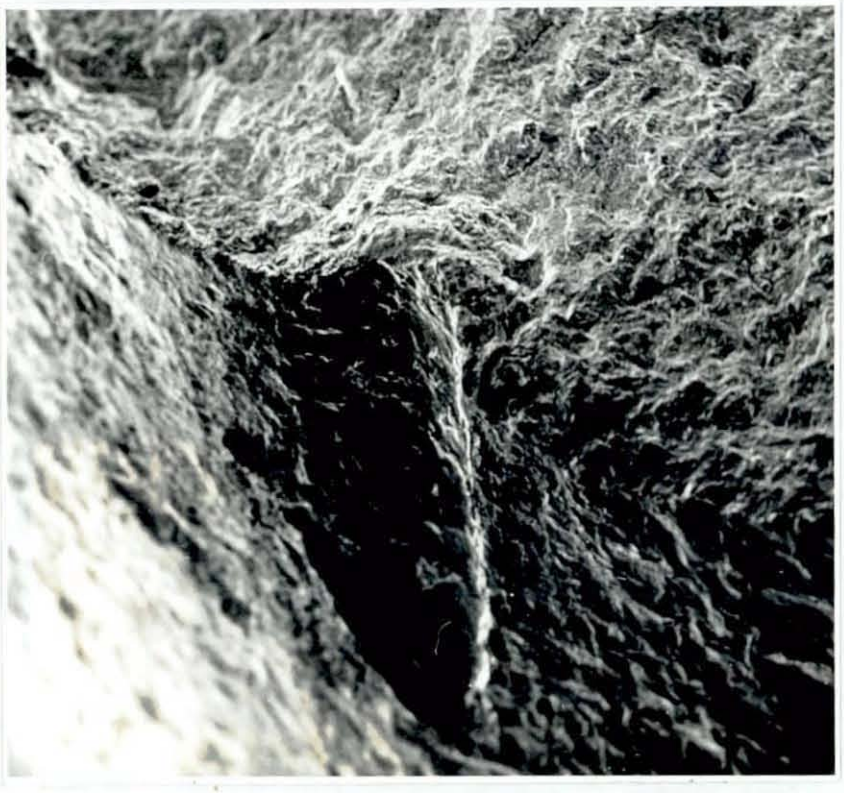

Fig. 3.18 Fracture initiation from an existing dent, also beach markings can be seen at the transition zone (magnification factor 65).

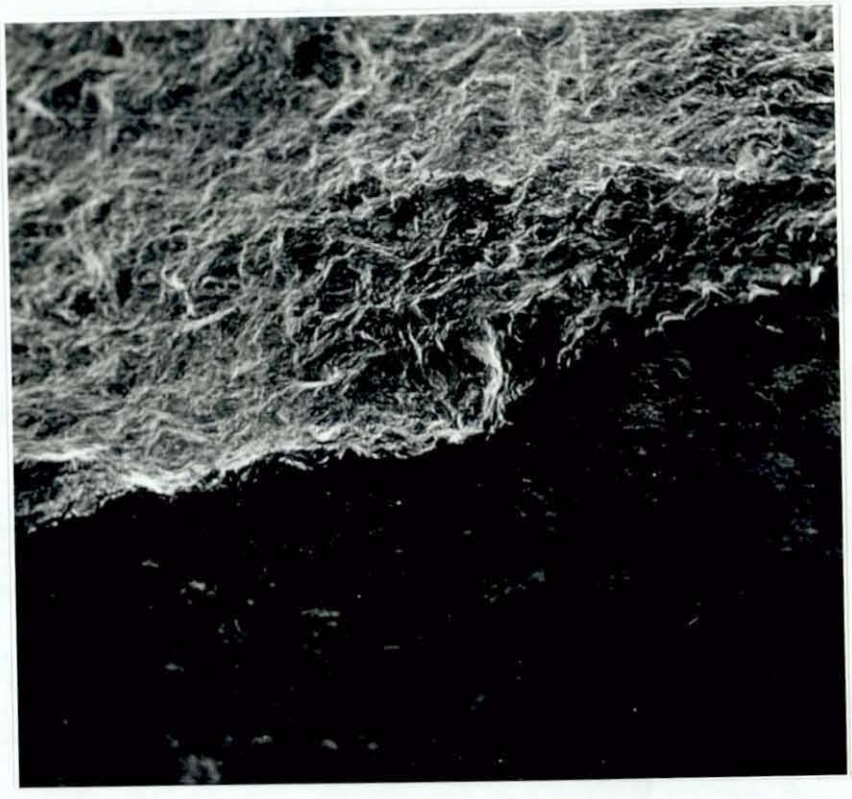

Fig. 3.19 Possible fracture initiation zone showing beach marking at the transition zone (magnification factor 130).

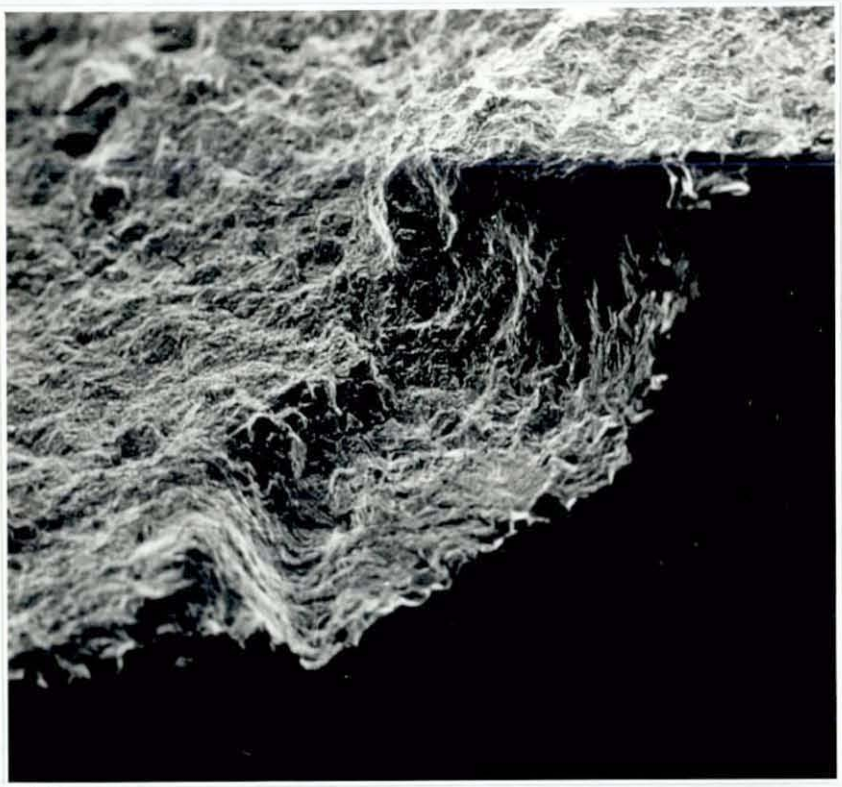

Fig. 3.16 Fracture initiation from an existing dent at the weld (magnification factor 130).

Fig. 3.17 Fracture initiation at two possible locations and rachet markings at the weld (magification factor 25).

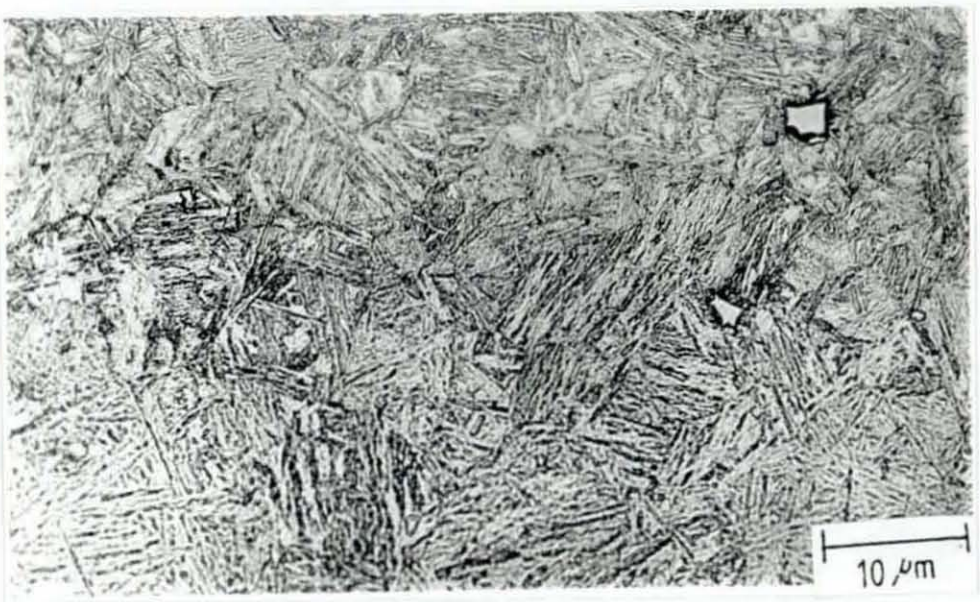

Fig. 3.20a General quenched and tempered structure (containing inclusions).

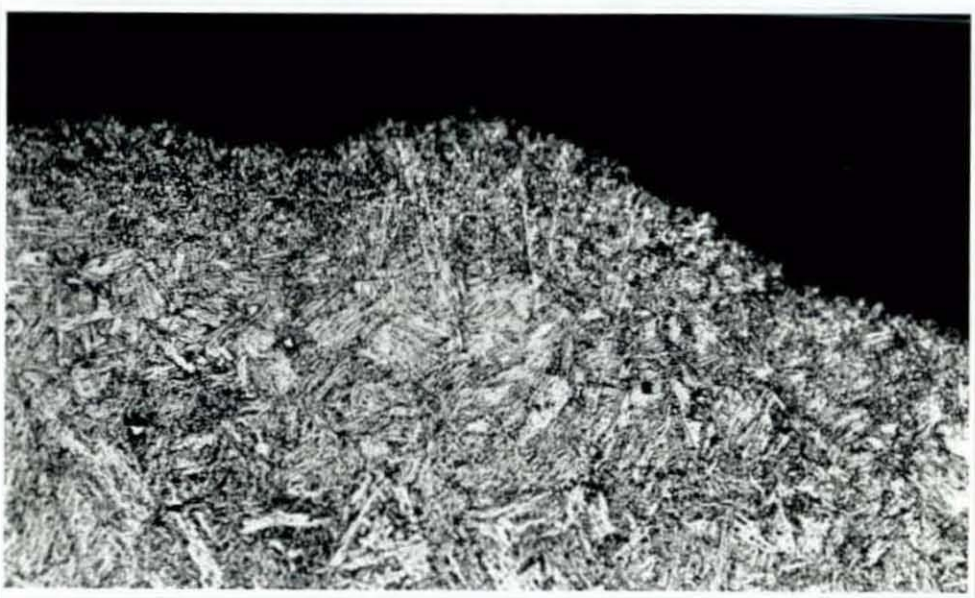

Fig. 3.20b The cross-section of a chain link with thickened grain boundries at the edge.

Fig. 3.21 Different locations of the fatigue fracture.

Fig. 3.22 Location of fracture in chain due to tensile (left) testing and fatigue testing.

Location of Fracture	Load level, kN								
	13	14	15	16	18	19	20	22	24
Trans.	0.0	73.3	80.0	54.4	22.2	11.1	22.2	20.0	14.0
Crown	0.0	0.0	0.0	14.0	5.6	66.7	25.0	35.0	22.0
Weld	100.	26.7	20.0	31.6	72.2	22.2	52.5	45.0	64.0
Centre	88.9	20.0	10.0	47.4	55.6	22.2	17.5	47.5	42.0
End	11.1	80.0	90.0	52.6	44.4	77.8	82.5	52.5	58.0

Table 3.2 Effect of load level, and centre and end links on the fracture location (in percentage).

Location of fracture	Calibration load, kN				
	0	20	30	38	50
Trans.	41.8	60.0	29.3	21.3	21.8
Crown	6.3	0.0	16.0	31.9	34.6
Weld	51.9	40.0	54.7	46.8	43.6
Centre	43.0	20.0	41.3	51.1	30.9
End	57.0	80.0	58.7	48.9	69.1

Table 3.3 Effect of calibration load and centre and end links on the fracture location (in percentage).

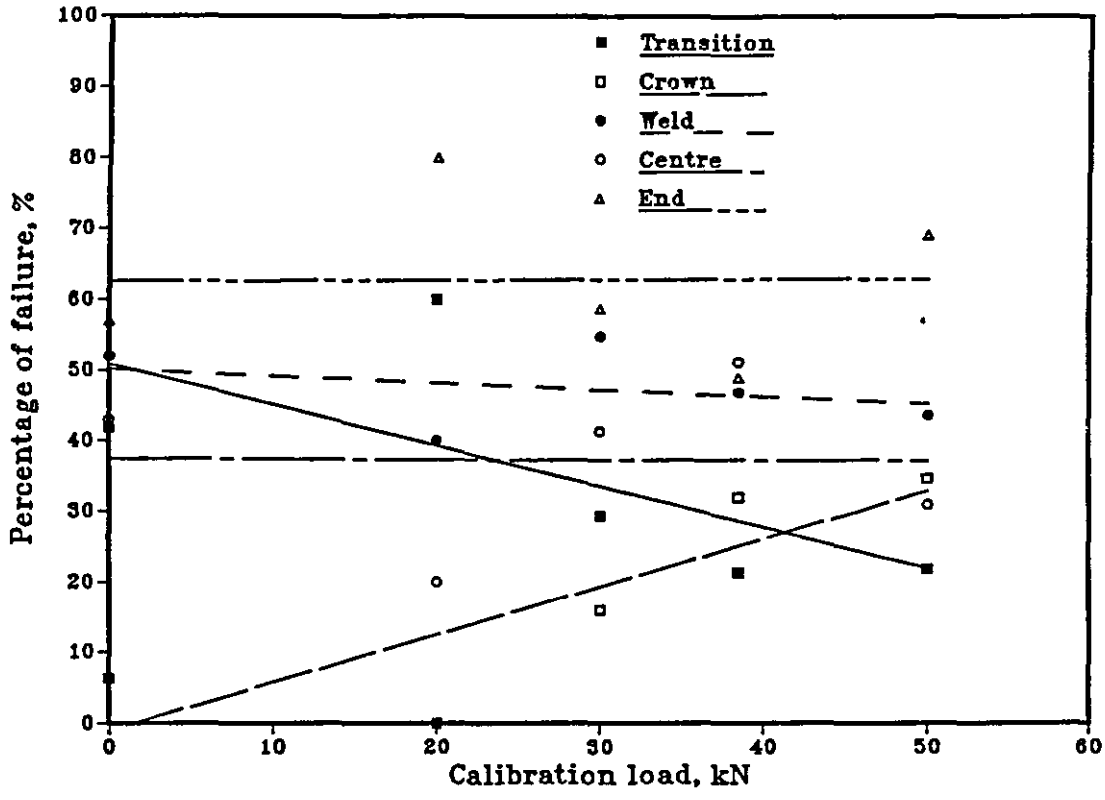

Fig. 3.23 Effect of calibration load on the position of fatigue fracture (transition, crown, weld, centre and end).

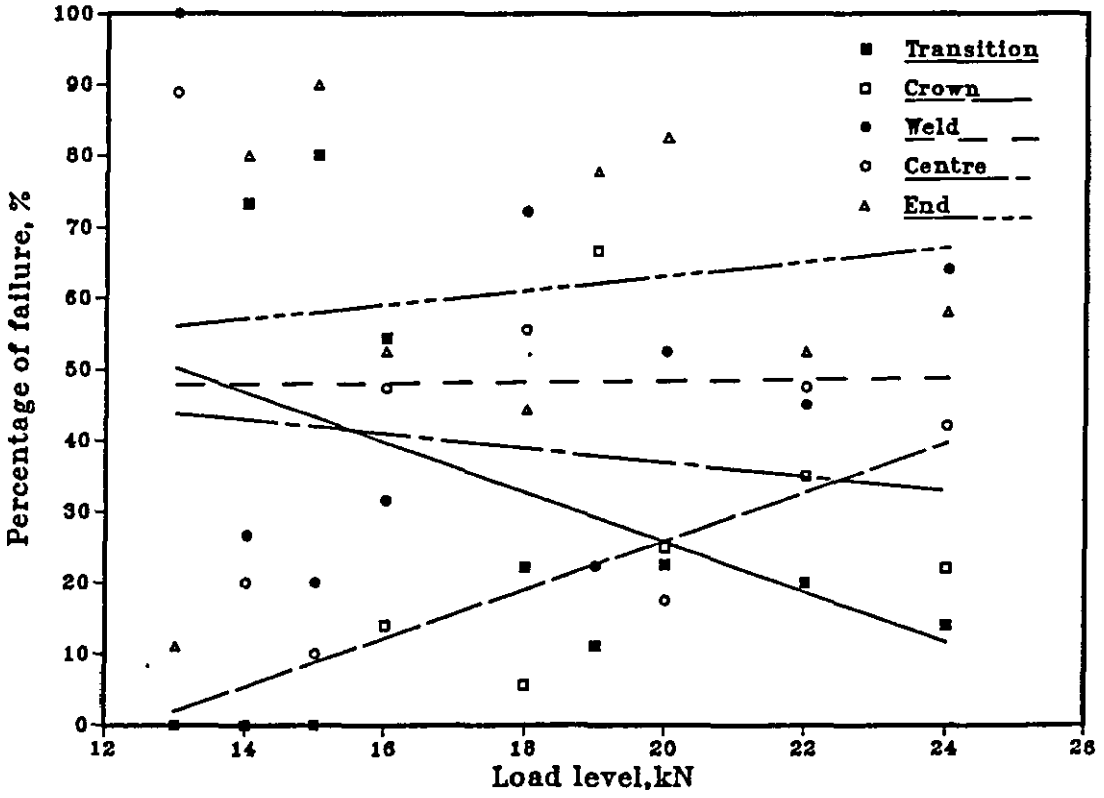

Fig. 3.24 Effecf of load level on the position of fatigue fracture (transition, crown, weld, centre and end).

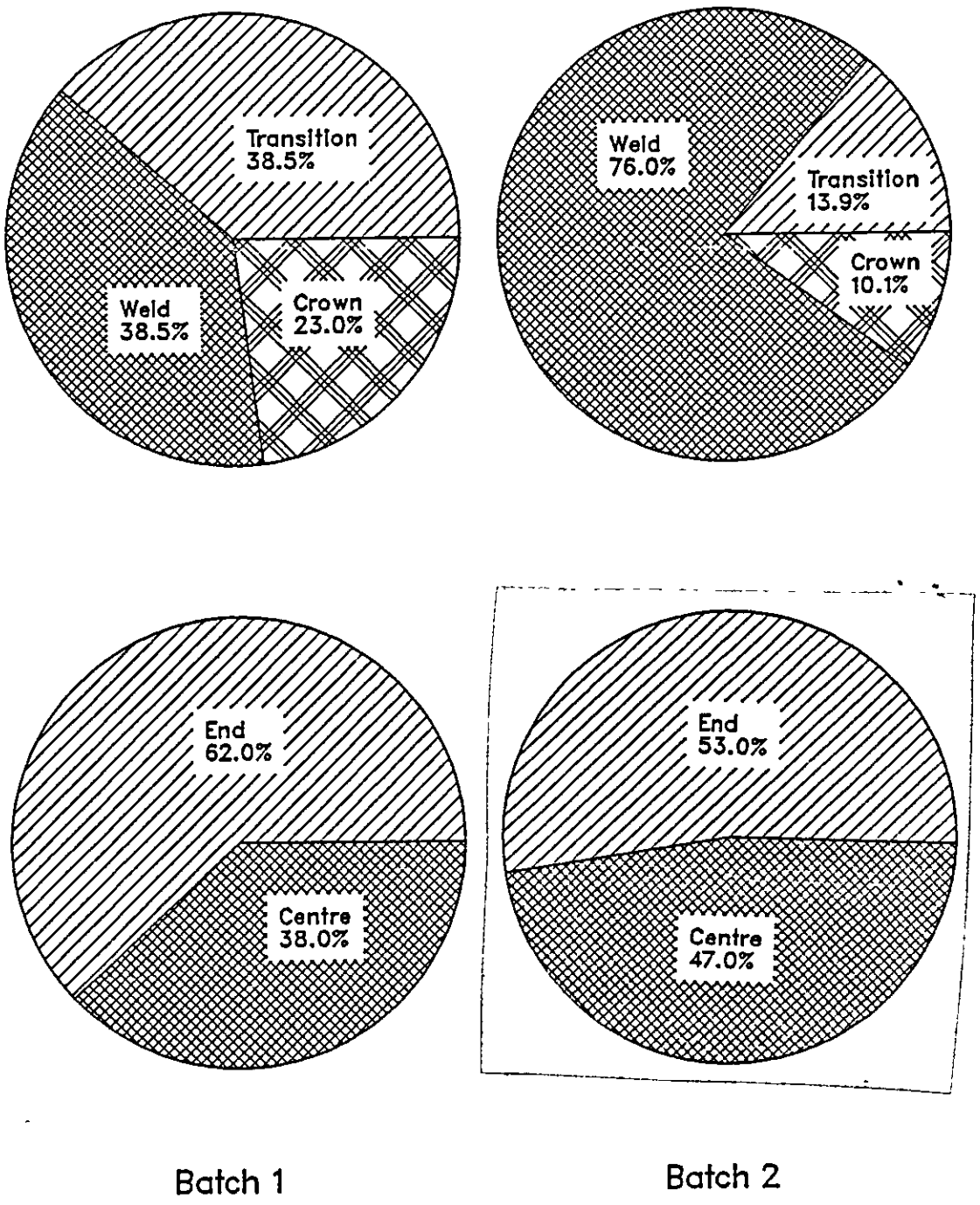

Fig. 3.25 Effect of different batches of chain on the position of the fatigue fracture (transition, weld and crown regions and centre and end links).

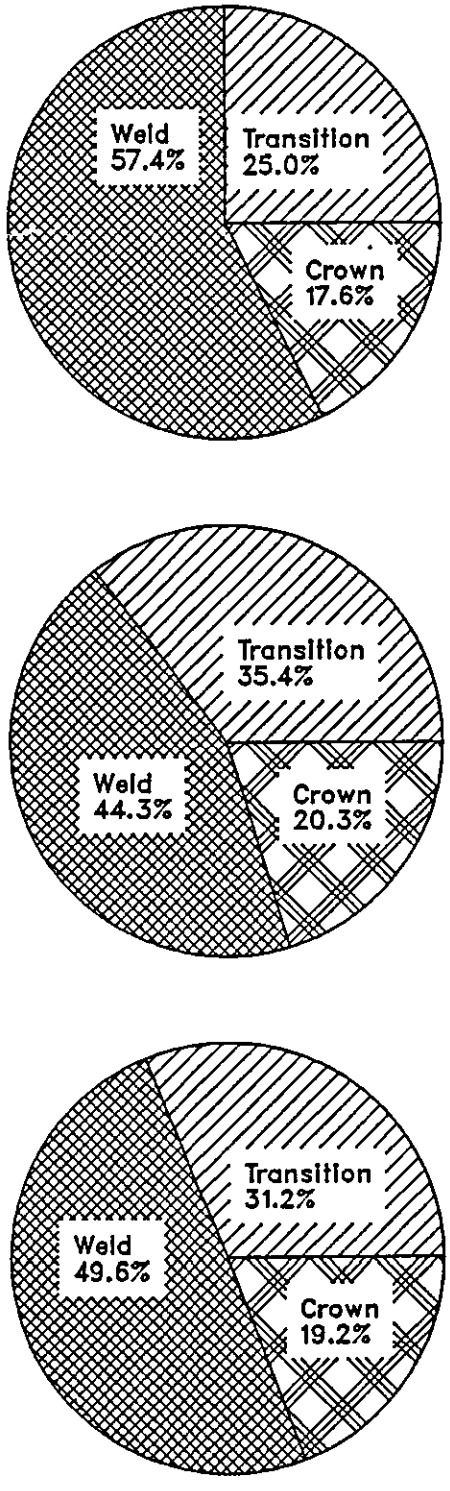

Fig. 3.26 Effect of centre or end links on the position of the fatigue fracture (total is the sum of the centre and end links).

Type	Area reduction (%)	Elongation (%)	Max. load (kN)	Tensile strength (MPa)	Yield load (kN)	Yield stress (MPa)	Diameter (mm)
Plain	60	7	22.5	1390	20.00	1235	4.54
	55	8	22.8	1403	18.75	1169	4.52
	55	7	22.3	1390	18.75	1169	4.52
Ave.				1394		1191	
Welded	55	14	19.6	1227	18.00	1127	4.51
	57	8	22.5	1408	17.50	1095	4.51
	50	14	19.6	1221	17.50	1091	4.52
Ave.				1285		1104	

Table 3.4 Tensile testing of chain link material (Ave. tensile strength, 1340 MPa and yield stress is 1148 MPa).

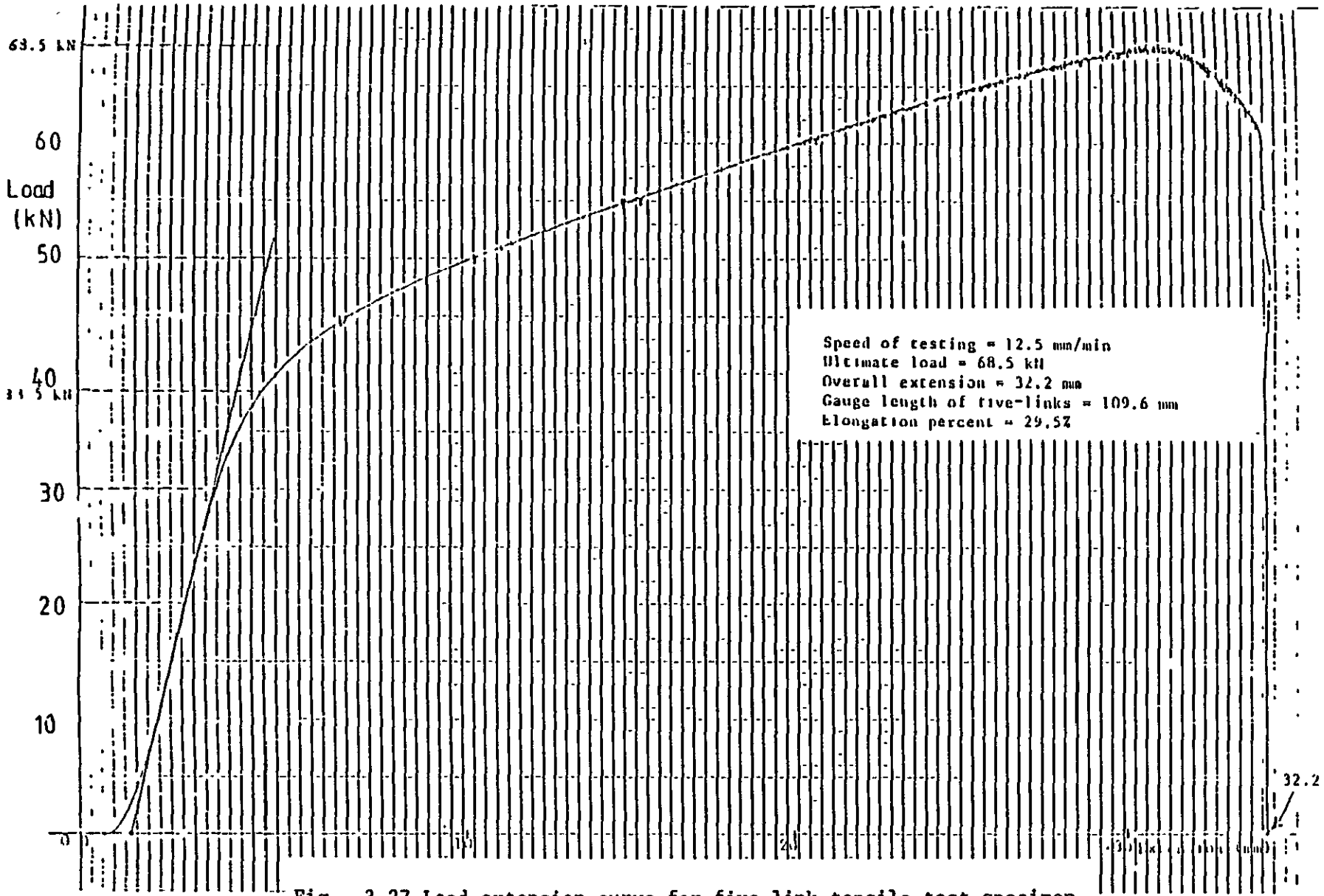

Fig. 3.27 Load-extension curve for five-link tensile test specimen.

Specimen type	Trial number	D1	D2	Dave.	VHN
1	1	367	352	359	432
	2	361	363	362	425
	3	366	363	364	420
	4	362	355	358	434
	5	368	360	364	420
	6	354	360	357	436
Average					428
2	1	360	365	363	422
	2	355	353	354	444
	3	351	357	354	444
	4	360	350	355	441
	5	357	353	355	441
Average					438

Table 3.5 Vickers pyramid hardness number for two specimens.

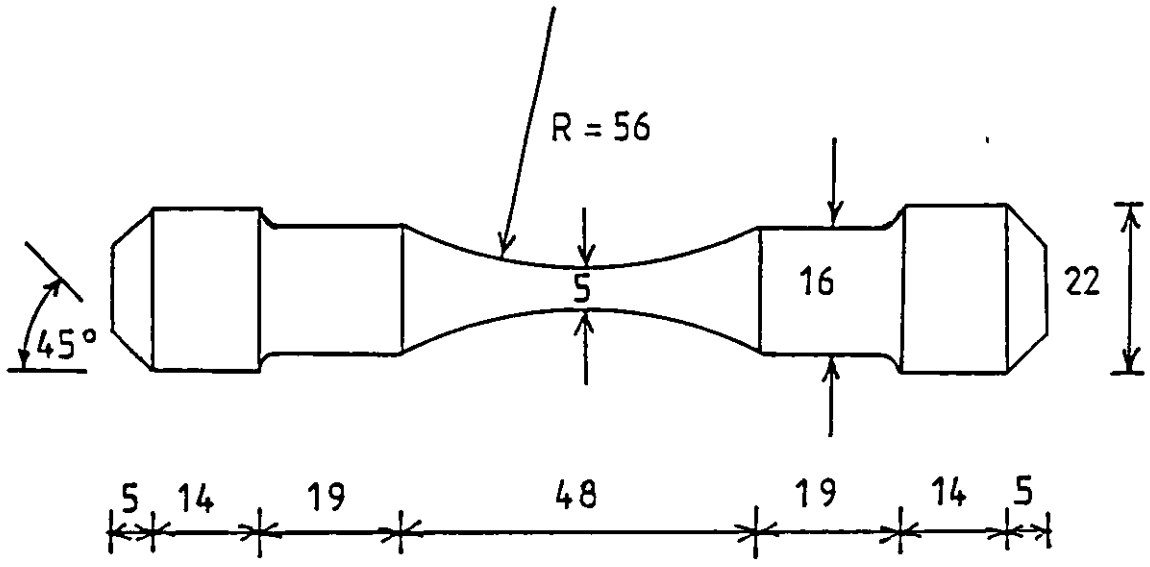

Fig. 3.28 Detail drawing of the chain material fatigue specimen (all dimensions in mm).

Rank order	Mean load, kN (amplitude is 8.35 kN)				
	10.73	7.06	3.34	-1.45	-6.27
1	51530	51830	57440	84610	2000000+
2	94060	80610	81610	157090	2000000+
3	95850	108720	120290	198620	
4	110330	131710	229540	232370	
Mean	87943	93218	122220	168173	2000000+

Table 3.6 Effect of reduction in mean stress on fatigue life of chain material,mean stress varies in the range of 546 to -319 MPa (i.e. corresponding to the mean load of 10.73 to -6.27 kN.), as-polished.

Rank order	Mean load, kN (amplitude is 8.35 kN)	
	10.73	7.58
1	32250	39130
2	42310	82330
Mean	37280	60780

Table 3.7 Effect of mean stress on fatigue life of chain material, as-machined.

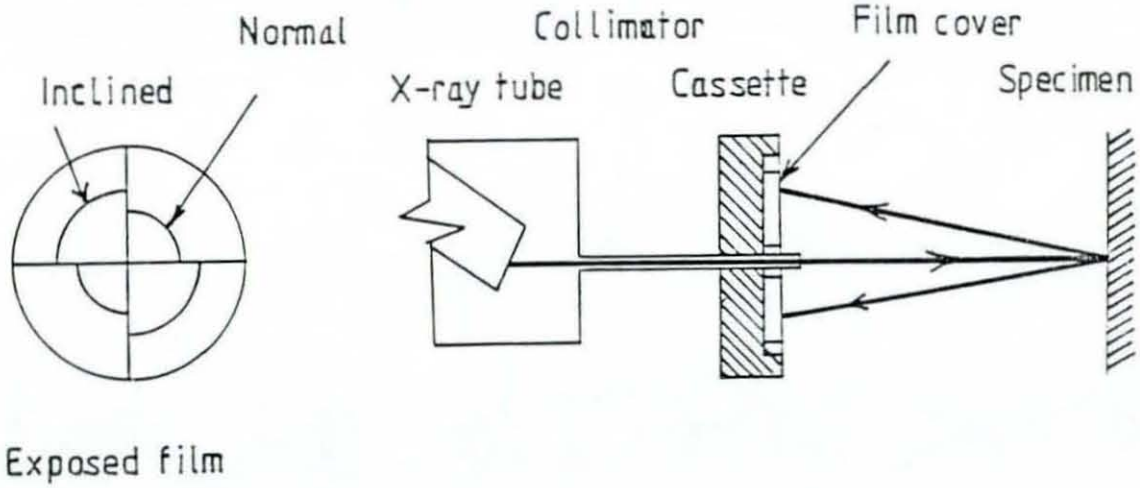

Fig. 4.1 Schematic diagram of back reflection method.

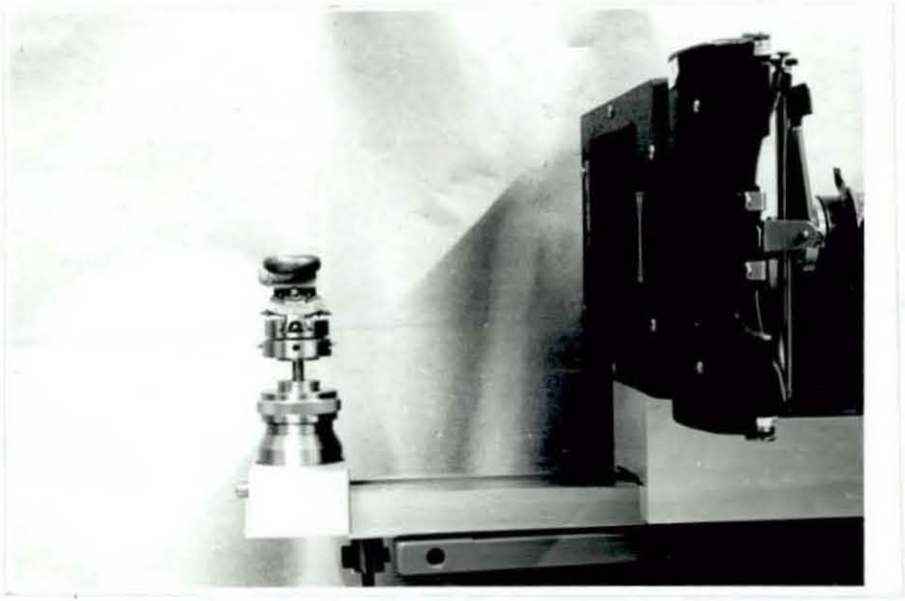

Fig. 4.2 Back reflection experimental set-up.

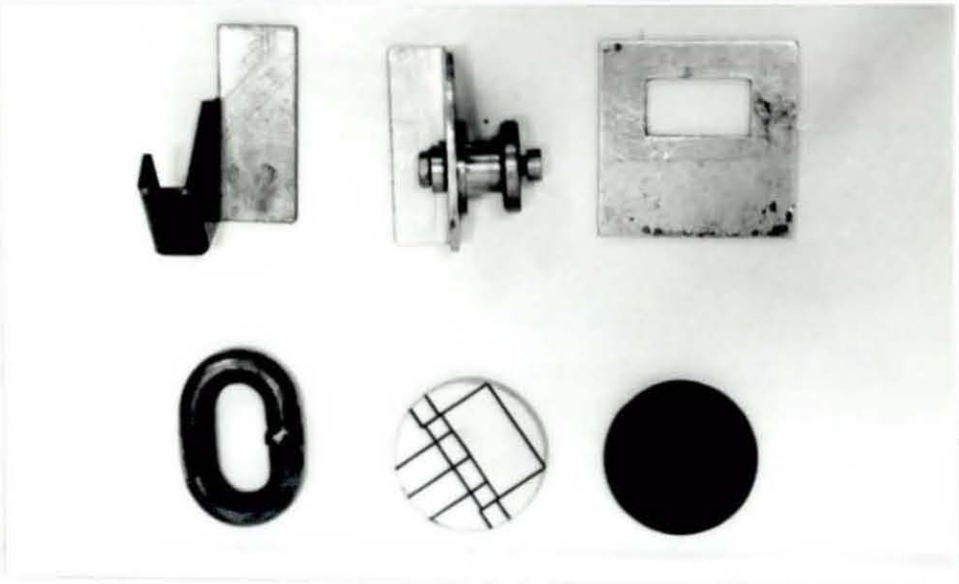

Fig. 4.3 Accessories used for the back reflection and x-ray diffraction experiments (flourescent disc, standard silicon sample, chain link and various specimen holders for diffractometer).

Fig. 4.4 Typical photograph of a double exposure rings.

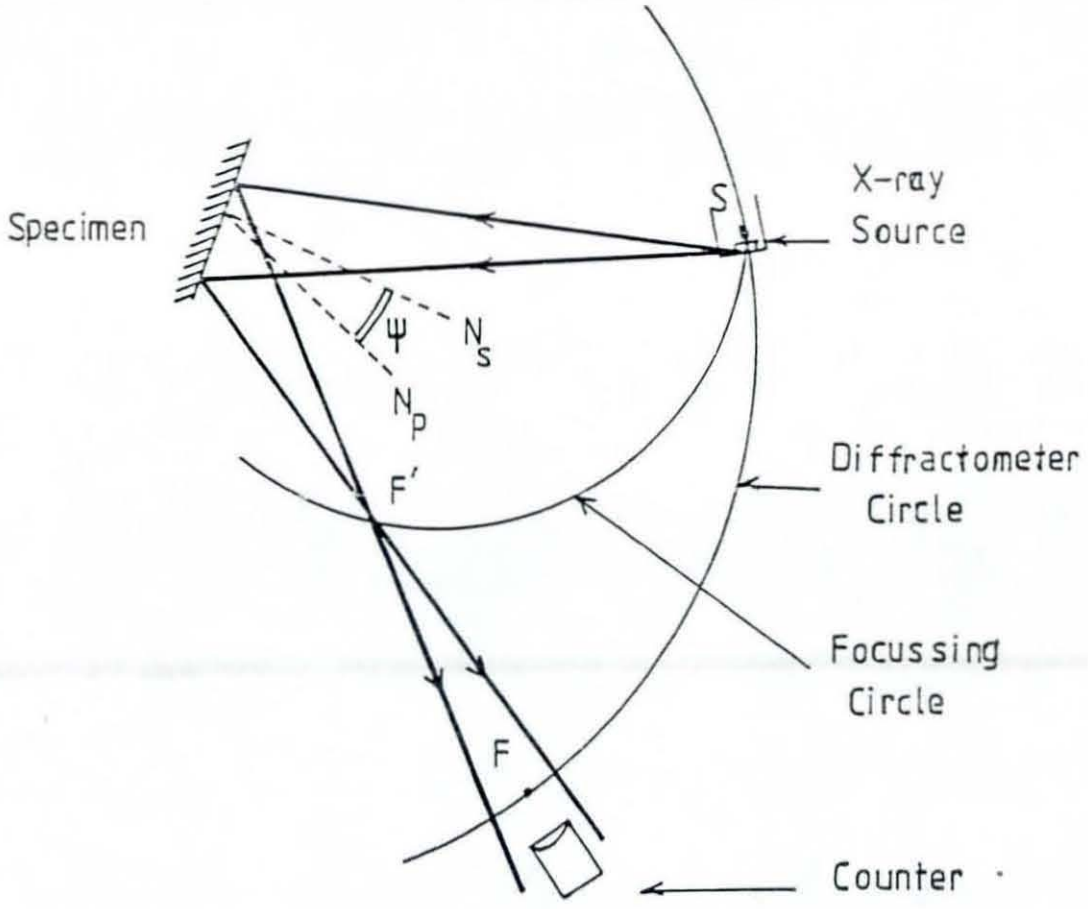

Fig. 4.5 Schematic diagram of diffractometer.

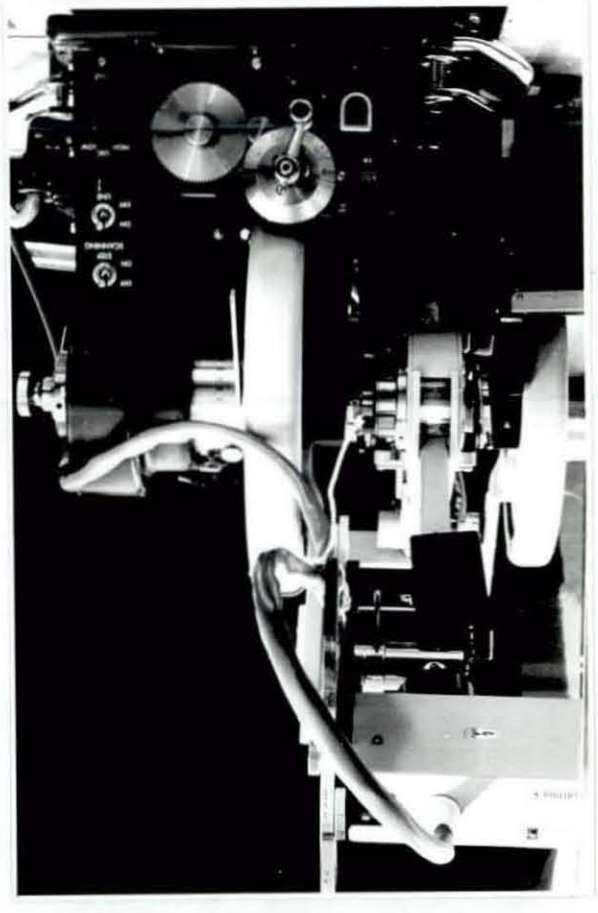

(a)

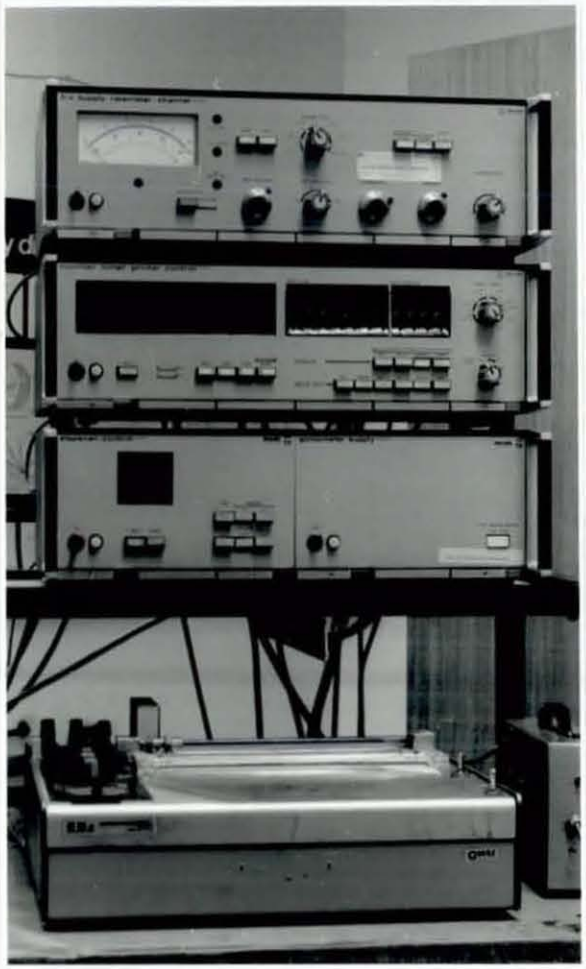

(b)

Fig. 4.6 Photographs of the laboratory x-ray diffractometer. a) x-ray diffractometer. b) recording equipments.

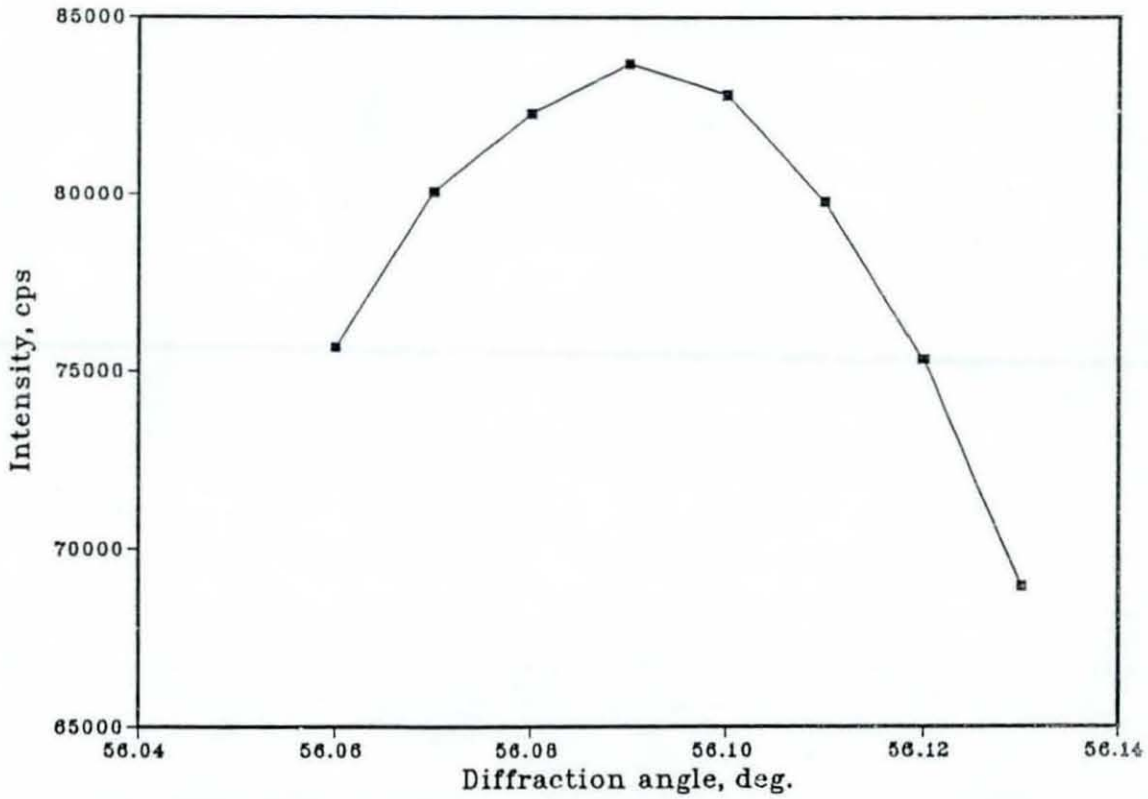

Fig. 4.7 Peak profile of the standard silicon specimen (56.09 deg. compared with 56.12 deg. expected for the standard) to check the alignment of the diffractometer. Scanning step=.01 deg.

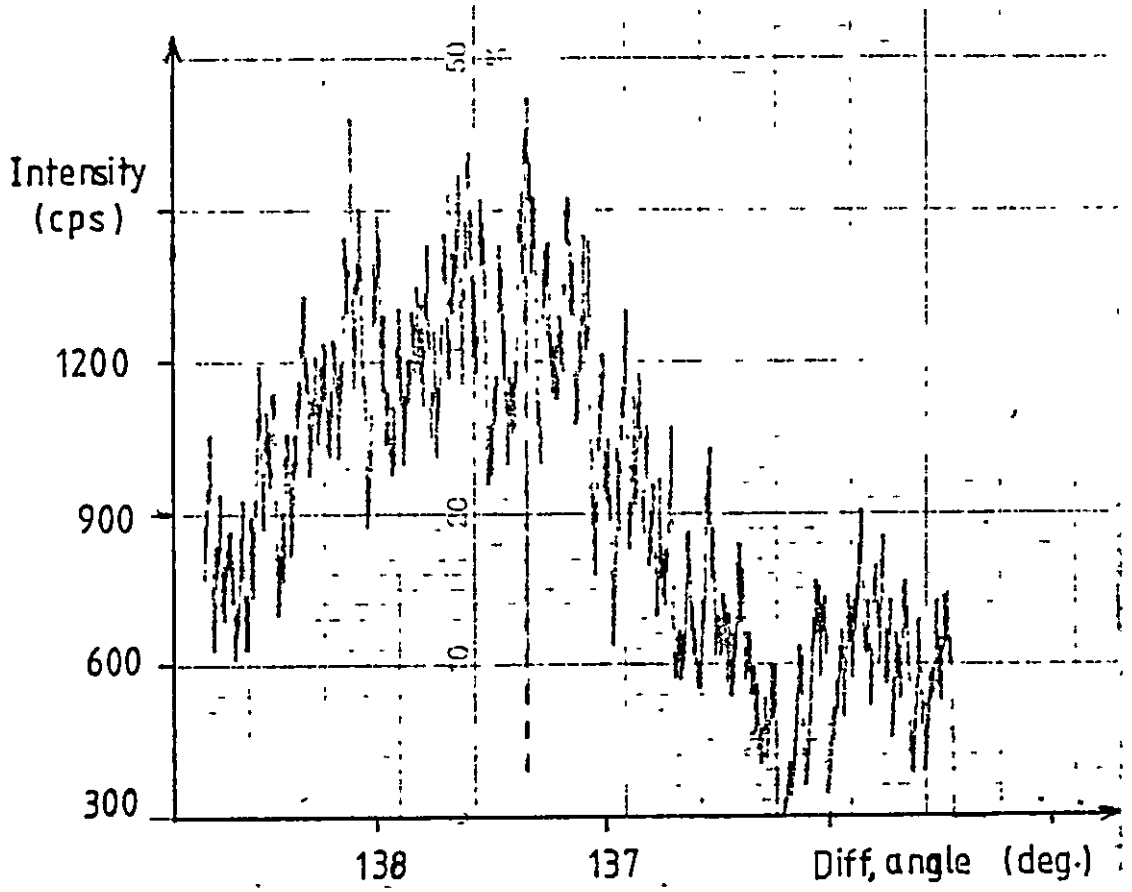

Fig. 4.8 Recorded intensity (cps) versus diffraction angle (deg.) for a typical chain link measurement (45° the right).

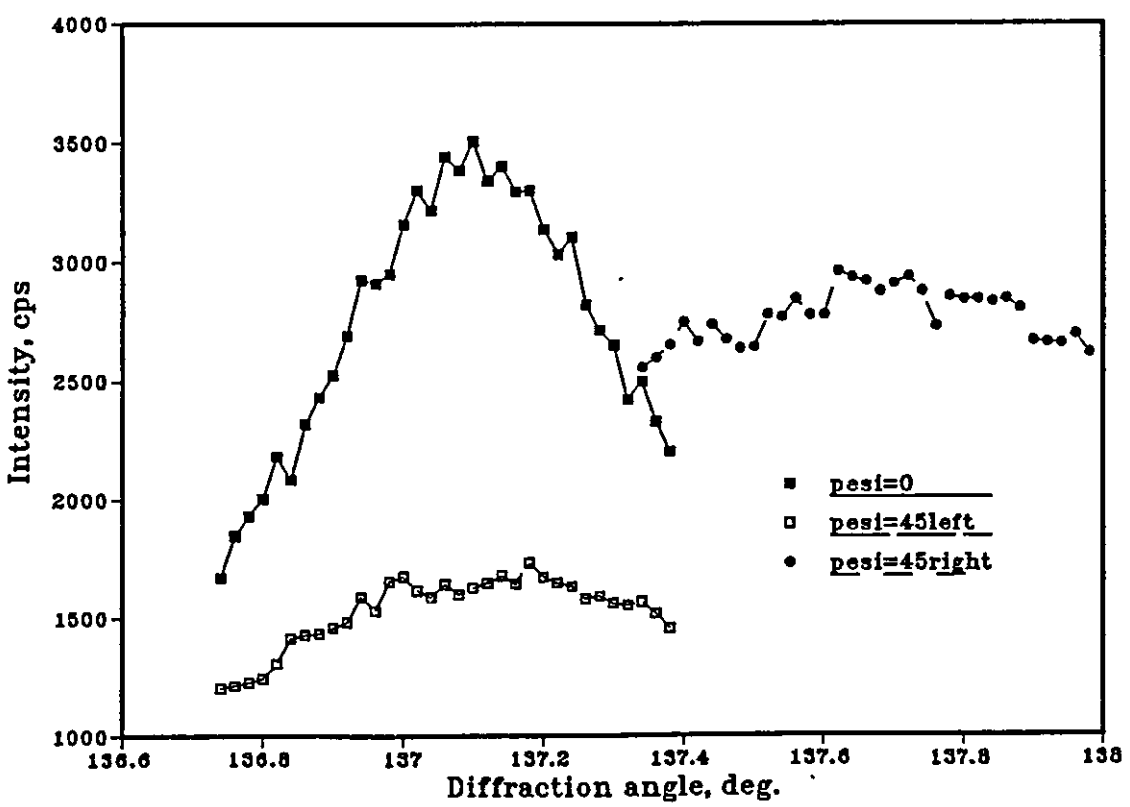

Fig. 4.9 Typical peak profile of 7 mm lifting chain tempered at 600 deg. C (at pesi angle of 0 and 45 deg. to the right and left). Scanning time and steps are 3 minutes and .02 deg. respectively.

Tempering time	State of calibration	Position	$\psi = 0^{o}$	$\psi = 45^{o}$	
				to left	to right
3 Hours	Non-cal.	Centre	136.95	137.00	137.60
		5 mm right	136.90	137.20	137.75
		5 mm left	137.00	137.20	137.60
	Calibrated	Centre	136.95	137.45	137.45
2 Hours	Non-cal.	Centre	136.90	137.25	137.25
	Calibrated 1	Centre	136.95	137.20	137.40
	Calibrated 2	Centre	136.95	137.30	137.15

Table 4.1 Diffraction peak angles for various samples at different positions on the 7 mm lifting chain.

Tempering time	State of calibration	Position	Residual stress, MPa, $\psi=45^{o}$	
			To left	To right
3 Hours	Non-cal.	Centre	- 62	- 806
		5 mm right	- 372	- 1054
		5mm left	- 248	- 744
	Calibrated	Centre	- 620	- 620
2 Hours	Non-cal.	Centre	- 434	- 434
	Calibrated 1	Centre	- 310	- 558
	Calibrated 2	Centre	- 434	- 248

Table 4.2 Residual stresses for the measurements of Table 4.1 for various samples.

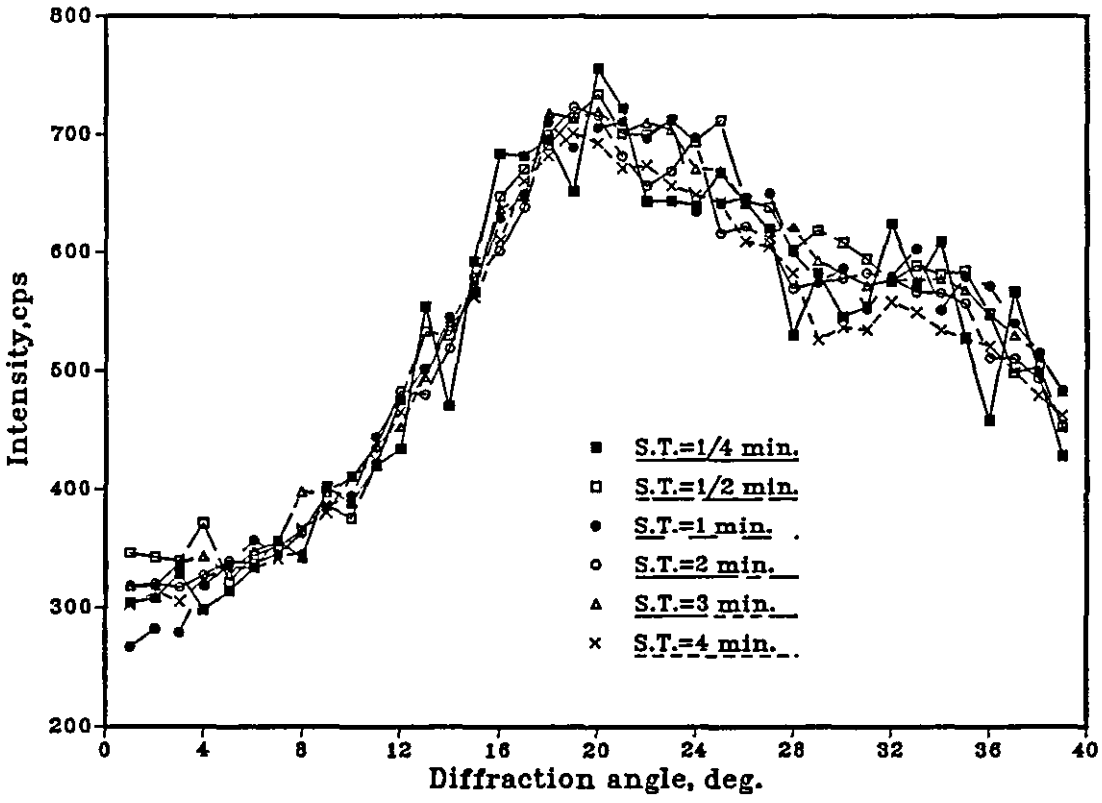

Fig.4.10 Effect of scanning time (S.T.) on the peak profile patterns of 7 mm lifting chain tempered at 600 deg. C (scanning step=.05 deg. and pesi=45 deg.).

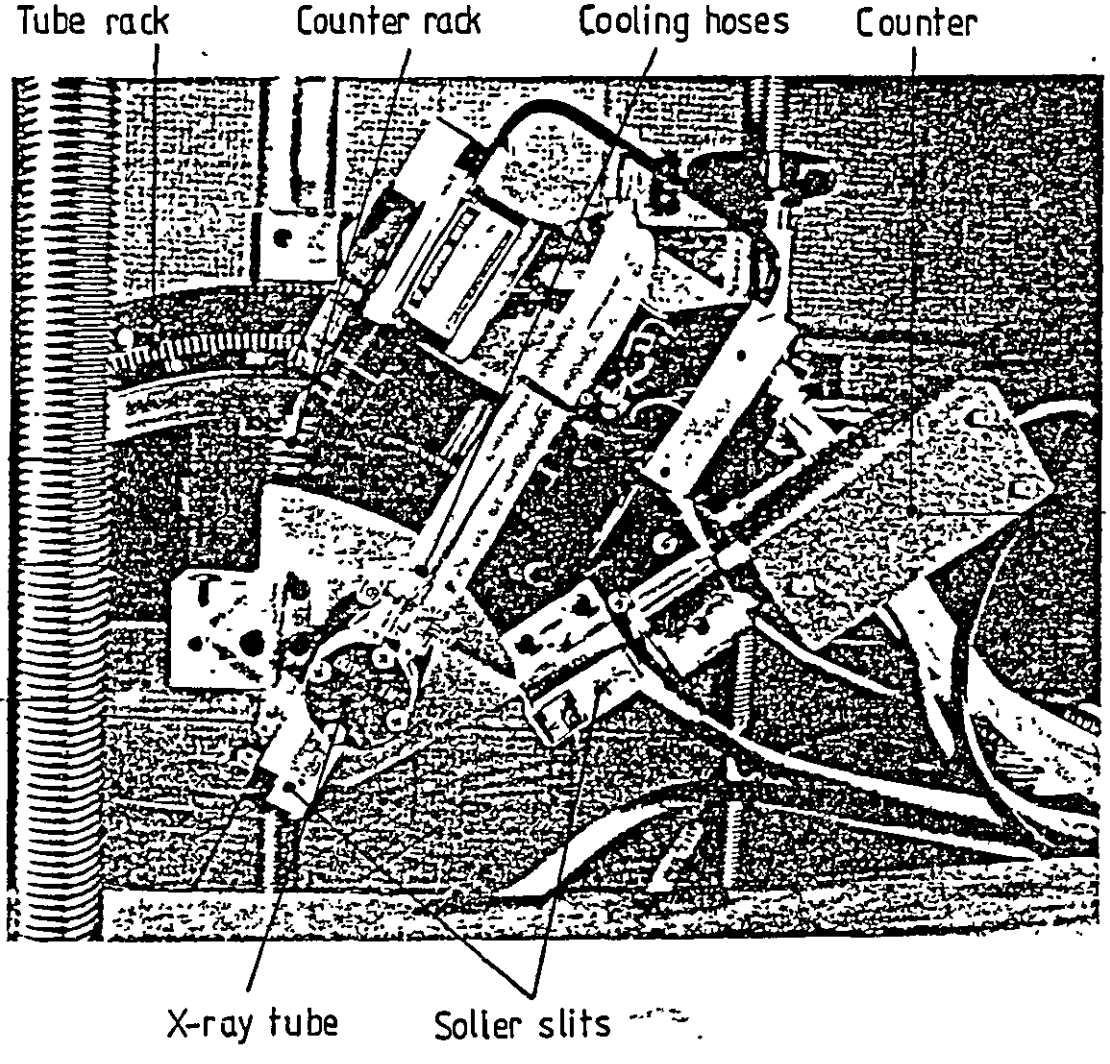

Fig. 4.11 x-ray goniometer of Strainflex.

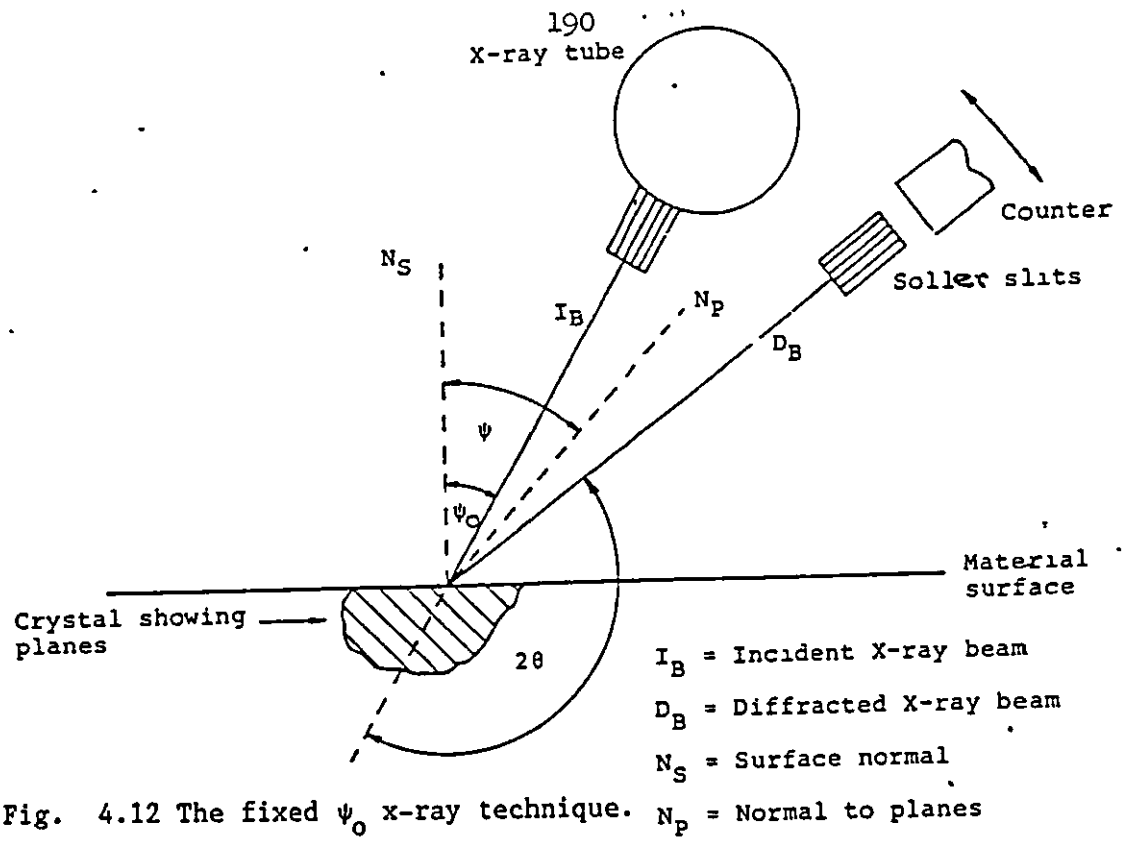

Fig. 4.12 The fixed ψ_o x-ray technique.

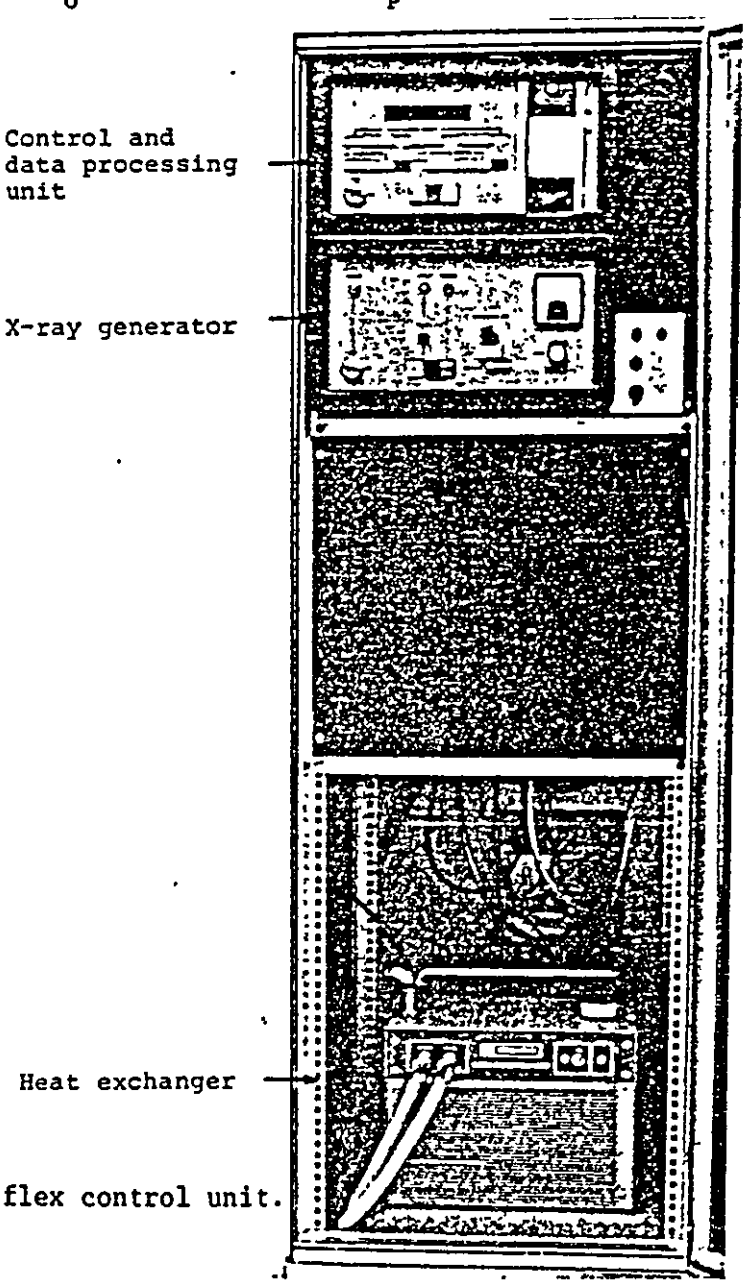

Fig. 4.13 Strainflex control unit.

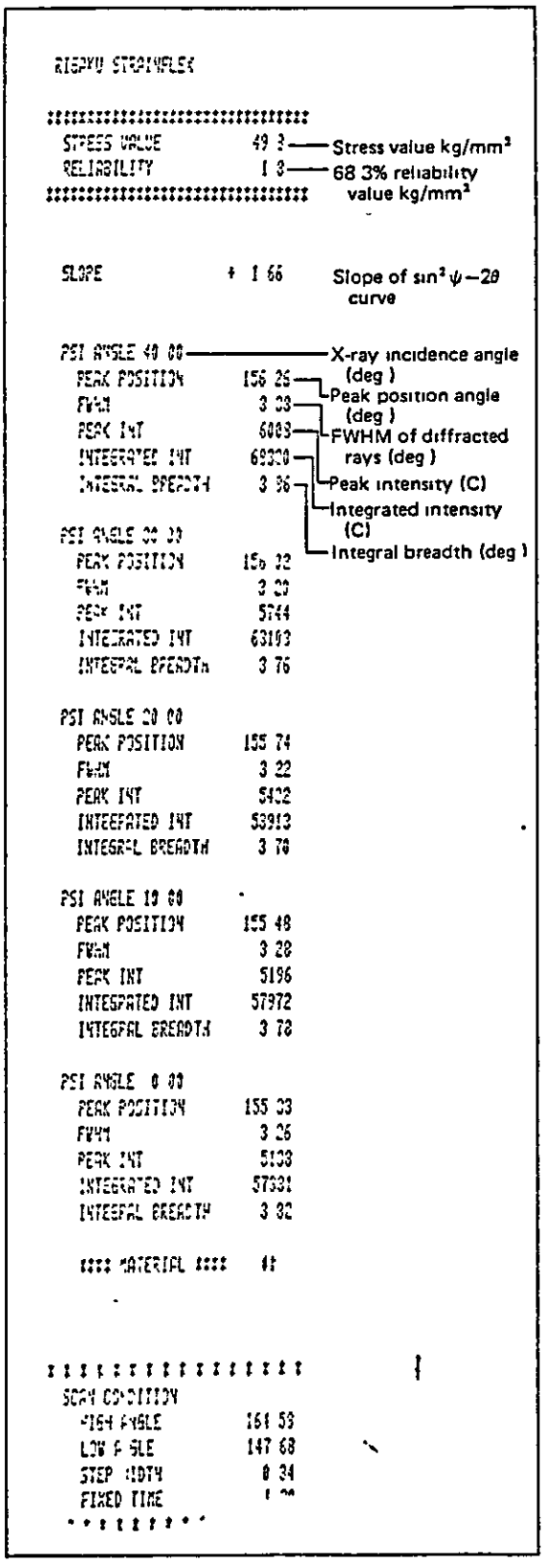

Fig. 4.14 A typical analyser output (parameters definitions given in Fig. 4.16).

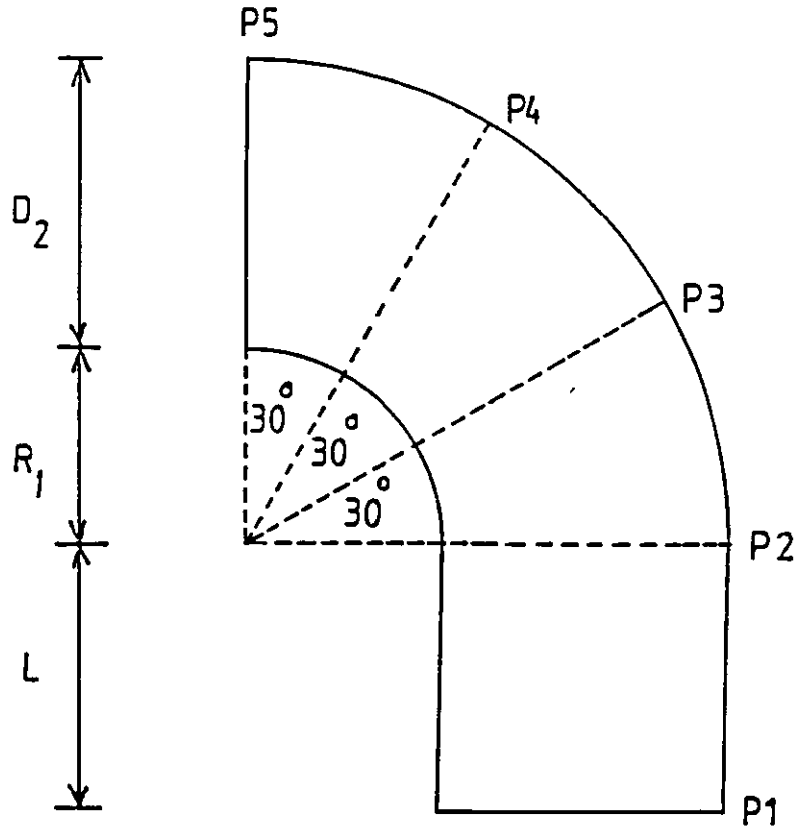

Fig. 4.15 A quarter of the chain link showing the location of stress measurements.

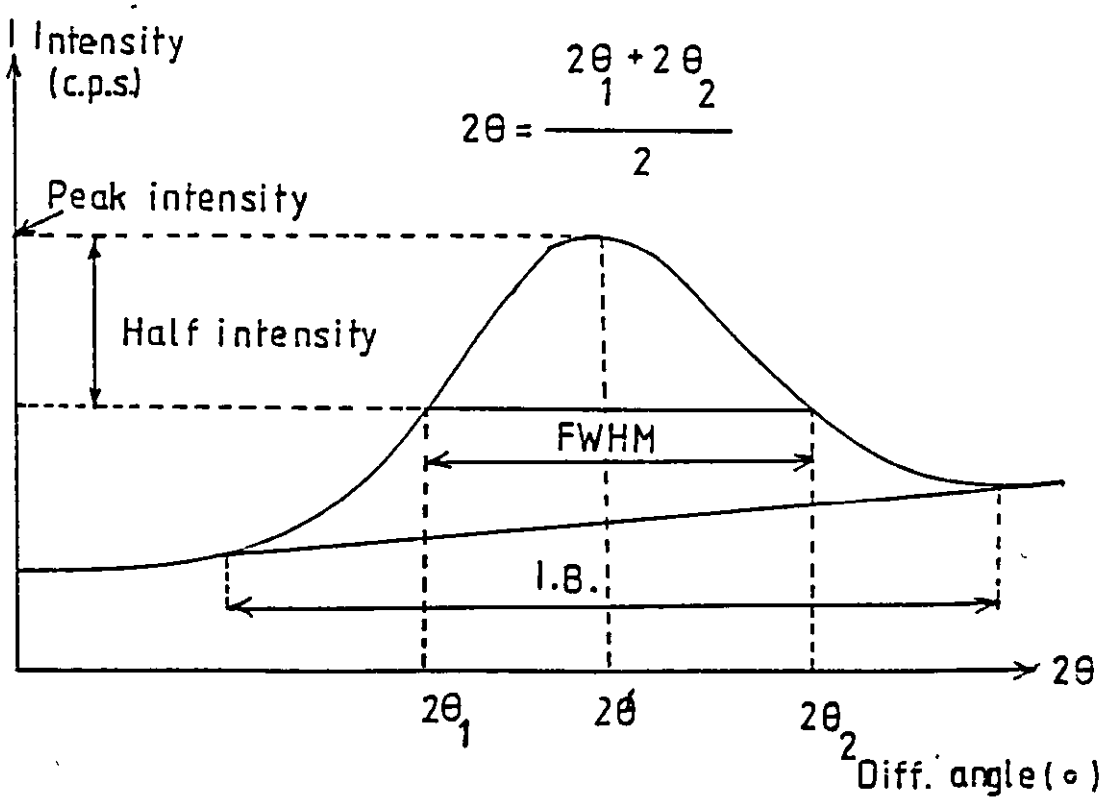

Fig. 4.16 Illustration of some of the parameters used in the Rigaku/Strainflex measurements. (FWHM, full width at half maximum intensity; I.B., integral breadth). $2\theta=156.2^{\circ}$ at $\psi=30^{\circ}$ was taken for Cotθ calculation in the stress formula.

Calibration load (kN)	Residual stresses at various positions, MPa				
	P1	P2	P3	P4	P5
0	- 53				- 53
30	- 69				- 251
38.5	- 157	- 122	- 141	- 174	- 311
50	- 117				- 306

Table 4.3 Residual stresses in 7 mm lifting chain links at various positions at the surface.

Calibration load (kN)	Residual stresses at various positions, MPa				
	P1	P2	P3	P4	P5
0	- 304 (-335)				- 257 (-264)
260	- 167				- 321
320	- 153	- 276	- 374	- 170	- 226
380	- 280				- 270

Table 4.4 Residual stresses in 19 mm mining chain links, as water quenched (the stresses inside the brackets correspond to electro-polished case).

Calibration load (kN)	Residual stresses, MPa	
	P1	P5
0	- 82	- 59
260	- 235	- 268
320	- 288	- 253

Table 4.5 Residual stresses in 19 mm mining chain link as air cooled.

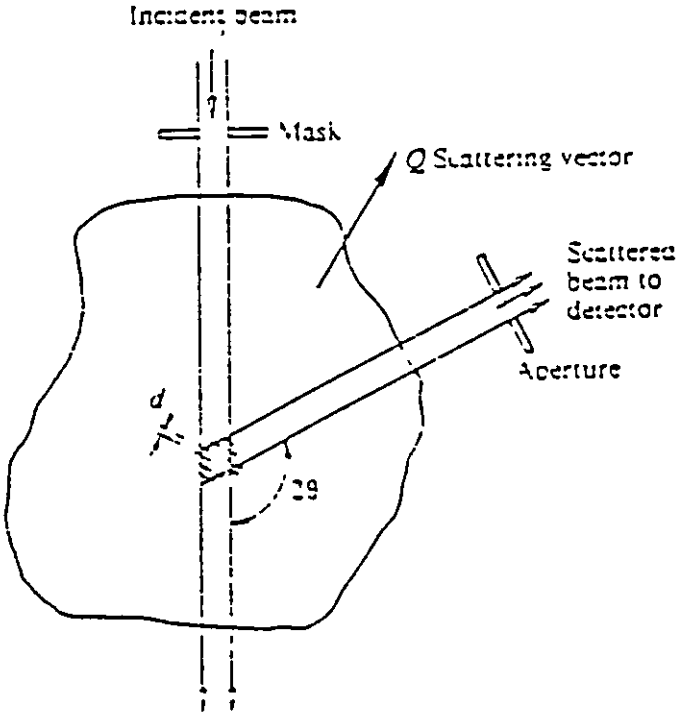

Fig. 4.17 Principles of the neutron diffraction technique showing Bragg reflection from crystal planes d apart.

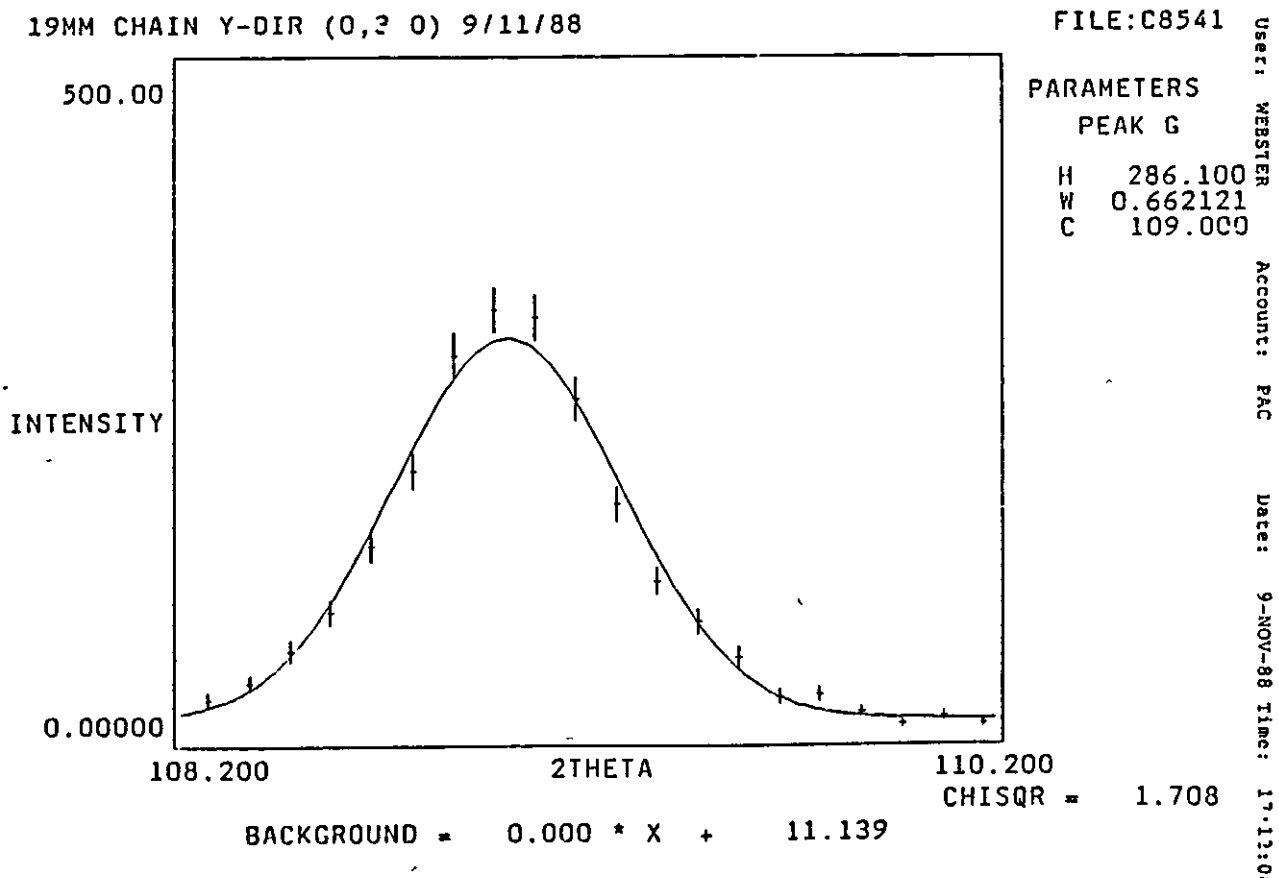

Fig. 4.18 A typical neutron diffraction pattern.

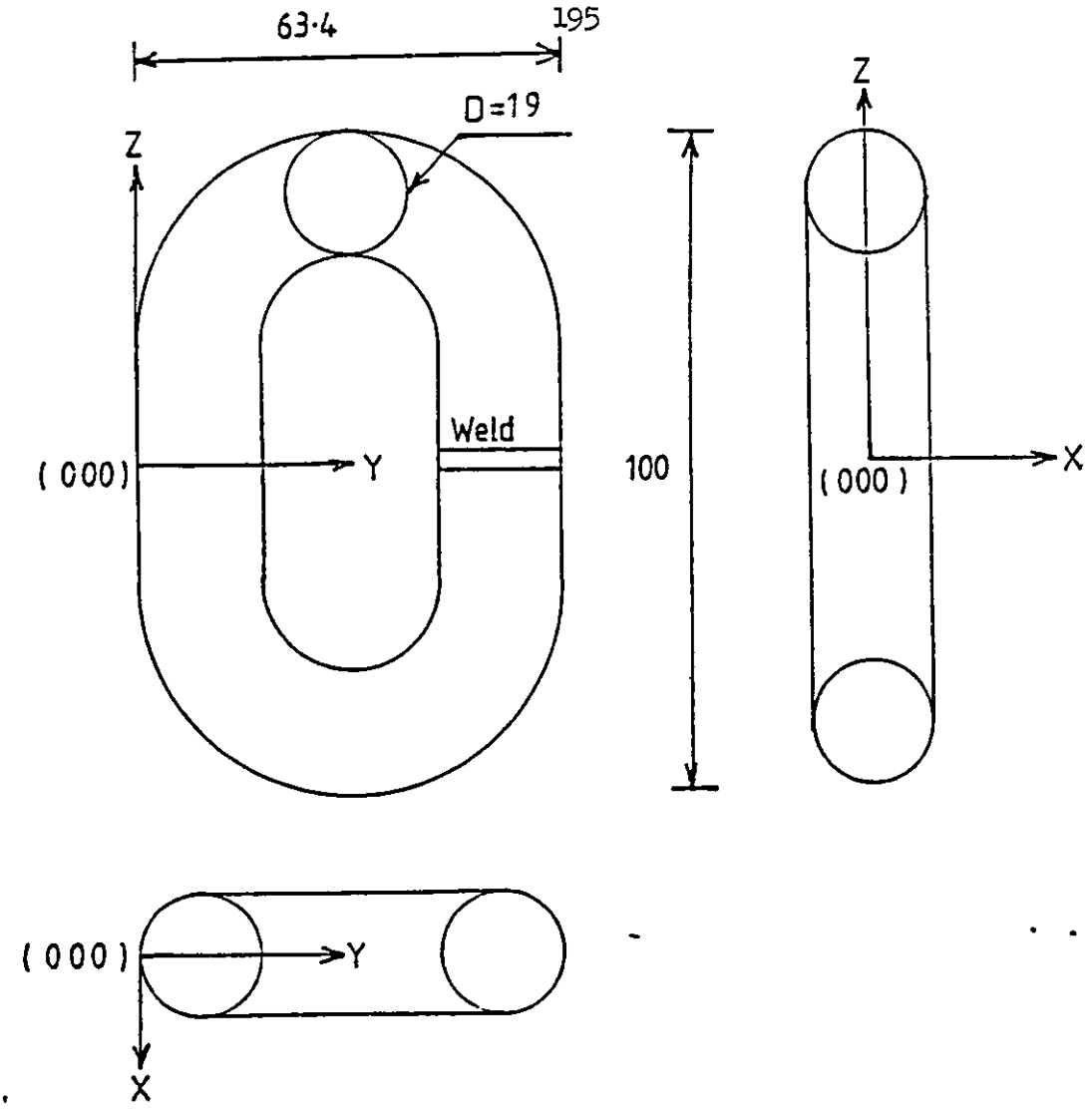

Fig. 4.19 Chain link dimensions and coordinate system used.

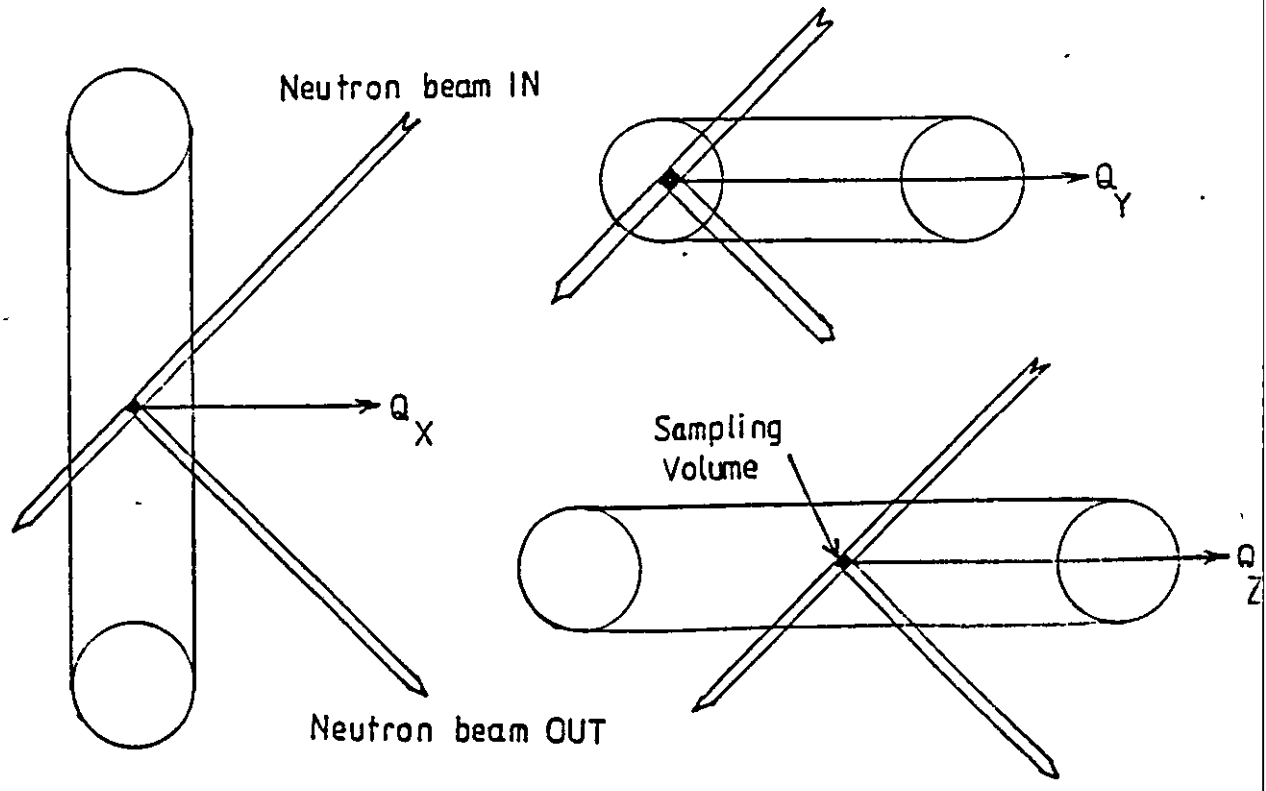

Fig. 4.20 Measuring positions for chain link - plane view.

FILE	HEIGHT	WIDTH	CENTRE	AREA	BAG	CHISQ	X	Y	Z
7 0									
R8252	188.	0.705	109.075	141.27	8.6	1.21	0.0	1.0	0.0
R8251	275.	0.700	109.026	205.21	17.3	1.57	0.0	3.0	0.0
R8250	217.	0.693	109.203	160.54	19.9	1.00	0.0	6.0	0.0
R8249	214.	0.730	109.214	166.00	30.7	1.06	0.0	9.5	0.0
R8248	170.	0.744	109.130	134.76	28.2	1.43	0.0	13.0	0.0
R8247	172.	0.802	109.071	147.03	19.1	1.15	0.0	16.0	0.0
R8246	184.	0.792	109.074	154.92	4.8	1.67	0.0	18.0	0.0

*** -- ACCURACY -- ***

FILE	HEIGHT	WIDTH	CENTRE	AREA	BAG	CHISQ	X	Y	Z
7 0									
R8252	7.	0.021	0.009	6.51	1.3	1.21	0.0	1.0	0.0
R8251	8.	0.018	0.008	8.05	1.8	1.57	0.0	3.0	0.0
R8250	7.	0.023	0.009	7.54	2.2	1.00	0.0	6.0	0.0
R8249	7.	0.027	0.010	8.41	2.8	1.06	0.0	9.5	0.0
R8248	7.	0.030	0.012	7.70	2.5	1.43	0.0	13.0	0.0
R8247	6.	0.029	0.011	7.69	2.2	1.15	0.0	16.0	0.0
R8246	6.	0.022	0.010	6.79	1.1	1.67	0.0	18.0	0.0

Table 4.6 (211) diffraction peak data for the x-direction (0, Y, 0) scan.

FILE	HEIGHT	WIDTH	CENTRE	AREA	BAG	CHISQ	X	Y	Z
7 0									
R8540	299.	0.697	109.020	221.64	10.1	1.24	0.0	1.0	0.0
R8541	286.	0.662	109.000	201.65	11.1	1.71	0.0	3.0	0.0
R8543	405.	0.610	109.220	262.82	22.4	1.69	0.0	6.0	0.0
R8544	331.	0.778	109.218	274.15	23.2	1.50	0.0	9.5	0.0
R8545	331.	0.750	109.158	263.74	24.0	1.47	0.0	13.0	0.0
R8547	228.	0.745	109.100	181.07	17.5	1.32	0.0	16.0	0.0
R8548	263.	0.744	109.036	208.48	18.7	1.42	0.0	18.0	0.0

••• -- ACCURACY -- •••

FILE	HEIGHT	WIDTH	CENTRE	AREA	BAG	CHISQ	X	Y	Z
7 0									
R8540	8.	0.016	0.007	7.99	1.5	1.24	0.0	1.0	0.0
R8541	8.	0.016	0.007	7.70	1.5	1.71	0.0	3.0	0.0
R8543	11.	0.013	0.006	8.95	1.9	1.69	0.0	6.0	0.0
R8544	9.	0.021	0.007	10.33	3.1	1.50	0.0	9.5	0.0
R8545	8.	0.017	0.007	8.66	2.4	1.47	0.0	13.0	0.0
R8547	7.	0.025	0.009	8.33	2.4	1.32	0.0	16.0	0.0
R8548	8.	0.021	0.008	8.62	2.4	1.42	0.0	18.0	0.0

Table 4.6 Cont.(211) diffraction peak data for the y-direction (0,y,0) scan

FILE	HEIGHT	WIDTH	CENTRE	AREA	BAG	CHISQ	X	Y	Z
7 0									
R8239	136.	0.739	109.430	106.97	9.2	1.13	0.0	1.0	0.0
R8240	134.	0.776	109.570	110.51	11.1	1.28	0.0	3.0	0.0
R8241	54.	1.257	109.068	71.62	14.6	1.25	0.0	6.0	0.0
R8242	71.	0.761	108.919	57.68	14.8	1.11	0.0	9.5	0.0
R8243	57.	0.876	109.174	53.28	10.6	1.68	0.0	13.0	0.0
R8244	77.	0.727	109.346	59.34	13.7	1.34	0.0	16.0	0.0
R8245	92.	0.778	109.440	76.23	8.9	1.25	0.0	18.0	0.0

××× -- ACCURACY -- ×××

FILE	HEIGHT	WIDTH	CENTRE	AREA	BAG	CHISQ	X	Y	Z
7 0									
R8239	6.	0.030	0.011	6.18	1.7	1.13	0.0	1.0	0.0
R8240	6.	0.032	0.012	6.40	1.9	1.28	0.0	3.0	0.0
R8241	5.	0.159	0.036	11.11	4.8	1.25	0.0	6.0	0.0
R8242	5.	0.050	0.020	5.27	1.6	1.11	0.0	9.5	0.0
R8243	4.	0.068	0.022	5.47	2.0	1.68	0.0	13.0	0.0
R8244	5.	0.047	0.017	5.27	1.8	1.34	0.0	16.0	0.0
R8245	5.	0.043	0.015	5.68	1.8	1.25	0.0	18.0	0.0

Table 4.6 Cont.(211) diffraction peak data for the z-direction (0,y,0) scan

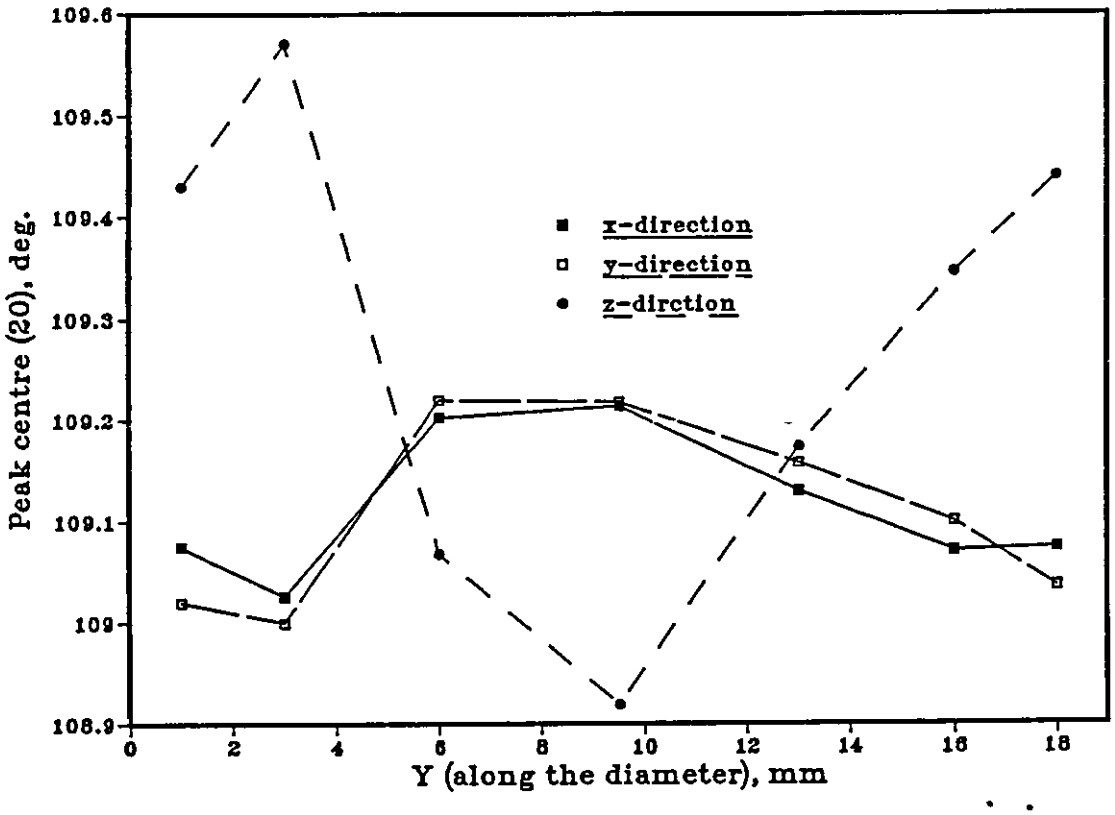

Fig. 4.21 (211) Peak centre positions for the X, Y and Z orientations for the (0, Y, 0) scans.

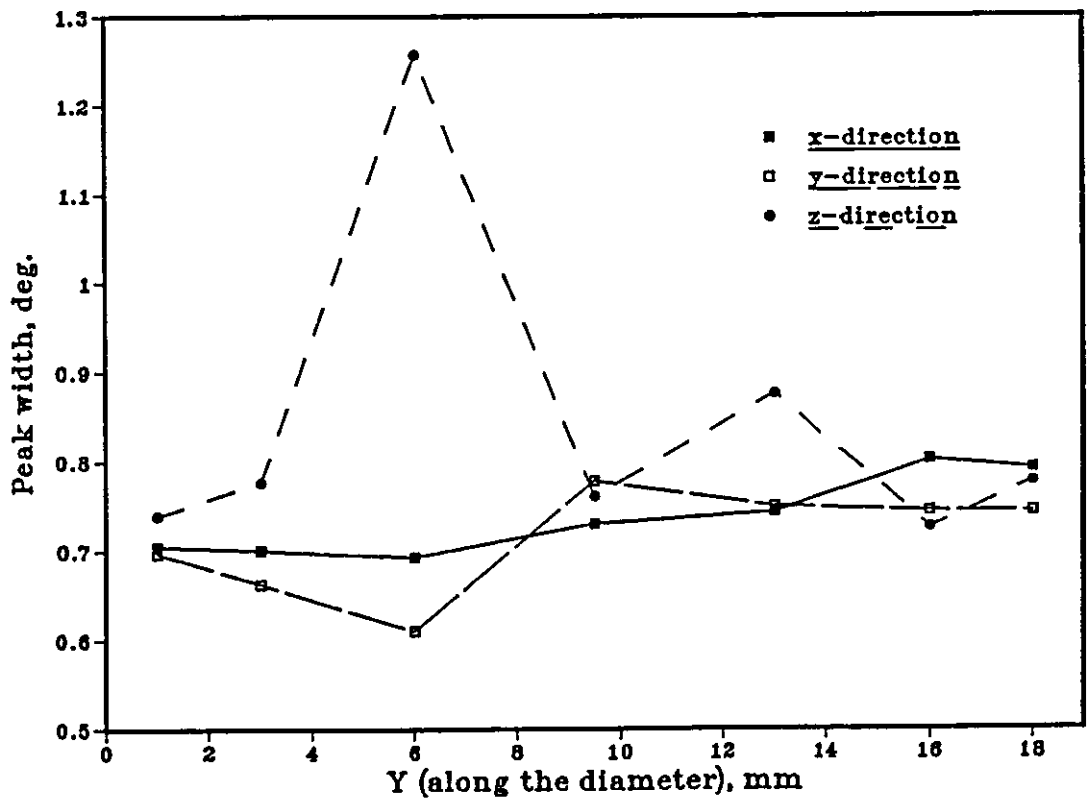

Fig. 4.22 (211) Peak widths for the X, Y and Z orientations for the (0, Y, 0) scans.

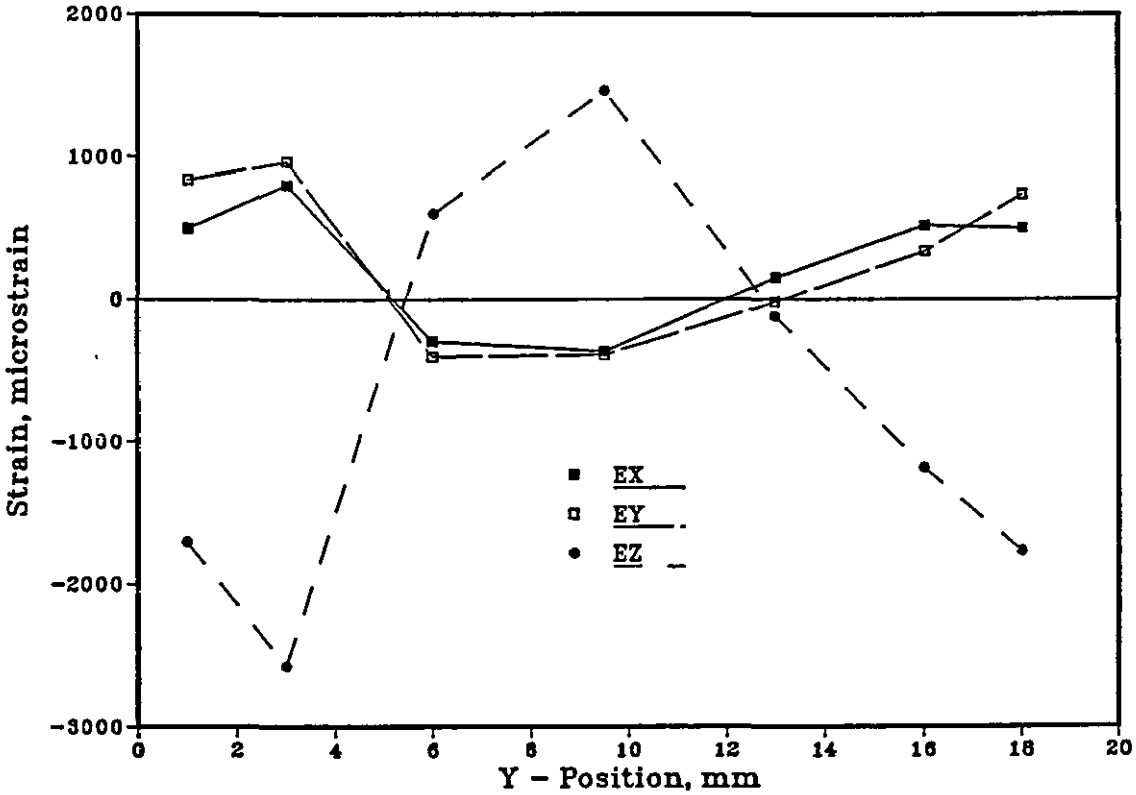

Fig. 4.23 Strains for the X, Y and Z orientations for the (0, Y, 0) scans.

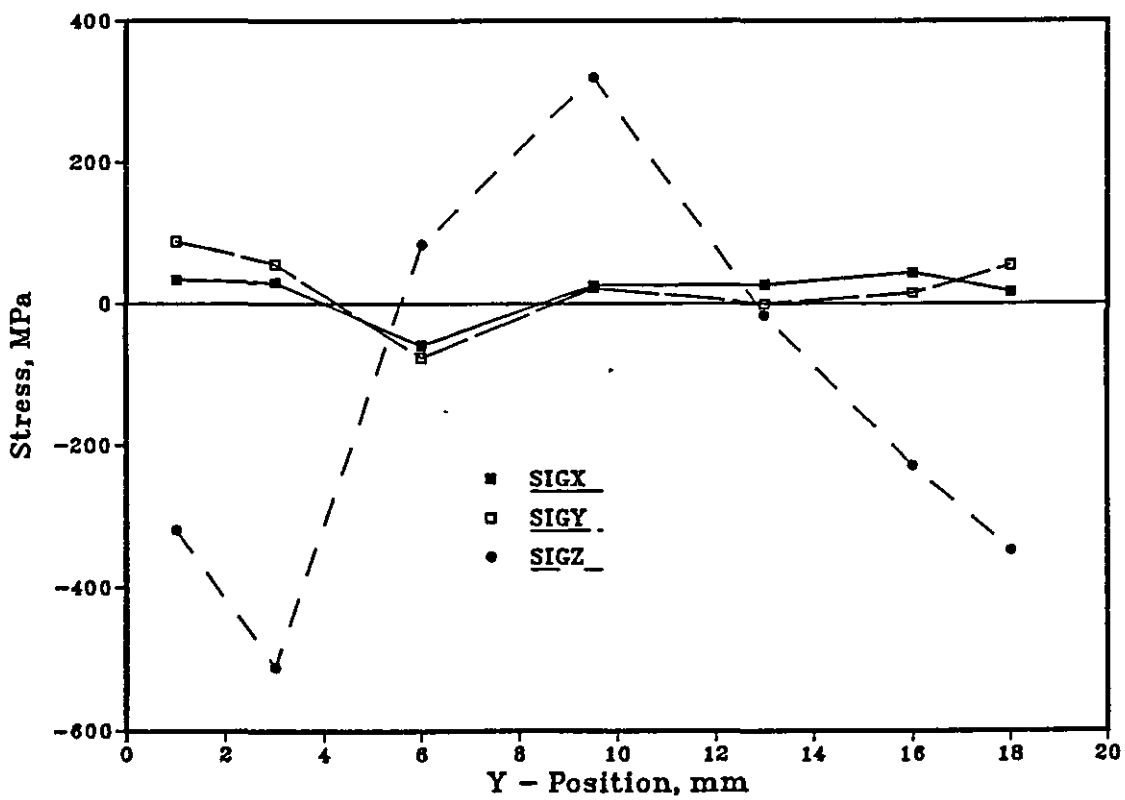

Fig. 4.24 Stresses for the X, Y and Z orientations for the (0, Y, 0) scans.

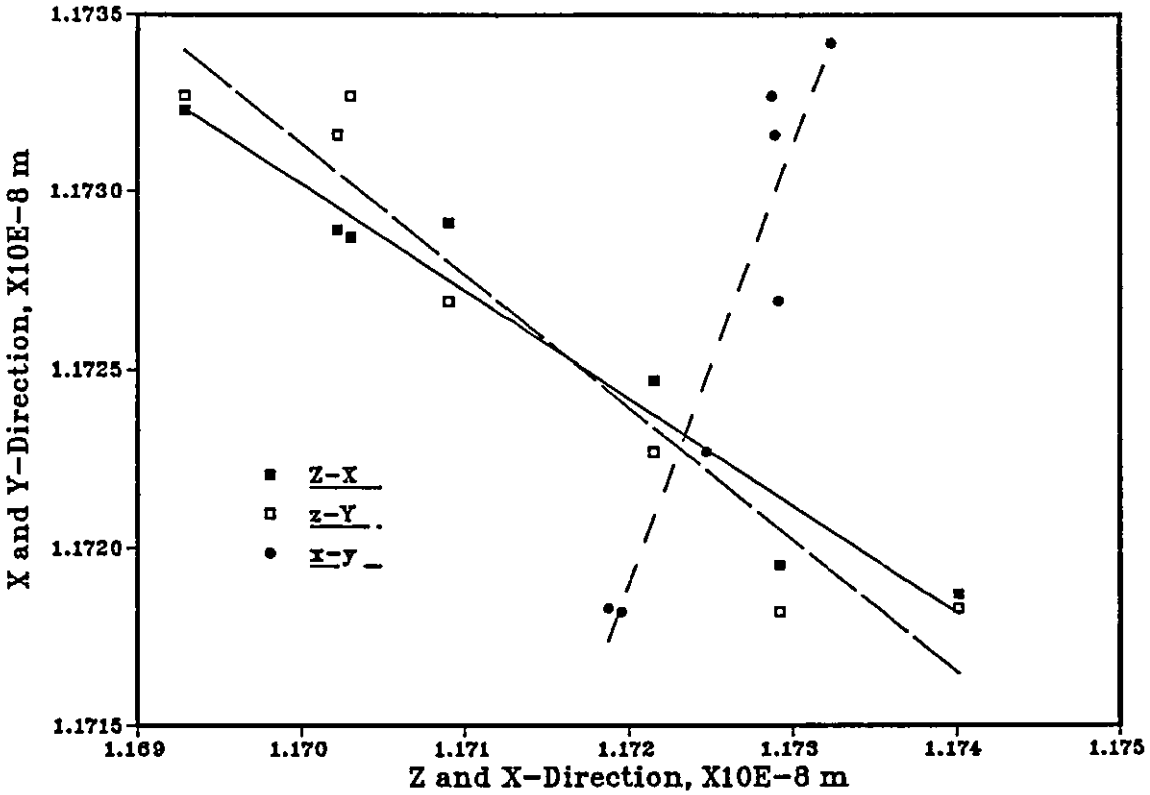

Fig. 4.25 Determination of equal lattice spacings in X, Y and Z-direction (stress free state).

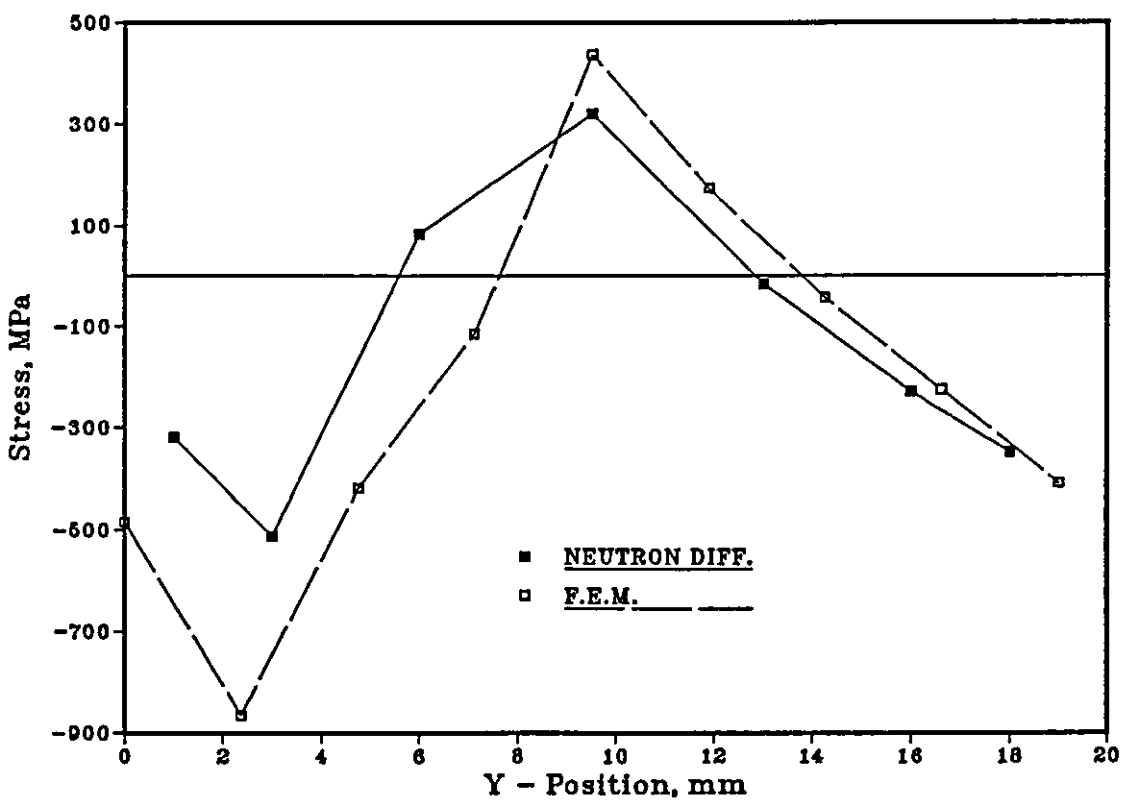

Fig. 4.26 Comparison of residual stresses from the finite element analysis and neutron diffraction measurements.

Distance mm	X-Direction		Y-Direction		Z-Direction	
	2θ deg.	d nm	2θ deg.	d nm	2θ deg.	d nm
1	109.075	.117287	109.020	.117327	109.430	.117030
3	109.026	.117323	109.000	.117342	109.570	.116929
6	109.202	.117195	109.220	.117182	109.068	.117292
9.5	109.213	.117187	109.218	.117183	109.919	.117401
13	109.130	.117247	109.158	.117227	109.174	.117215
16	109.070	.117291	109.100	.117269	109.346	.117090
18	109.073	.117289	109.036	.117316	109.440	.117022

Table 4.7 Lattice spacing measured by the neutron diffraction method in the direction through a section at the centre of the 19 mm mining chain barrel.

X mm	Y mm	Z mm	ε_x $\mu\varepsilon^x$	ε_y $\mu\varepsilon^y$	ε_z $\mu\varepsilon^z$	σ_x MPa^x	σ_y MPa^y	σ_z MPa^z
0.0	1.0	0.0	497	838	-1707	35	90	-319
0.0	3.0	0.0	800	962	-2576	31	57	-512
0.0	6.0	0.0	-298	-404	602	-60	-77	84
0.0	9.5	0.0	-366	-391	1465	26	22	321
0.0	13.0	0.0	155	-19	-118	27	-1	-17
0.0	16.0	0.0	521	341	-1186	45	16	-230
0.0	18.0	0.0	503	739	-1769	17	55	-348

Table 4.8 Residual stress and strain distribution versus positiion Y for the (0, Y ,0) scan.

X mm	Y mm	Z mm	ε_x $\mu\varepsilon$	ε_y $\mu\varepsilon$	ε_z $\mu\varepsilon$	σ_x MPa	σ_y MPa	σ_z MPa
0.0	1.0	0.0	64	53	75	21	19	23
0.0	3.0	0.0	59	53	81	20	19	25
0.0	6.0	0.0	64	49	226	33	31	64
0.0	9.5	0.0	69	53	128	26	23	38
0.0	13.0	0.0	81	53	140	29	25	41
0.0	16.0	0.0	75	64	110	26	24	33
0.0	18.0	0.0	69	59	98	24	22	30

Table 4.9 Accuracy of residual stress and strain distribution veses Y for the (0, Y ,0) scan. Note : $\Delta\theta = 2\theta - 109.154^{o}$

Distance mm	2θ deg.	Δθ deg.	ε με
-9.5	109.204	.050	-310
-8.5	109.212	.058	-360
-6.5	109.221	.067	-416
-3.5	109.198	.044	-273
-0.0	109.210	.056	-348

Table 4.10 Residual stresses at a section through the centre of the barrel of 19 mm mining chain (in radial direction).

Y, mm	σ_1	σ_2	σ_3
0.000	-484	-116	27
2.375	-865	-38	152
4.750	-419	-71	55
7.125	-114	-42	107
9.500	-49	-21	437
11.875	-47	-22	174
14.250	-43	-41	-14
16.625	-228	-6	-3
19.000	-409	-4	45

Table 4.11 Residual stresses through the centre of the 19 mm mining chain from the finite element analysis (3-D).

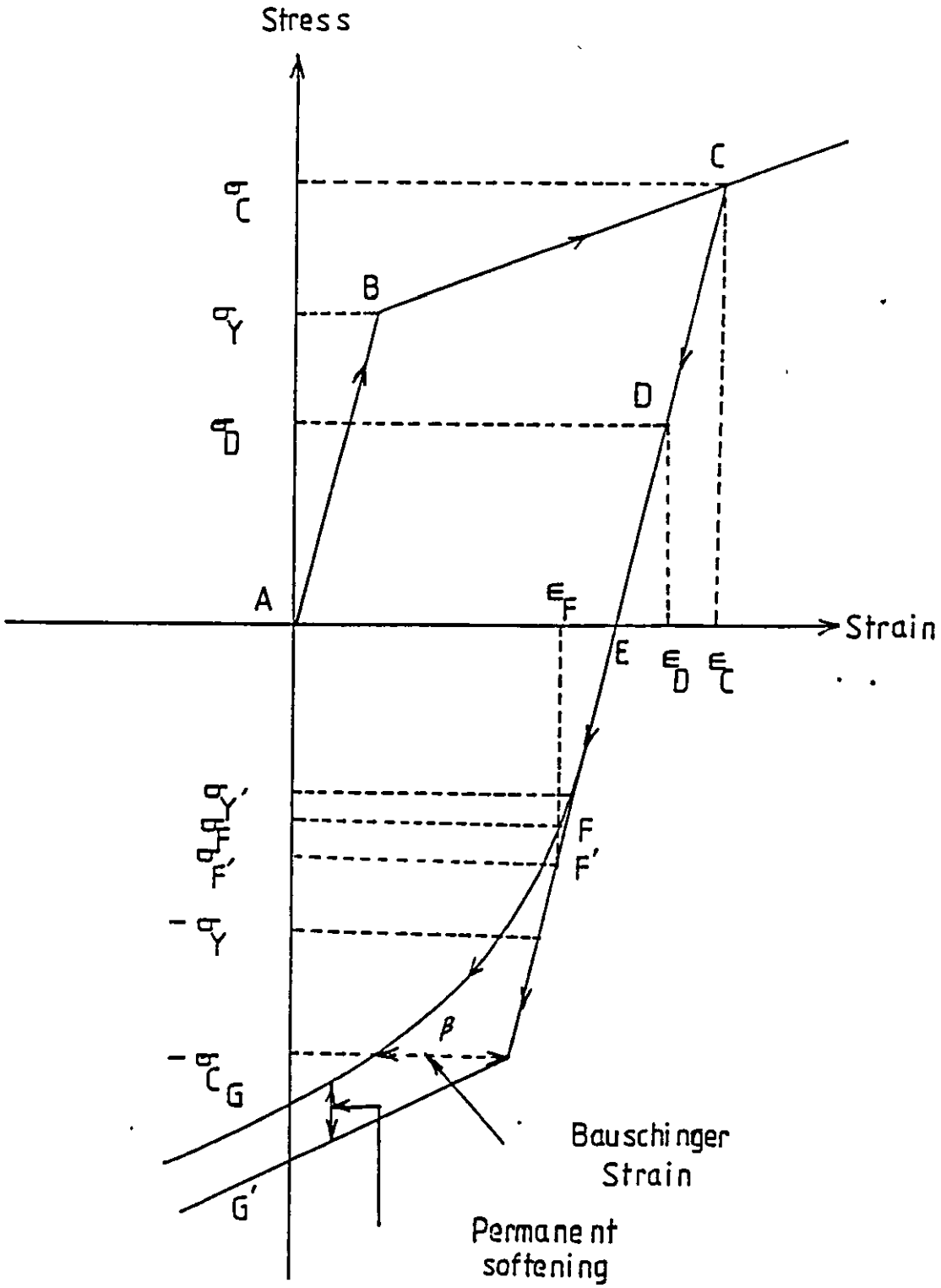

Fig. 5.1 Schematic presentation of the uniaxial stress-strain behaviour of chain material during forward and reverse tests.

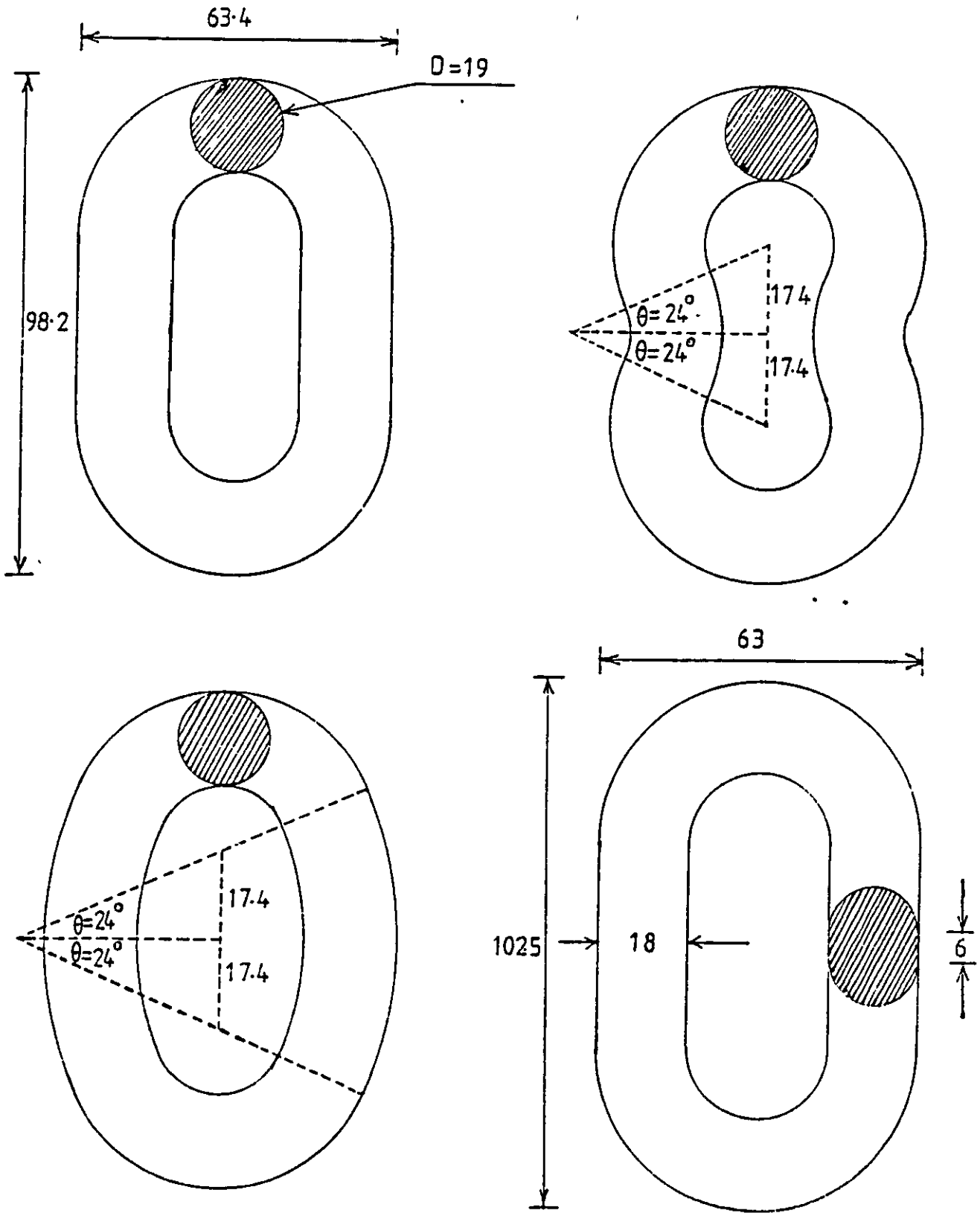

Fig. 5.2a Different link geometries (standard, eight shape, elliptical and oval-link).

Fig. 5.2b All the geometries used in the strain gauge work.

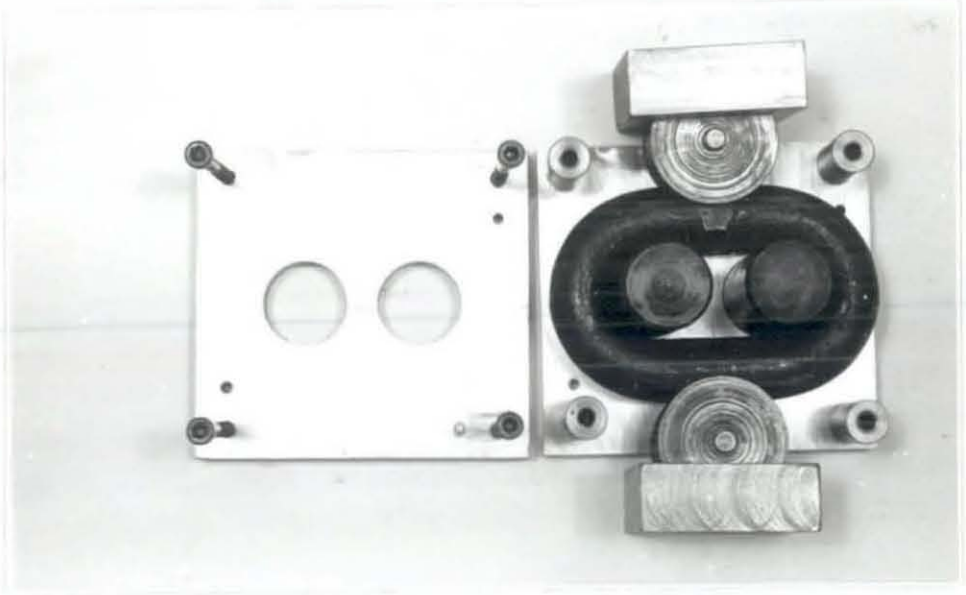

Fig. 5.3a Rollers, pins and packing plates to form the eight shape 19 mm mining cahin.

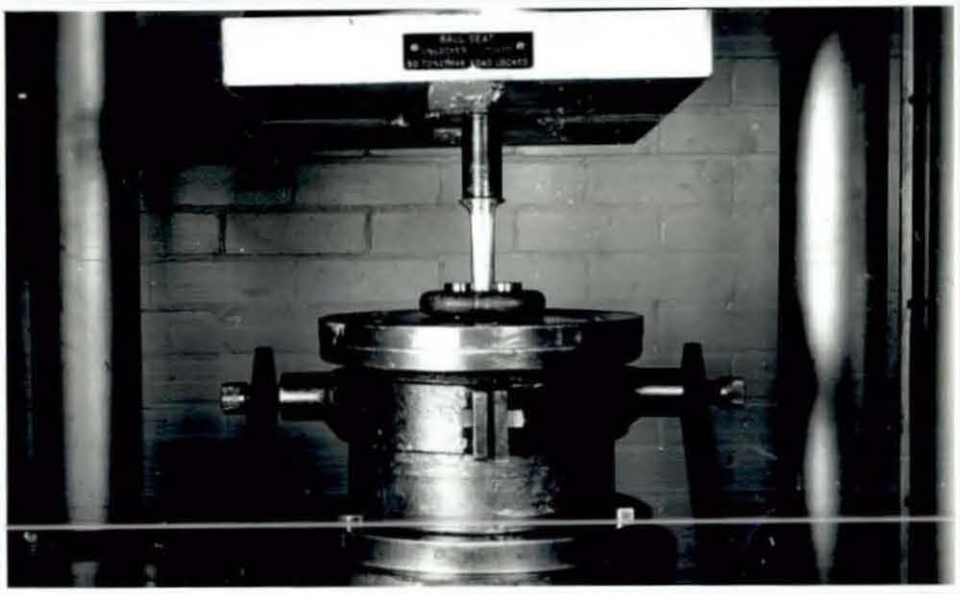

Fig. 5.3b Pins and punch used to form the elliptical 19 mm mining chain under the press.

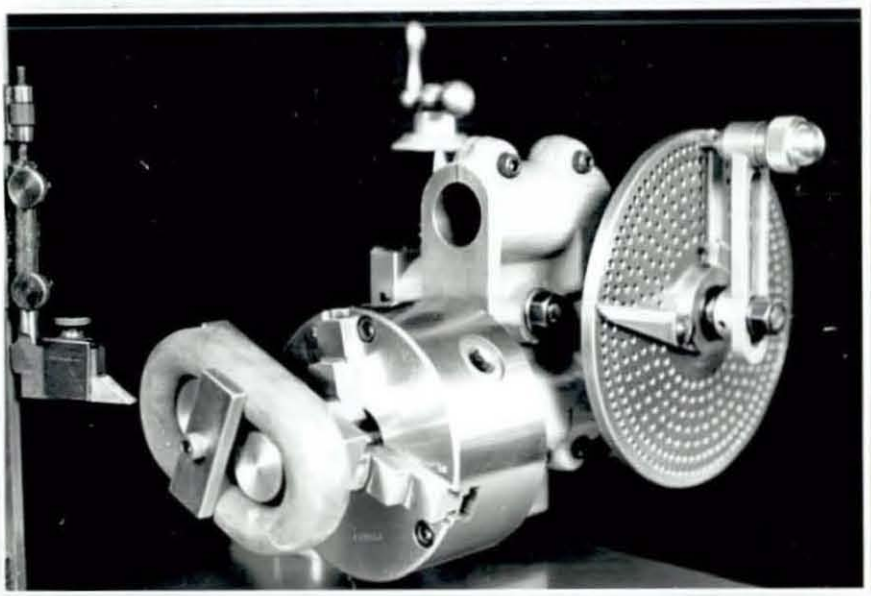

Fig. 5.4 Divider head with holding jigs used to mark off the strain gauge positions on various link geometries.

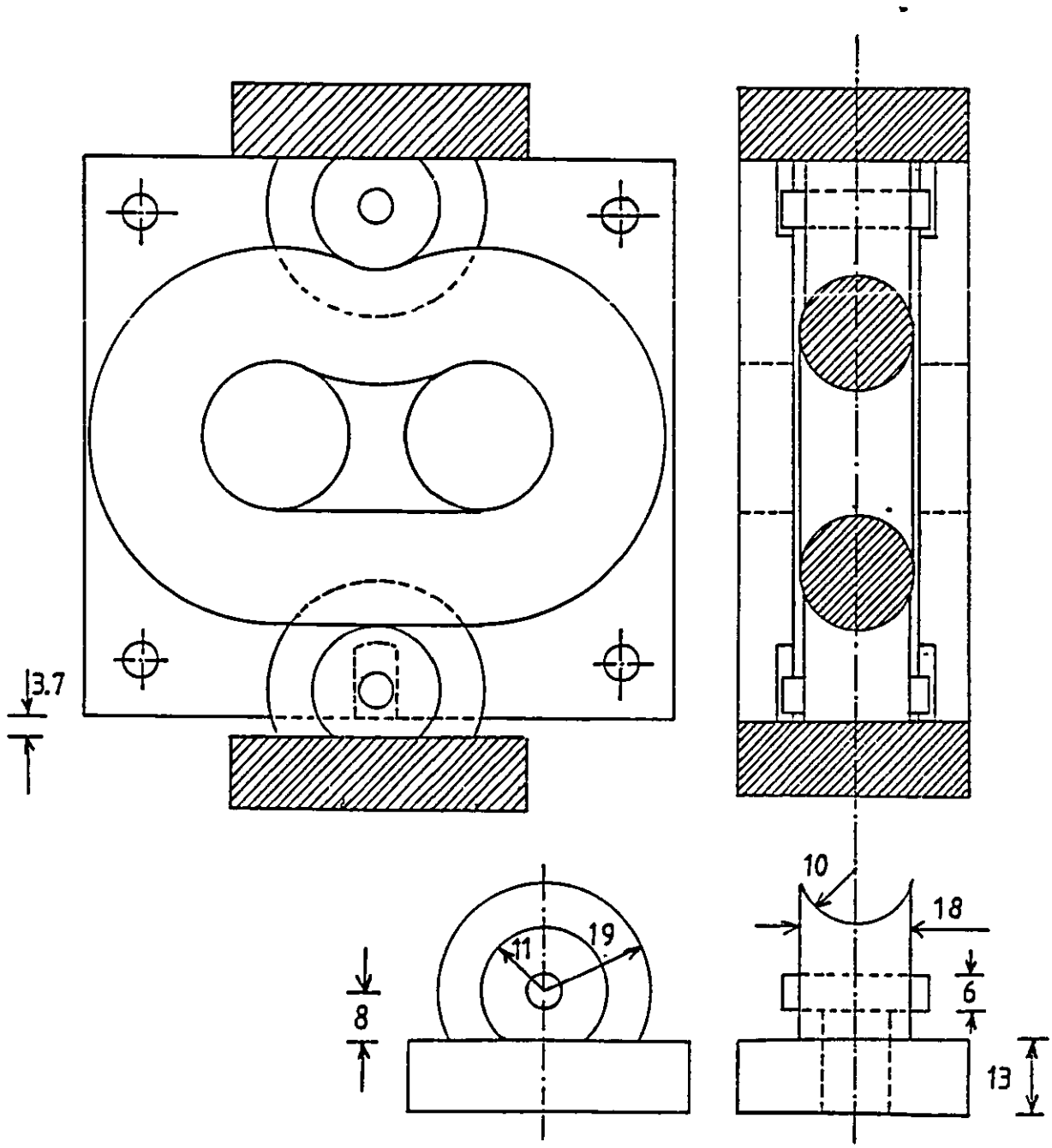

Fig. 5.3c Sketch of the arrangements used to form eight shape link.

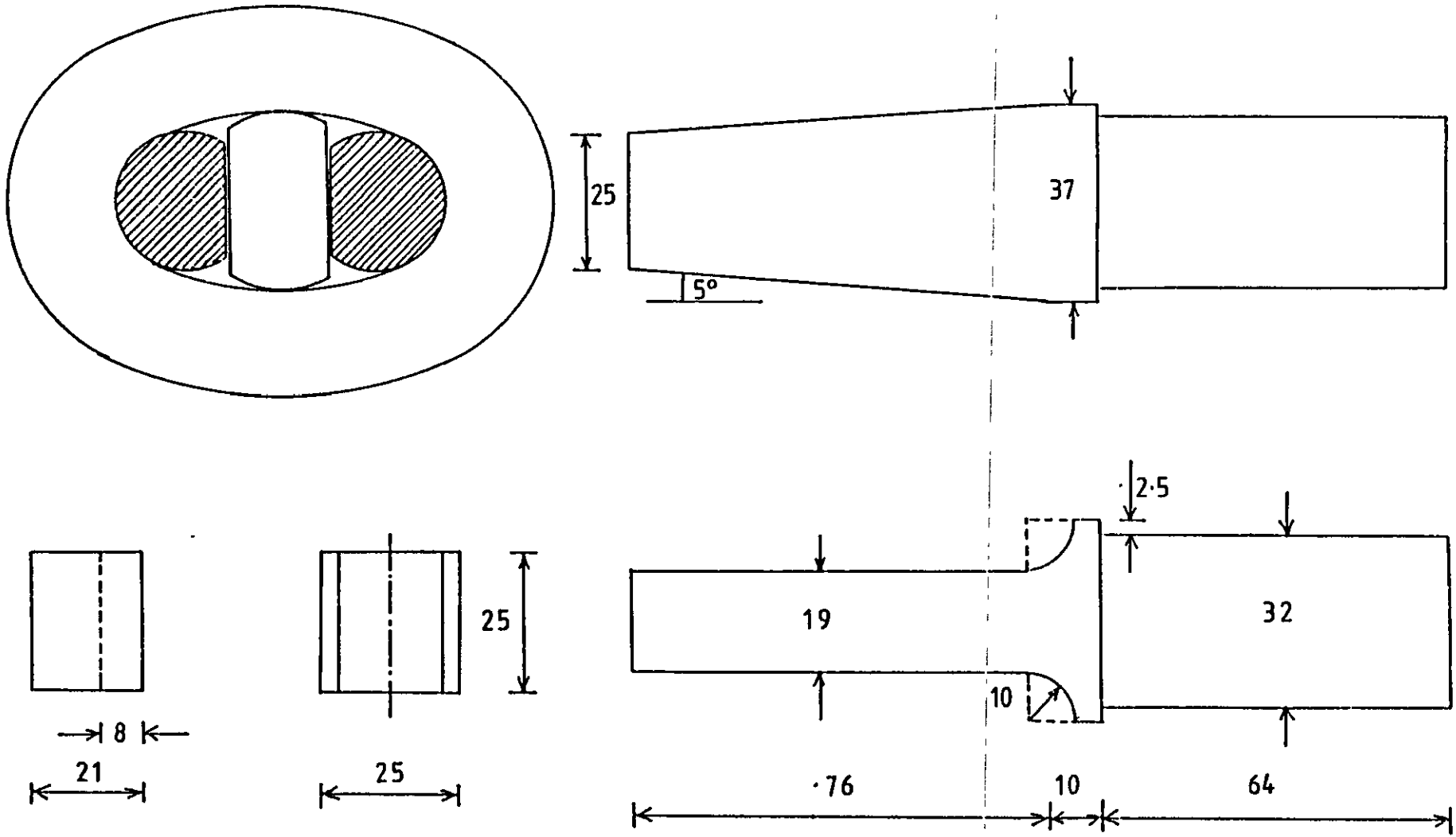

Fig. 5.3d Sketch of the arrangements used to form elliptical shape link.

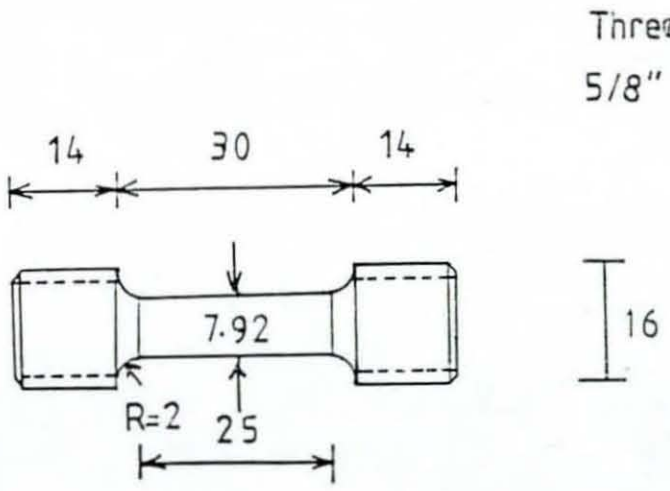

Fig. 5.5 Detail drawing of the material test specimen used to obtain the stress-strain curves under tension and compression (all dimensions in mm).

Fig. 5.6 two holders patially ground for calibration of chain links (19 mm mining).

Fig. 5.7a Instron testing machine used for tensile testing of the chain material.

Fig. 5.7b Instron testing machine with compression bed used for comparison testing of chain material.

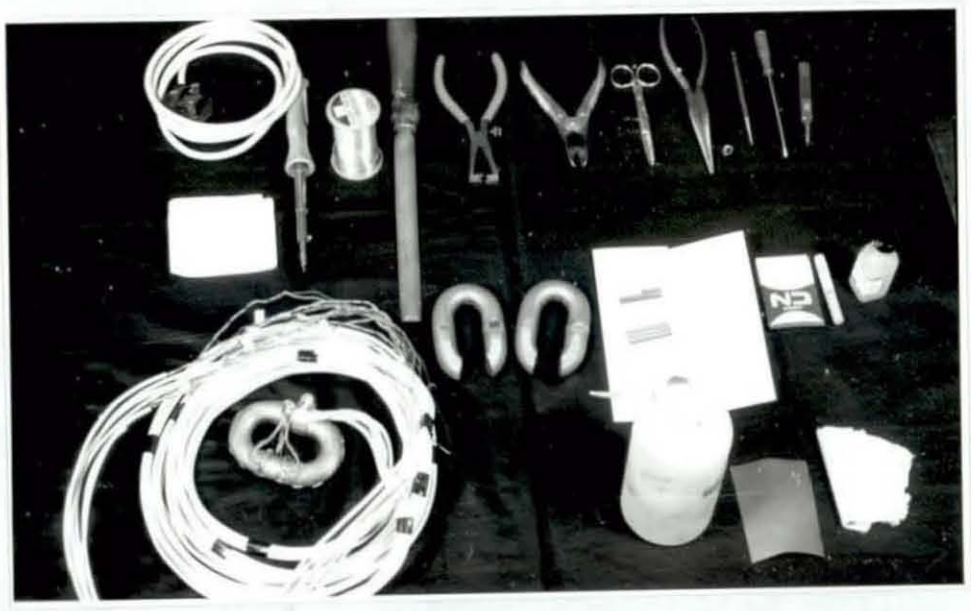

Fig. 5.8 Accessories used in the strain gauge installation.

Fig. 5.9 The data logger with its peripherals used in calibration processes.

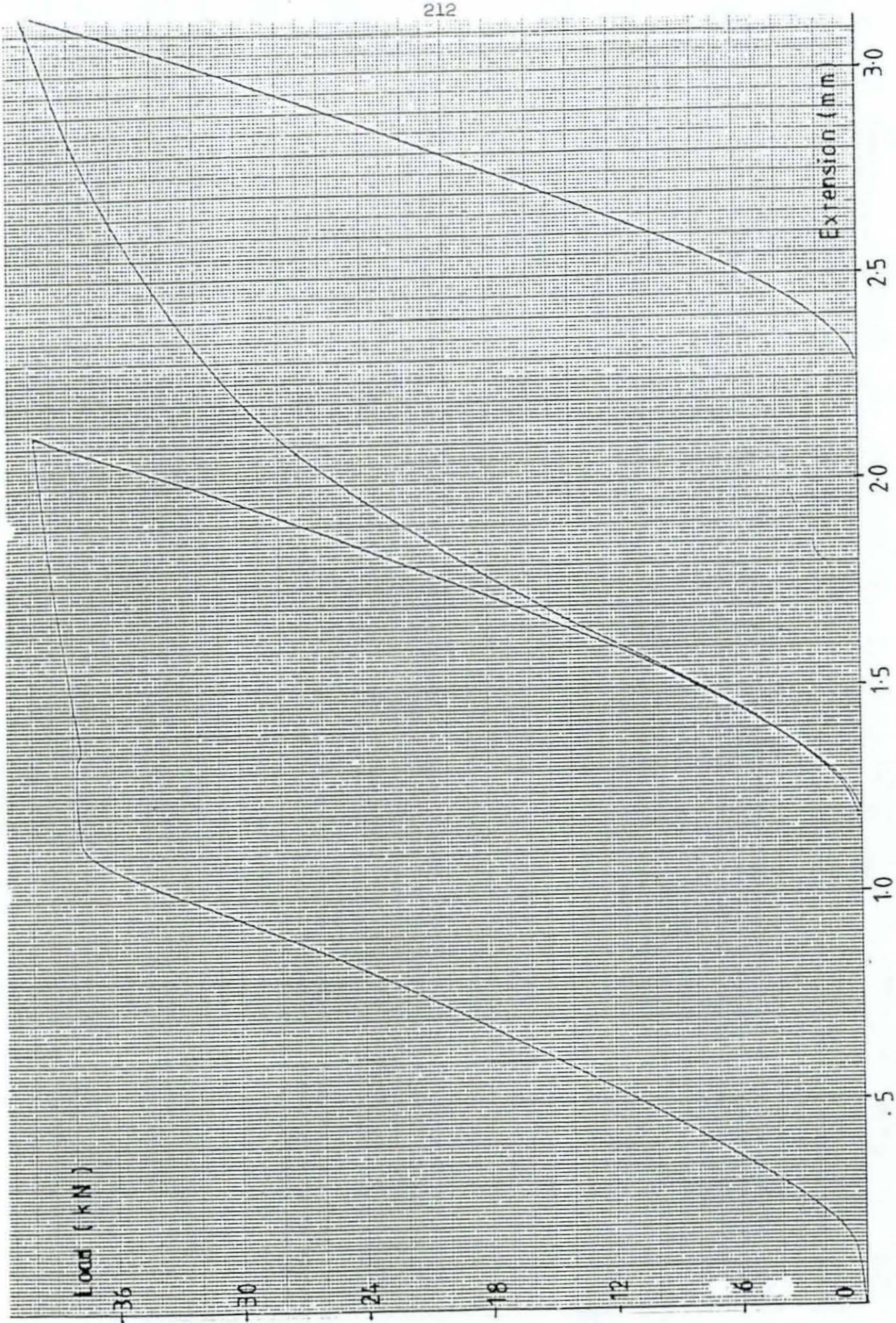

Fig. 5.10 Typical load-extension curve for test 3 of material 2 using Instron testing machine.

Fig. 5.11 Amsler testing machine used in the calibration of the chain link (for material 1 and 2).

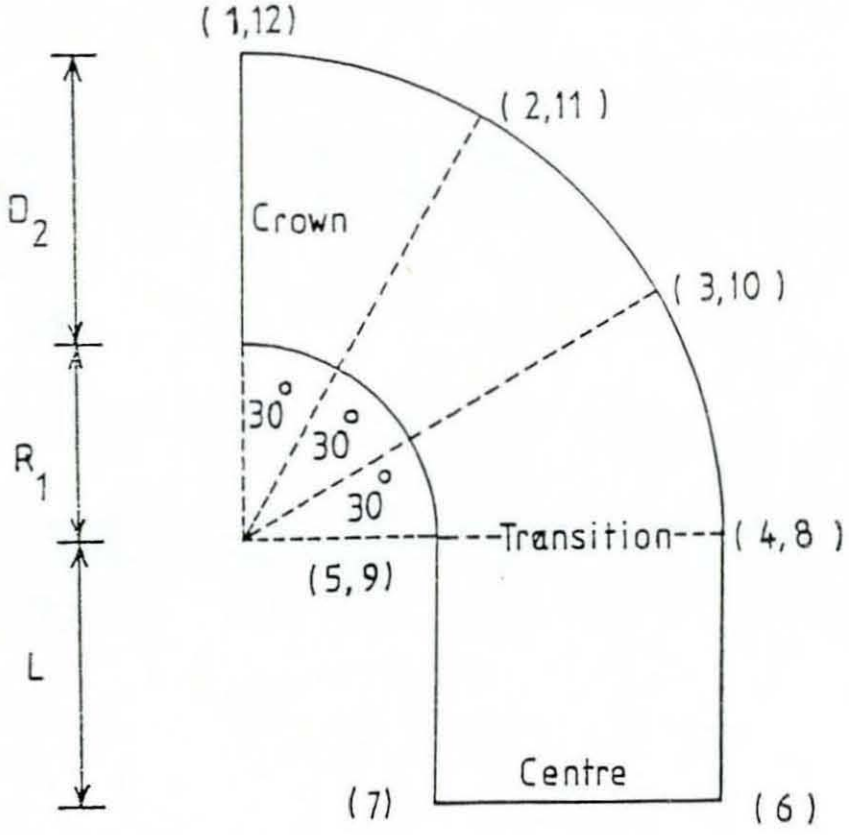

Fig. 5.12 Position of attachment of strain gauges.

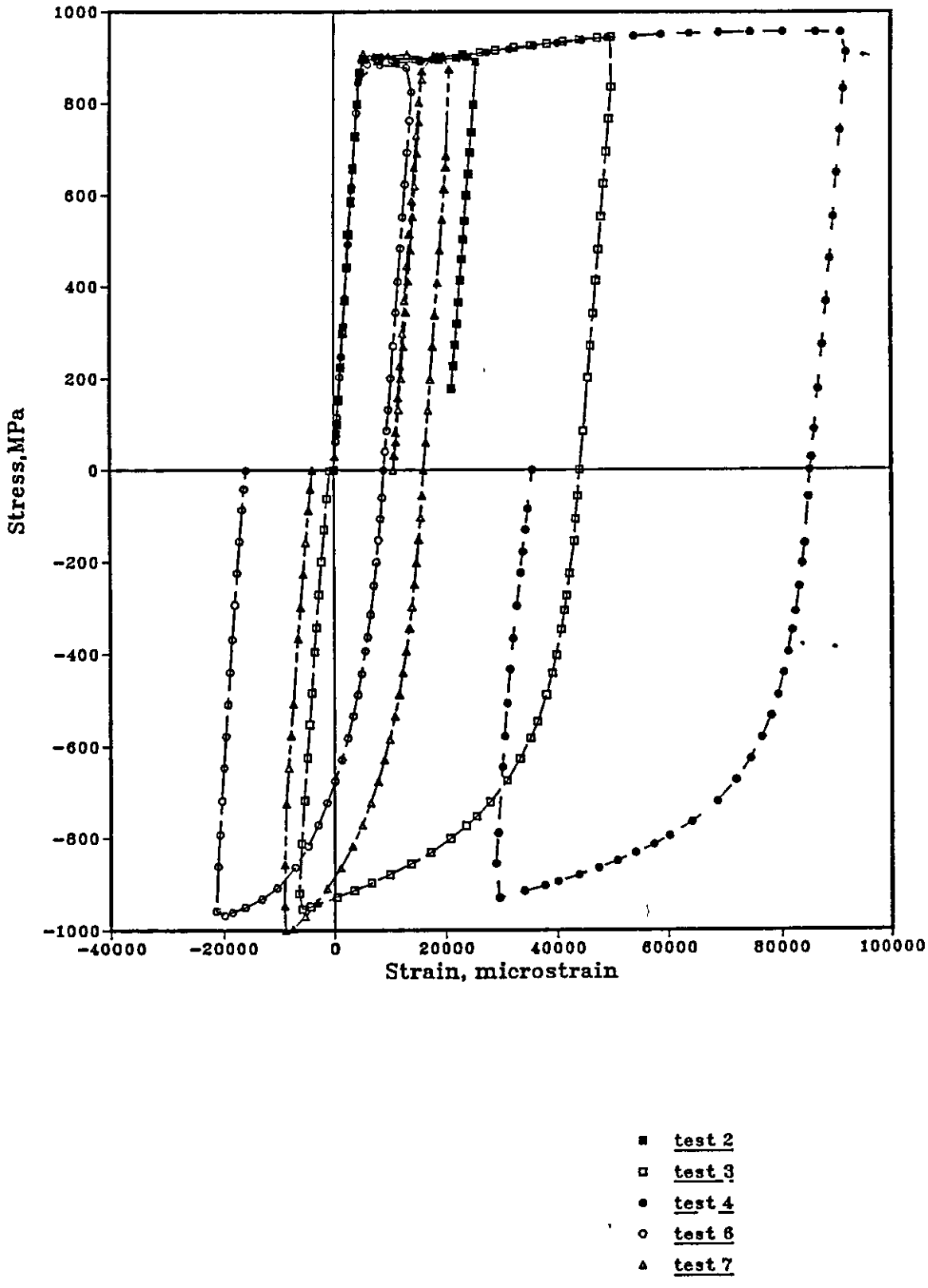

Fig. 5.13 Stress–strain curve of the material 1 (water quenched).

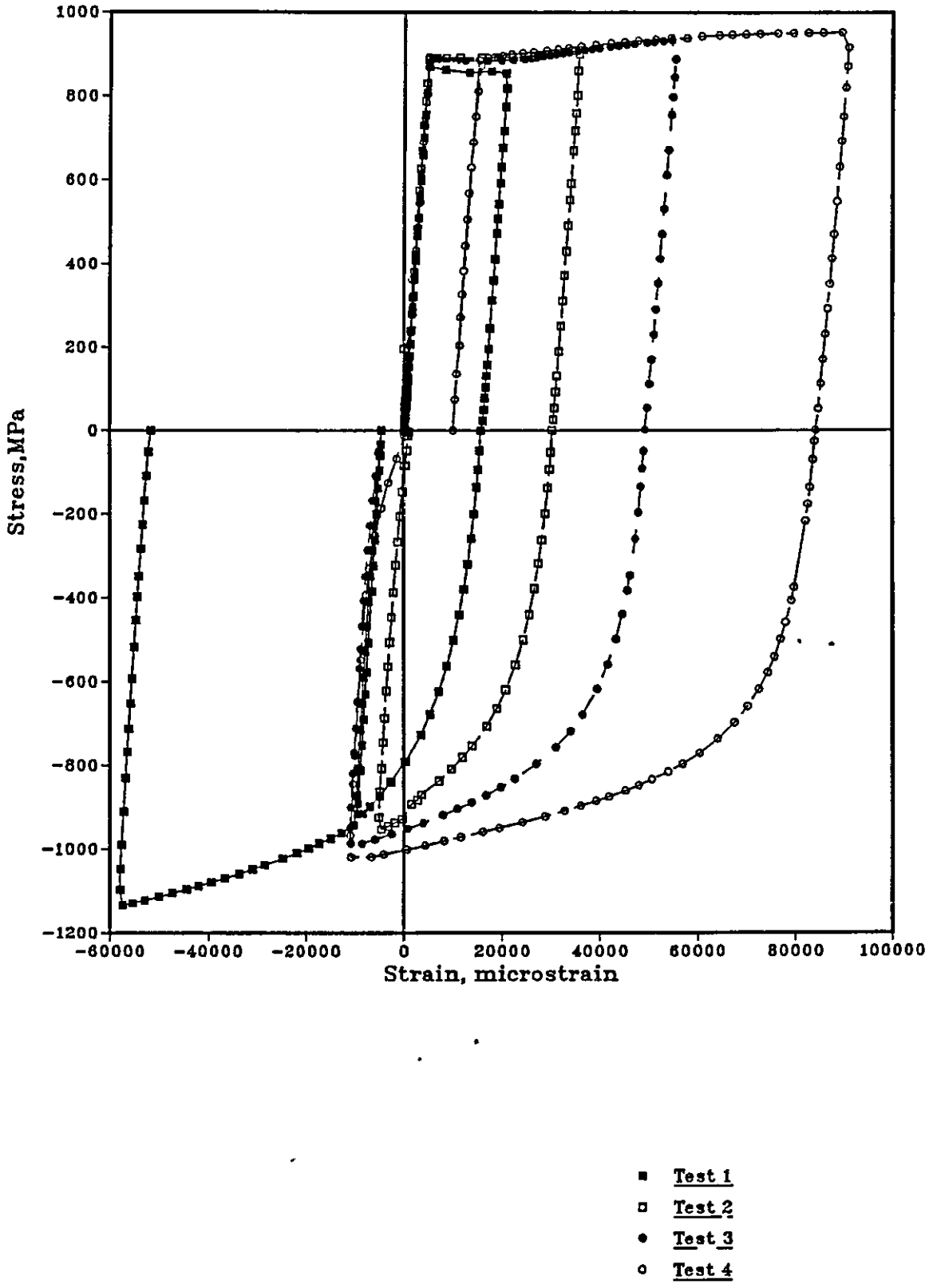

Fig. 5.14 Stress-strain curve of the material 2 (air cooled).

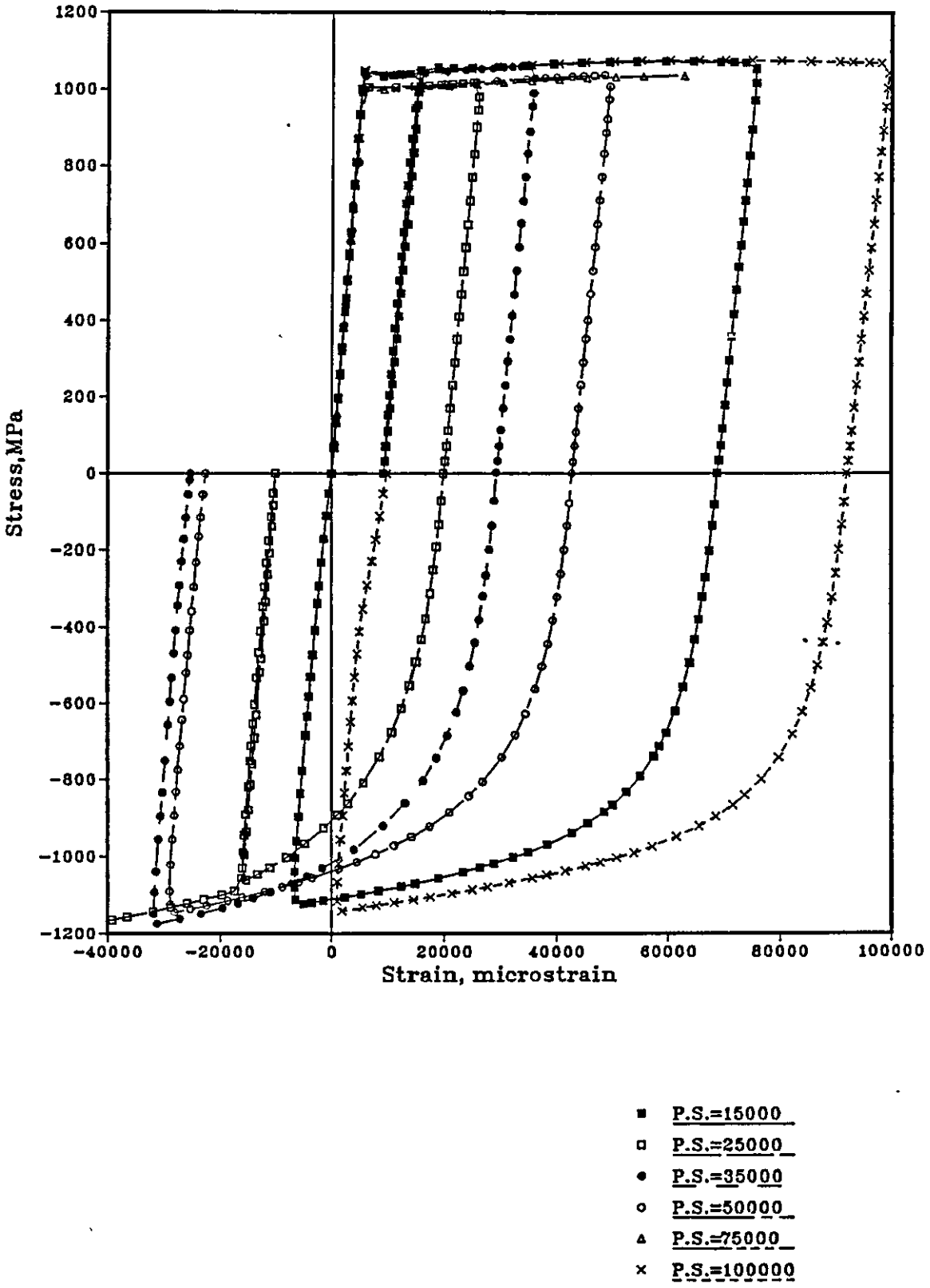

Fig. 5.15 Stress–strain curve of the material 3 (manufacturer's heat treatment). P.S. is the prestraining before unloading.

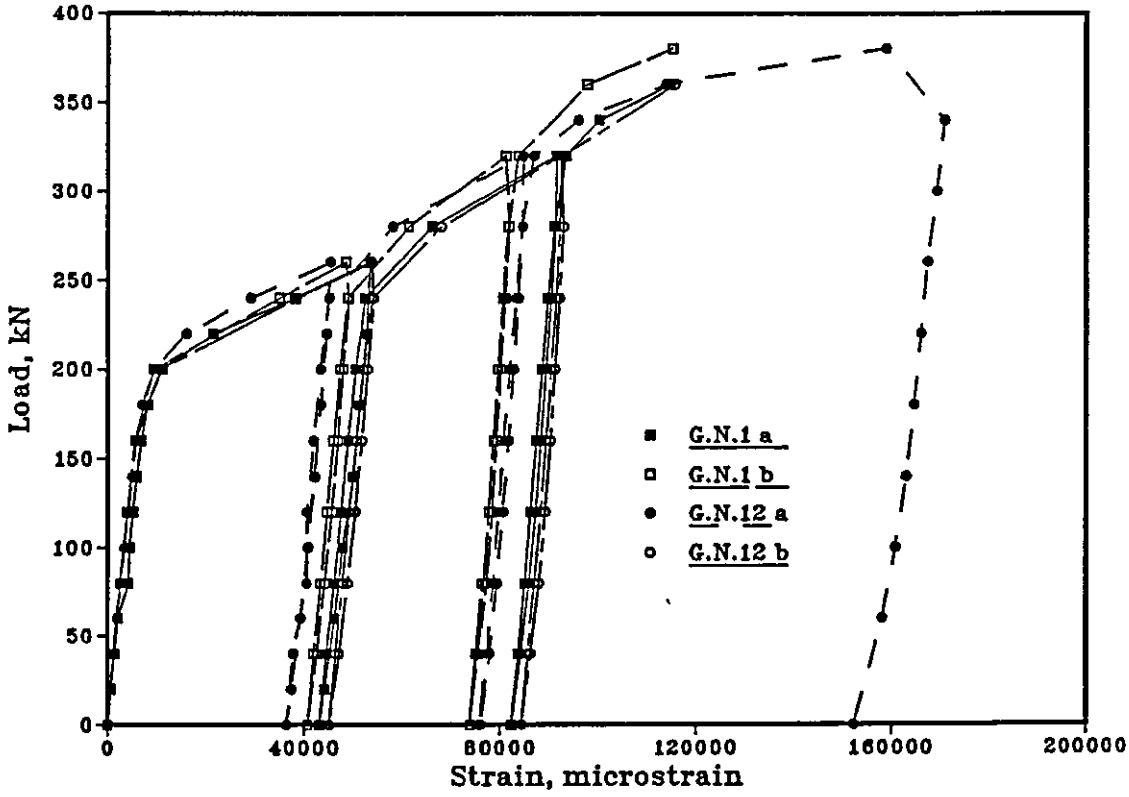

Fig. 5.16 Strain–load curve of strain gauges 1 and 12for the standard link (material 1, links a and b).

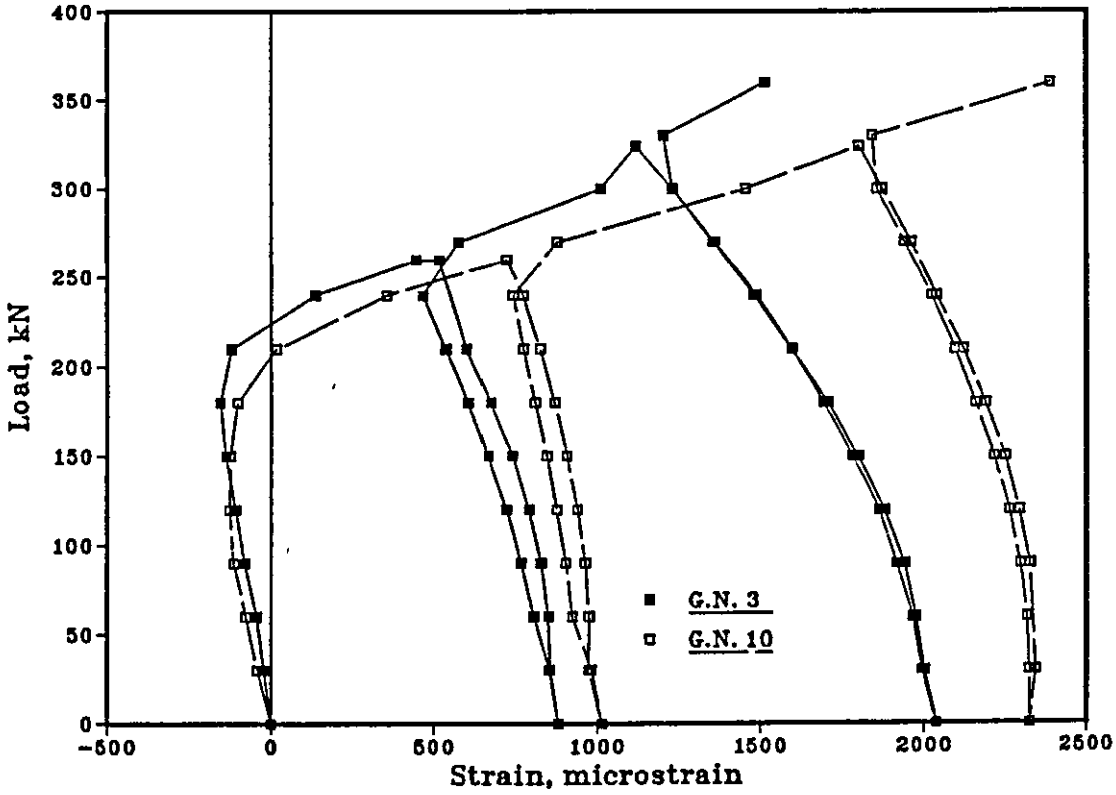

Fig. 5.17 Strain–load curve of strain gauges 3 and 10 for the standard link (material 3, link a).

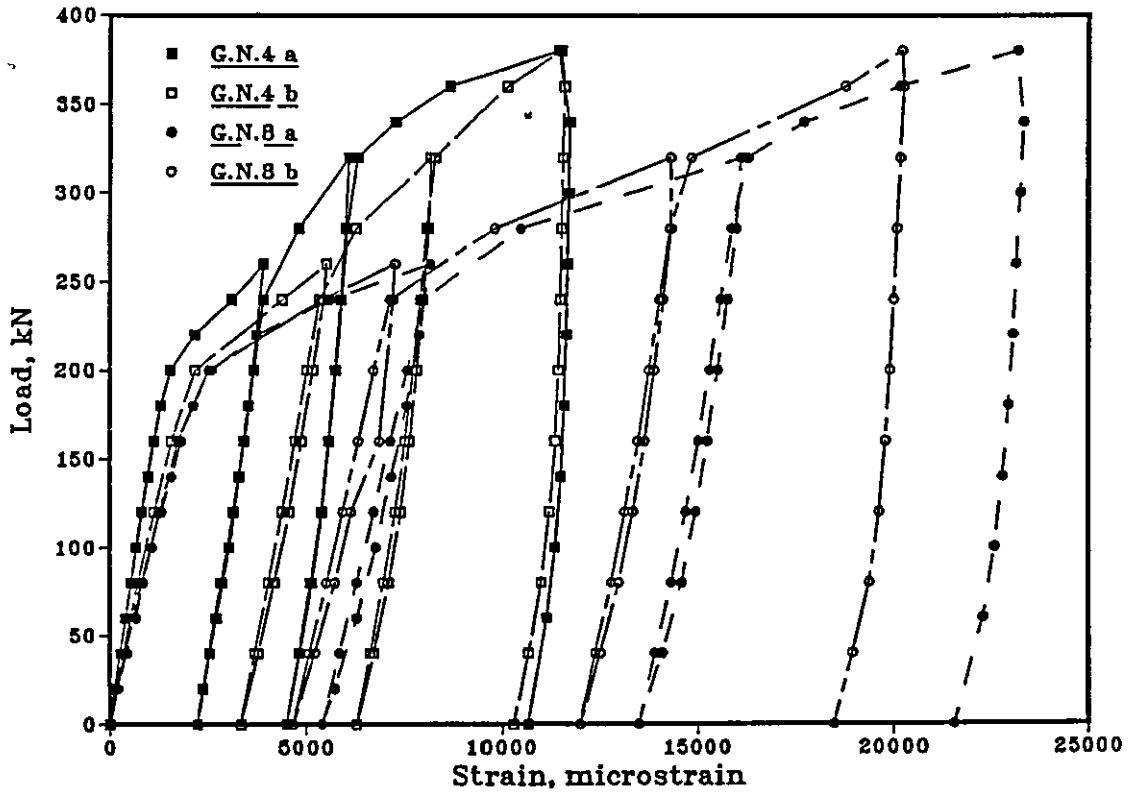

Fig. 5.18 Strain–load curve of strain gauges 4 and 8 for the standard link (material 1, links a and b).

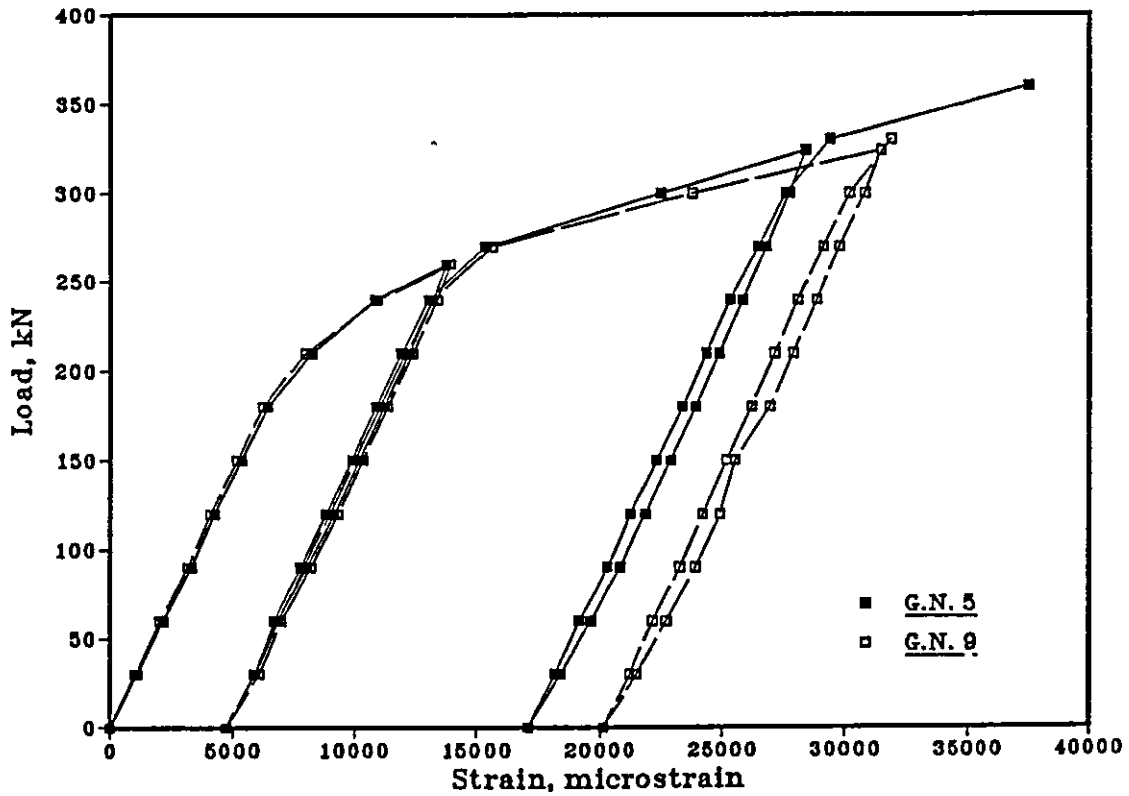

Fig. 5.19 Strain–load curve of strain gauges 5 and 9 for the standard link (material 3, link a).

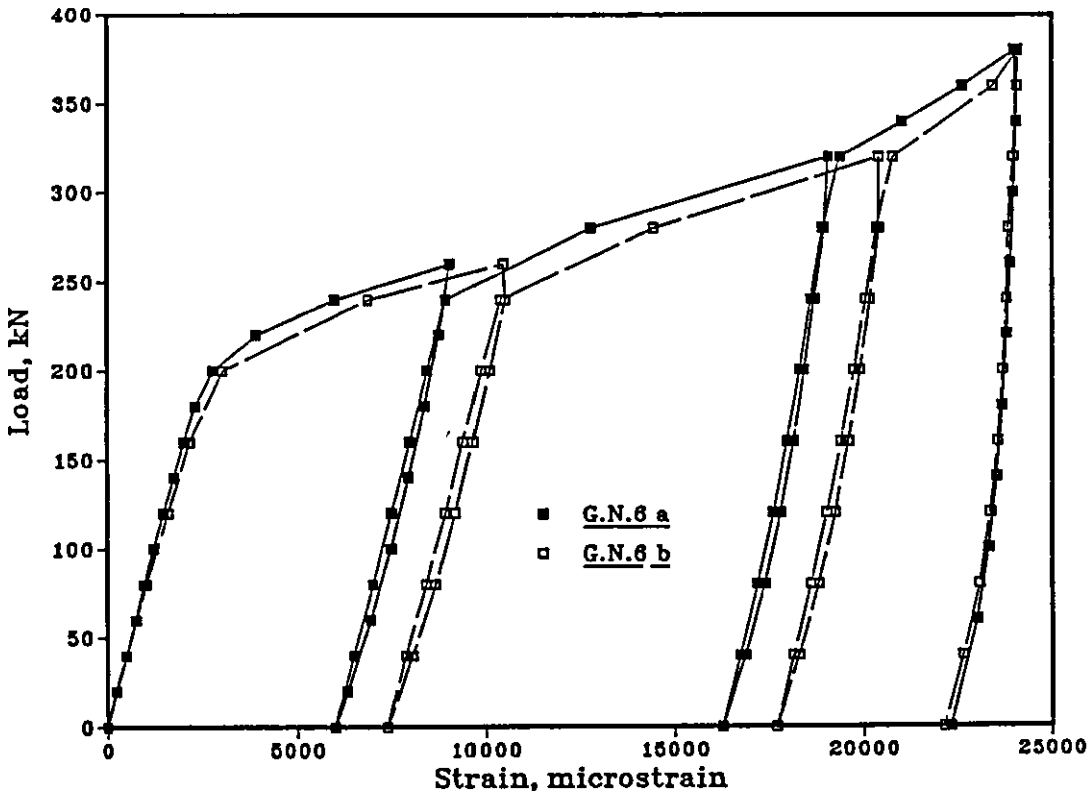

Fig. 5.20 Strain–load curve of strain gauge 6 for the standard link (material 1, links a and b).

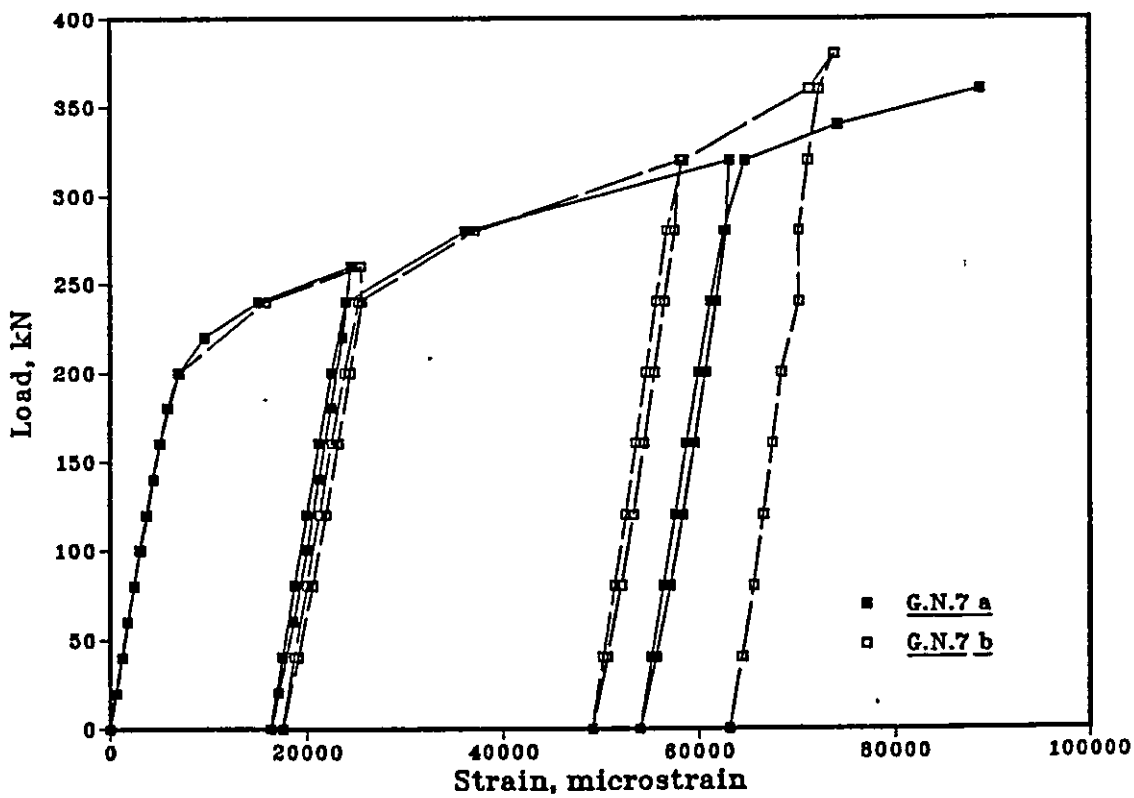

Fig. 5.21 Strain–load curve of strain gauge 7 for the standard link (material 1, links a and b).

G. N.	Cal. load = 260 kN		Cal. load = 320 kN		Cal. load = 380 kN	
	Loaded με	Unloaded με	Loaded με	Unloaded με	Loaded με	Unloaded με
1	53412 48604	43163 40738	91377 81214	82266 73961	115097	
12	45323 53783	36384 45131	84725 92230	75907 84370	158778	152369
2	4135	-625 -846	8563 7430	3011 1876	53435 52159	47529 46920
11	3148	-1357	3968	-1240	27026	21519
3	-360	-1084 -1250	-751 -737	-2192 -2287	-4705 -4381	-6950 -6809
10	-1010 -1550	-1653 -1539	-2910 -2854	-3158 -3388	-8091 -7641	-9431 -9531
4	-3909 -5516	-2228 -3325	-6103 -8174	-4505 -6305	-11429 -11503	-10658 -10277
8	-8166 -7255	-5395 -4680	-16090 -14289	-13483 -11980	-23152 -20211	-21528 -18432
5	16031	8209	29864	20700	55526	46044
9	24155 24295	15096 15387	51325 53713	41153 43898	96578	86893
6	-9047 -10436	-5993 -7396	-19073 -20400	-16250 -17680	-24003 -24077	-22302 -22128
7	24536 25543	16300 17501	63152 58180	53931 49152	73916	63119

Table 5.1 Strains at extreme load levels for material 1 (first row and second row are for first and second links).

G. N.	Cal. load = 260 kN		Cal. load = 320 kN		Cal. load = 350 kN	
	Loaded με	Unloaded με	Loaded με	Unloaded με	Loaded με	Unloaded με
1	58121 49197	51172 41155	88097	80105		
12	92923 51549	85369 43227				
2	4348	-128	20495	17045	47173	61292
11	2854	-1589	40558	36441	70761	
3	-319	-979	-1658	-2867	-3824	-10535
10	-2839	-3183	-6843	-8693	-11555	-32722
4	-4556	-2691	-7566	-6109	-9727	-12129
8	-15743	-13598	-21757	-20243	-23450	-29670
5	17963	10509	38143	29946	54243	
9	67223	57332				
6	-15129 -9358 -5458	-12514 -6310 -2822	-20552 -19555 -8992	-18576 -16737 -6712	-20983	-23811
7	61044	53318	106829	98625	125322	131880

Table 5.2 Strains at extreme load levels for material 2 (first row and second row are for first and second links).

G. N.	Cal. load = 260 kN		Cal. load = 320 kN		Cal. load = 380 kN	
	R.S. MPa	$R.S_{av.}$ MPa	R.S. MPa	$R.S_{av.}$ MPa	R.S. MPa	$R.S_{av.}$ MPa
1	-398 -156	-242	-320 0	-255		320
12	-250 -164		-242 -203		320	
2	-131 -173	-196	109 -242	-131	125 125	44
11	-284		-259		-117	
3	-227 -261	-289	-458 -478	-576	-898 -898	-898
10	-345 -322		-660 -708		-898 -898	
4	-466 -695	-509	-492 -437	-421	-664 -664	-664
8	-398 -477		-351 -405		-719 -609	
5	-305	-326	-469	-391	-305	-297
9	-336 -336		-375 -328		-289	
6	-297 -294	-296	-484 -422	-453	-719 -719	-719
7	-289 -274	-282	-274 -274	-274	-430	-430

Table 5.3 Residual stresses at various calibration loads for material 1.

G. N.	Cal. load = 260 kN		Cal. load = 320 kN		Cal. load = 350 kN	
	R.S. MPa	$R.S_{av.}$ MPa	R.S. MPa	$R.S_{av.}$ MPa	R.S. MPa	$R.S_{av.}$ MPa
1	-173					
	-293	-256	-220	-220		
12	-220					
	-339					
2	-27		53		1013	
		-180		113		1013
11	-332		173			
3	-205		-599		-892	
		-435		-744		-902
10	-665		-888		-912	
4	-562		-679		-892	
		-541		-649		-899
8	-519		-619		-905	
5	-299		-313			
		-383		-313		
9	-466					
6	-459		-413		-905	
	-126	-297	-333	-393		-905
	-306		-433			
7	-266	-266	-213	-213	-985	-985

Table 5.4 Residual stresses at various calibration loads for material 2.

G. N.	Cal. load = 260 kN		Cal. load = 320 kN		Cal. load = 380 kN	
	Stress MPa	Stress$_{av.}$ MPa	stress MPa	Stress$_{av.}$ MPa	Stress MPa	Stress$_{av.}$ MPa
1	937 929	931	969 961	965	984	100
12	929 929		961 969		1023	
2	864	761	898 898	875	937 937	92
11	658		829		907	
3	-75	-203	-157 -154	-379	-890 -890	-894
10	-211 -324		-608 -596		-898 -898	
4	-817 -898	-878	-898 -898	-901	-902 -902	-904
8	-898 -898		-906 -902		-907 -906	
5	906	907	907	927	932	951
9	907 907		937 937		969	
6	-898 -898	-898	-910 -910	-910	-907 -907	-907
7	910 910	910	945 937	941	953	953

Table 5.5 Stresses at extreme load levels for material 1.

G. N.	Cal. load = 260 kN		Cal. load = 320 kN		Cal. load = 350 kN	
	Stress MPa	$Stress_{av.}$ MPa	stress MPa	$Stress_{av.}$ MPa	Stress MPa	$Stress_{av.}$ MPa
1	925 919	932	953	953		
12	959 929					
2	890	730	889	901	915	927
11	596		912		939	
3	-67	-330	-346	-618	-799	-843
10	-593		-890		-886	
4	-890	-888	-890	-890	-885	-892
8	-886		-890		-899	
5	889	912	909	909	925	925
9	935					
6	-892 -885 -885	-887	-892 -892 -885	-890	-892	-892
7	932	932	972	972	992	992

Table 5.6 Stresses at extreme load levels for material 2.

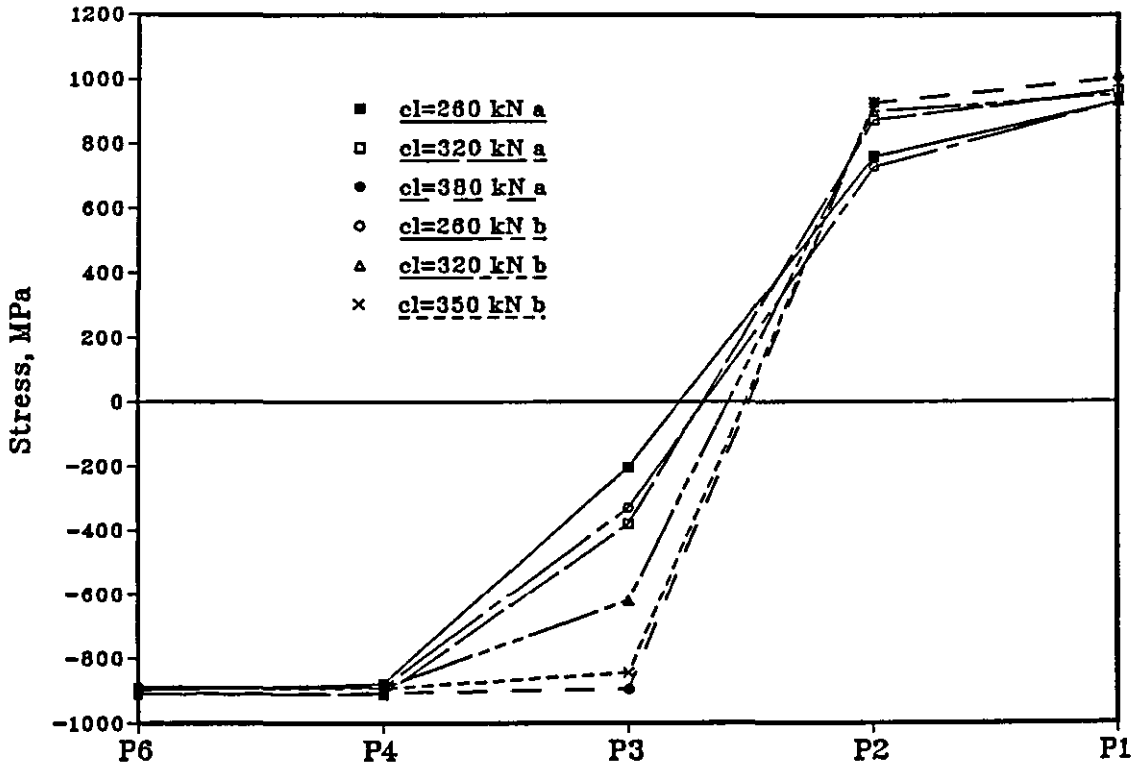

Fig. 5.22 Effect of calibration load (cl) on the stress pattern of the standard 19 mm mining chain link using the strain gauge method (material 1 and 2, links a and b).

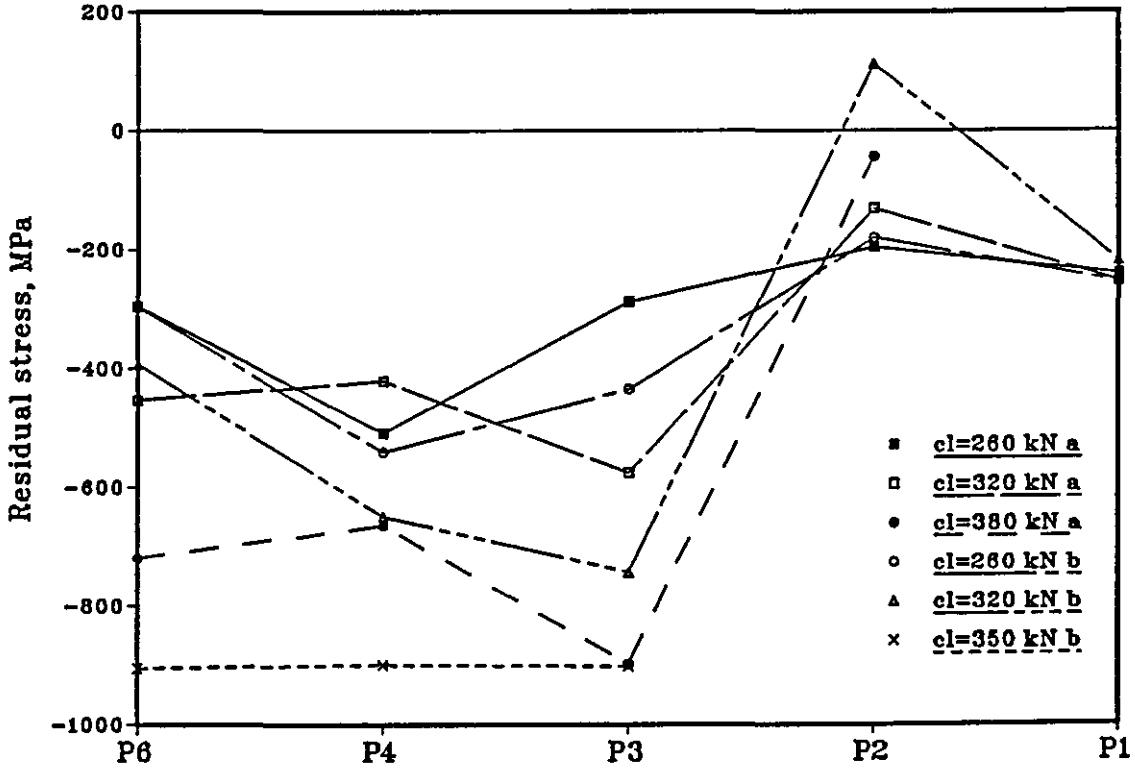

Fig. 5.23 Effect of calibration load (cl) on the residual stress pattern of the 19 mm standard mining chain link using strain gauge method (material 1 and 2, links a and b).

Stress type	Position	Cal. loads, material 1			Cal. loads, material 2		
		260 kN	320 kN	380 kN	260 kN	320 kN	350 kN
Res. stress	Tran. (5 and 9)	-326	-391	-297	-383	-313	
	Centre (7)	-282	-274	-430	-266	-213	-985
Total stress	Tran. (5 and 9)	907	927	951	912	909	925
	Centre (7)	910	941	953	932	972	992

Table 5.7 Residual and total stresses at the inside transition and centre of 19 mm minimg chain at various calibration loads for materials 1 and 2.

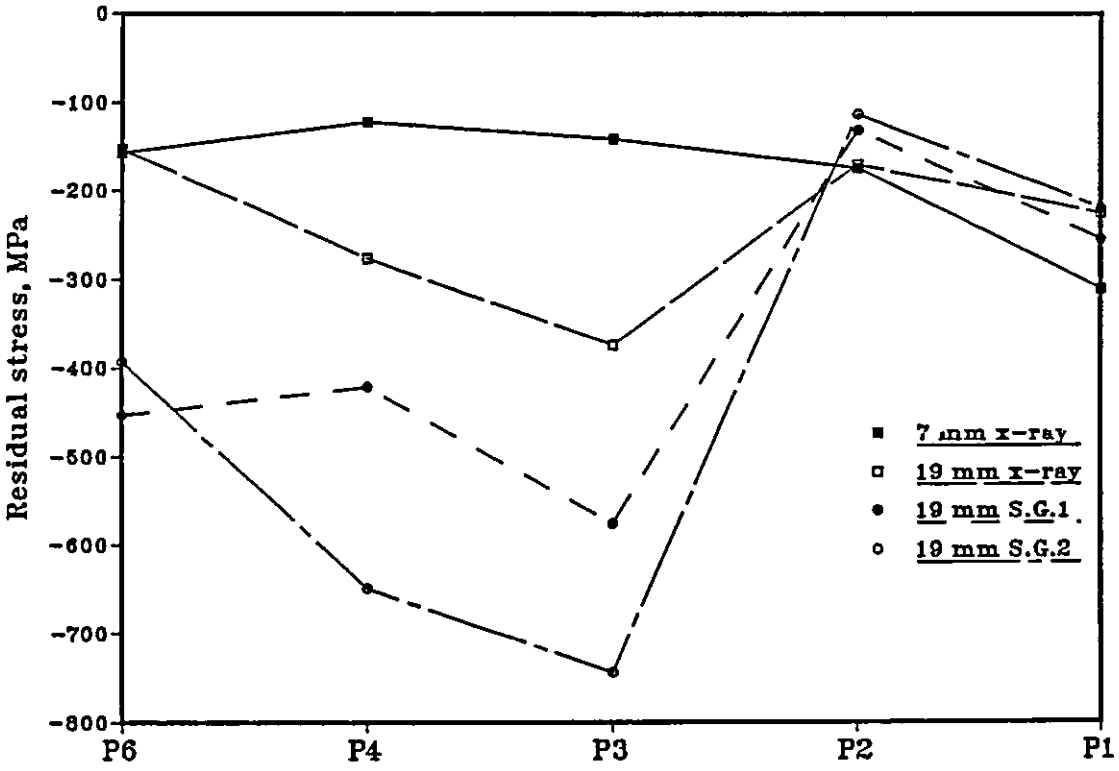

Fig. 5.24 Comparison of residual stress measurements on the 19 mm mining (cl=320 kN) and 7 mm lifting chains (cl= 38.5 kN) for material 1 and 2 (i.e. S.G.1 and S.G.2 respectively).

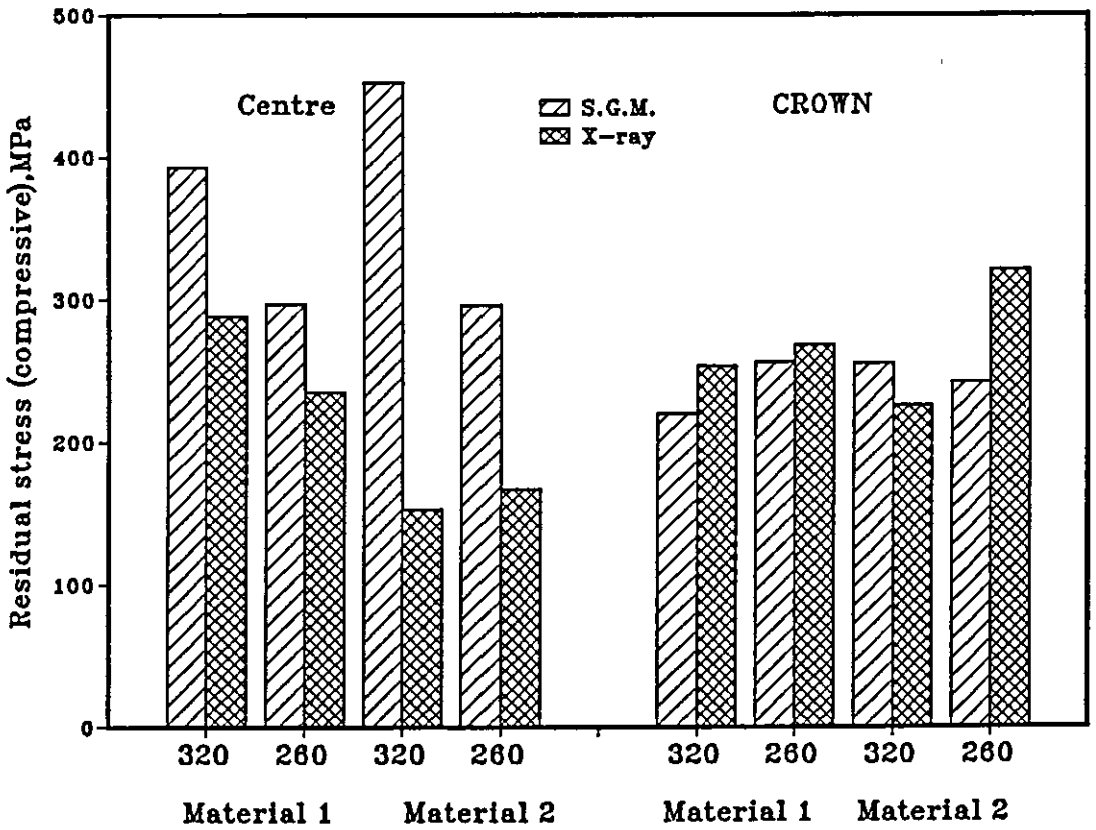

Fig. 5.25 Comparison of residual stress measurements using the x-ray and strain gauge methods for material 1 and 2.

G. N.	Cal. load = 260 kN		Cal. load = 320 kN		Cal. load = 380 kN	
	Loaded με	Unloaded με	Loaded με	Unloaded με	Loaded με	Unloaded με
1	23675 10779	14051 2585	56013 26963	45093 16833	50986	40405
12	26333 9722	15806 2168	68318 20922	56419 11776	36520	27050
2	4411 4741	-703 -125	4987 5865	-1139 -58	10181	3472
11	4493 4578	-815 2	4705 5859	-1585 239	9727	3293
3	-445 427	-878 -31	-1115 508	-2038 -277	709	-614
10	-721 496	-1013 5	-1801 704	-2324 -188	986	-489
4	-4179 -2455	-1567 -203	-7281 -3744	-4500 -1150	-4657	-2151
8	-4302 -2418	-1667 -166	-8741 -3628	-5739 -1072	-4547	-2110
5	13734 10397	4540 1504	28384 16133	17046 4996	23996	11172
9	13901 10452	4740 1408	31467 15628	20132 4428	23040	10222
6	-5417 -3509	-1964 -543	-13714 -6996	-9854 -3467	-14876	-11344
7	12447 9973	3878 2293	21246	11373	47607	36257

Table 5.8 Strains at extreme load levels for standard links (material 3).

G. N.	Cal. load = 260 kN		Cal. load = 320 kN		Cal. load = 380 kN	
	Loaded με	Unloaded με	Loaded με	Unloaded με	Loaded με	Unloaded με
1	7892 9663	1573 2539	18718 23761	11108 14792	32507 42582	24054 33130
12	9567 9332	2390 2408	23933 23027	15234 14334	42236 37932	32792 28823
2	4415 4046	139 -125	5025 4299	-251 -819	6461 5285	572 -546
11	4009 4621	-188 -242	4176 5182	-959 -560	5015 10289	-841 3735
3	825 -306	-18 -140	335 -1300	-871 -1256	-844 -3203	-2473 -3470
10	-410 632	-210 -138	-1586 -157	-1479 -117	-3944 -1372	-4016 -2717
4	-1416 -2172	-51 -225	-2744 -4283	-1171 -1950	-4168 -7901	-2595 -5518
8	-2307 -1549	-333 -58	-4661 -3201	-2286 -1355	-9289 -5245	-6662 -3342
5	10187 13042	1390 2922	17867 26251	6559 12957	28330 50856	14691 35218
9	13982 11003	3503 1988	28828 21218	15204 9288	59356 36951	42594 22690
6	-892 -1135	71 99	-1622 -2095	-844 -925	-1561 -2488	-1482 -2006
7	4076 4192	-112 -135	5087 5259	98 107	5480 5740	170 246

Table 5.9 Strains at extreme load levels for eight shape links (material 3).

G. N.	Cal. load = 260 kN		Cal. load = 320 kN		Cal. load = 380 kN	
	Loaded με	Unloaded με	Loaded με	Unloaded με	Loaded με	Unloaded με
1	41792	30728	80856	70239	98821	84993
12	47033	35282	88812	77629	102535	92231
2	3845 4997	-1148 -664	5140 13346	-915 6422	7129 33583	213 26452
11	3842 5377	-1619 -535	5349 15790	-1043 8561	8126 40656	897 32795
3	-1497 -290	-1527 -901	-1114 122	-1690 -1159	-936 577	-2164 -1427
10	-1761 5	-1977 -970	-1244 392	-1971 -1267	-1108 524	-2428 -1711
4	-8661 -5349	-4964 -2115	-12391 -7092	-8794 -4013	-14067 -7381	-11018 -4746
8	-9956 -5384	-6325 -2147	-14180 -7555	-10636 -4414	-16271 -8773	-13277 -5947
5	16361 10282	7748 2593	24512 14946	14577 6007	31995 17077	21112 7465
9	19009 10810	10522 3106	29123 17046	19342 8000	38566 22130	27842 12199
6	-28461 -15328	-23141 -10063	-57069 -43668	-51652 -38267	-81054 -64376	-76424 -59609
7	72957 42352	60453 29442	131150	116629		

Table 5.10 Strains at extreme load levels for elliptical links (material 3).

G. N.	Cal. load = 393 kN		Cal. load = 489 kN		Cal. load = 574 kN	
	Loaded με	Unloaded με	Loaded με	Unloaded με	Loaded με	Unloaded με
1	10219 31334	3160 22640	26317 43827	18106 35540	41194 60036	33121 52444
12	13004 43929	5209 34619	39559 59328	29860 50567	57215 75693	47782 67303
2	4262 5730	-185 448	5592 11492	326 5738	11358 42380	5613 36399
11	3268 3666	-549 -1257	3649 5252	-1264 -295	5783 32232	56 26042
3	1058 1327	-193 -1016	1393 1206	-820 -2158	1722 -1092	-1589 -5184
10	-688 -2142	-516 -2400	-1927 -2852	-1884 -4114	-2486 -5146	-3294 -8252
4	988 1524	179 1111	1156 1084	831 1381	504 2382	1039 3111
8	2699 6692	643 4373	5993 7957	3496 6300	8771 7753	6615 7339
5	6105 11588	435 3896	9006 16255	2119 6587	11341 39428	3084 28551
9	10096 31634	2428 19961	24499 48783	14015 35532	42465 75574	30157 61977
6	-2422 -5353	-342 -3140	-4279 -5458	-2062 -3912	-4849 -5495	-3143 -4891
7	6507 15549	588 7297	11729 22278	4273 12997	17668 31891	9055 21865

Table 5.11 Strains at extreme load levels for oval-links (material 3).

G. N.	Cal. load = 260 kN		Cal. load = 320 kN		Cal. load = 380 kN	
	R.S. MPa	$R.S_{av.}$ MPa	R.S. MPa	$R.S_{av.}$ MPa	R.S. MPa	$R.S_{av.}$ MPa
1	-357		-357			
	-348	-337	-311	-378	-366	-343
12	-412		-513			
	-229		-330		-330	
2	-127		-206			
	-23	0	-10	-115	-183	-151
11	148		-287			
	0		43		-119	
3	-159		-369			
	-6	-48	-50	-219	-111	-109
10	-183		-421			
	1		-34		-89	
4	-284		-513			
	-37	-163	-208	-328	-389	-386
8	-302		-395			
	-30		-194		-382	
5	-403		-495			
	-431	-401	-522	-541	-568	-568
9	-376		-623			
	-412		-522		-568	
6	-355	-227	-379	-403	-433	-433
	-98		-426			
7	-348	-316		-256		-431
	-284		-256		-431	

Table 5.12 Residual stresses at various calibration loads for standard links (materail 3).

G. N.	Cal. load = 260 kN		Cal. load = 320 kN		Cal. load = 380 kN	
	R.S. MPa	$R.S_{av.}$ MPa	R.S. MPa	$R.S_{av.}$ MPa	R.S. MPa	$R.S_{av.}$ MPa
1	-200 -213	-210	-292 -347	-324	-284 -312	-325
12	-213 -213		-292 -363		-371 -331	
2	25 -23	-19	-45 -148	-118	-71 -99	-114
11	-34 -44		-174 -101		-152 -134	
3	-3 -25	-23	-158 -227	-169	-448 -628	-574
10	-38 -25		-268 -21		-727 -492	
4	-9 -41	-30	-212 -353	-306	-470 -537	-561
8	-60 -10		-414 -245		-552 -605	
5	-355 -489	-433	-497 -600	-565	-623 -670	-653
9	-458 -426		-608 -552		-679 -647	
6	13 18	16	-153 -167	-160	-268 -363	-315
7	-20 -25	-23	18 19	19	31 45	38

Table 5.13 Residual stresses at various calibration loads for eight shape links (material 3).

G. N.	Cal. load = 260 kN		Cal. load = 320 kN		Cal. load = 380 kN	
	R.S. MPa	$R.S_{av.}$ MPa	R.S. MPa	$R.S_{av.}$ MPa	R.S. MPa	$R.S_{av.}$ MPa
1	-181	-239	-245	-261	-237	-223
	-308		-205		-87	
12	-245		-347		-355	
	-221		-245		-213	
2	-33	-70	59	-91	-142	0
	81		-142		47	
11	-99		-229		10	
	-228		-53		87	
3	-35	-187	-148	-414	-288	-705
	-184		-391		-938	
10	-93		-341		-596	
	-434		-775		-1002	
4	32	210	150	437	188	543
	201		250		563	
8	116		632		529	
	489		718		892	
5	79	-264	-316	-430	-355	-501
	-331		-410		-497	
9	-268		-450		-568	
	-537		-544		-584	
6	-62	-315	-373	-541	-569	-727
	-568		-708		-885	
7	-71	-142	-316	-328	-355	-403
	-213		-339		-450	

Table 5.14 Residual stresses at various calibration loads for elliptical links (material 3).

G. N.	Cal. load = 393 kN		Cal. load = 489 kN		Cal. load = 575 kN	
	R.S. MPa	$R.S_{av.}$ MPa	R.S. MPa	$R.S_{av.}$ MPa	R.S. MPa	$R.S_{av.}$ MPa
1	-165	-238	-211	-238	-156	-149
	-229		-183		0	
12	-266		-321		-284	
	-293		-238		-156	
2	-33	-110	59	-79	-92	-43
	-81		-92		-192	
11	-99		-229		10	
	-228		-53		103	
3	-35	-187	-148	-406	288	-708
	-184		-391		-938	
10	-93		-341		-596	
	-434		-745		-1010	
4	32	239	150	436	188	565
	201		250		563	
8	116		633		643	
	608		710		864	
5	79	-218	-165	-391	-330	-481
	-247		-431		-513	
9	-284		-400		-513	
	-421		-568		-568	
6	-62	-315	-373	-560	-569	-727
	-568		-747		-885	
7	-55	-133	-247	-284	-293	-339
	-211		-321		-385	

Table 5.15 Residual stresses at various calibration loads for oval-links (material 3).

G. N.	Cal. load = 260 kN		Cal. load = 320 kN		Cal. load = 380 kN	
	Stress MPa	$Stress_{av.}$ MPa	stress MPa	$Stress_{av.}$ MPa	Stress MPa	$Stress_{av.}$ MPa
1	1018 1010	1015	1034 1018	1027	1034	1032
12	1022 1010		1041 1014		1030	
2	798 858	825	903 1006	942	1010	1010
11	813 829		852 1006		1010	
3	-81 -77	-95	-202 92	-77	128	153
10	-131 -90		-326 127		178	
4	-756 -444	-604	-1006 -678	-838	-843	-833
8	-779 -438		-1010 -657		-823	
5	1010 1010	1010	1026 1010	1018	1018	1018
9	1010 1010		1026 1010		1018	
6	-980 -635	-808	-1010 -1006	-1008	-1010	-1010
7	1010 1010	1010	1014	1014	1034	1034

Table 5.16 Stresses at extreme load levels for standard links (material 3).

G. N.	Cal. load = 260 kN		Cal. load = 320 kN		Cal. load = 380 kN	
	Stress MPa	$Stress_{av.}$ MPa	stress MPa	$Stress_{av.}$ MPa	Stress MPa	$Stress_{av.}$ MPa
1	1010 1010	1010	1010 1018	1013	1026 1026	1026
12	1010 1010		1018 1018		1026 1026	
2	799 732	773	910 778	846	1006 957	970
11	726 836		756 938		908 1010	
3	149 -55	34	61 -235	-122	-152 -580	-424
10	-74 114		-287 -28		-714 -248	
4	-256 -393	-337	-497 -775	-674	-754 -1010	-931
8	-418 -280		-844 -579		-1010 -949	
5	1010 1010	1010	1014 1022	1018	1022 1034	1029
9	1010 1010		1022 1014		1038 1022	
6	-161 -205	-183	-294 -379	-337	-283 -450	-367
7	738 759	749	920 952	936	992 1006	999

Table 5.17 Stresses at extreme load levels for eight shape links (material 3).

G. N.	Cal. load = 260 kN		Cal. load = 320 kN		Cal. load = 380 kN	
	Stress MPa	$Stress_{av.}$ MPa	stress MPa	$Stress_{av.}$ MPa	Stress MPa	$Stress_{av.}$ MPa
1	1026	1028	1045	1047	1057	1053
12	1030		1049		1049	
2	696 904	817	930 1010	980	1006 1026	1017
11	695 973		968 1010		1010 1026	
3	-271 -52	-160	-202 22	-84	-169 104	-43
10	-319 1		-225 71		-201 95	
4	-1010 -968	-991	-1010 -1010	-1010	-1010 -1010	-1010
8	-1010 -975		-1010 -1010		-1010 -1010	
5	1010 1010	1011	1018 1010	1017	1026 1014	1020
9	1014 1010		1026 1014		1026 1014	
6	-1018 -1010	-1014	-1034 -1026	-1030	-1045 -1041	-1043
7	1041 1026	1034	1073	1073		

Table 5.18 Stresses at extreme load levels for elliptical links (material 3)

G. N.	Cal. load = 393 kN		Cal. load = 489 kN		Cal. load = 575 kN	
	Stress MPa	$Stress_{av.}$ MPa	stress MPa	$Stress_{av.}$ MPa	Stress MPa	$Stress_{av.}$ MPa
1	1010 1026	1018	1022 1026	1027	1026 1034	1035
12	1010 1026		1026 1034		1034 1045	
2	771 1006	758	1006 1010	907	1010 1026	1022
11	592 664		660 951		1006 1026	
3	191 240	-20	252 218	-99	311 -195	-330
10	-124 -388		-349 -516		-500 -931	
4	179 276	488	209 196	605	91 431	636
8	489 1006		1006 1010		1010 1010	
5	1006 1010	1013	1010 1010	1018	1010 1026	1027
9	1010 1026		1018 1034		1026 1045	
6	-438 -969	-704	-774 -988	-881	-878 -995	-937
7	1010 1010	1010	1010 1014	1012	1014 1026	1020

Table 5.19 Stresses at extreme load levels for oval-links (material 3).

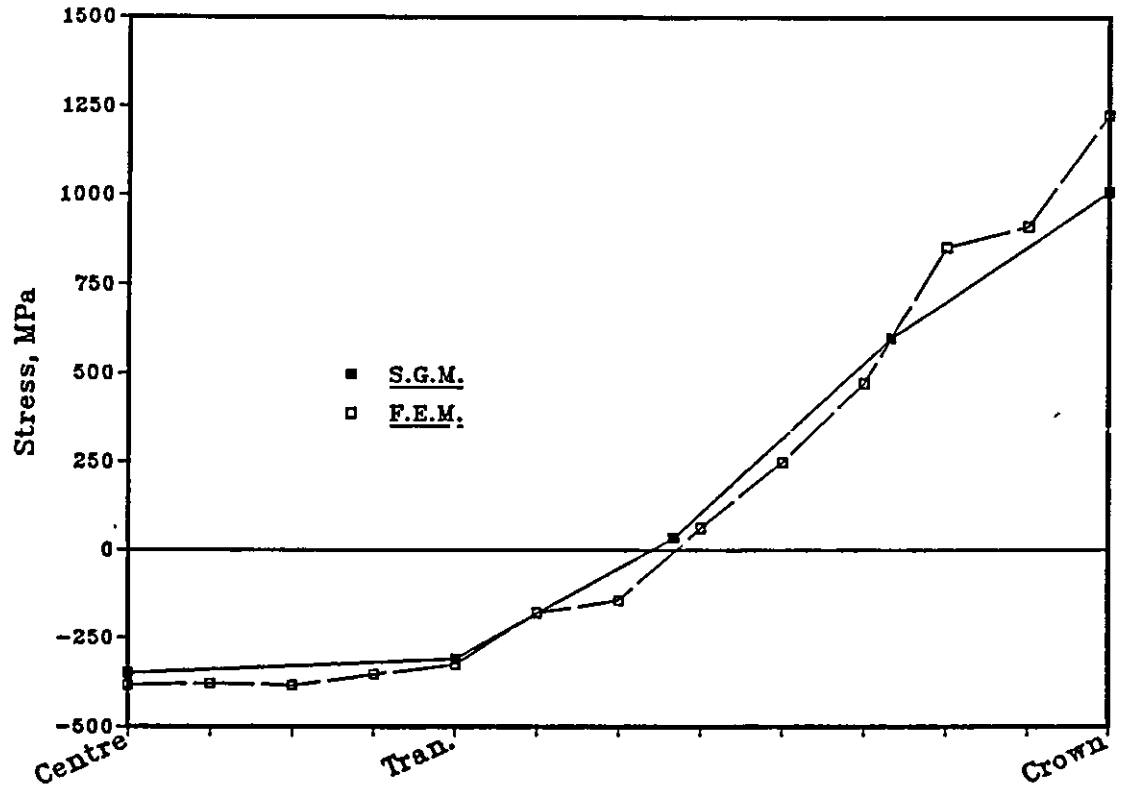

Fig. 5.26 Stresses in the 19 mm standard mining chain link at the outside, elastic stresses (nominal stress, 265 MPa).

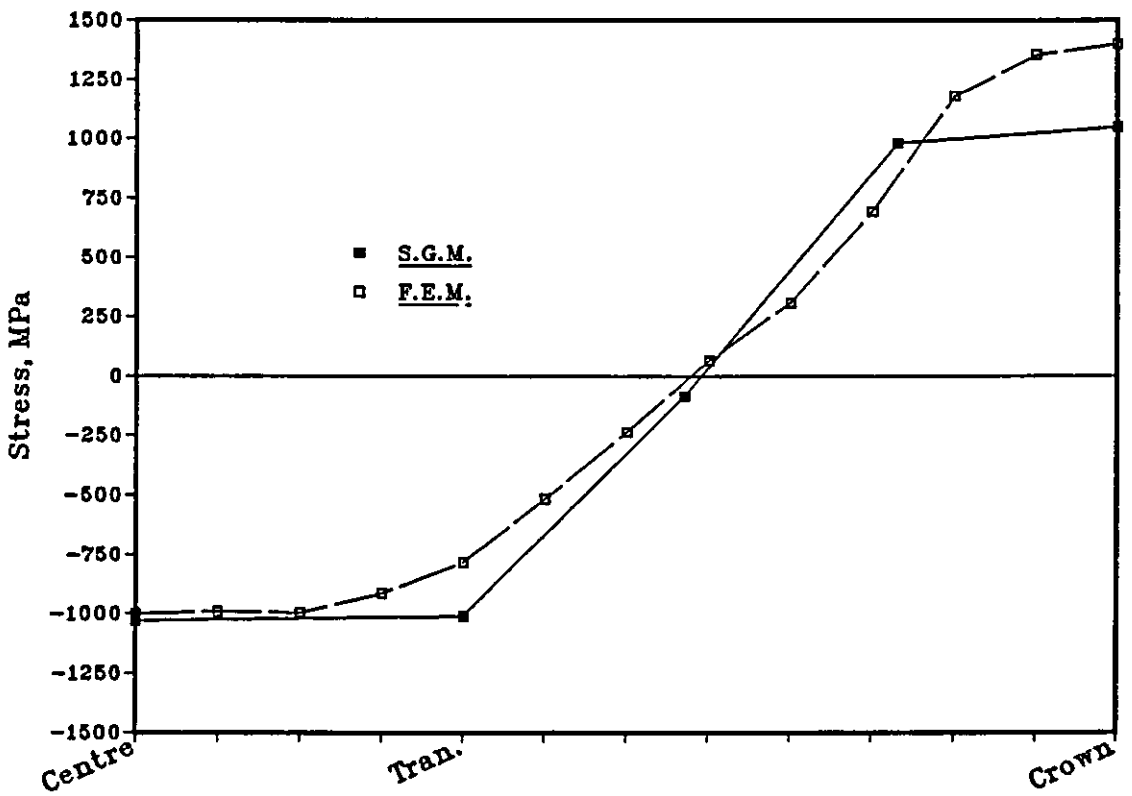

Fig. 5.27 Stresses in the 19 mm standard mining chain link at the outside after the onset of plastic flow (nominal stress, 526 MPa).

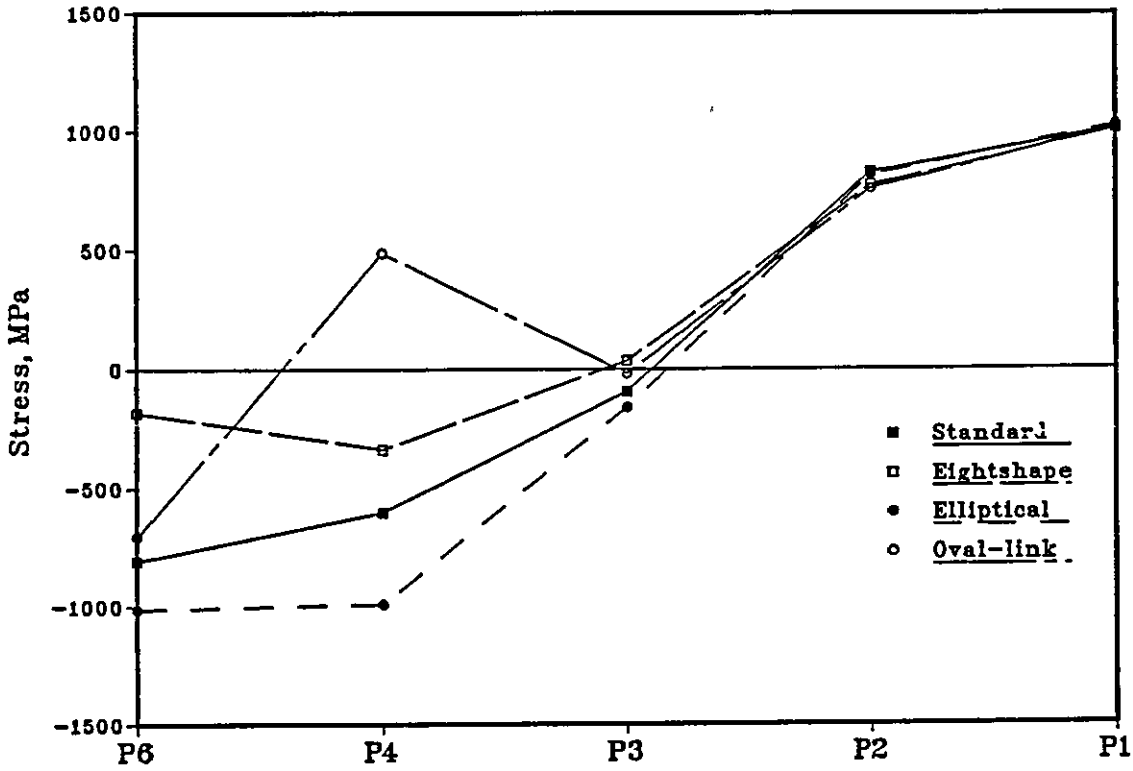

Fig. 5.28 Effect of link geometry on the total stresses under the calibration load of 260 kN (393 kN for the oval-link chain).

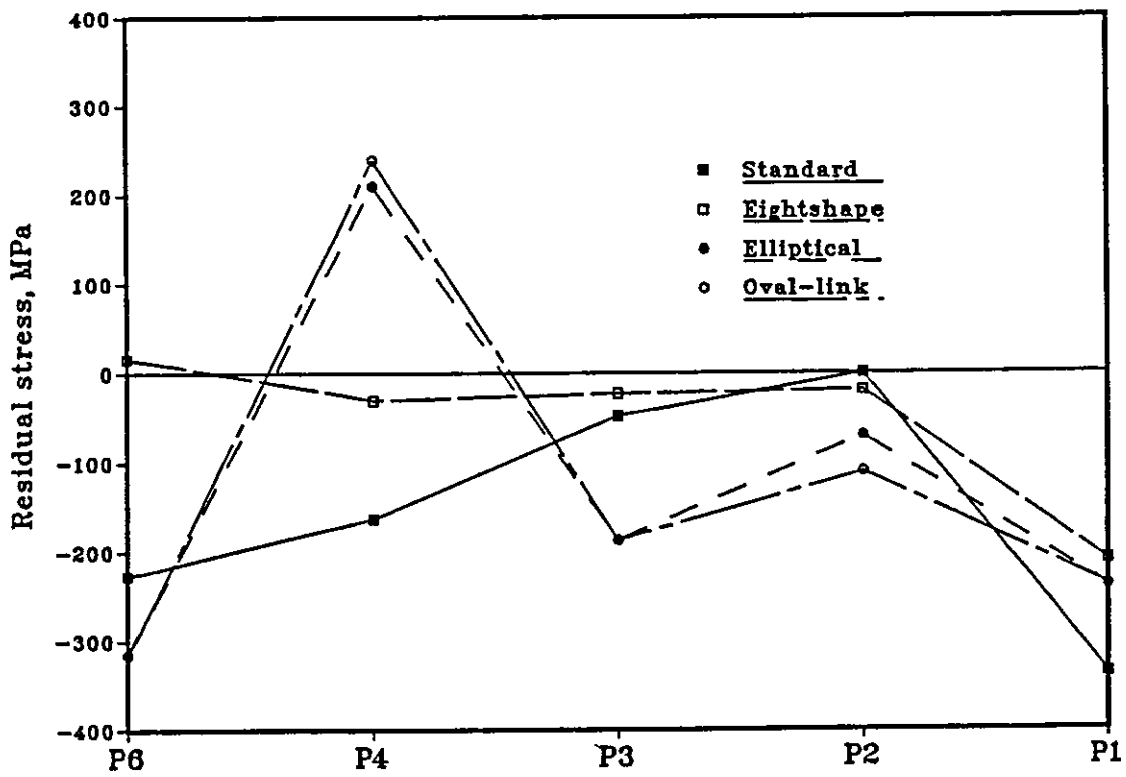

Fig. 5.29 Effect of link geometry on the residual stresses under the calibration load of 260 kN (393 kN for oval-link chain).

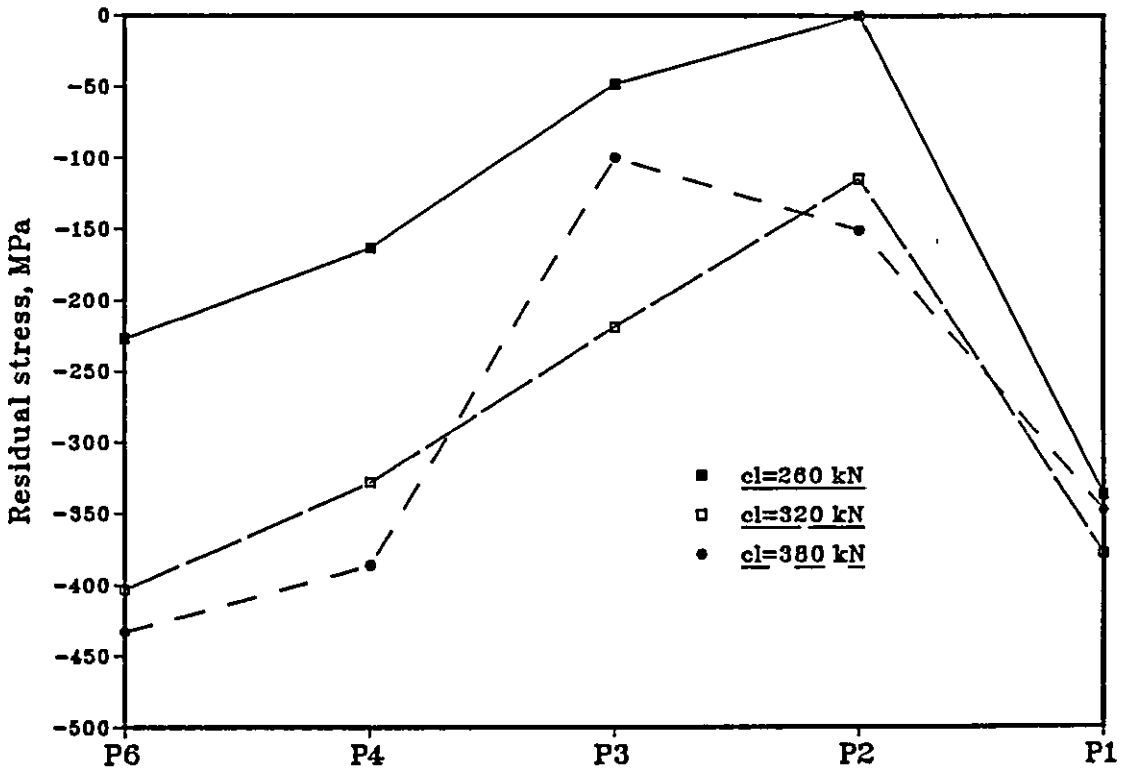

Fig. 5.30 Effect of increase in calibration load (cl) on the residual stress pattern of the 19 mm standard mining chain link (material 3).

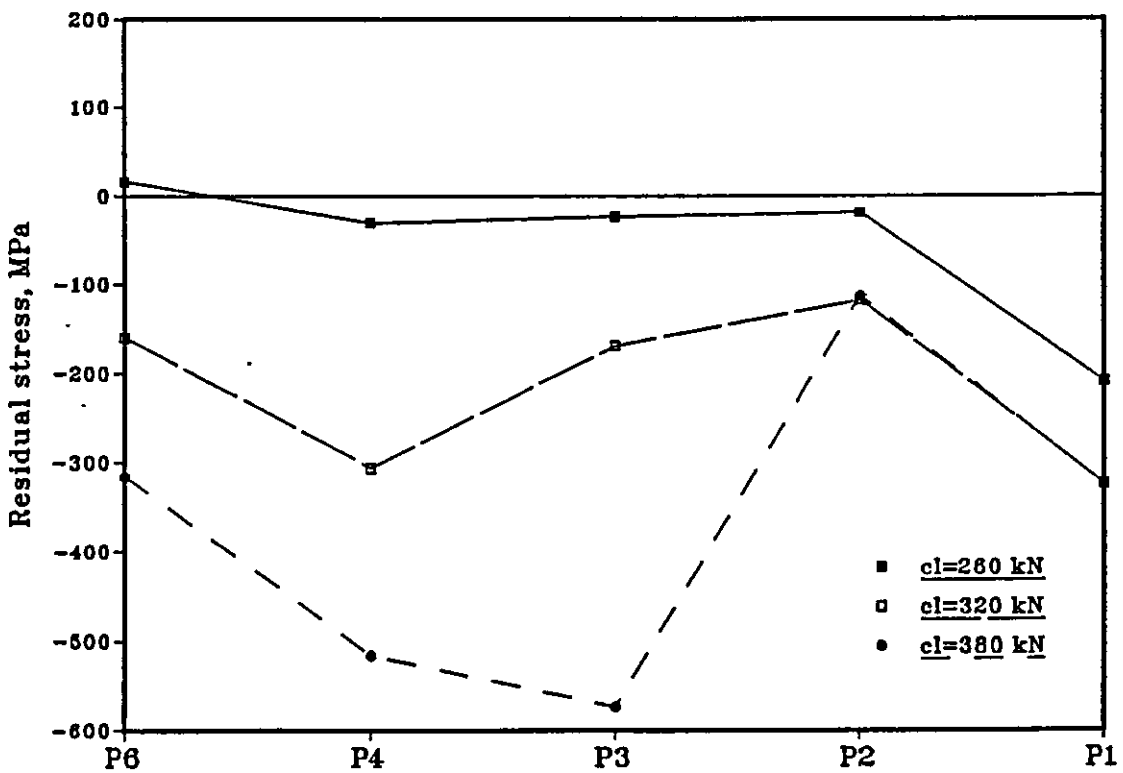

Fig. 5.31 Effect of increase in calibration load (cl) on the residual stress pattern of the 19 mm eight shape mining chain link (material 3).

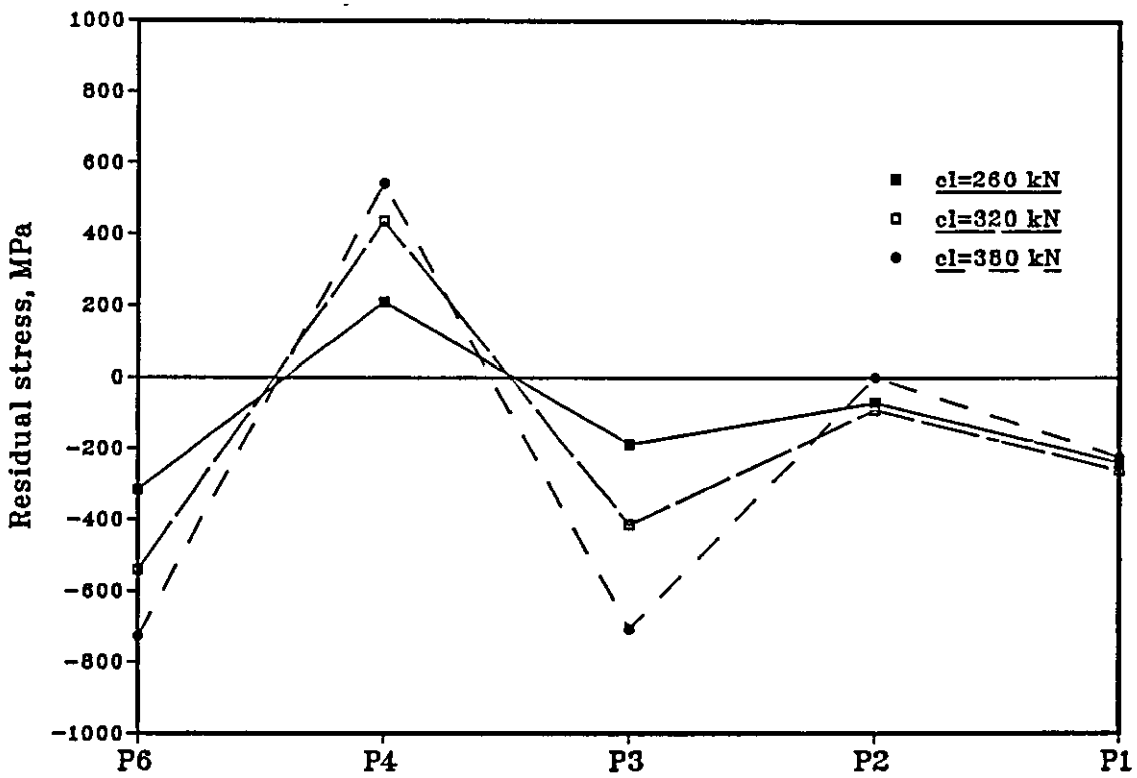

Fig. 5.32 Effect of increase in calibration load (cl) on the residual stress pattern of the 19 mm elliptical mining chain link (material 3).

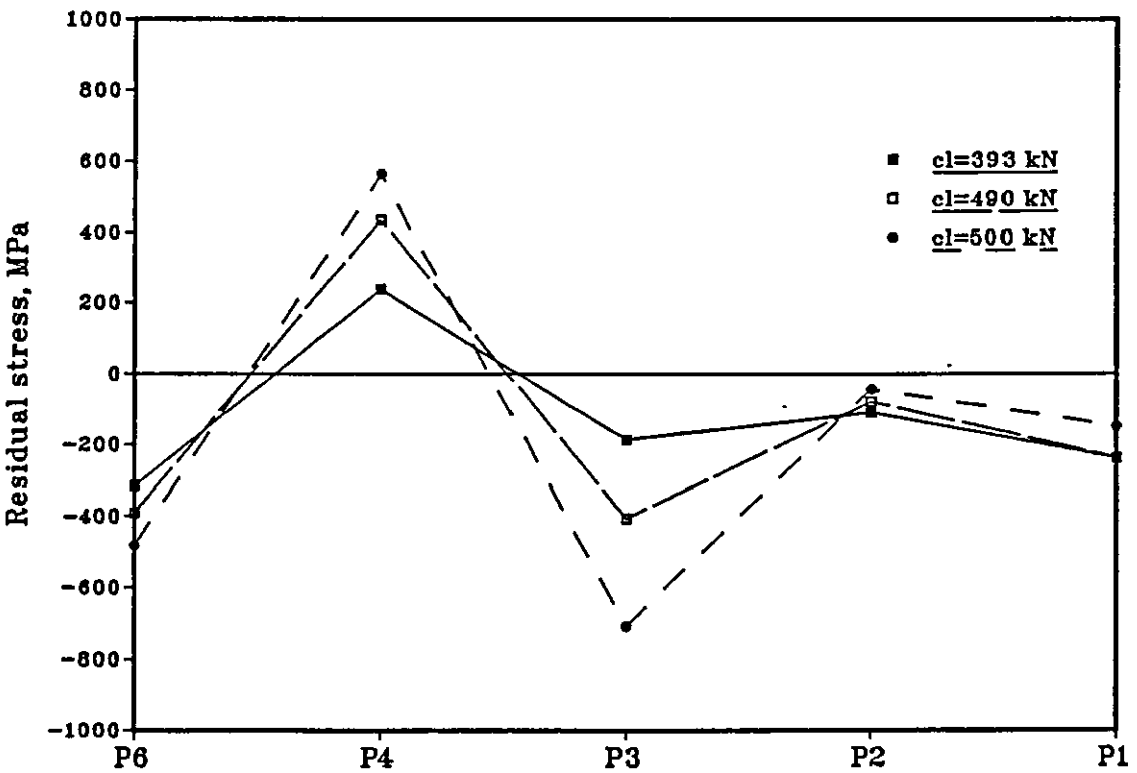

Fig. 5.33 Effect of increase in calibration load (cl) on the residual stress pattern of the oval-link mining chain link (material 3).

Stress type	Position	Cal. loads, standard			Cal. loads, eight shape		
		260 kN	320 kN	380 kN	260 kN	320 kN	380 kN
Res. stress	Tran. (5 and 9)	-401	-541	-568	-433	-565	-655
	Centre (7)	-316	-256	-431	-23	19	38
Total stress	Tran. (5 and 9)	1010	1018	1018	1010	1018	1029
	Centre (7)	1010	1014	1034	749	936	999

Table 5.20 Residual and total stresses at the inside transition and centre of 19 mm mining chain at various calibration loads.

Stress type	Position	Cal. loads, elliptical			Cal. loads, oval		
		260 kN	320 kN	380 kN	393 kN	489 kN	574 kN
Res. stress	Tran. (5 and 9)	-264	-430	-501	-218	-391	-481
	Centre (7)	-142	-328	-403	-113	-284	-339
Total stress	Tran. (5 and 9)	1011	1018	1020	1013	1018	1027
	Centre (7)	1034	1073		1010	1012	1020

Table 5.20 cont. Residual and total stresses at the inside transition and centre of 19 mm mining chain under various calibration loads (material 3).

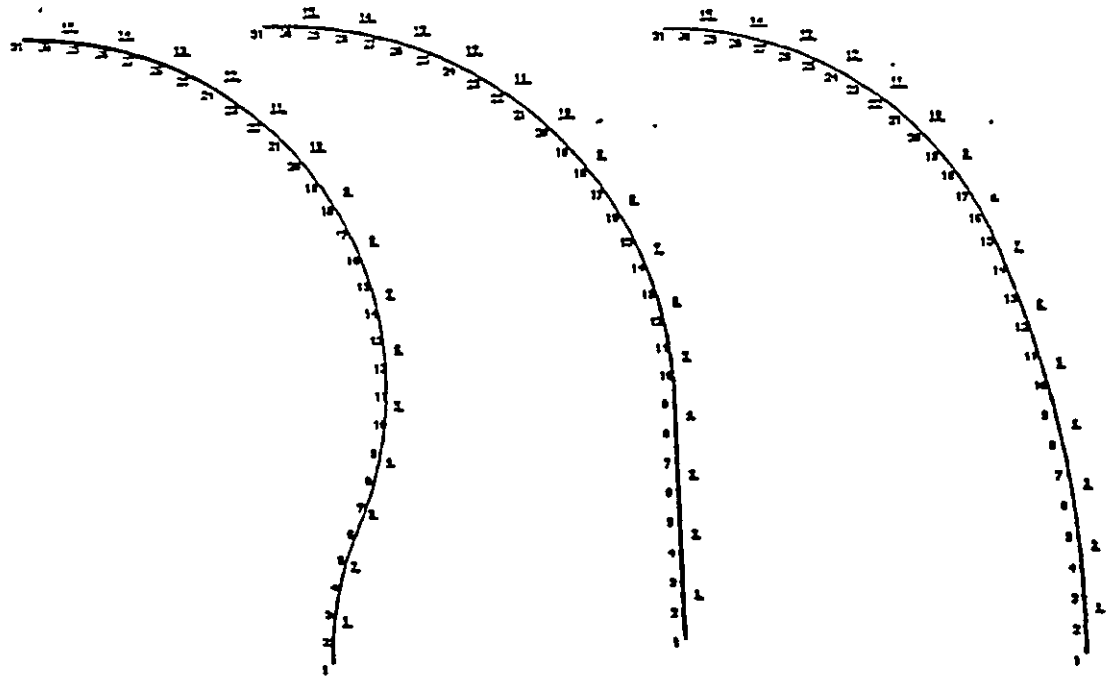

Fig. 6.1 Finite element mesh of different link shapes (standard, eight shape and elliptical).

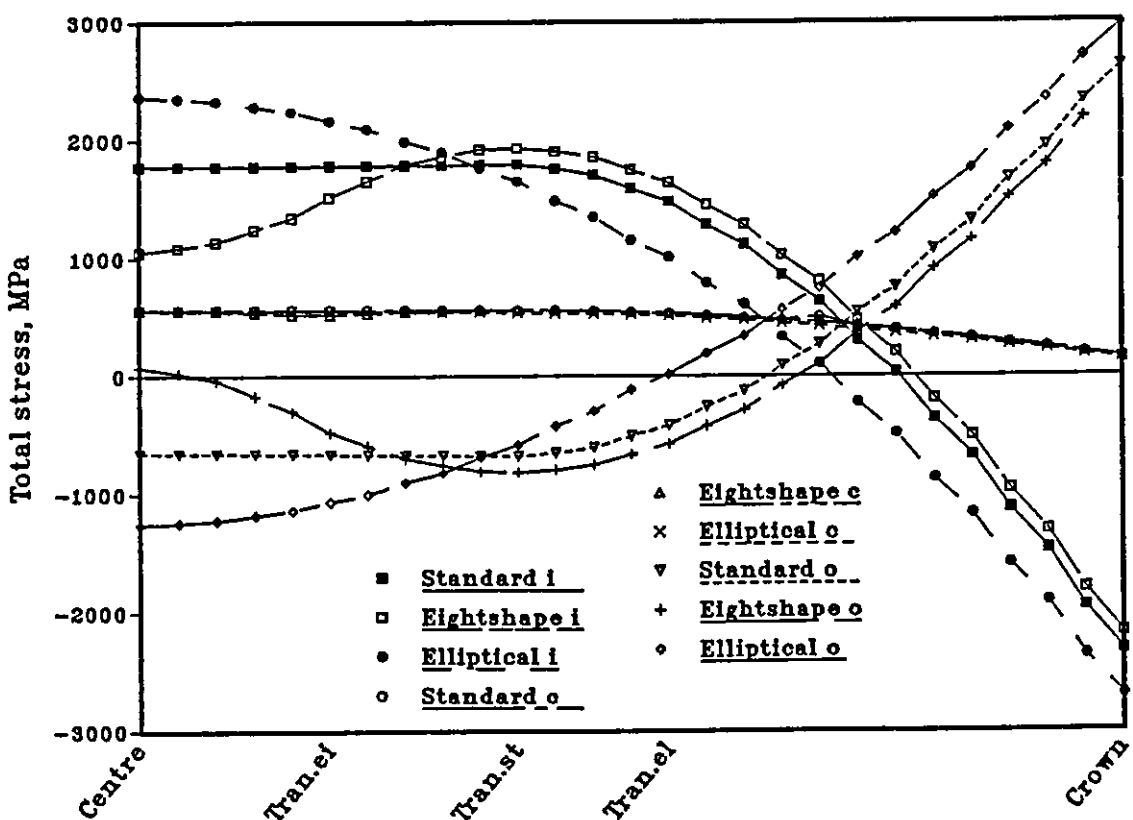

Fig.6.2 Total stresses of the 18 mm mining chain of different geometries at the inside (i), outside (o) and centre (c) under cl=320 kN.

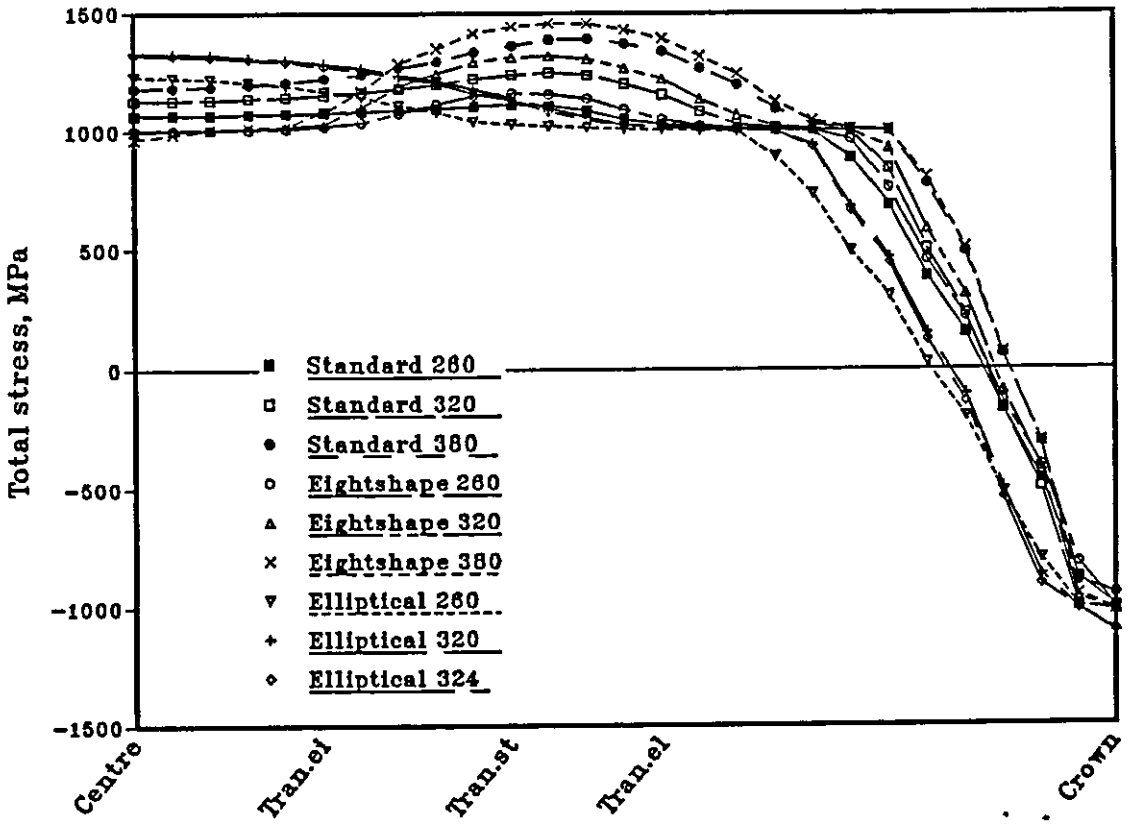

Fig.6.3 Total stresses of the 19 mm mining chain of different geometries at the outside for various calibration loads, kN.

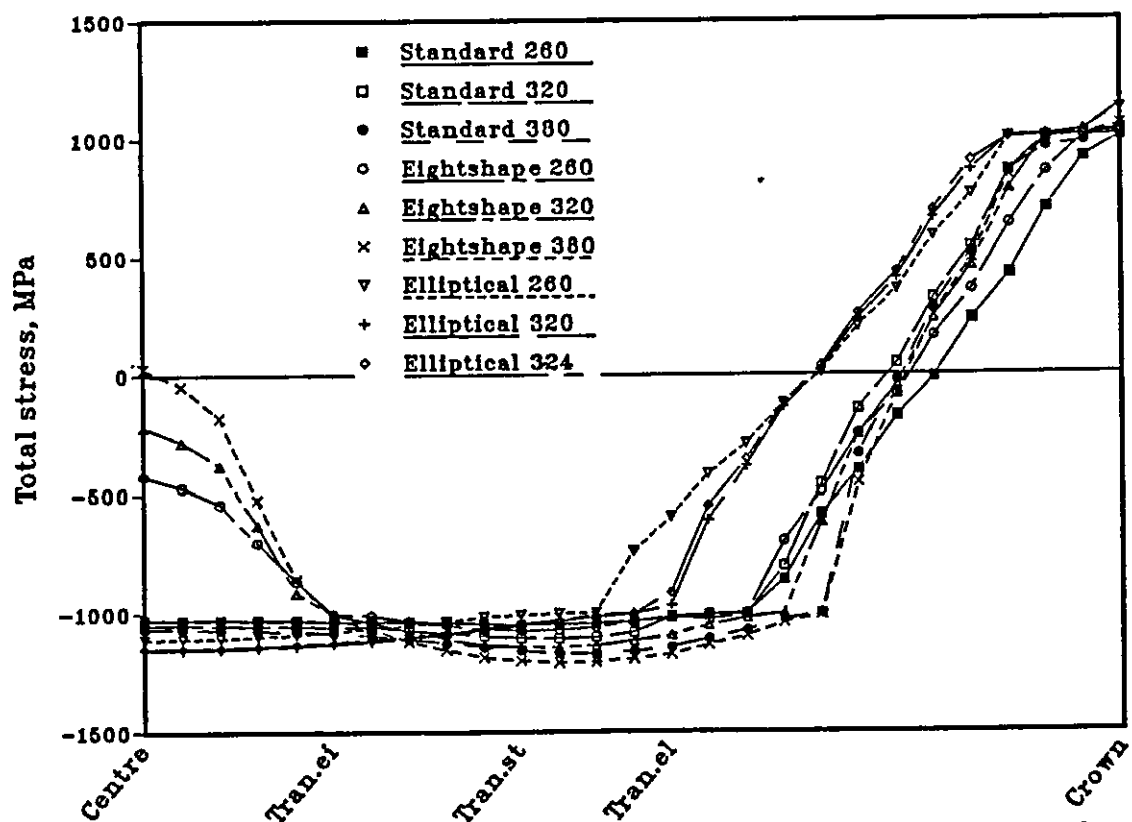

Fig. 6.4 Total stresses ofthe 19 mm mining chain of different geometries at the inside for various calibration loads, kN.

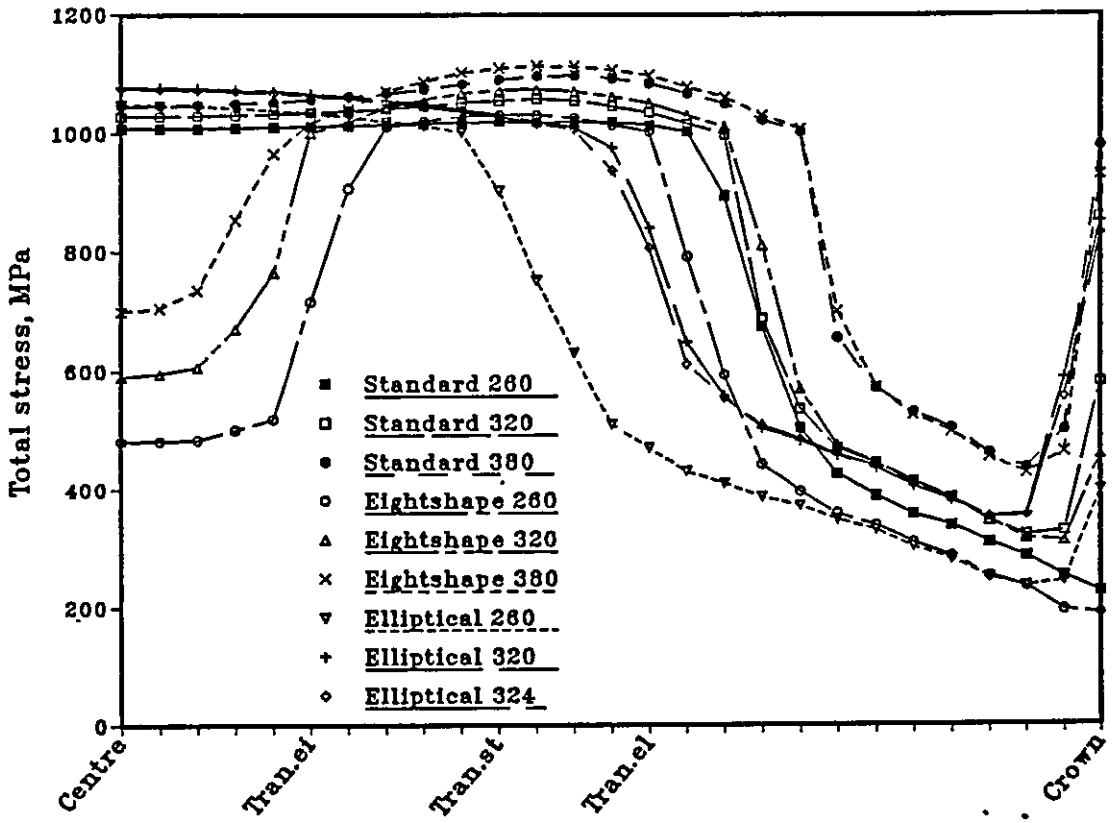

Fig. 6.5 Total stresses of the 19 mm mining chain of different geometries at the centre for various calibration loads, kN.

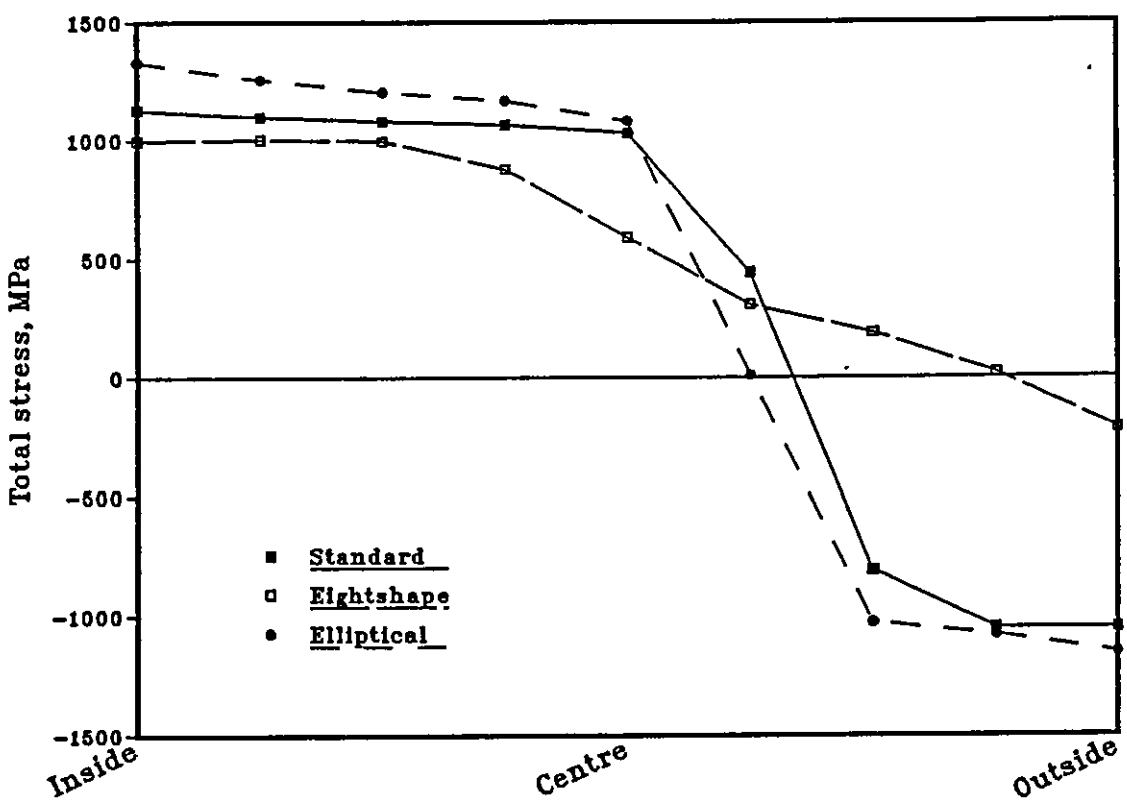

Fig. 6.6 Total stresses of the 19 mm mining chain of different geometries at the cross-section through the centre under calibration load of 320 kN.

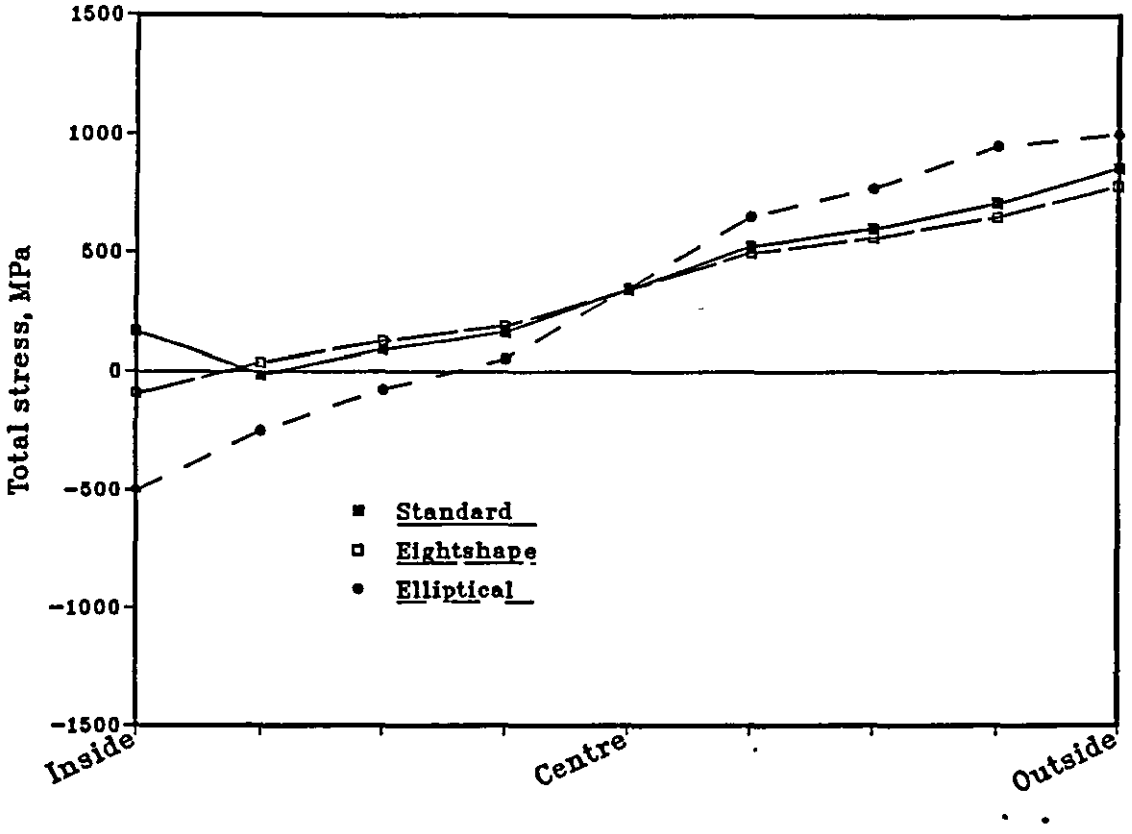

Fig. 6.7 Total stresses of the 19 mm mining chain of different geoemtries at the cross-section through 60 deg. to the crown under calibration load of 320 kN.

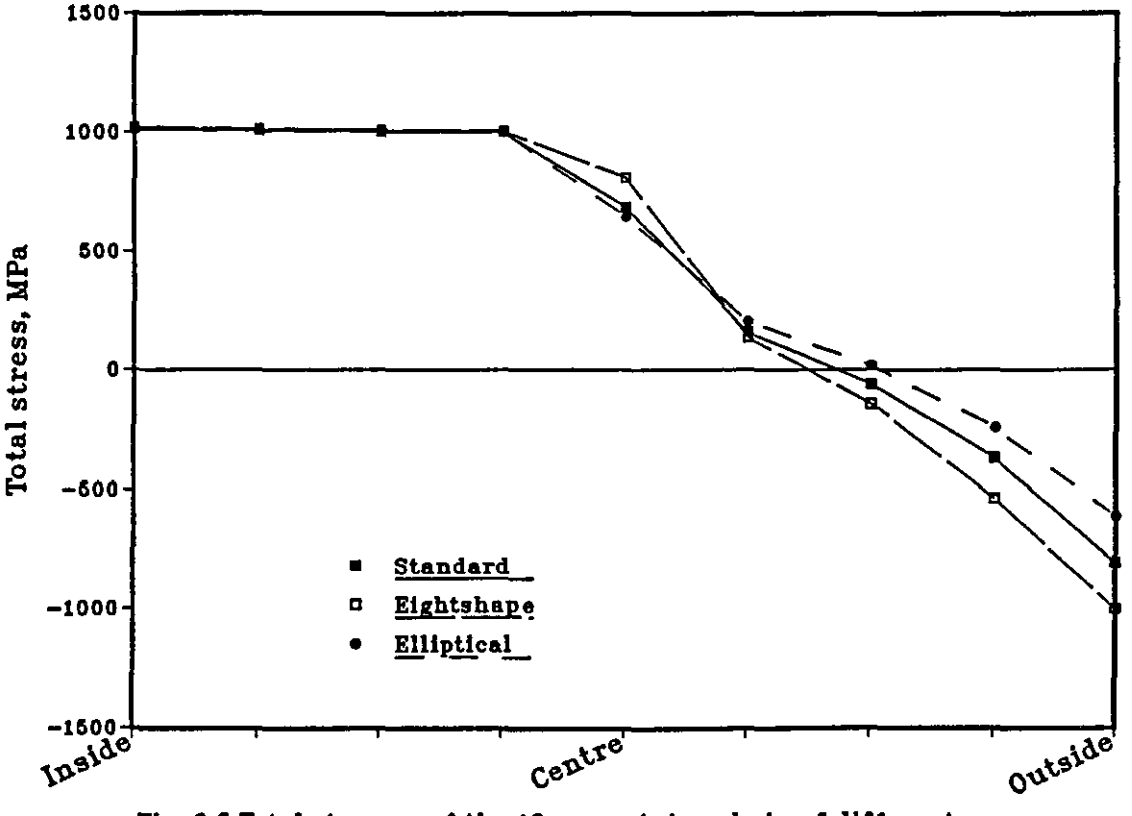

Fig. 6.8 Total stresses of the 19 mm mining chain of different geometries at the cross-section through the 30 deg. to the crown under calibration load of 320 kN.

Geometry	Centre (node 1), mm			Crown (node 31), mm		
Cal. load (kN)	cl=260	cl=320	cl=380	cl=260	cl=320	cl=380
Standard	-2.134	-4.164	-6.693	1.900	5.593	5.540
Eight shape	-1.649	-3.334	-5.306	1.570	3.354	3.137
Elliptical	-3.705	-6.120		2.952	4.722	4.553
Cal. load (kN)	cl=30	cl=38.5	cl=47	cl=30	cl=38.5	cl=47
Lifting	-.436	-1.198	-1.869	.424	1.086	1.648

Table 6.1 Displacements at the centre and crown of the mining (various geometries) and lifting chains under various calibration loads. For elliptical link, cl=380 kN was not achieved.

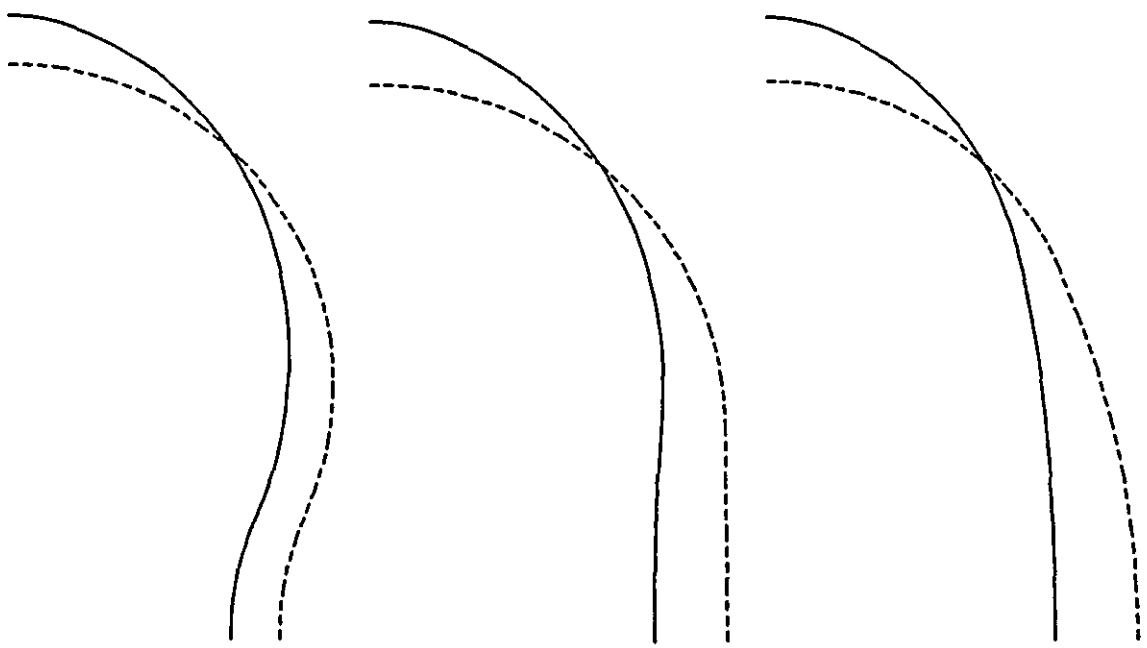

Fig. 6.9 Deformed shapes of the various link geometries under cl=320 kN (324 kN for elliptical).

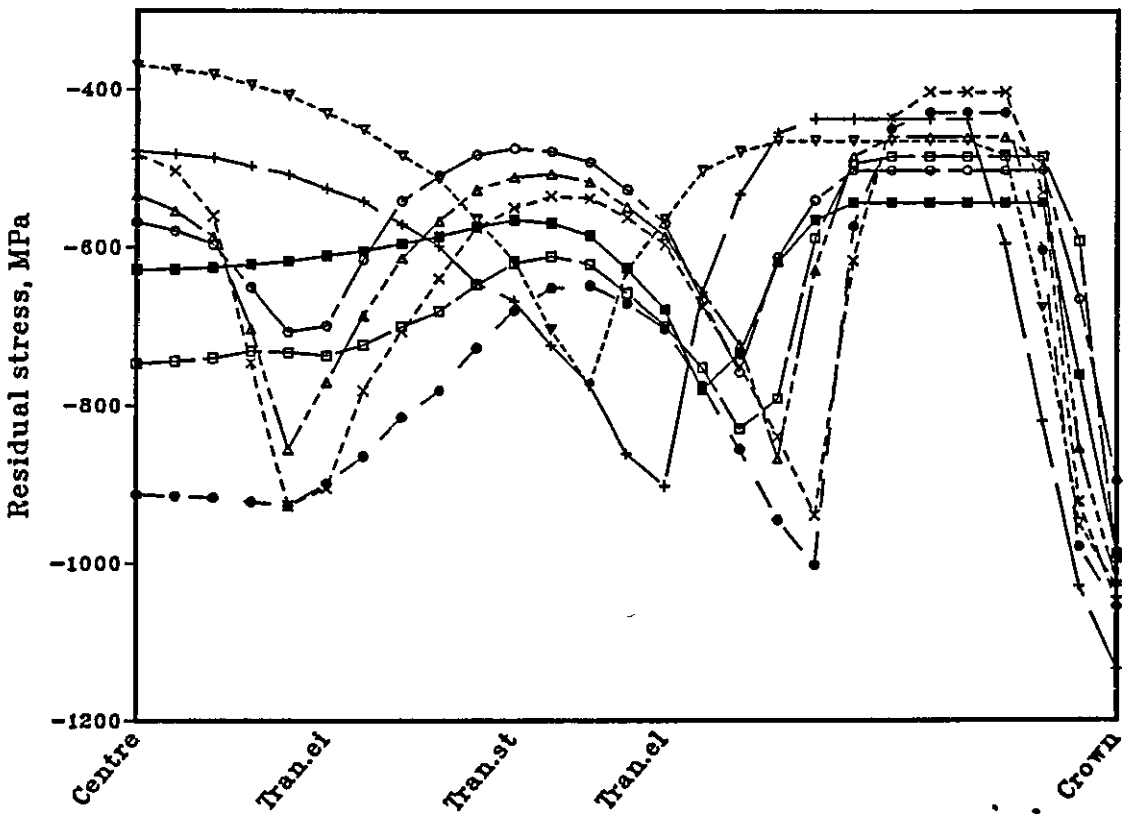

Fig. 6.10 Residual stresses of the 19 mm mining chain of different geometries at the outside for various calibration load, kN.

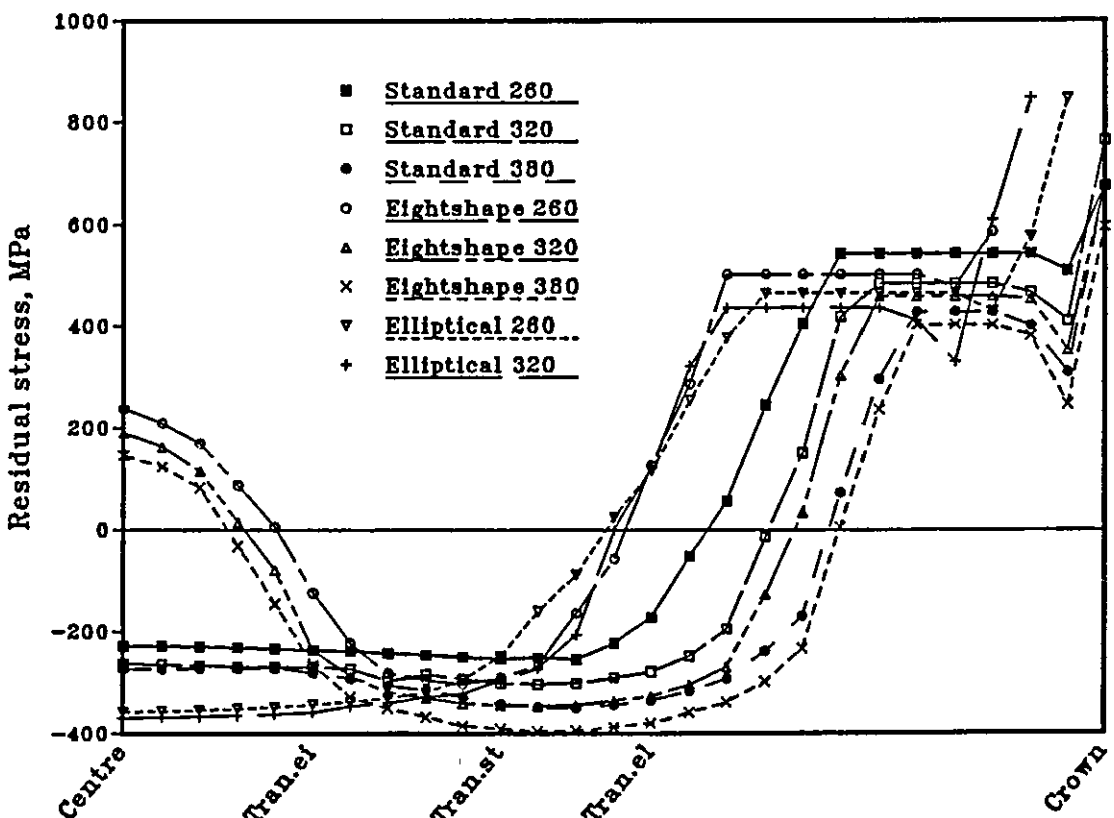

Fig. 6.11 Residual stresses of the 19 mm mining chain of different geometries at the inside for various calibration load, kN.

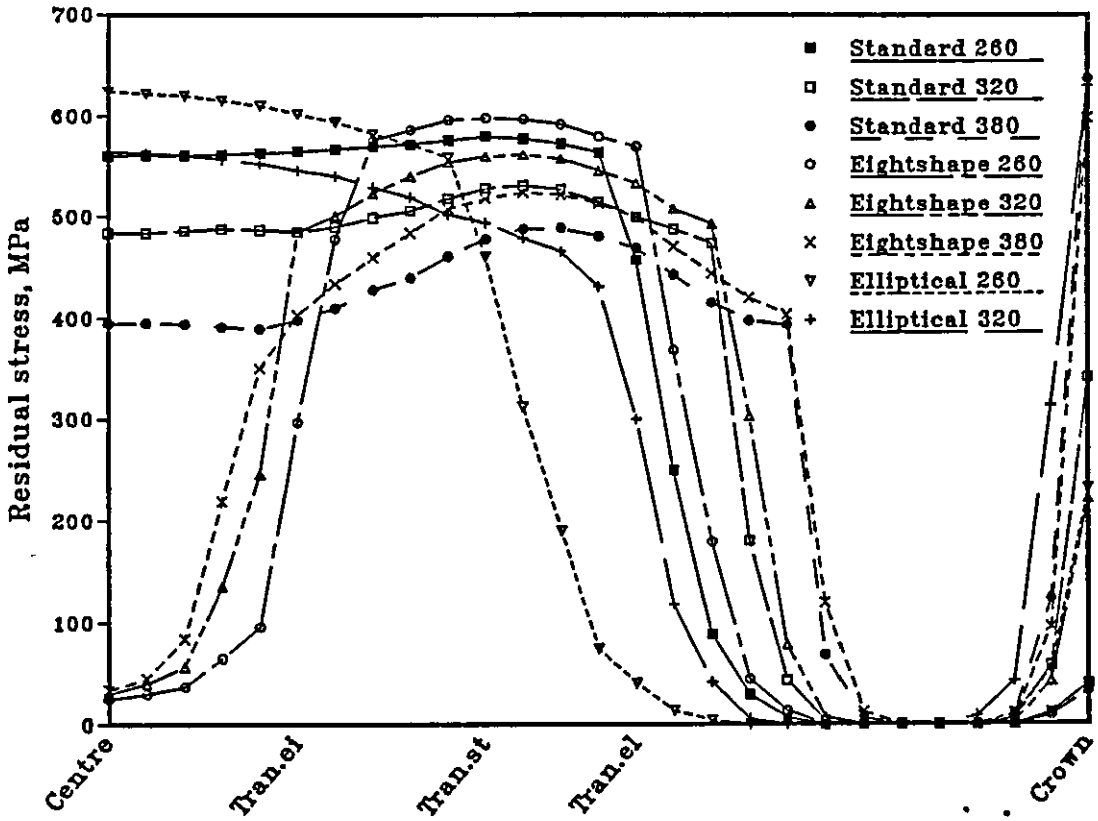

Fig. 6.12 Residual stresses of the 19 mm mining chain of different geometries at the centre for various calibration load, kN.

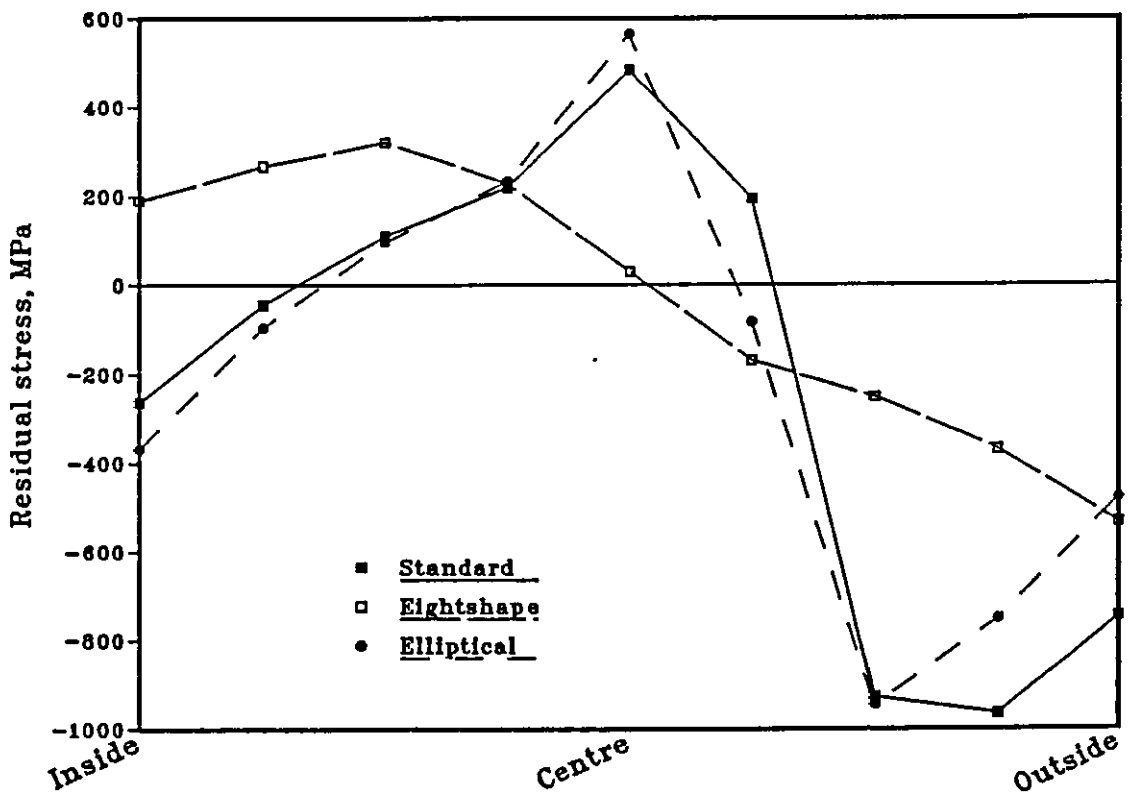

Fig. 6.13 Residual stresses of the 19 mm mining chain of different geometries at the cross-section through the centre under calibration load of 320 kN (as in neutron diffraction).

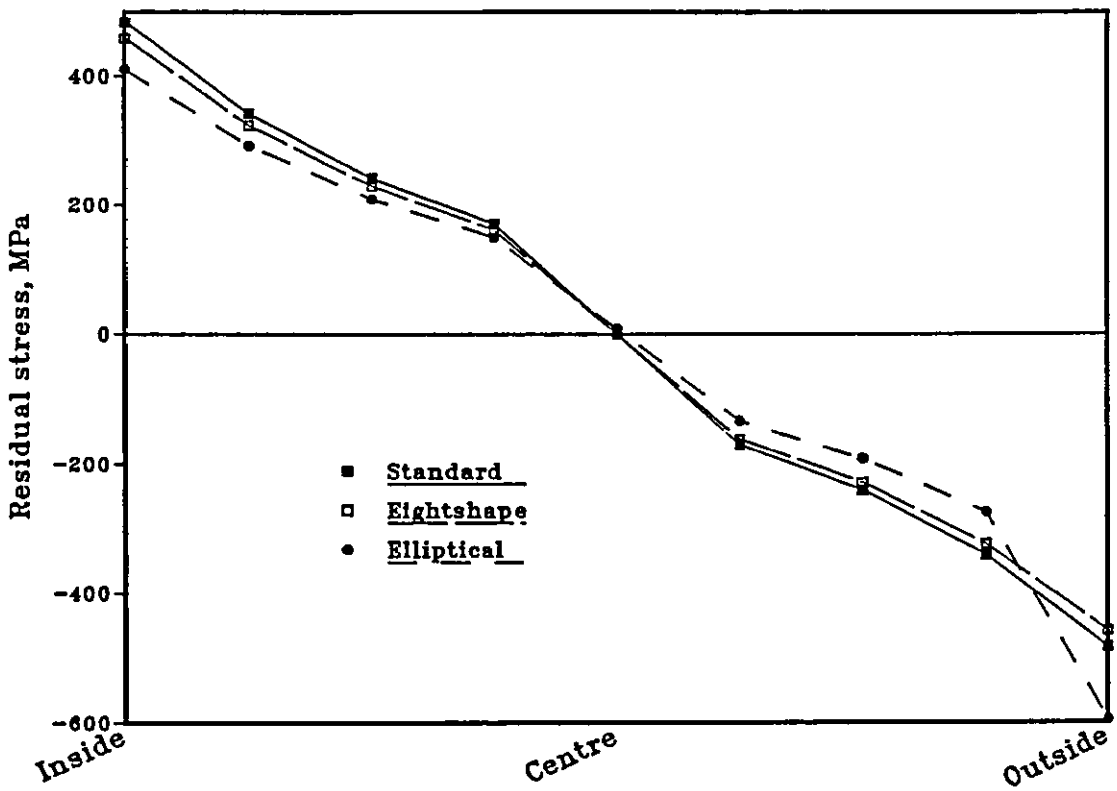

Fig. 6.14 Residual stresses of the 19 mm mining chain of different geometries at the cross-section through 60 deg. to the crown under calibration load of 320 kN.

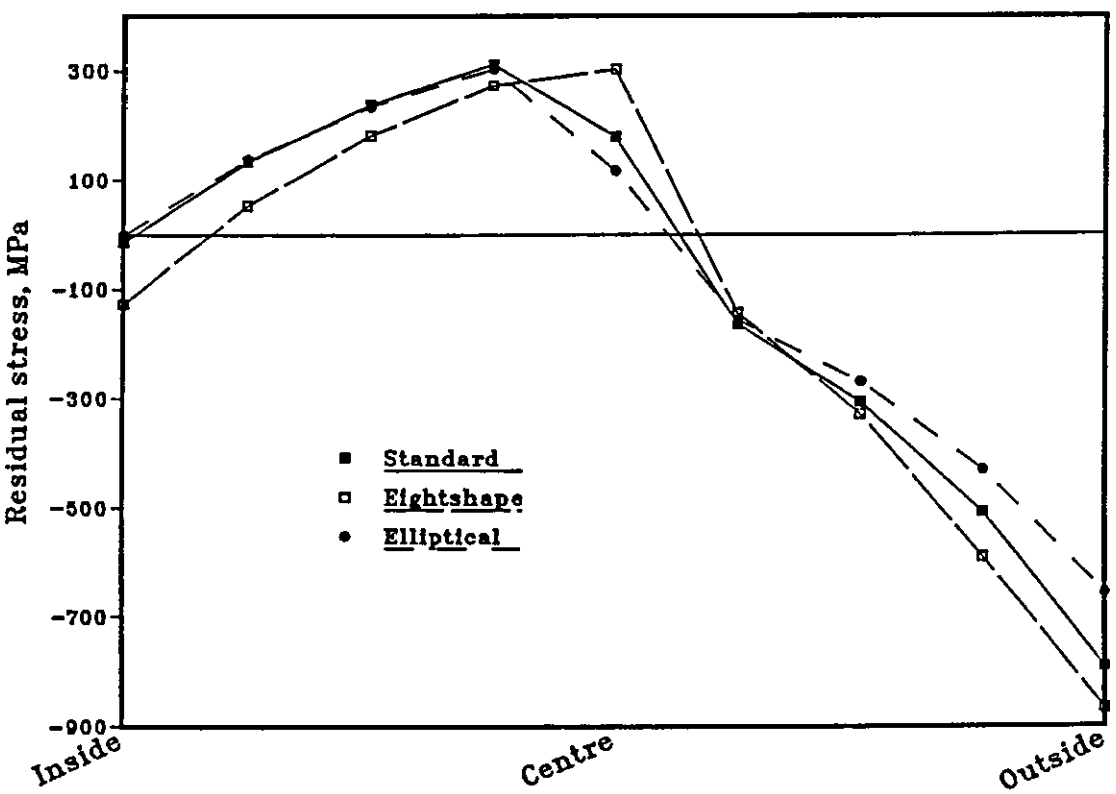

Fig. 6.15 Residual stresses of the 19 mm mining chain of different geometries at the cross-section through the 30 deg. to the crown under calibration load of 320 kN.

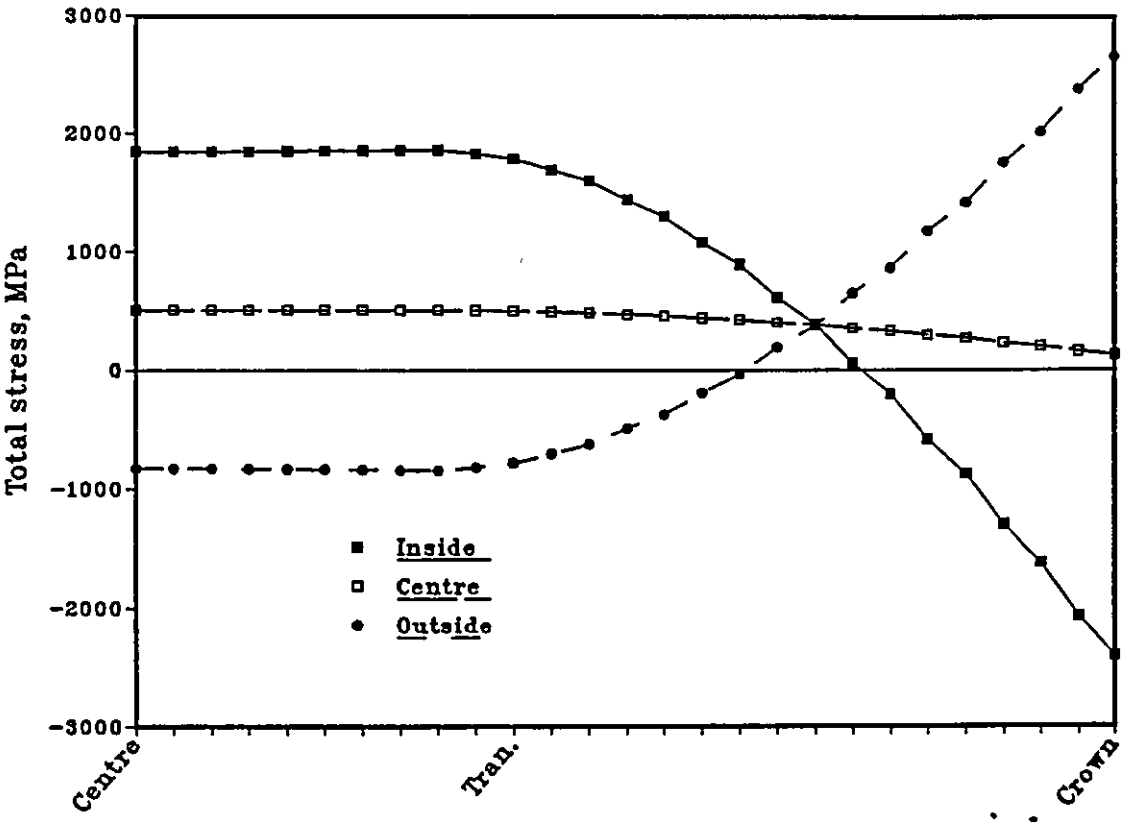

Fig. 6.16 Total stresses of the lifting chain under calibration load of 38.5 kN at the inside, centre and outside (elastic analysis).

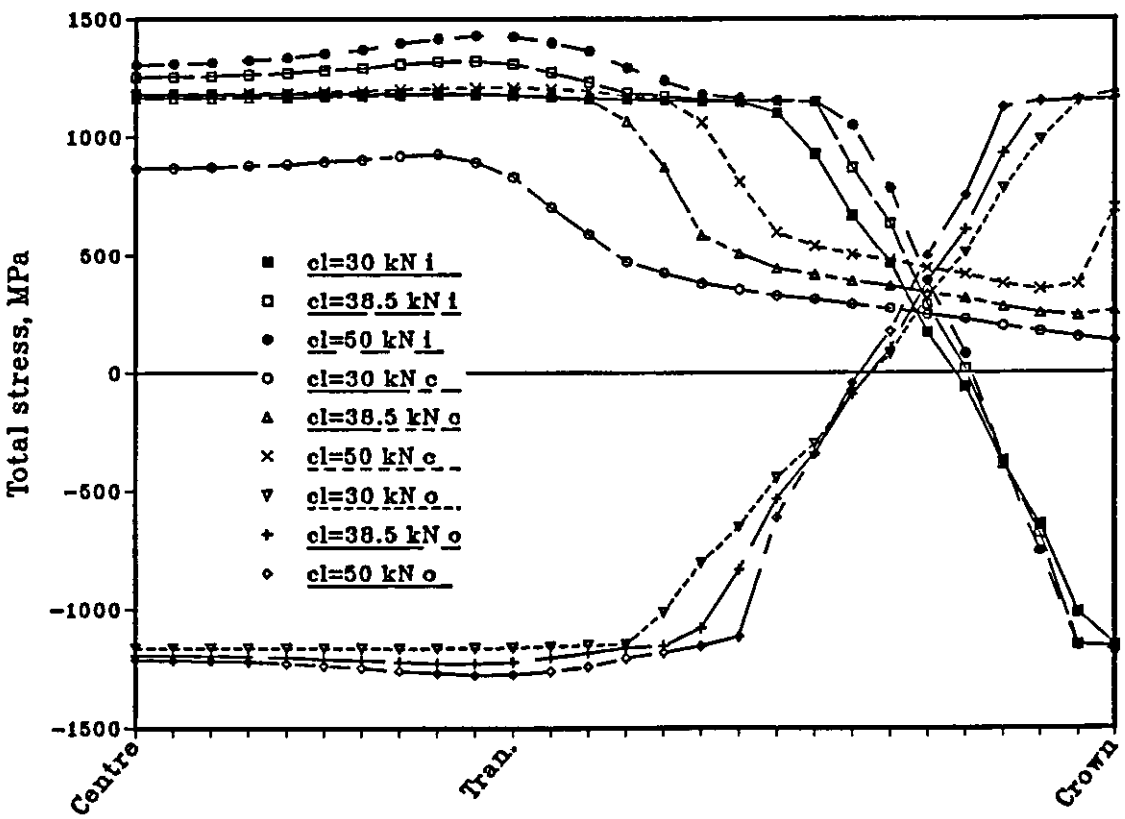

Fig. 6.17 Total stresses of lifting chain under various calibration loads at the inside (i), outside (o) and centre (c).

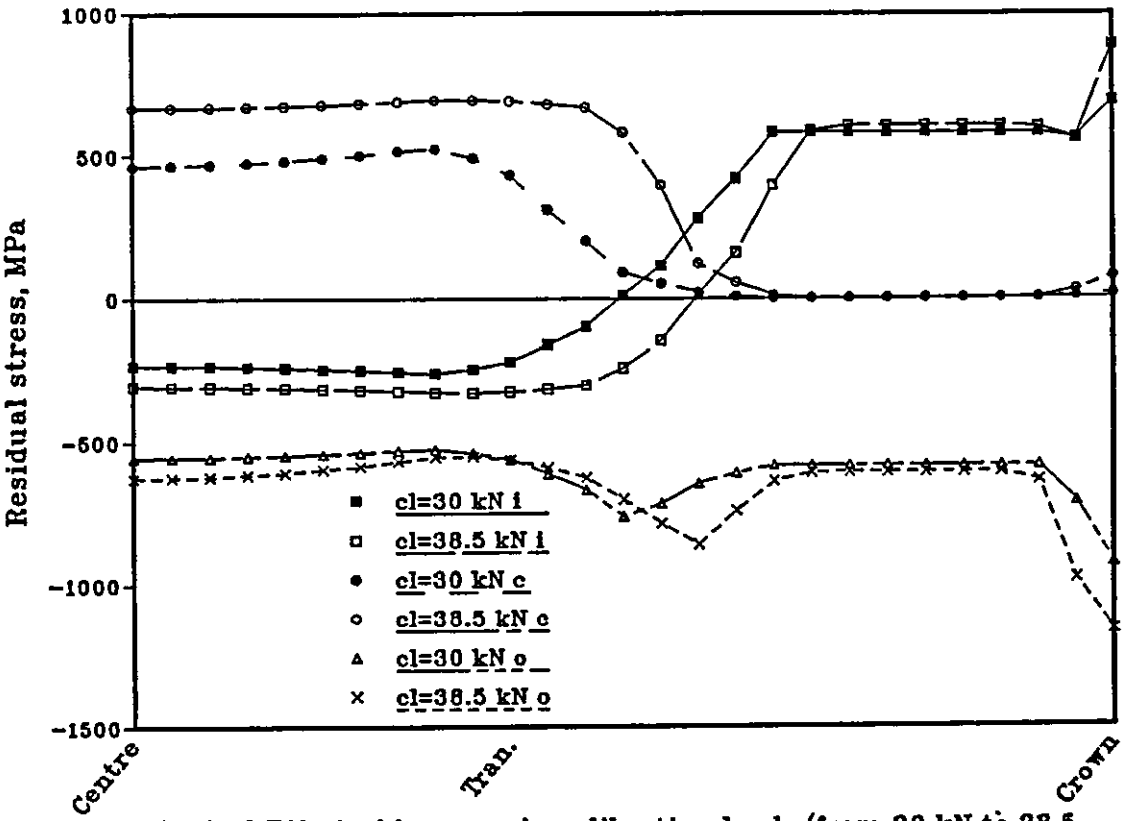

Fig. 6.18 Effect of increase in calibration loads (from 30 kN to 38.5 kN) on the residual stresses for the lifting chain at the inside (i), centre (c), and outside (o).

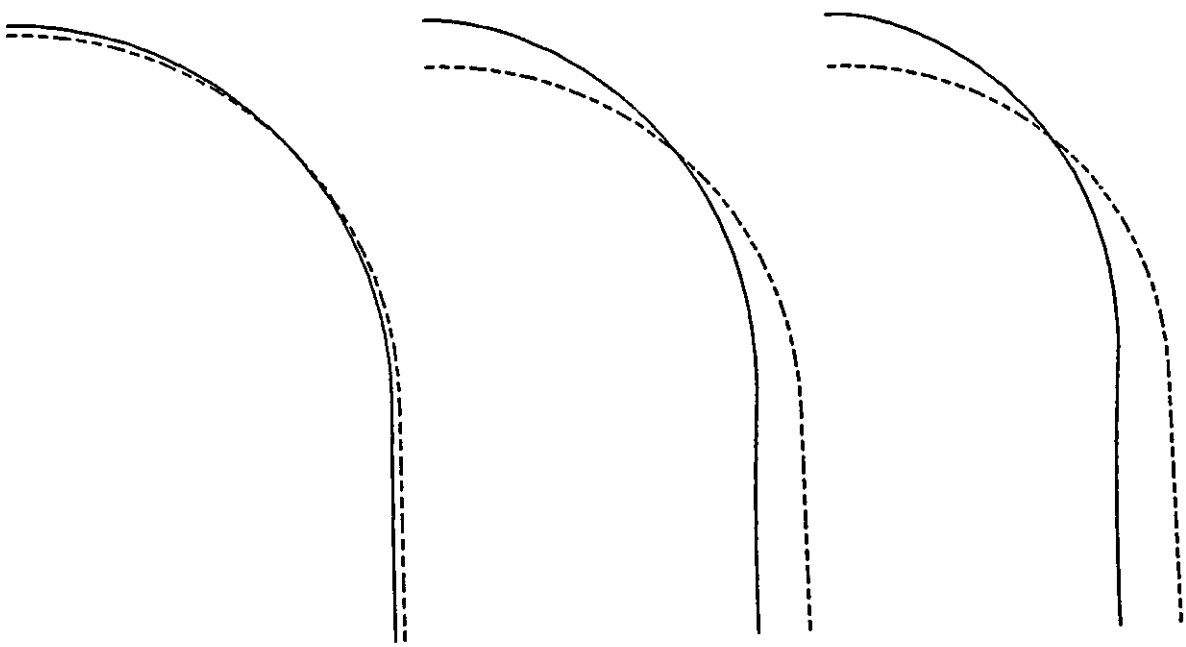

Fig. 6.19 Effect of increase in calibration load on the lifting chain , deformation (calibration loads are 28.8, 39.3 and 47 kN).

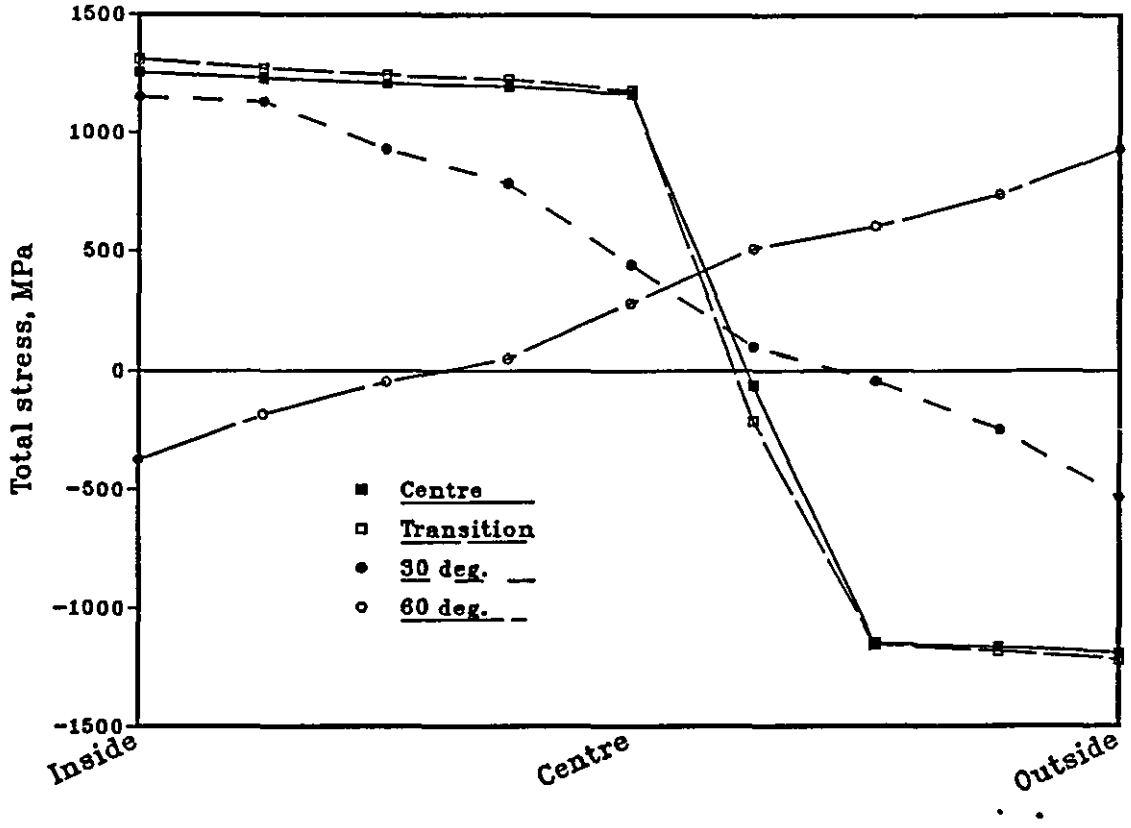

Fig. 6.20 Total stresses at various sections through the lifting chain.

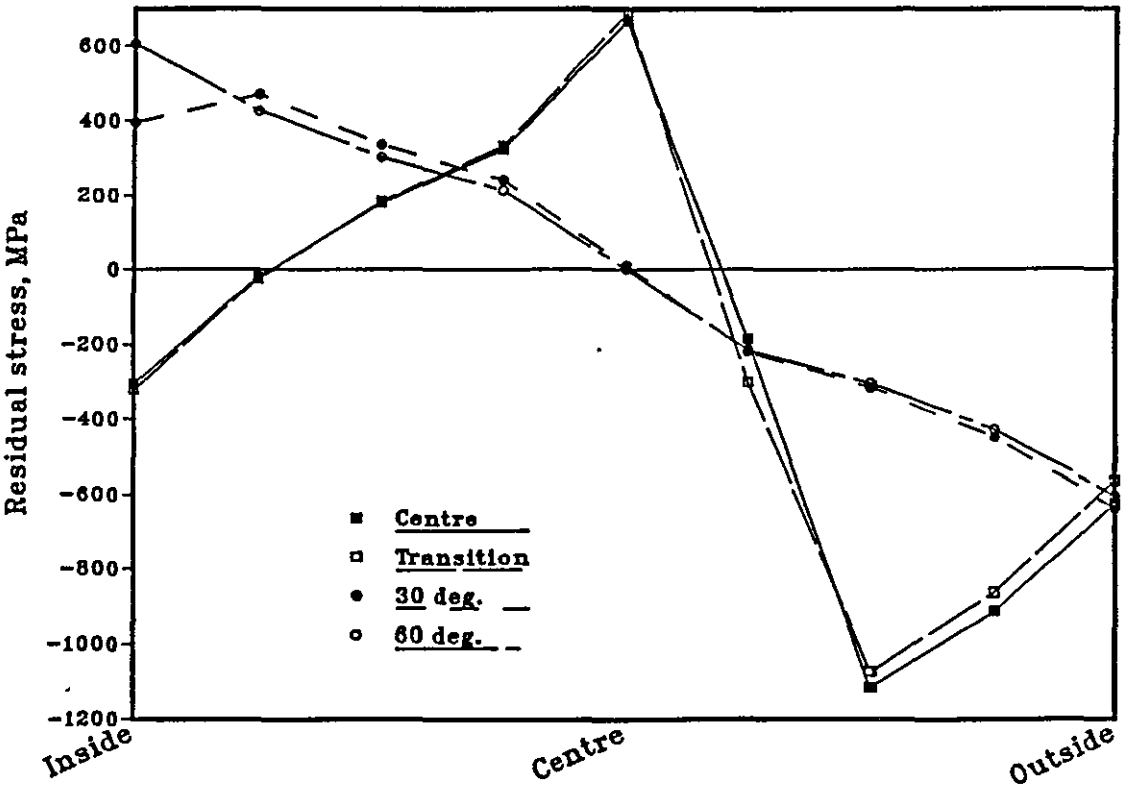

Fig. 6.21 Residual stresses at various sections through the lifting chain (at the centre the pattern is the same as the neutron diffraction results,Chapter 4).

Case	Load (P) (kN)	Major (minor) axis a, (mm)	Max. contact pressure, q_o (MPa)	Contact angle α, deg.
Mining chain	260	3.99	7811	17.9
	320	4.27	8370	19.2
	380	4.52	8860	20.3
	500	4.96	9713	22.3
Lifting chain	30	1.21	9370	12.5
	38.5	1.32	10573	13.6
	50	1.44	11536	14.9
	64	1.56	12525	16.1

Table 7.1 Maximum contact pressure and contact angle for mining and lifting chains under various calibration loads (elastic conditions assumed).

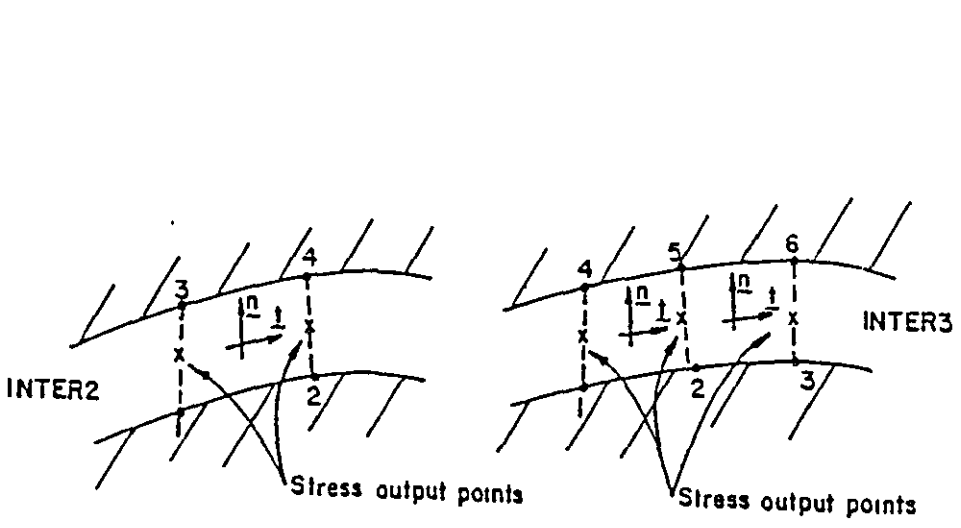

Fig. 7.1a Two and three-noded interface elements (INTER2 and INTER3).

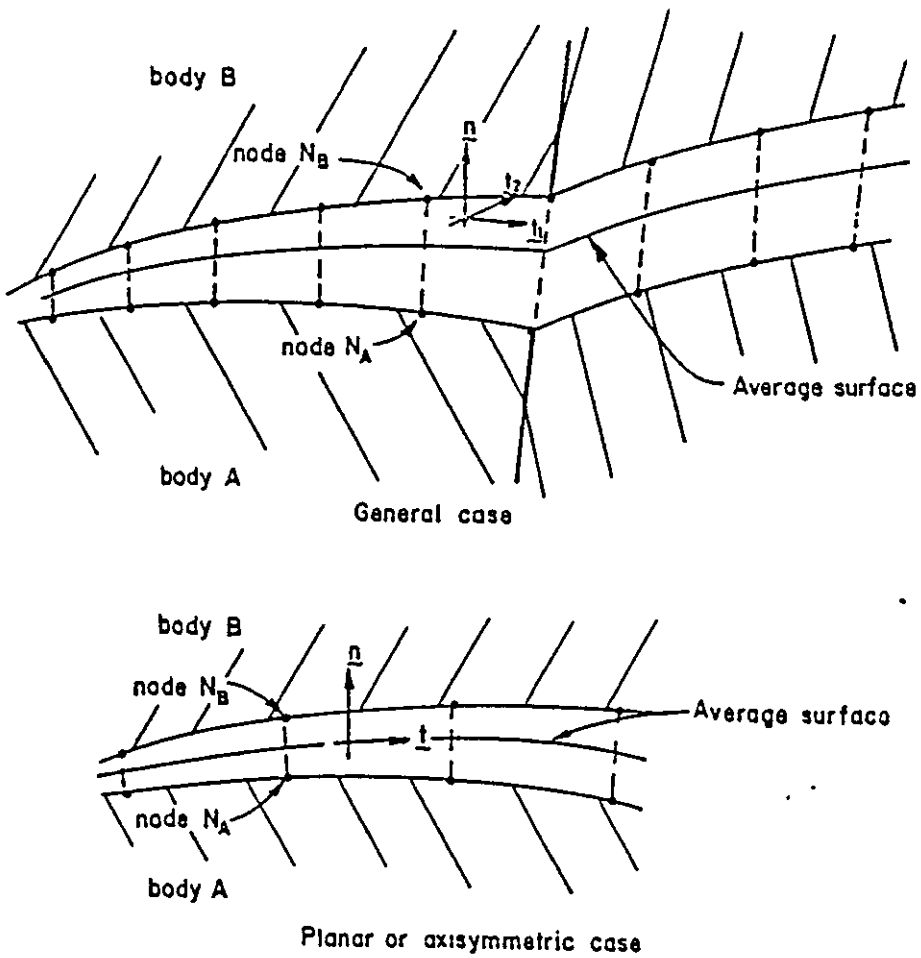

Fig. 7.1b Geometry of "average interface surfaces".

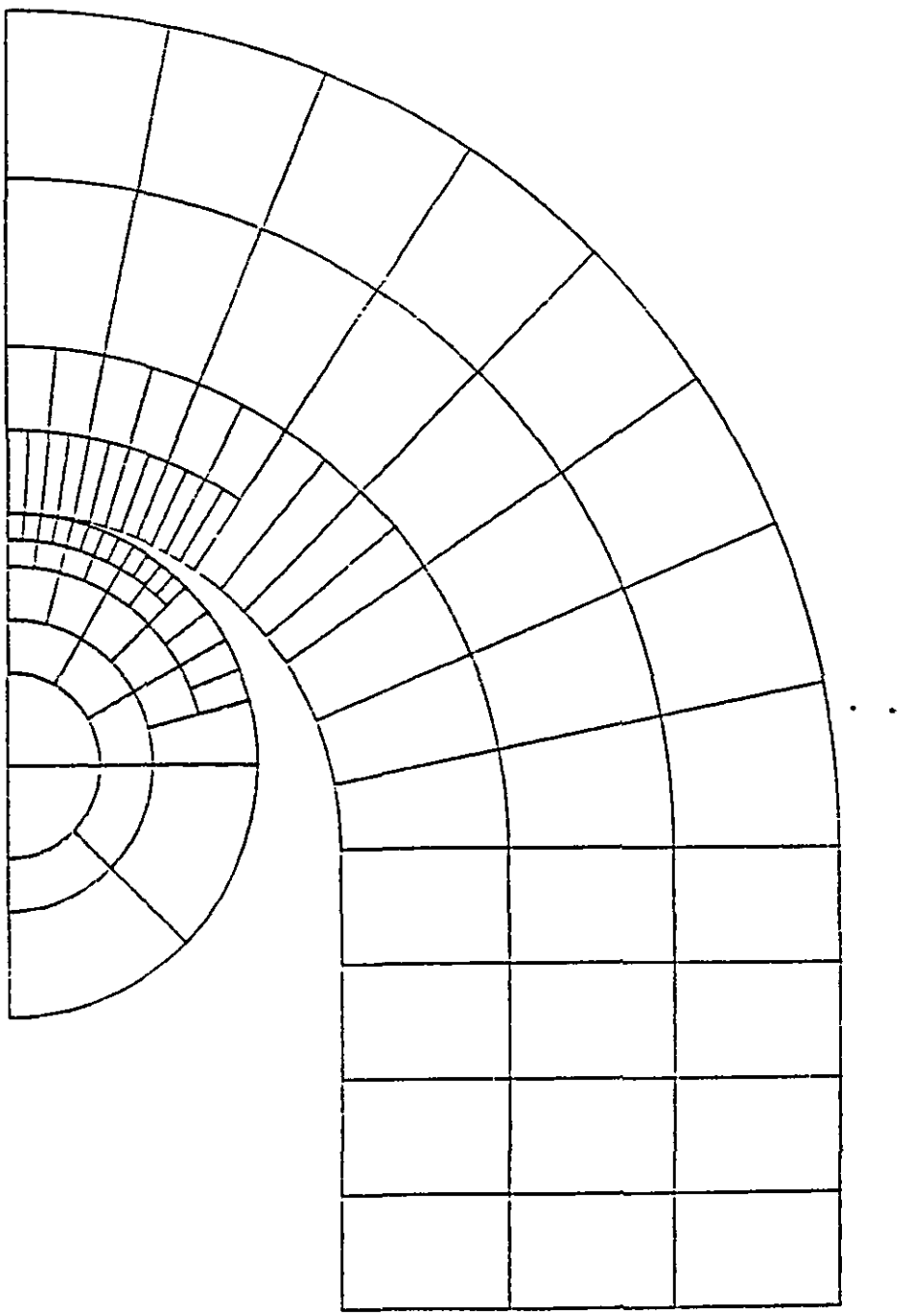

Fig. 7.2 Finite element mesh of the quarter of the 19 mm mining chain link.

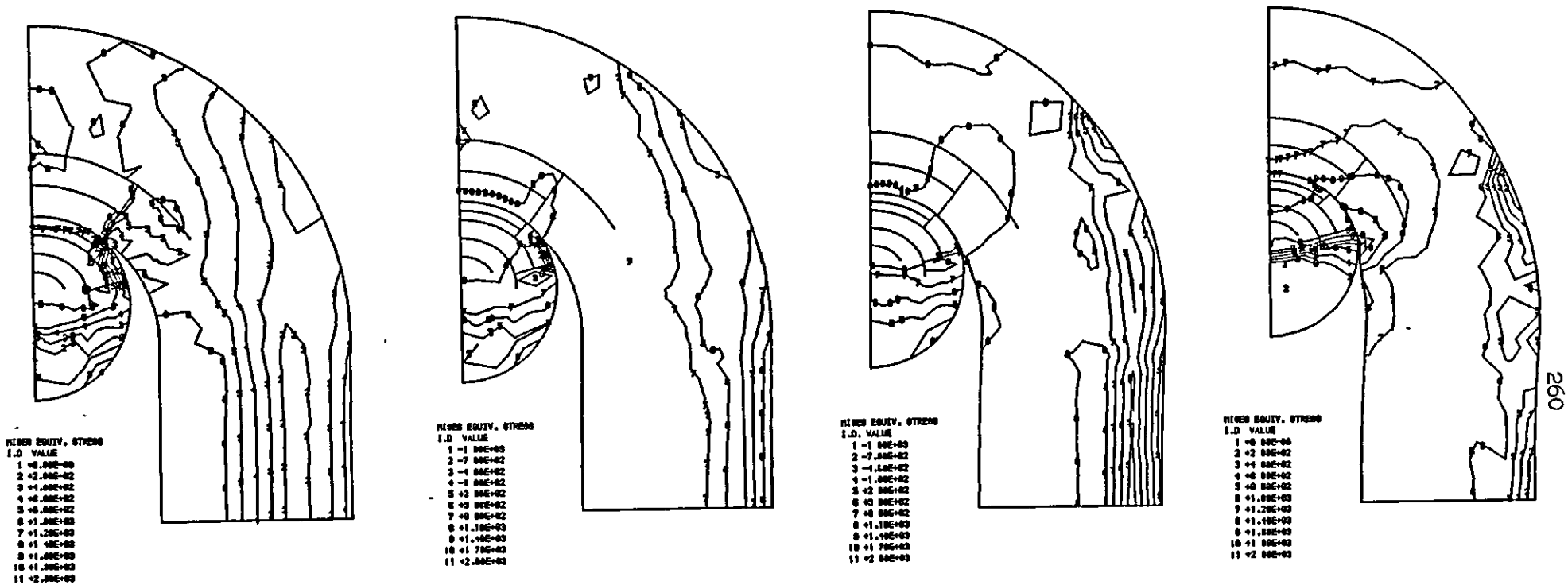

Fig. 7.3 Von Mises stress contours of the 19 mm mining chain under various calibration loads. a) 260 kN. b) 320 kN. c) 380 kN. d) 497 kN (plane stress).

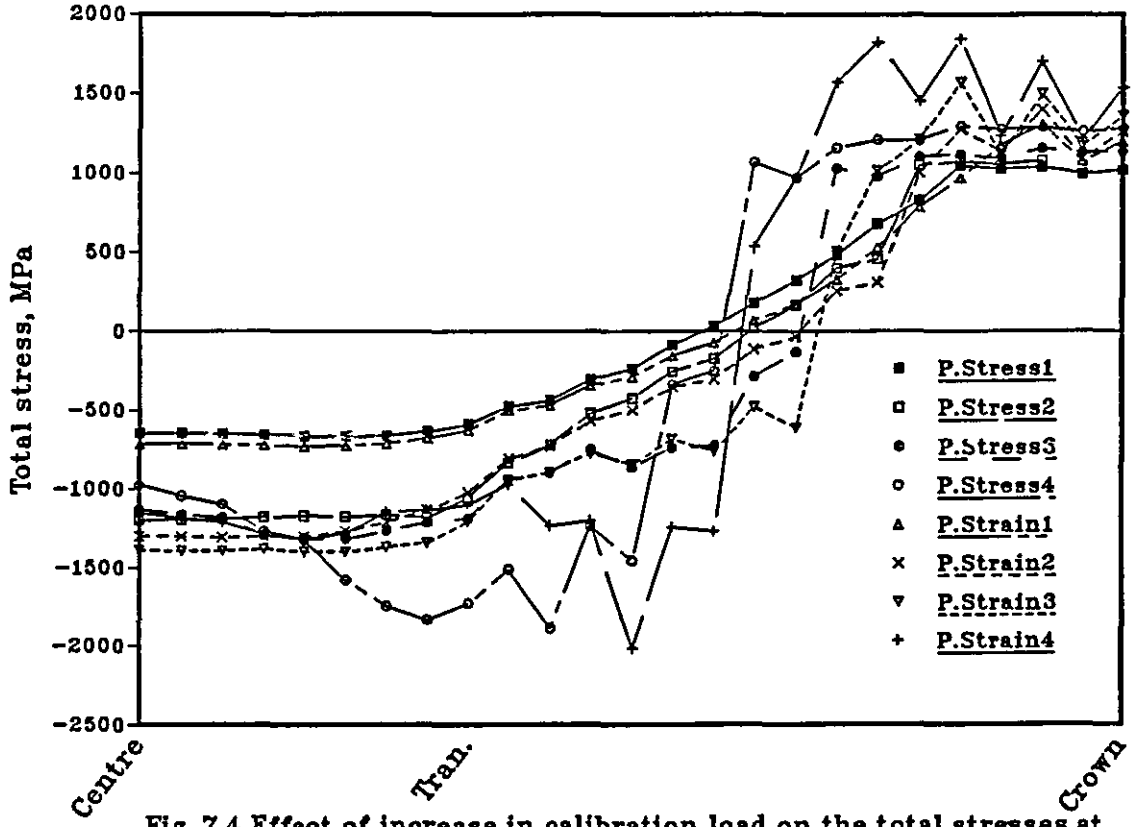

Fig. 7.4 Effect of increase in calibration load on the total stresses at the outside of the mining chain for plane stress/strain analysis (1, 260 kN, 2, 320 kN, 3, 380 kN, and 4 for 497kN).

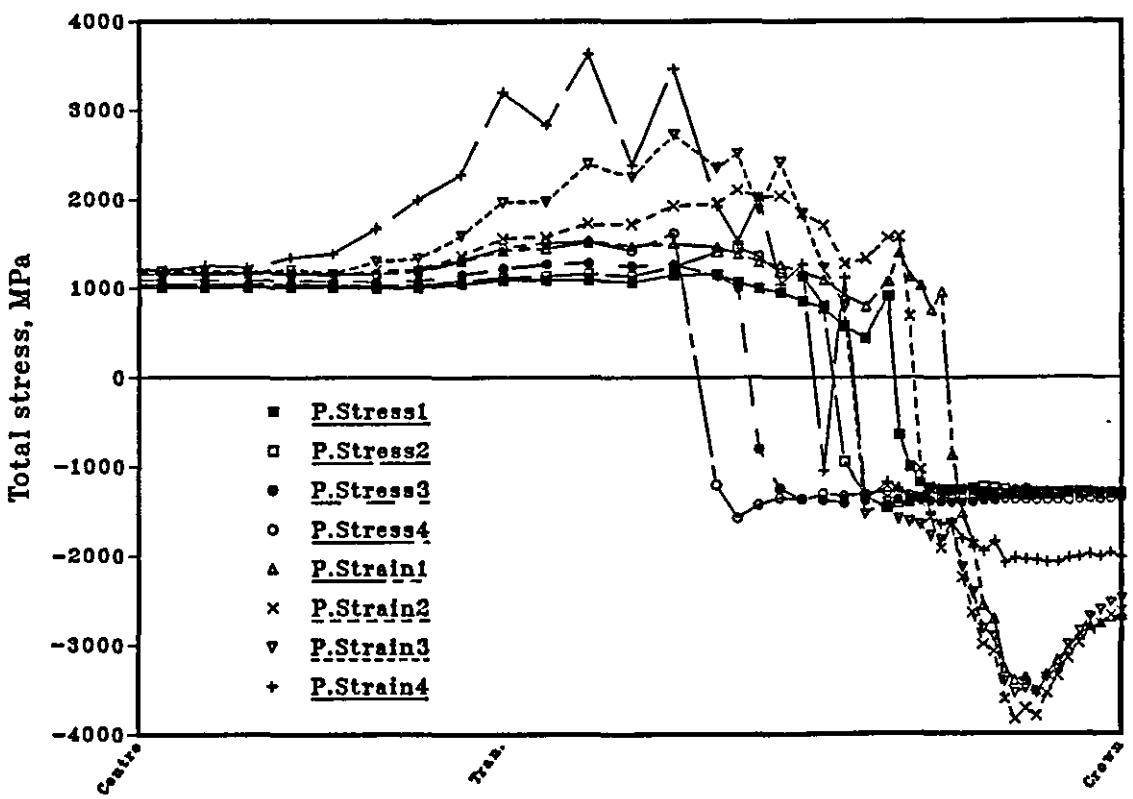

Fig. 7.5 Effect of increase in calibration load on the total stresses at the inside of the mining chain for plane stress/strain analysis (1, 260 kN, 2, 320 kN, 3, 380 kN, and 4 for 497kN).

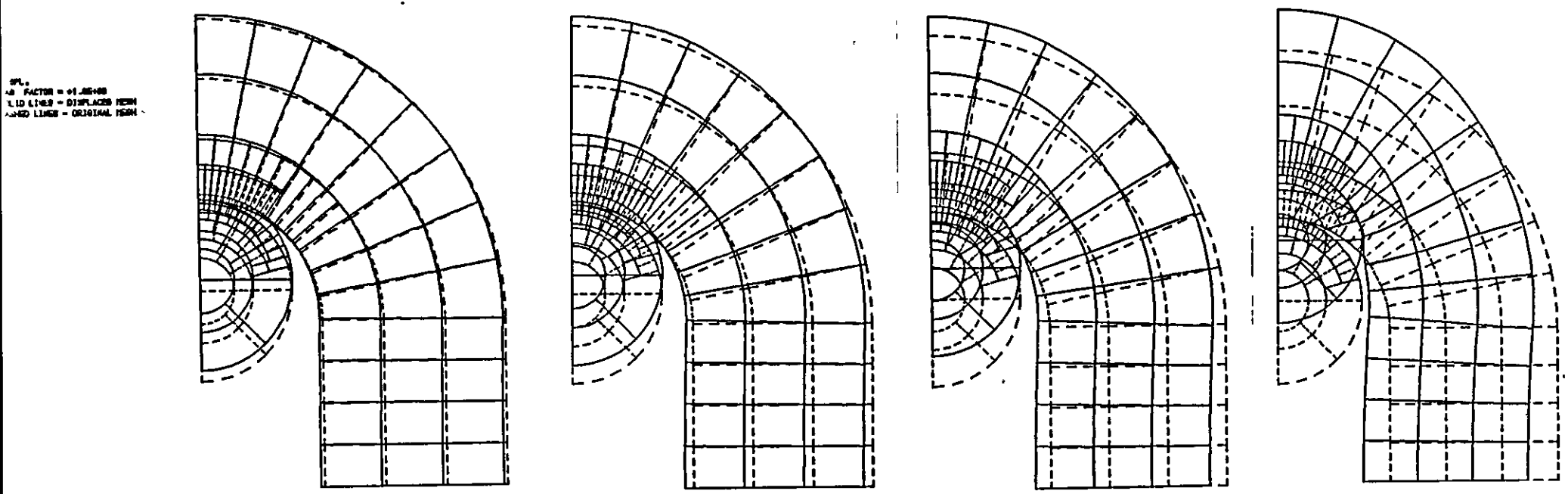

Fig. 7.6 Deformation of the 19 mm mining chain link under various calibration loads for plane stress case. .a) 260 kN. b) 320 kN. c) 380 kN. d) 497 kN.

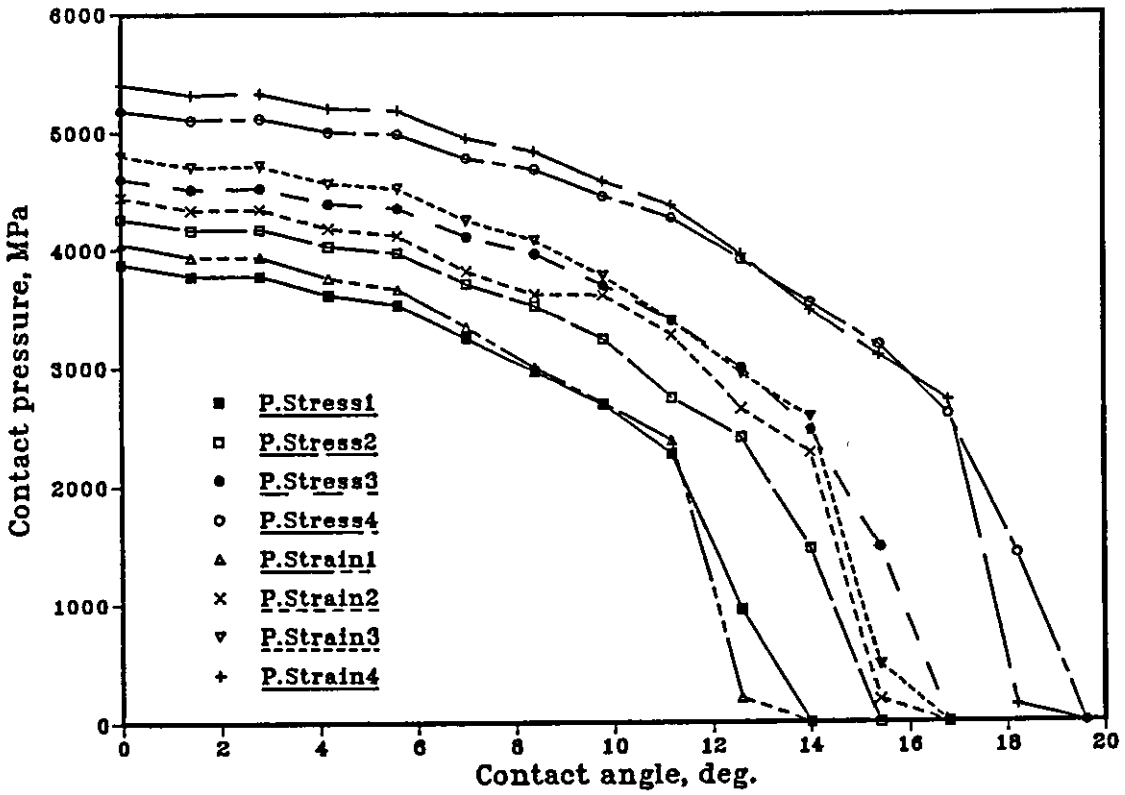

Fig 7.7 Effect of increase in calibration load on the contact angle and contact area of the mining chain for elastic planes stress/strain analysis (1, 260 kN, 2, 320 kN, 3, 380 kN and 4 for 497 kN.).

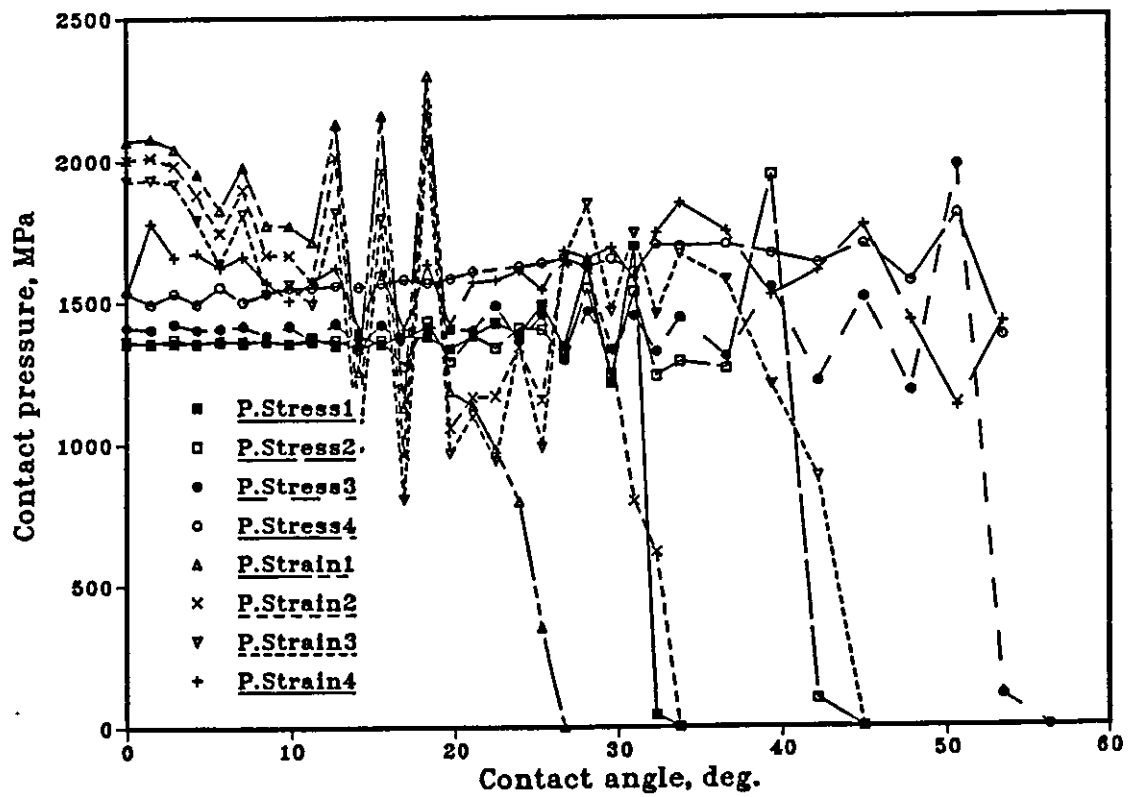

Fig 7.8 Effect of increase in calibration load on the contact angle and contact area of the mining chain for elasto-plastic planes stress/strain analysis (1, 260 kN, 2, 320 kN, 3, 380 kN and 4 for 497 kN.).

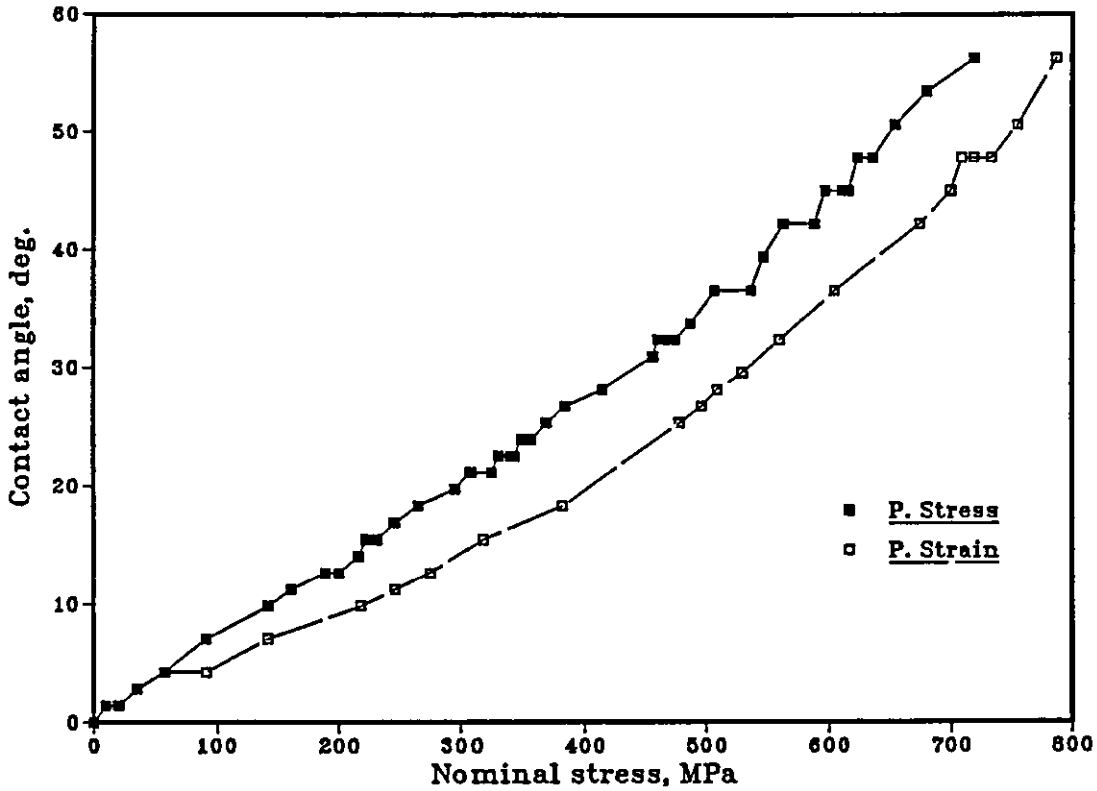

Fig. 7.9 Nominal stresses at the cross-section through the centre produced by calibration loads for plane stress/strain cases.

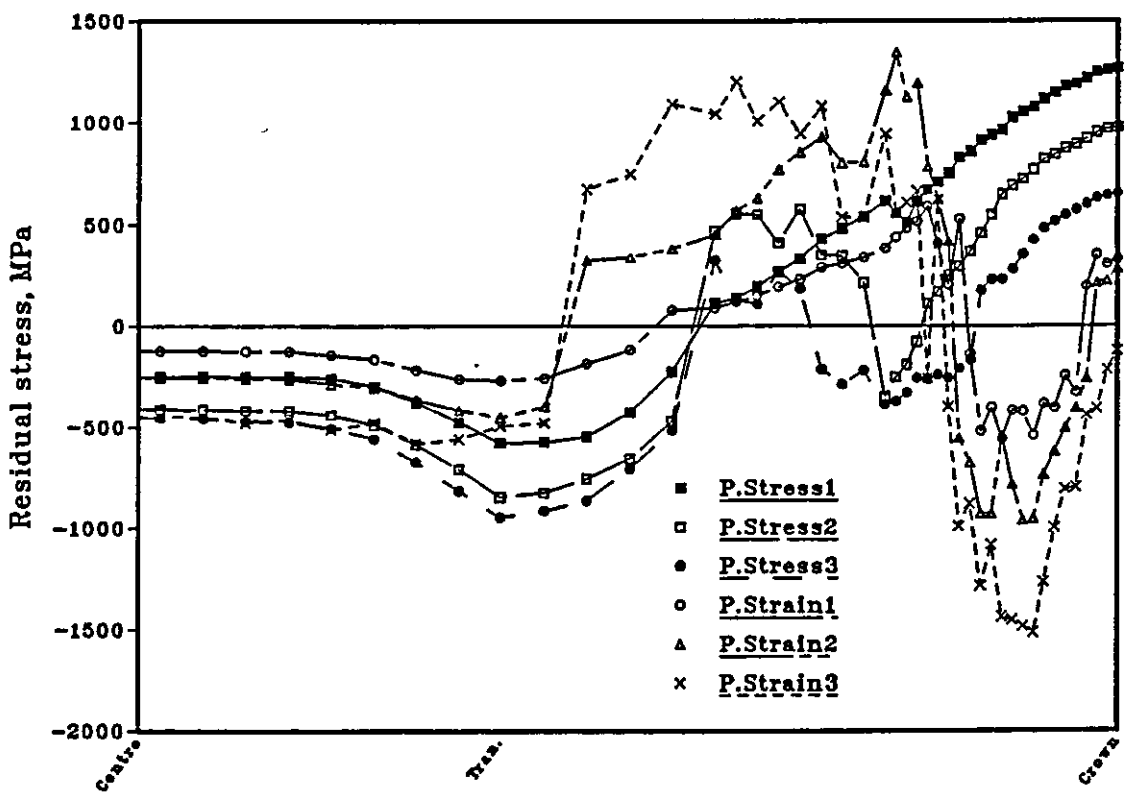

Fig. 7.11 Effect of increase in applied load on the total stresses at the inside of the mining chain for plane stress/strain analysis (1, 260 kN, 2, 320 kN, and 3, for 380 kN).

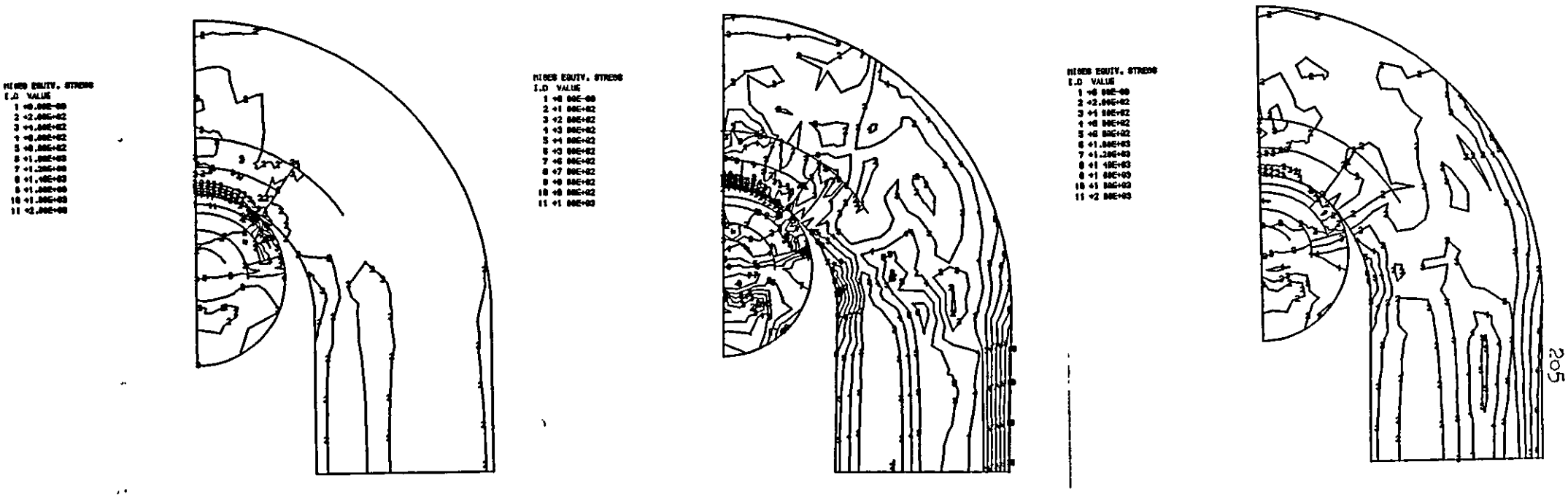

Fig. 7.10 Von Mises residual stress contours of the 19 mm mining chain under various calibration loads. a) 260 kN. b)320 kN. c) 380 kN (plane stress).

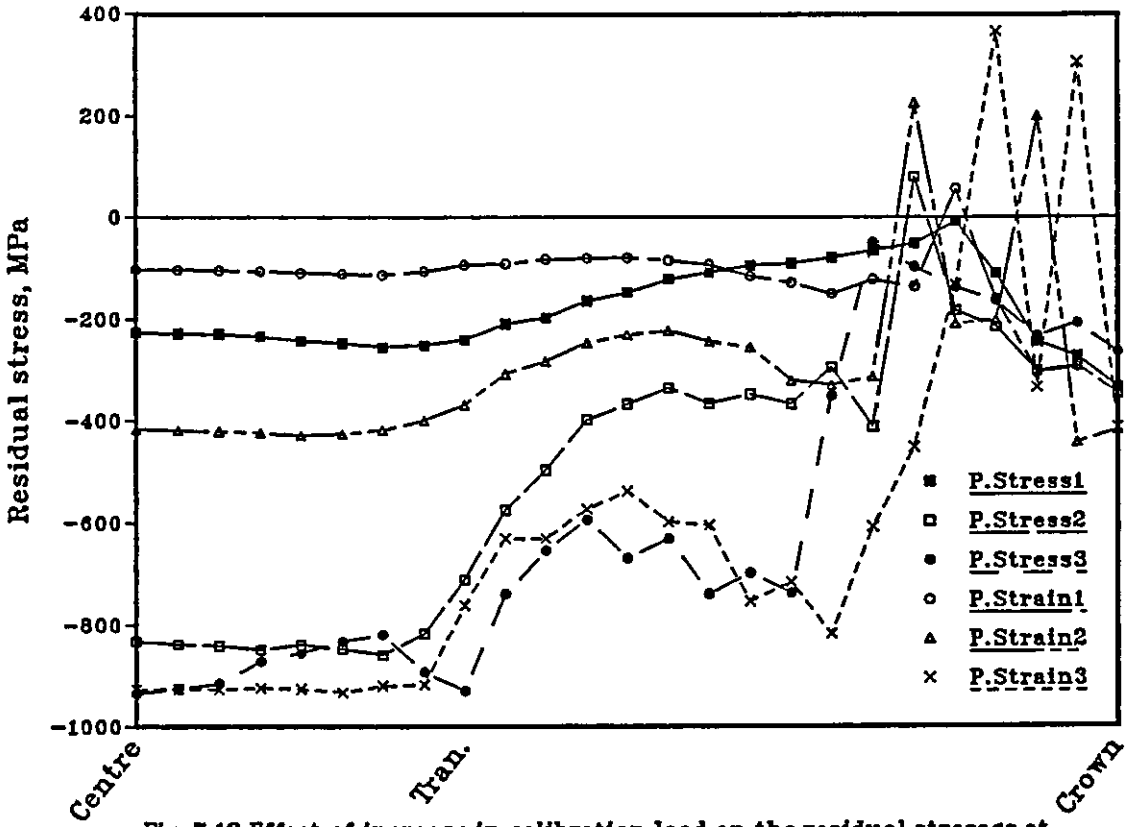

Fig. 7.12 Effect of increase in calibration load on the residual stresses at the outside of the mining chain for plane stress/strain analysis (1, 260 kN, 2, 320 kN and 3, for 380 kN).

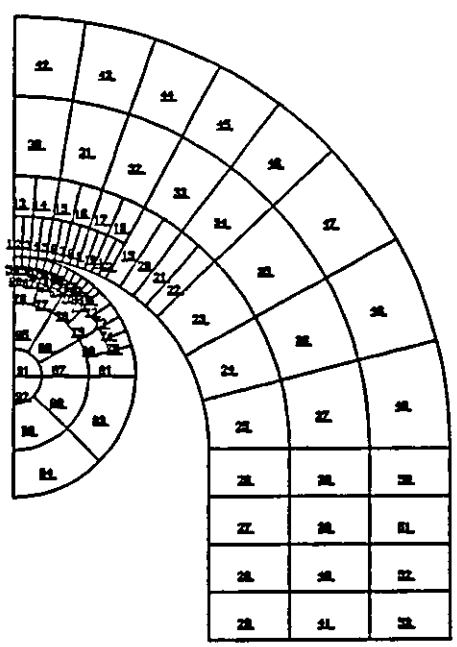

Fig. 7.13 FE mesh of 7 mm lifting chain

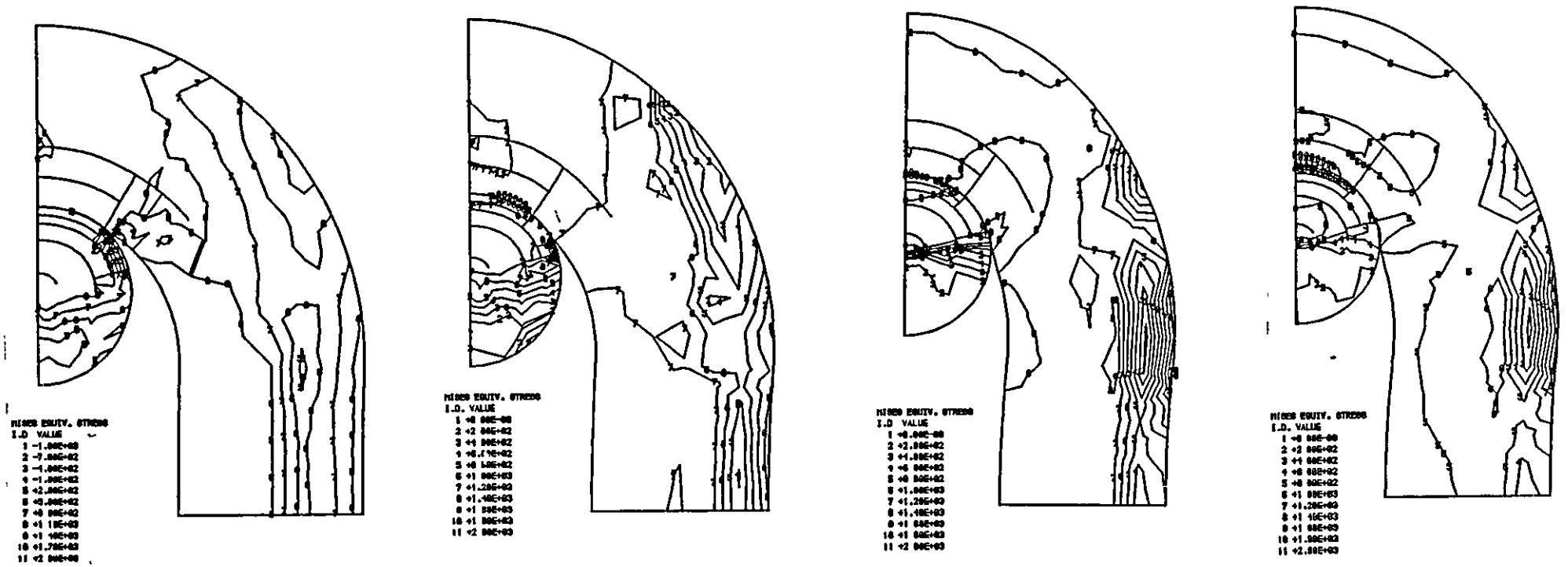

Fig. 7.14 Von Mises stress contours of the 7 mm lifting chain under various calibration loads. a) 30 kN. b) 38.5 kN. c) 50 kN. d) 64 kN.

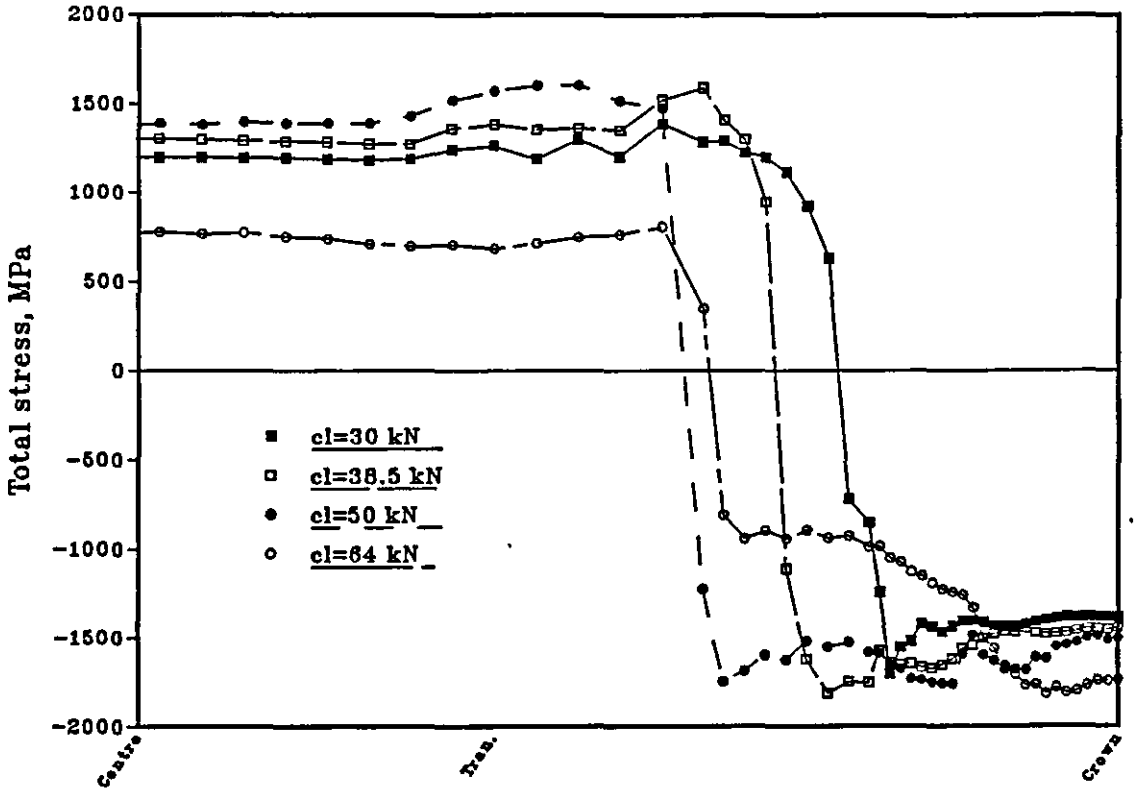

Fig. 7.15 Effect of increase in calibration load on the total stresses at the inside of the lifting chain for plane stress analysis (1, 30 kN, 2, 38.5 kN, 3, 50 kN, and 4, for 64 kN).

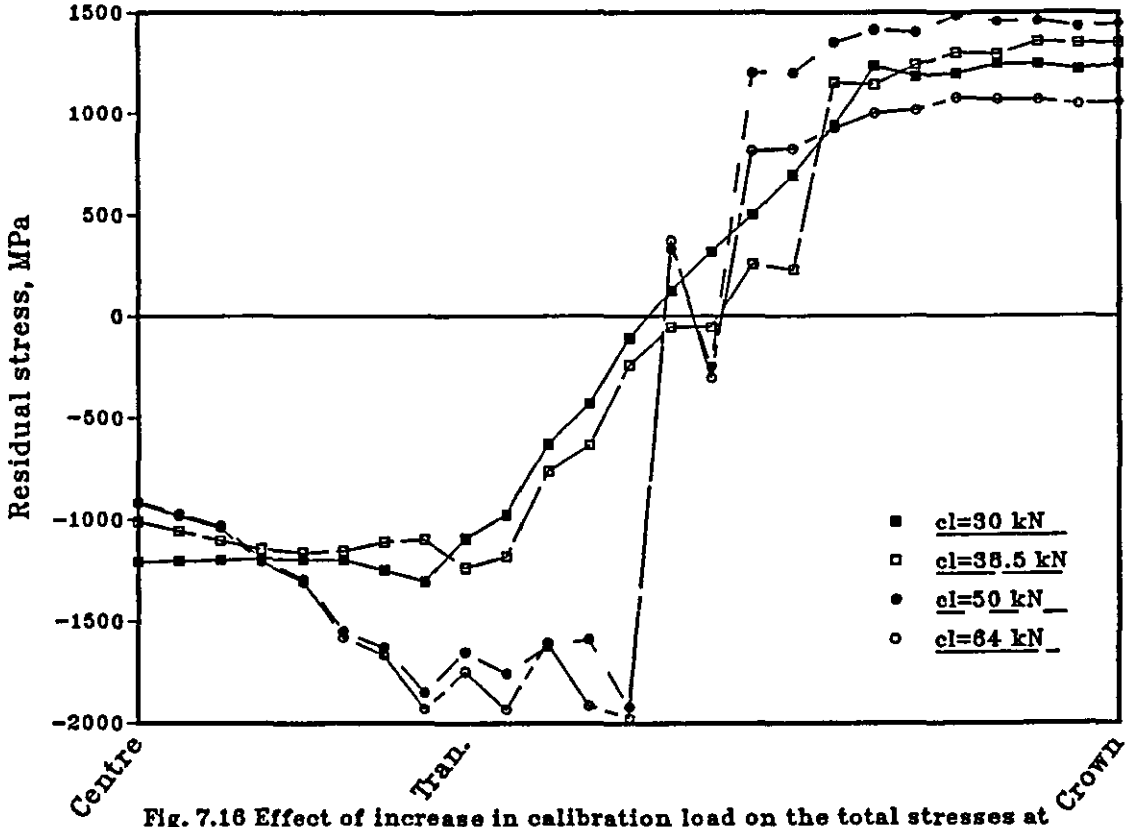

Fig. 7.16 Effect of increase in calibration load on the total stresses at the outside of the lifting chain for plane stress analysis (1, 30 kN, 2, 38.5 kN, 3, 50 kN and 4, for 64 kN).

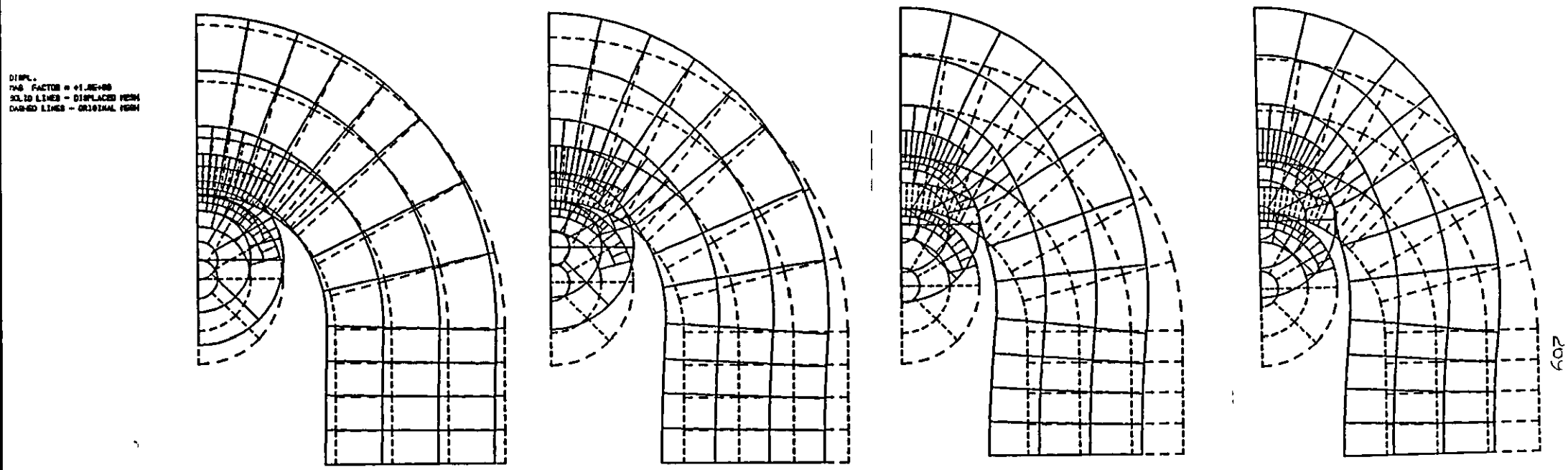

Fig. 7. 17 Deformation of the 7 mm lifting chain link under various calibration loads. a) 30 kN. b) 38.5 kN. c) 50 kN. d) 64 kN.

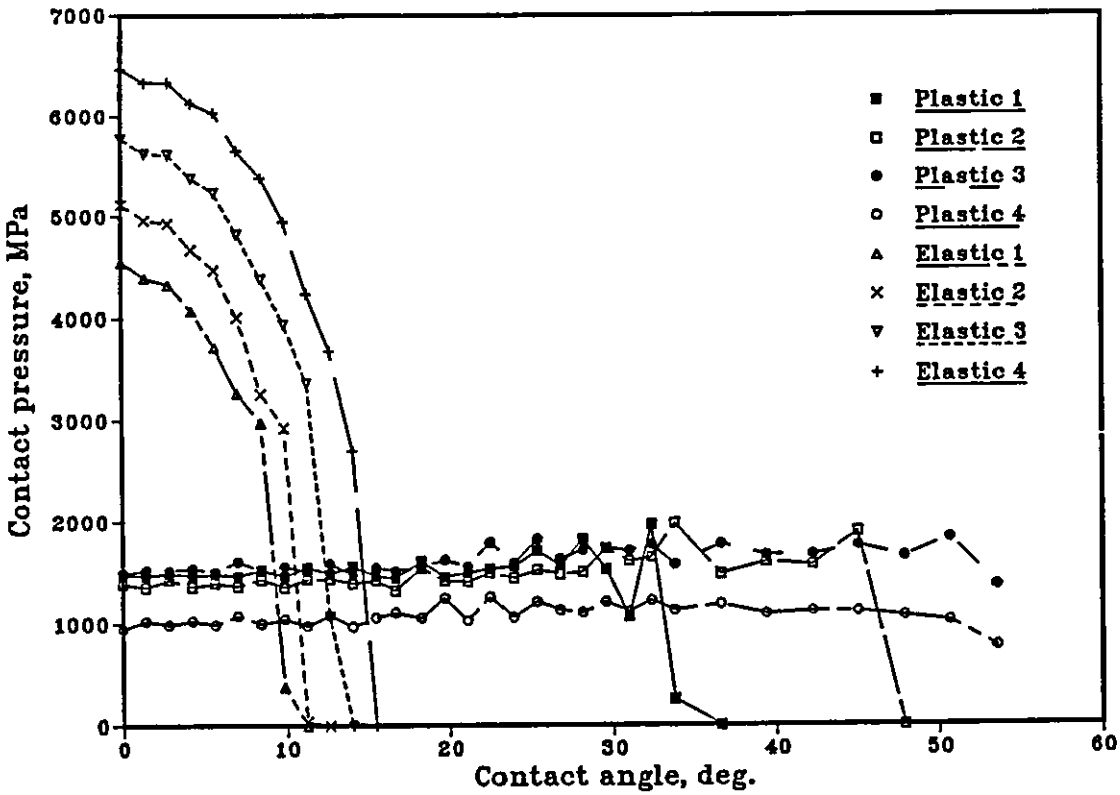

Fig. 7.18 Effect of increase in calibration load on the contact angle and contact pressure of the lifting chain for the plane stress analysis (1, 30 kN, 2, 38.5 kN, 3, 50 kN and 4, for 64 kN).

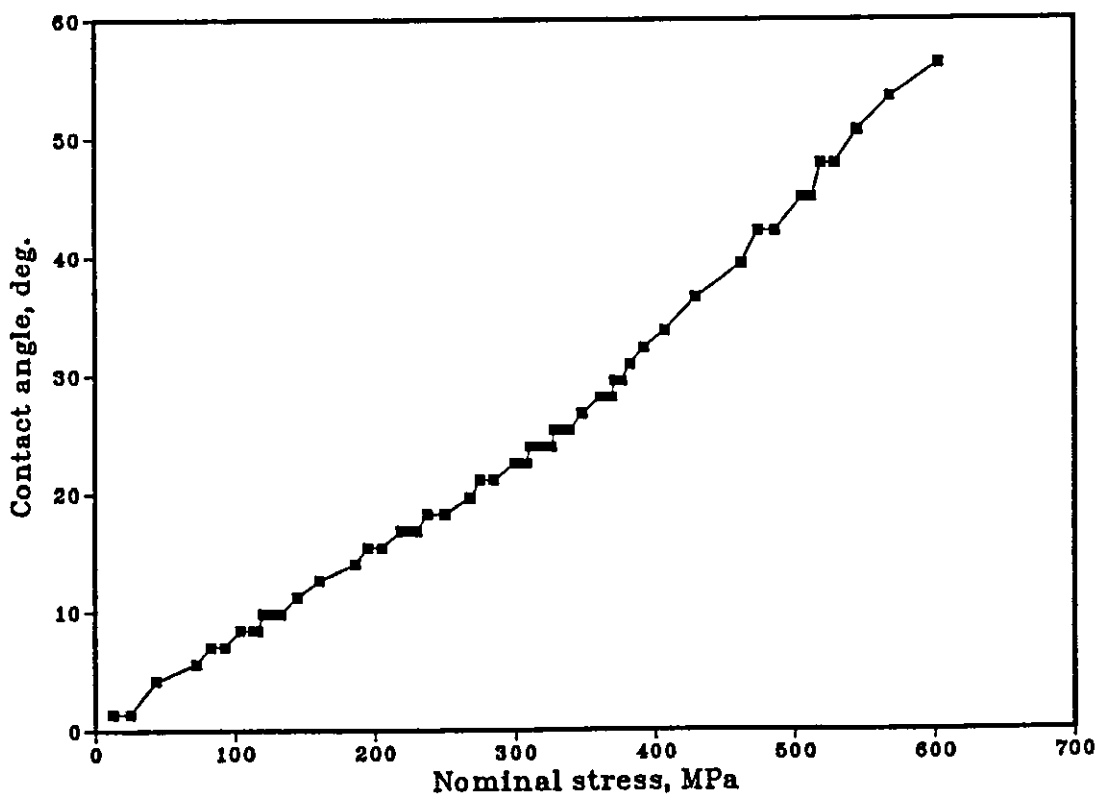

Fig. 7.19 Contact angle resulting from various level of calibration nominal stress at the section through the centre of the lifting chain.

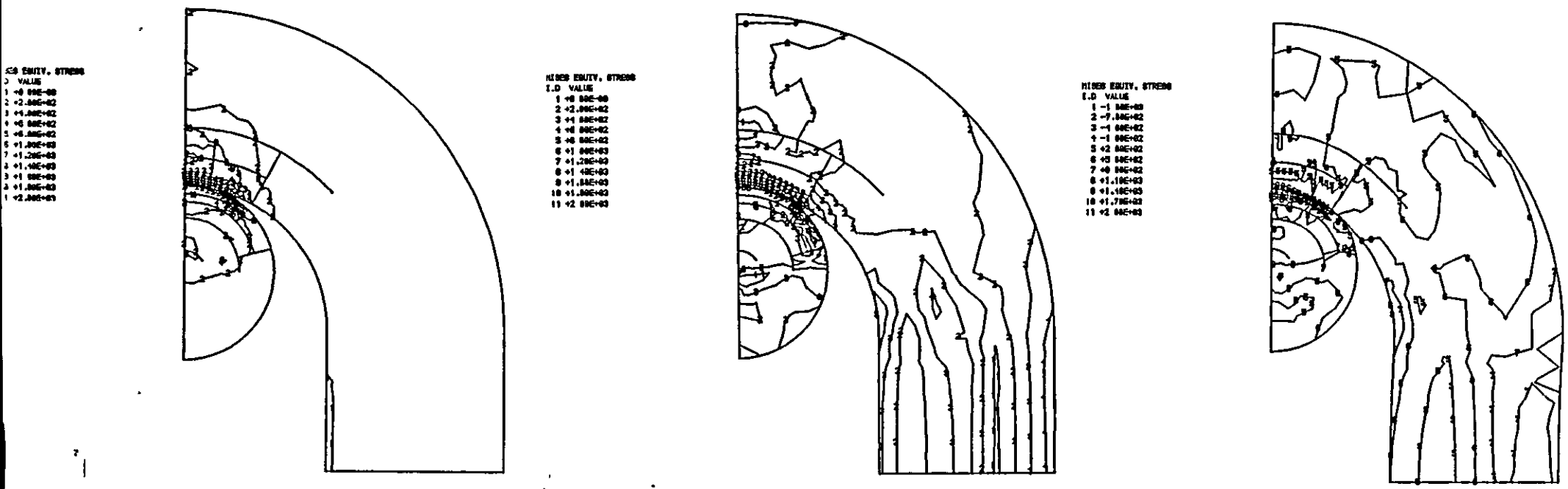

Fig. 7.20 Von Mises residual stress contours of the 7 mm lifting chain under various calibration loads. a) 30 kN. b) 38.5 kN. c) 50 kN.

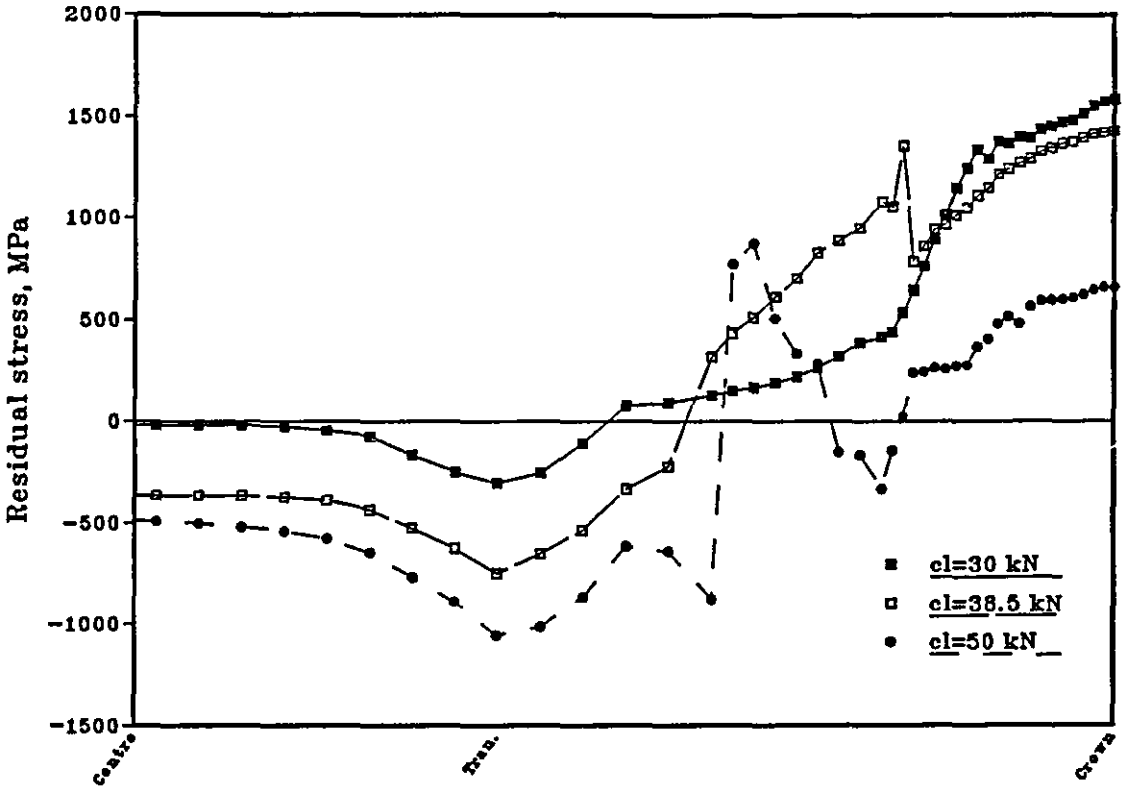

Fig. 7.21 Effect of increase in calibration load on the residual stresses at the inside of the lifting chain for plane stress analysis.

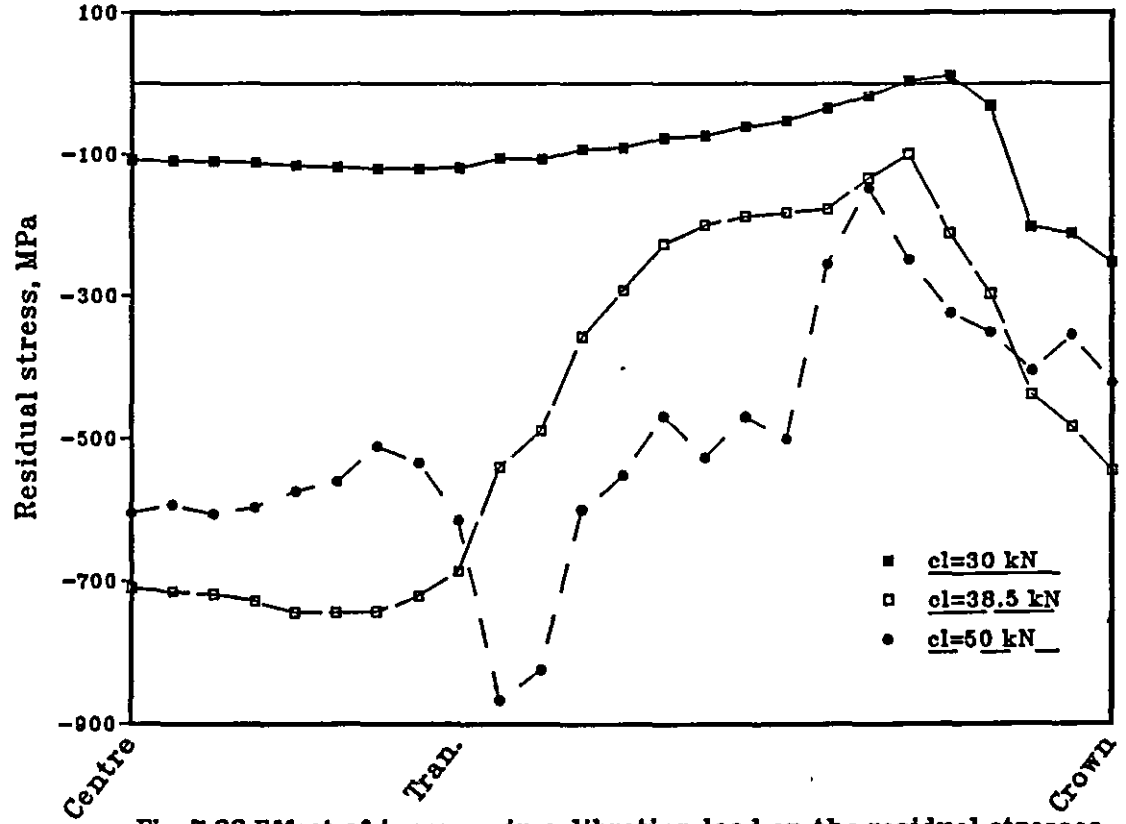

Fig. 7.22 Effect of increase in calibration load on the residual stresses at the outside the lifting chain for plane stress analysis.

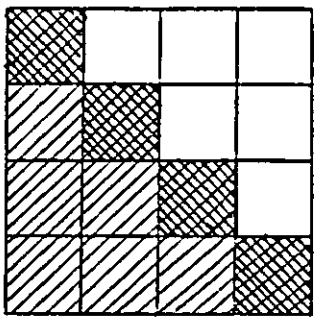

a) Circular cross-section.

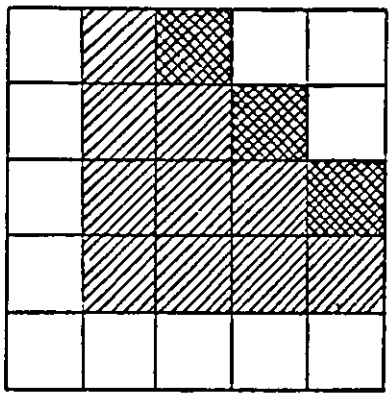

b)Oval cross-section.

3000 MPa 1000 MPa

Fig. 8.1 Assumed contact pressure for circular and oval cross-sectional chain links.

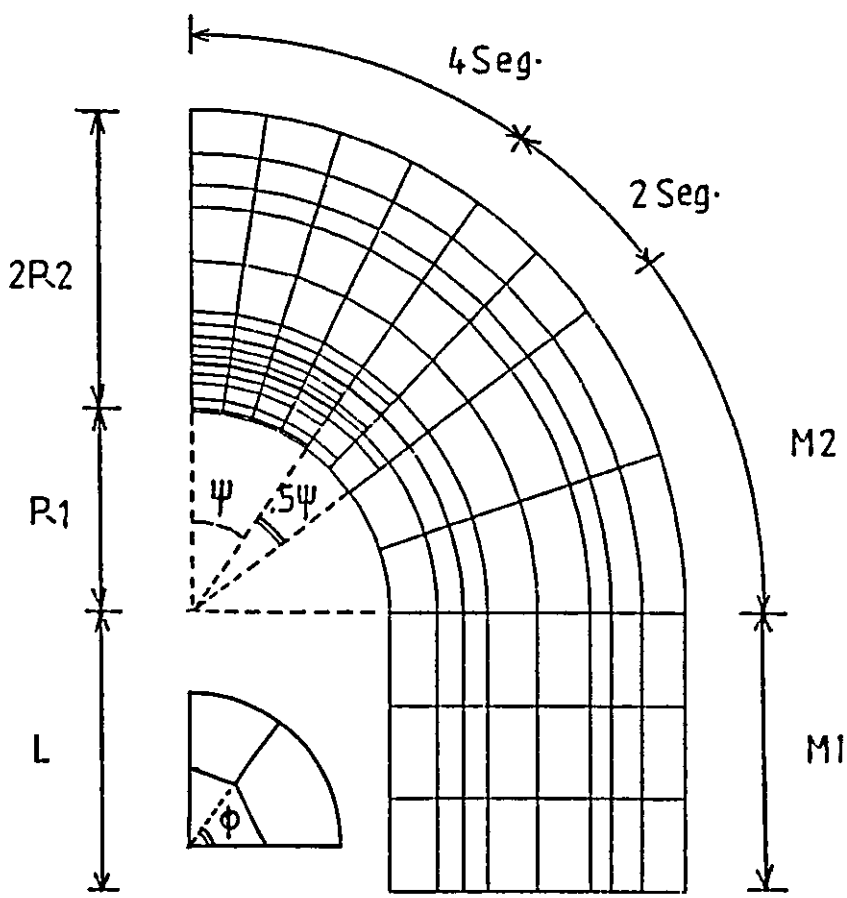

Fig. 8.2 An 1/8 of chain link (in plan view) showing refined zone for contact pressure application with various parameters used in the mesh generation.

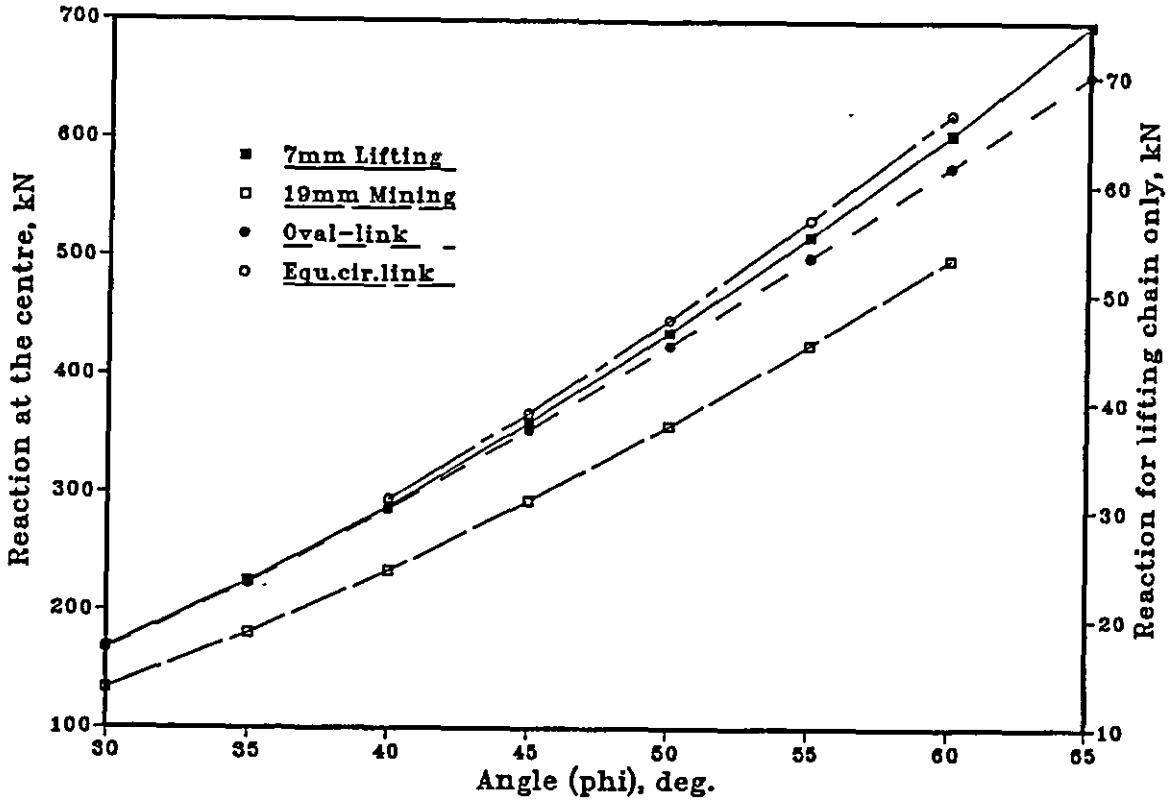

Fig. 8.3 Effect of increase in the contact angle on the reaction at the centre of various chain link geometries.

Cal. load	19 mm mining chain			7 mm lifting chain			Oval-link		Equ. Cir.	
	ϕ	ψ		ϕ	ψ		ϕ	ψ	ϕ	ψ
		2-D	3-D		2-D	3-D				
First	42.50	33.76	31.79	40.00	27.38	24.86	48.00	32.00	46.75	37.19
Second	47.50	45.01	35.53	45.00	36.57	27.97	54.50	36.33	52.75	41.97
Third	52.00	56.27	38.89	52.00	52.26	32.32	60.00	40.00	57.50	45.75
Failure	56.50		42.26	60.00		37.30	61.50	41.00	59.25	47.14

Table 8.1 Assumed and evaluated (2-D) angle of contact (deg.) for all grades of chain used in the he finite element analysis (3-D).

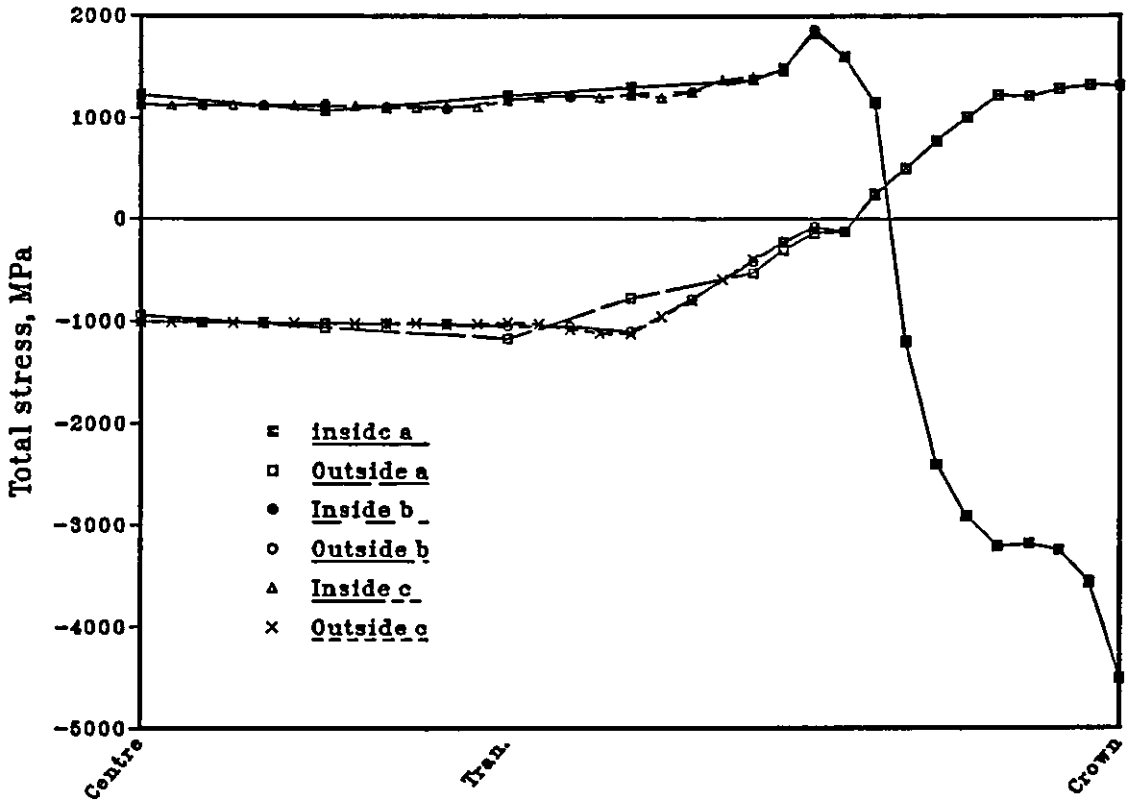

Fig. 8.4 Effect of mesh refinement on the total stresses at the inside and outside of the standard 19 mm mining chain under cl=320 kN.

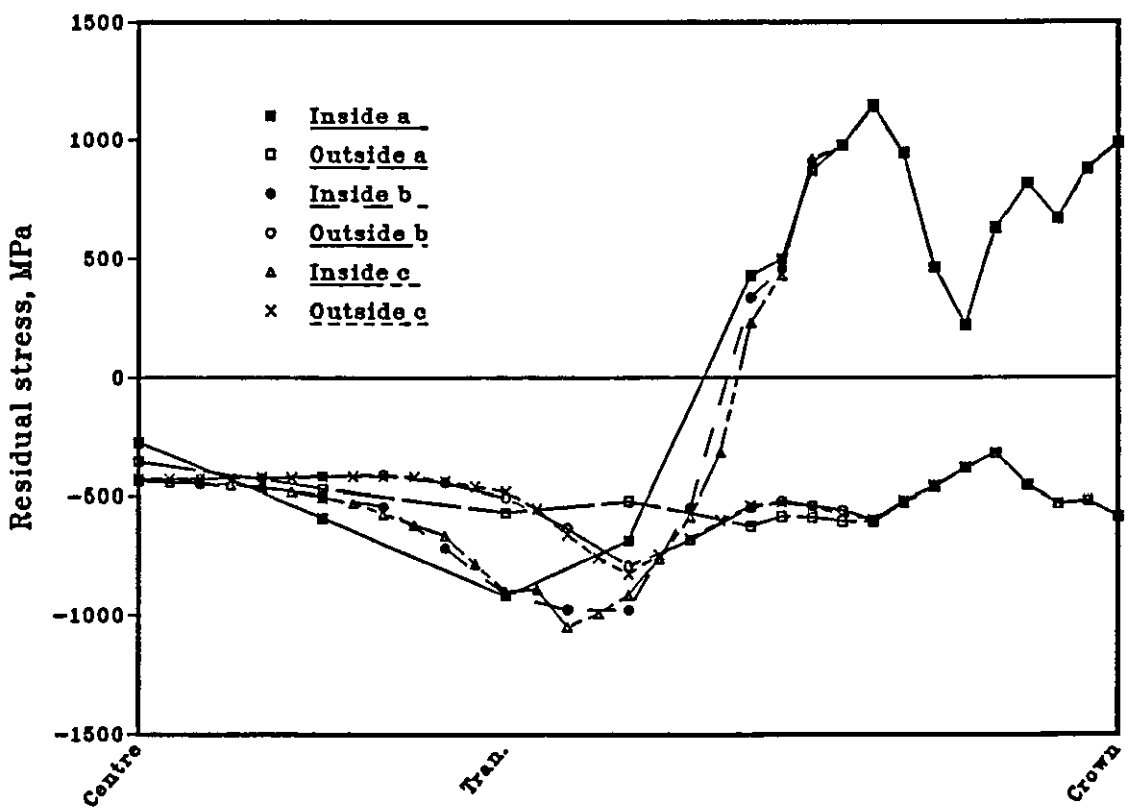

Fig. 8.5 Effect of mesh refinement on the residual stresses at the inside and outside of the standard 19 mm mining chain under cl=320 kN.

TITLE STRA.DAT 12.7 9.5 17.4 3 2 0.0 47.5 35.53

PAFEC

VIEW FROM X = 1.000
Y = 0.5941
Z = 1.879

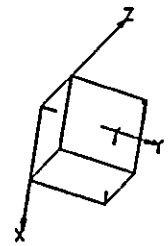

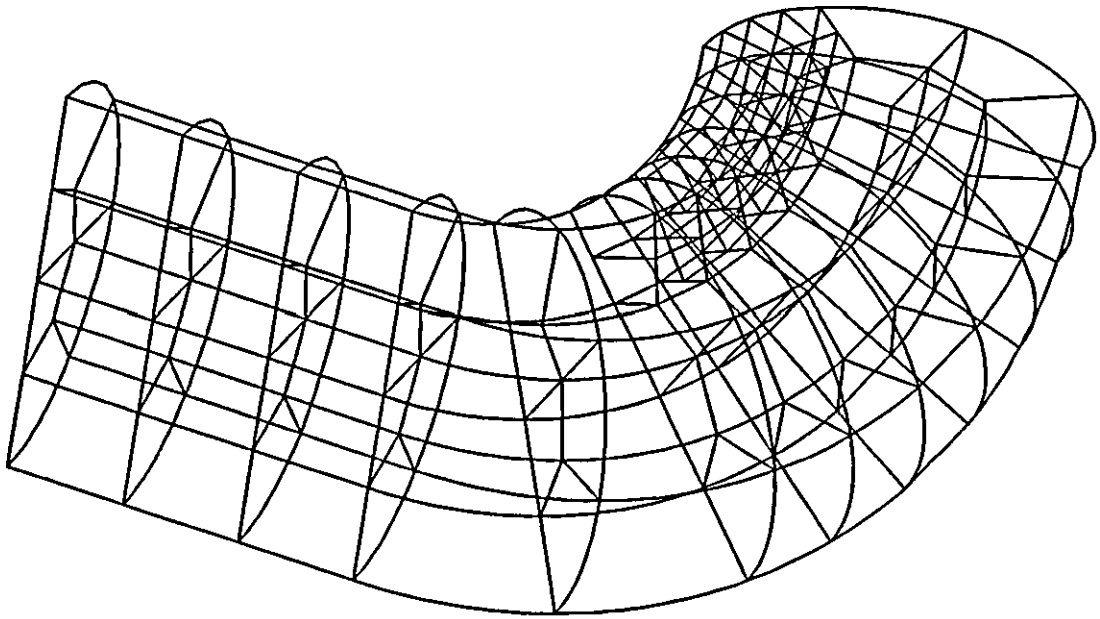

270

WHOLE STRUCTURE DRAWN

PRODUCED BY PAFWOR
ON 13/04/89 AT 2234 HOURS

Fig. 8.6a FE mesh of standard link.

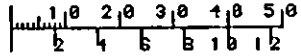

mm.
STRUCTURAL UNITS

DRAWING NO. 1
SCALE = 01000E-2
DRAWING TYPE= 2

11

TITLE 12.7 9.5 17.4 4 1 -24.0 47.7 35.53

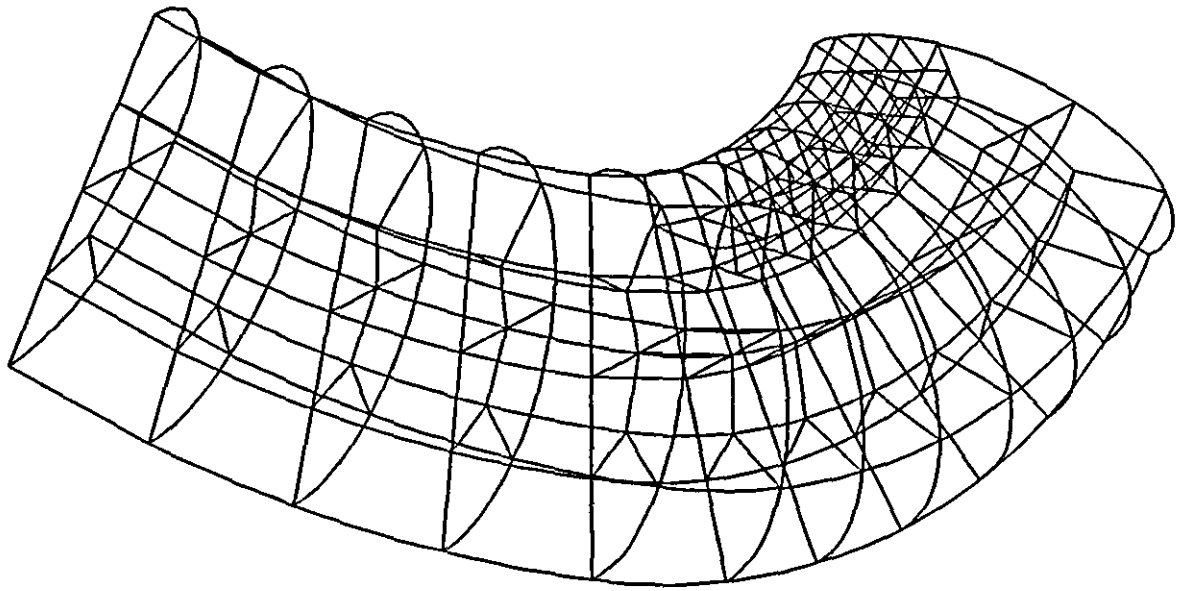

PAFEC

VIEW FROM X = 1.000
Y = 07137
Z = 2.076

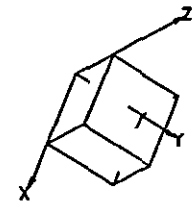

WHOLE STRUCTURE DRAWN

PRODUCED BY PAFWOR
ON 13/04/89 AT 2359 HOURS

Fig. 8.6b FE mesh of elliptical link.

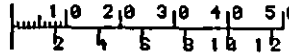

DRAWING NO. 1
SCALE = 01000 E-2 :1
DRAWING TYPE= 2

TITL 12.7 9.5 17.4 2 3 24.0 47.7 35.53

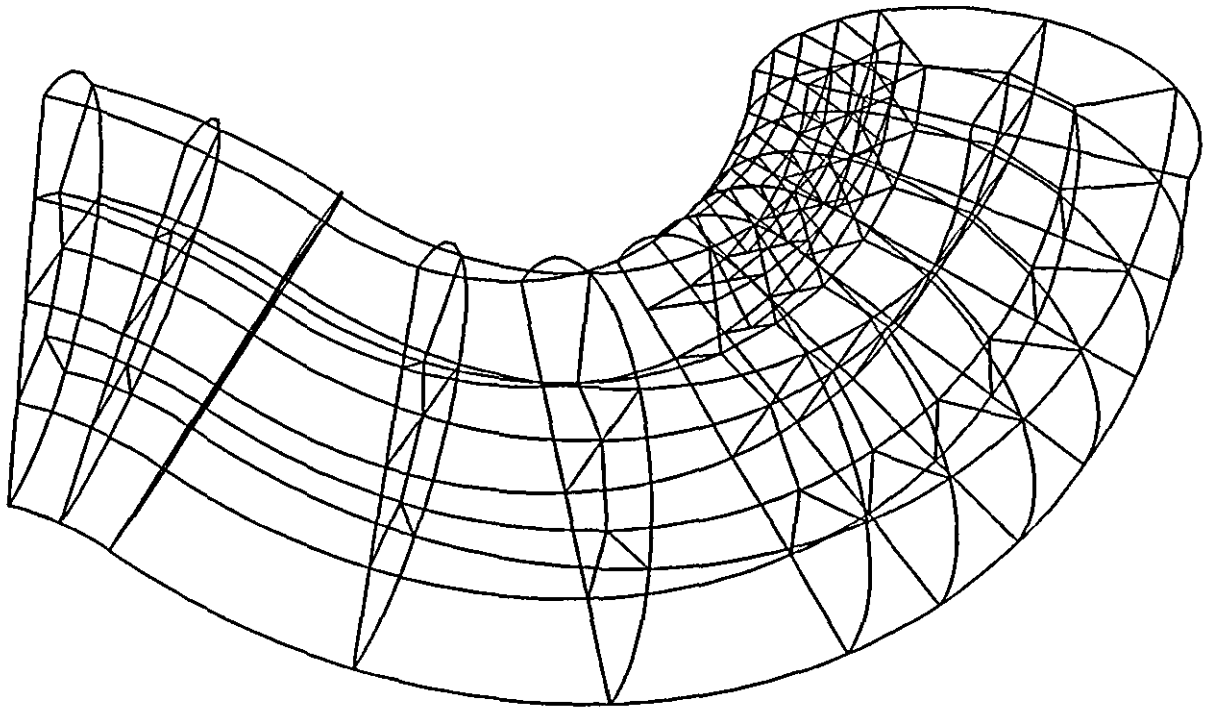

PAFEC

VIEW FROM X = 1.000
Y = 0.4944
Z = 1.717

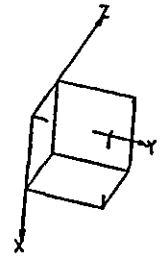

278

WHOLE STRUCTURE DRAWN

PRODUCED BY- PAFWOR
ON 13/04/89 AT 2329 HOURS

Fig. 8.6c FE mesh of eight shape link.

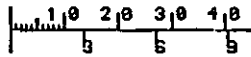

STRUCTURAL UNITS

DRAWING NO. 1
SCALE = 01500E-2
DRAWING TYPE= 2

11

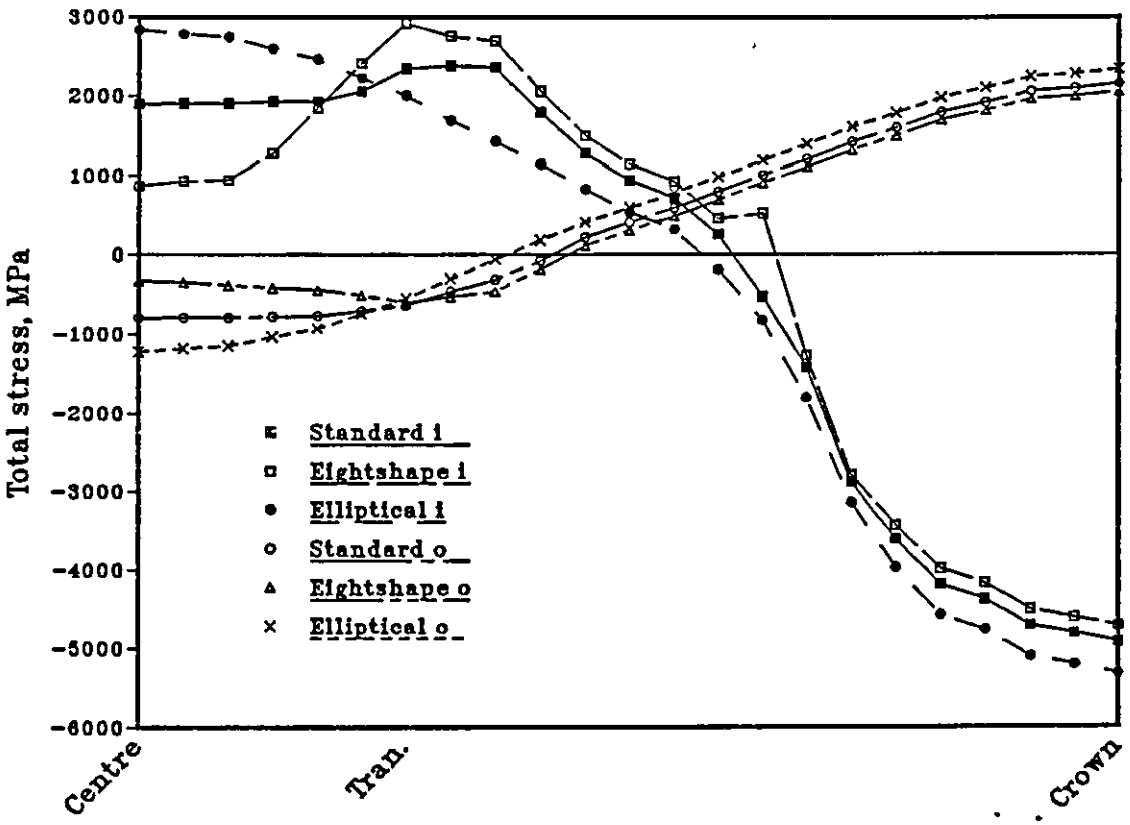

Fig. 8.7 Effect of link geometry on the total stresses of the 19 mm mining chain at the inside and outside under cl=320 kN for elastic analysis.

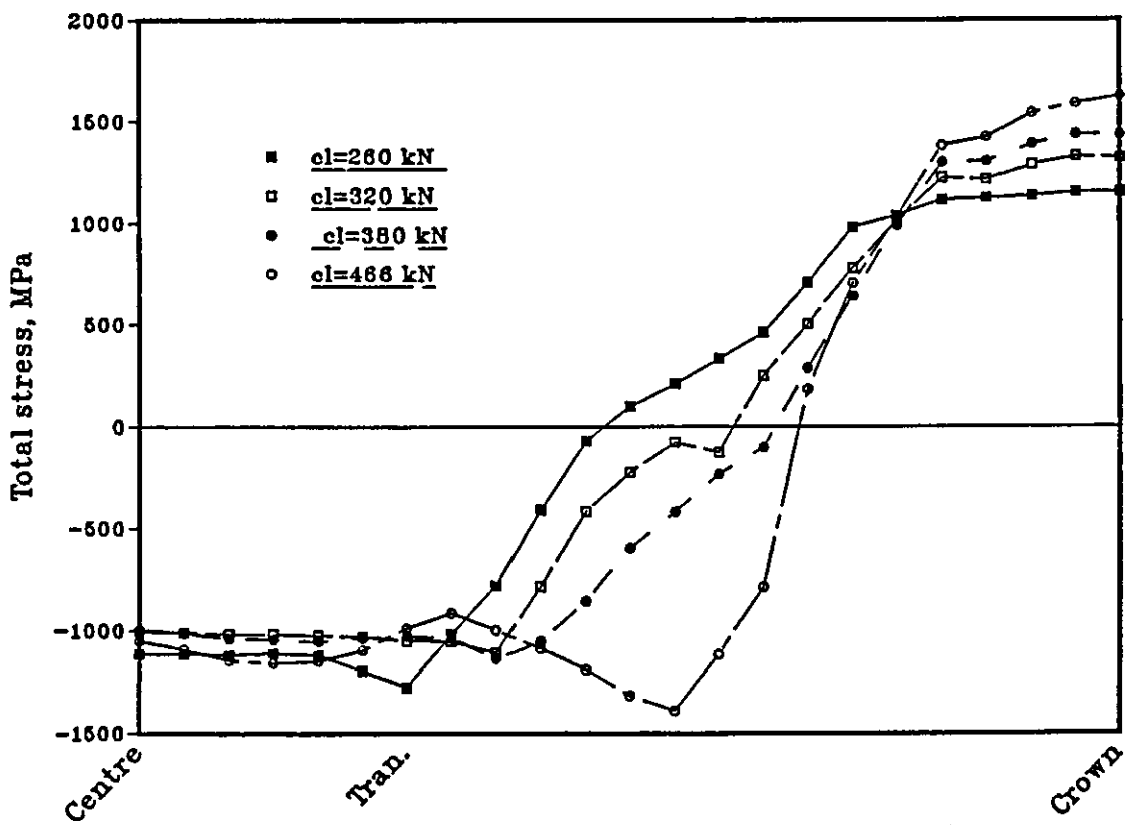

Fig. 8.8 Effect of increase in calibration load on the total stresses at the outside of the 19 mm standard mining chain.

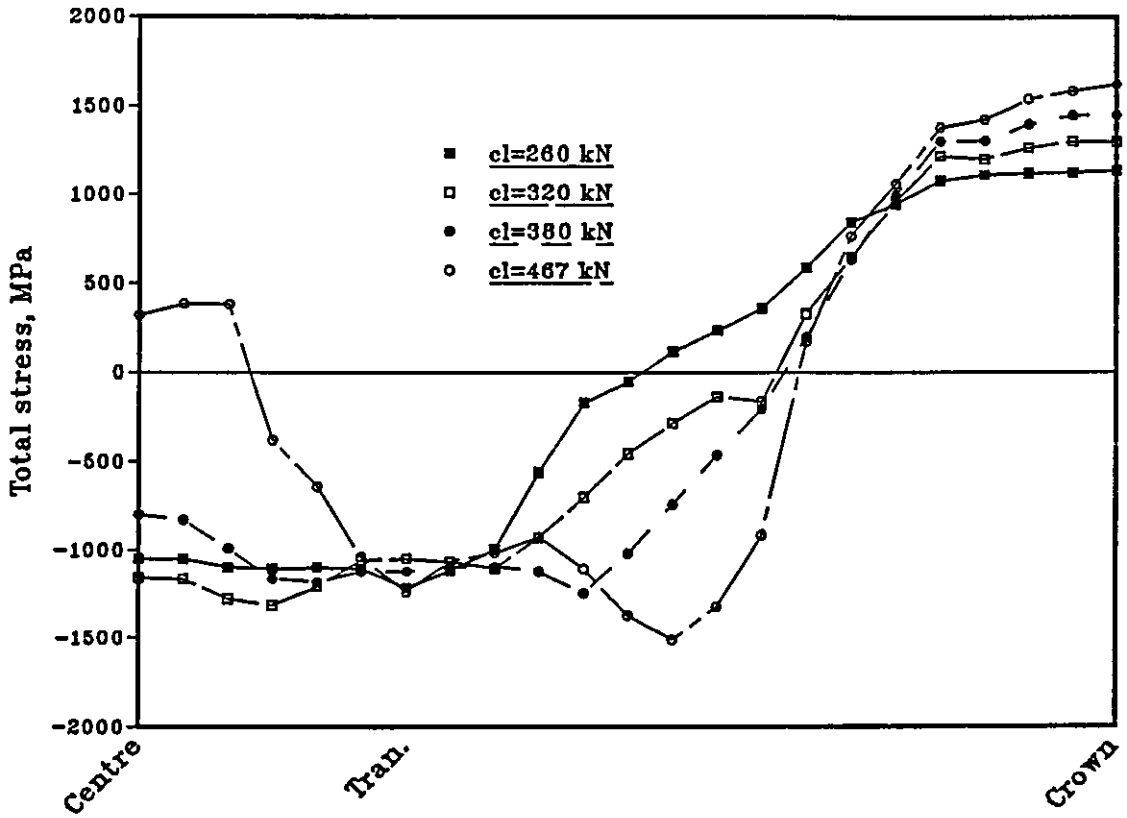

Fig. 9.9 Effect of increase in calibration load on the total stresses at the outside of the 19 mm eight shape mining chain.

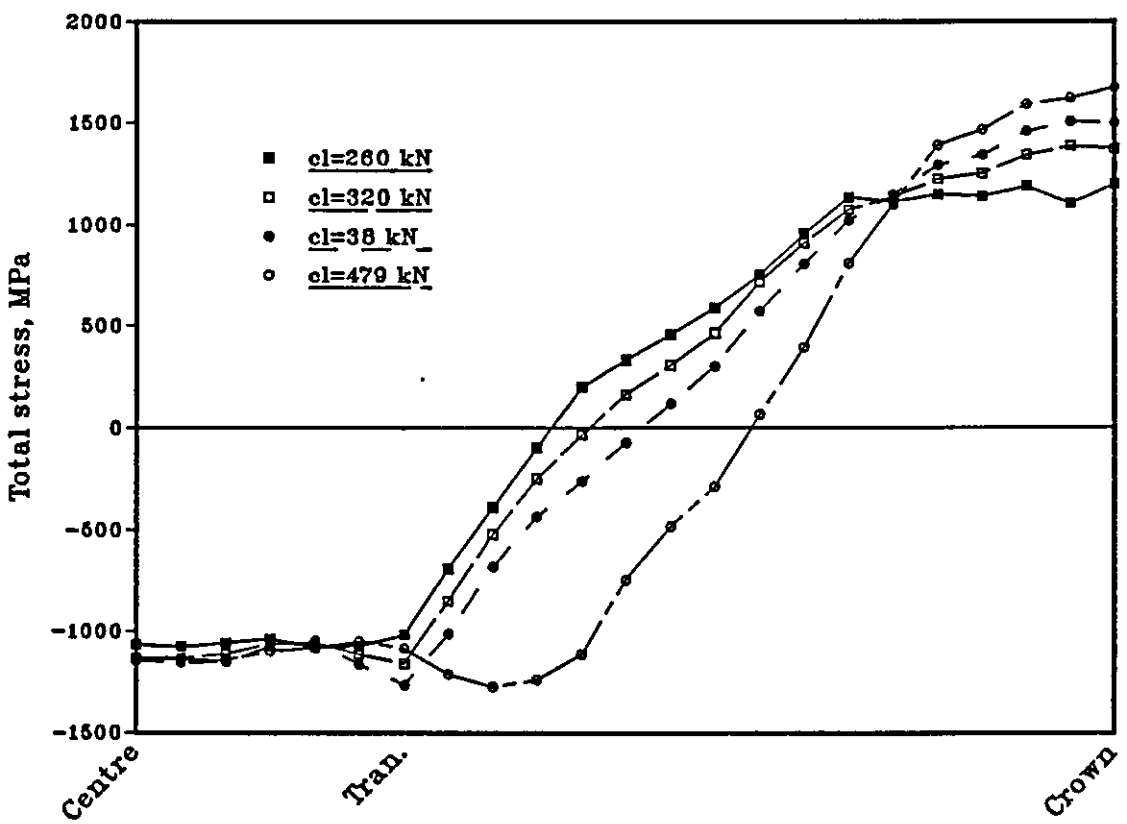

Fig. 8.10 Effect of increase in calibration load on the total stresses at the outside of the 19 mm elliptical mining chain.

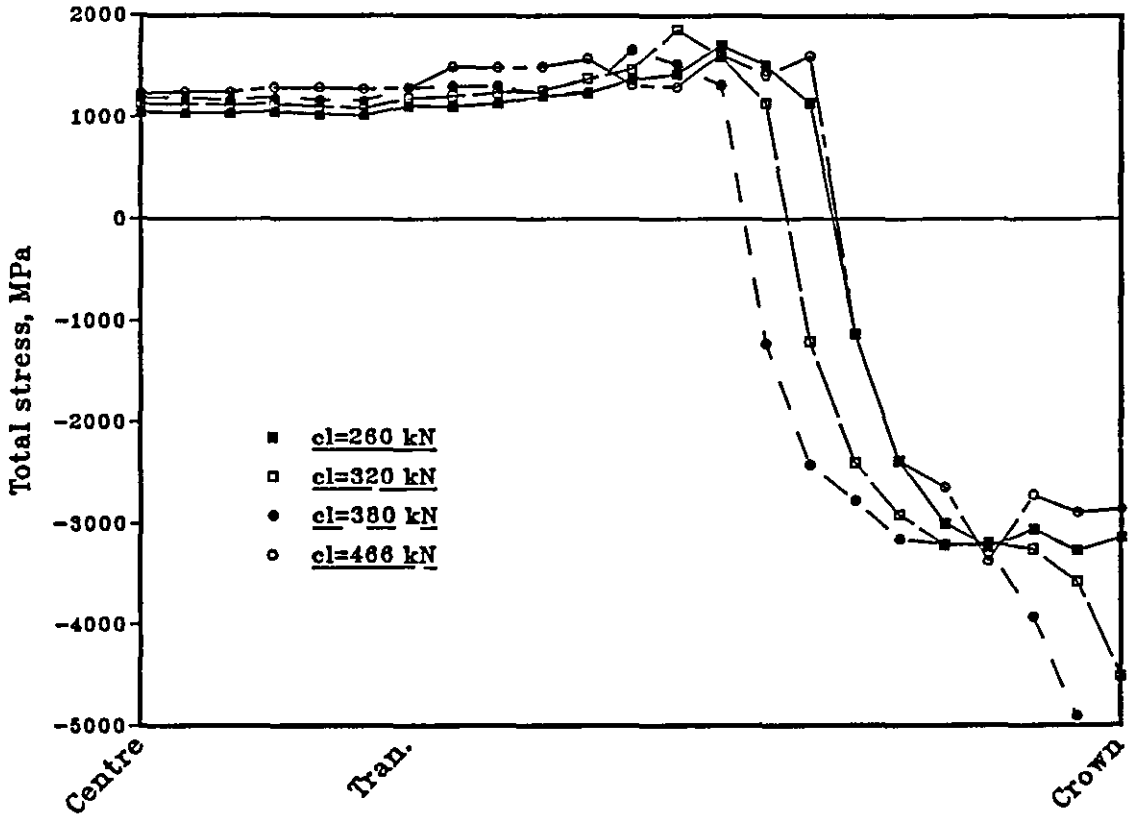

Fig. 8.11 Effect of increase in calibration load on the total stresses at the inside of the 19 mm standard mining chain.

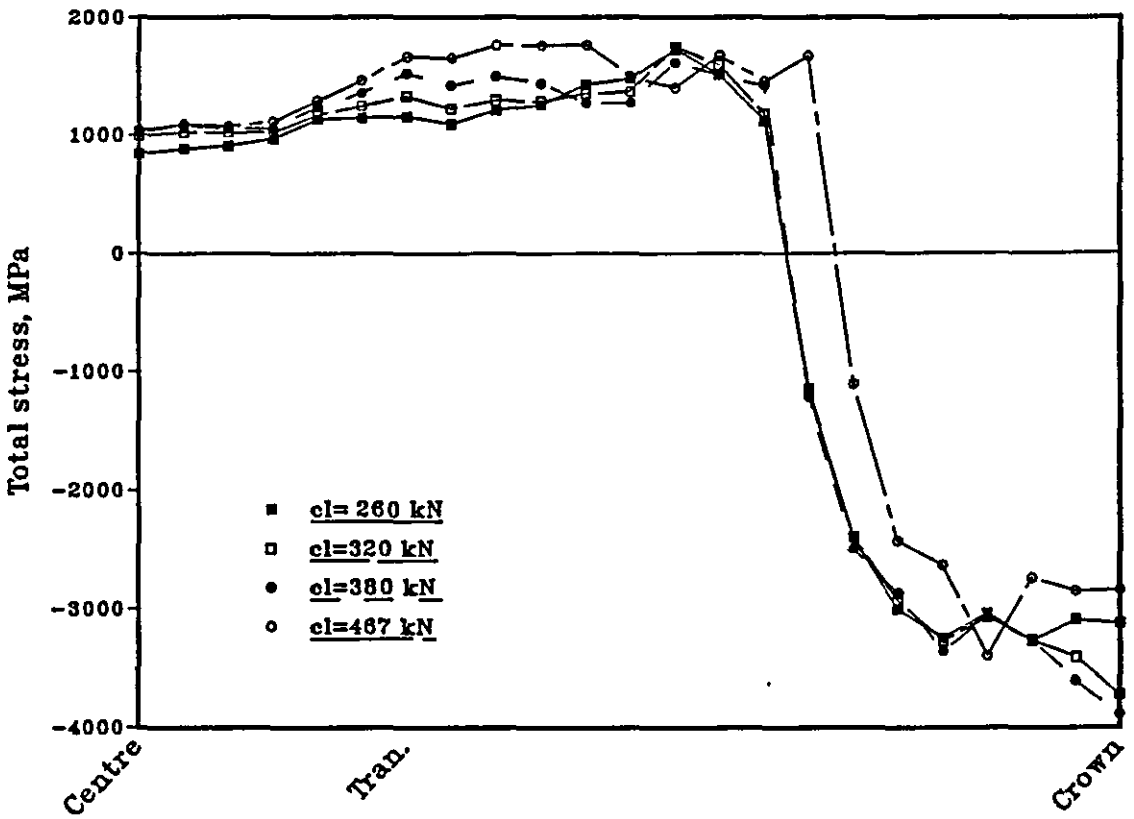

Fig. 8.12 Effect of increase in calibration load on the total stresses at the inside of the 19 mm eight shape mining chain.

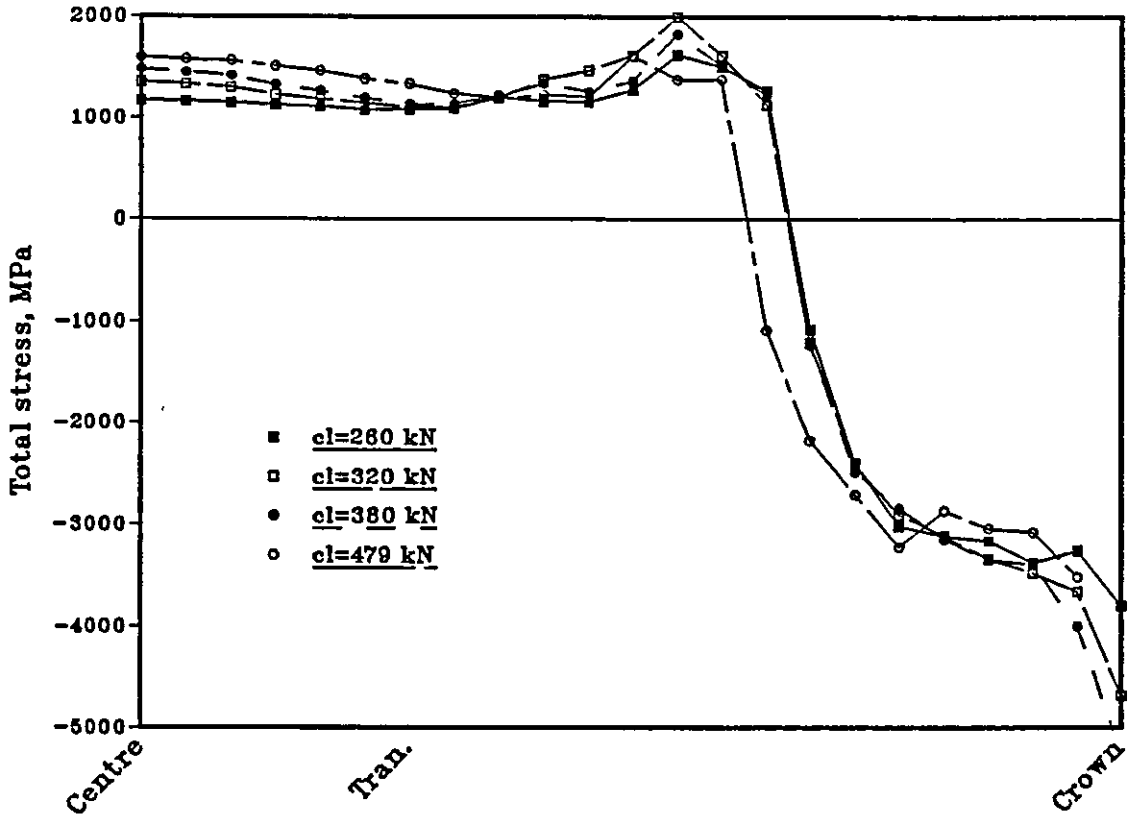

Fig. 8.13 Effect of increase in calibration load on the total stresses at the inside of the 19 mm elliptical mining chain.

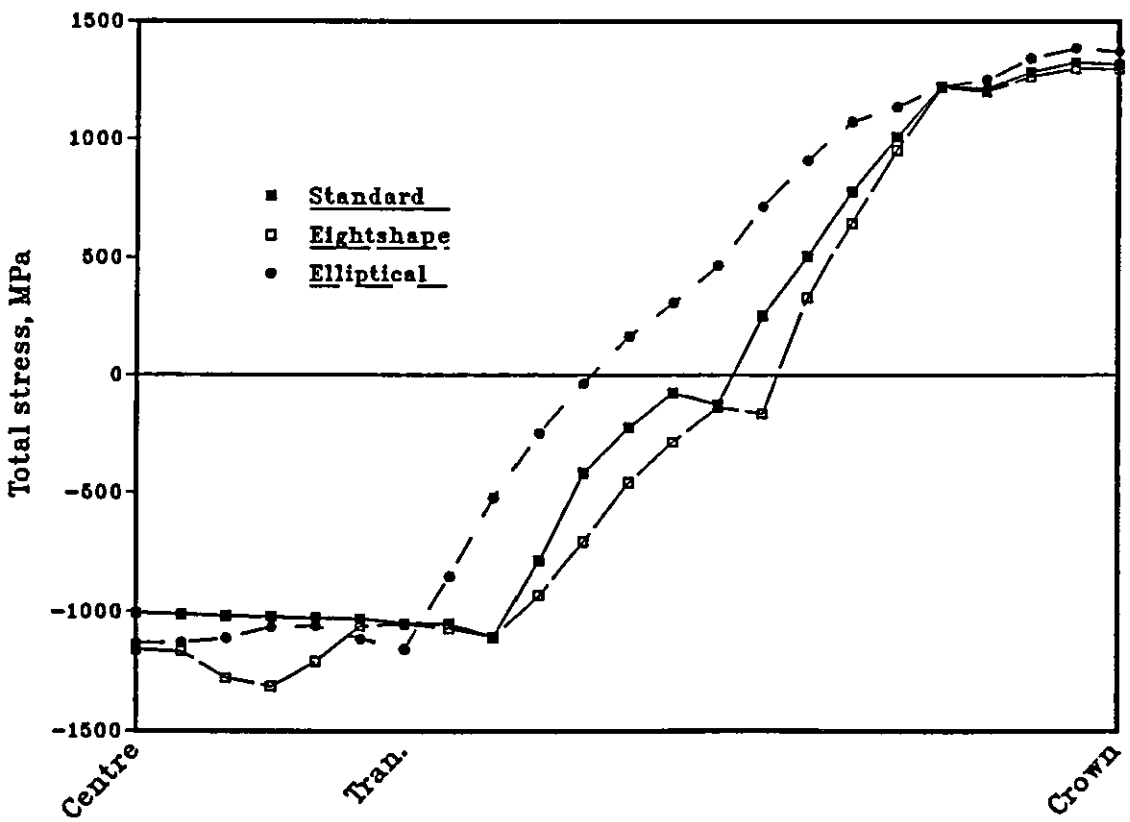

Fig. 8.14 Effect of link geometry on the total stresses at the outside of the 19 mm mining chain under catibration load of 320 kN.

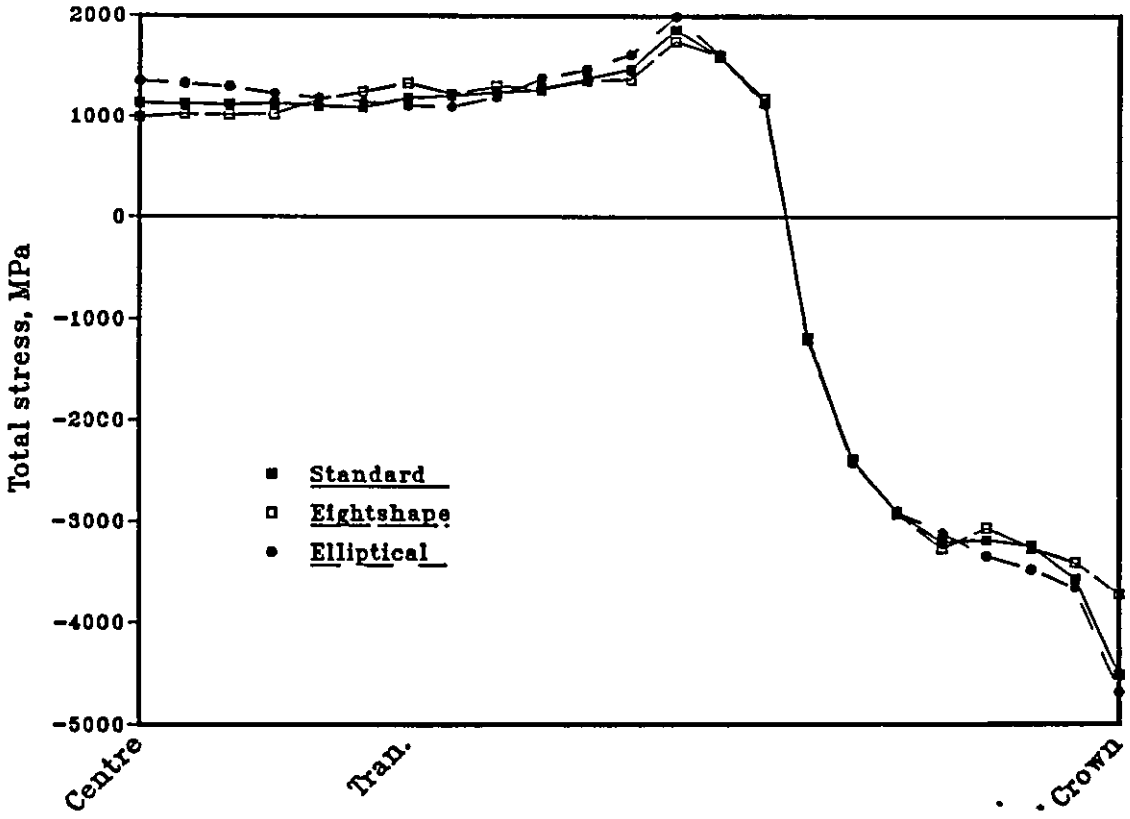

Fig. 8.15 Effect of link geometry on the total stresses at inside of the 19 mm mining chain under calibartion load of 320 kN.

Geometry	Number of increments	FE Failure load, kN	Exp. failure load, kN
Standard	28	466	497
Eight shape	27	467	510
Elliptical	19	479	476

Table 8.2 Comparison of failure load for various link geometries from the FE beam analysis and experiments.

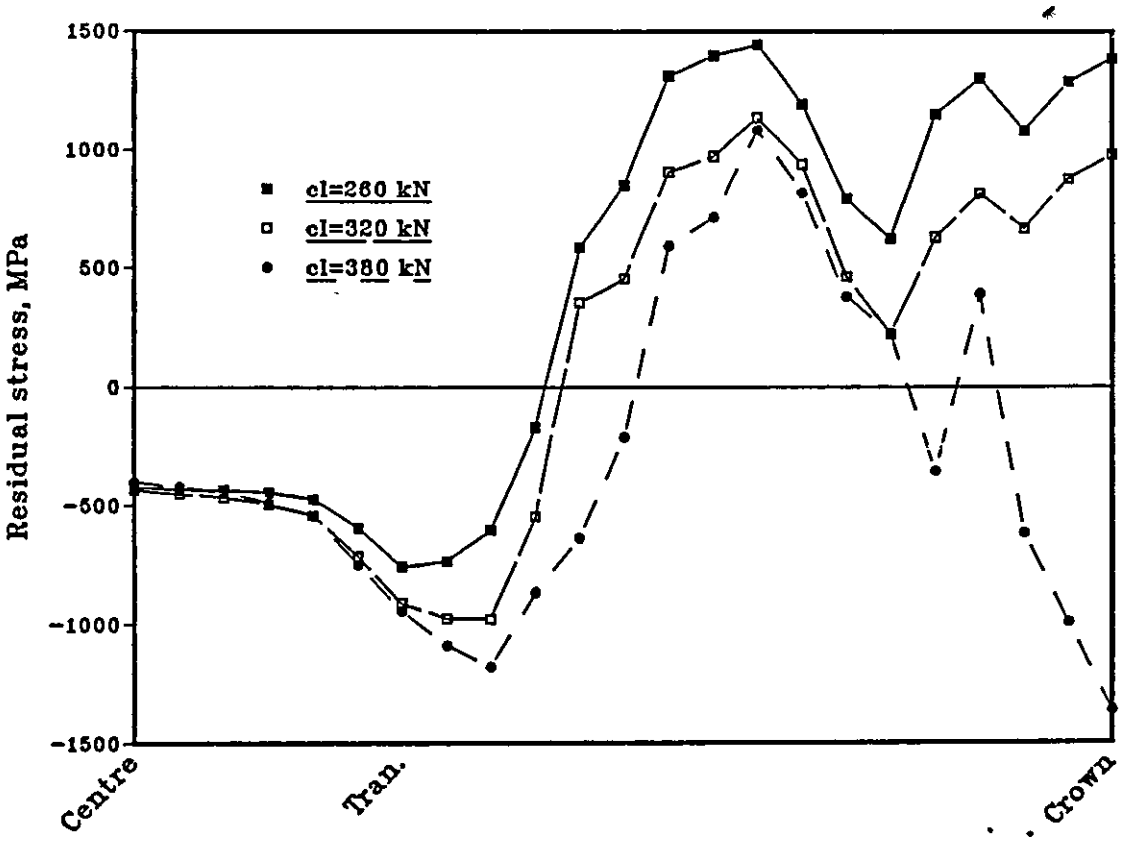

Fig. 8.16 Effect of increase in calibration load on the residual stresses at the inside of the 19 mm standard mining chain.

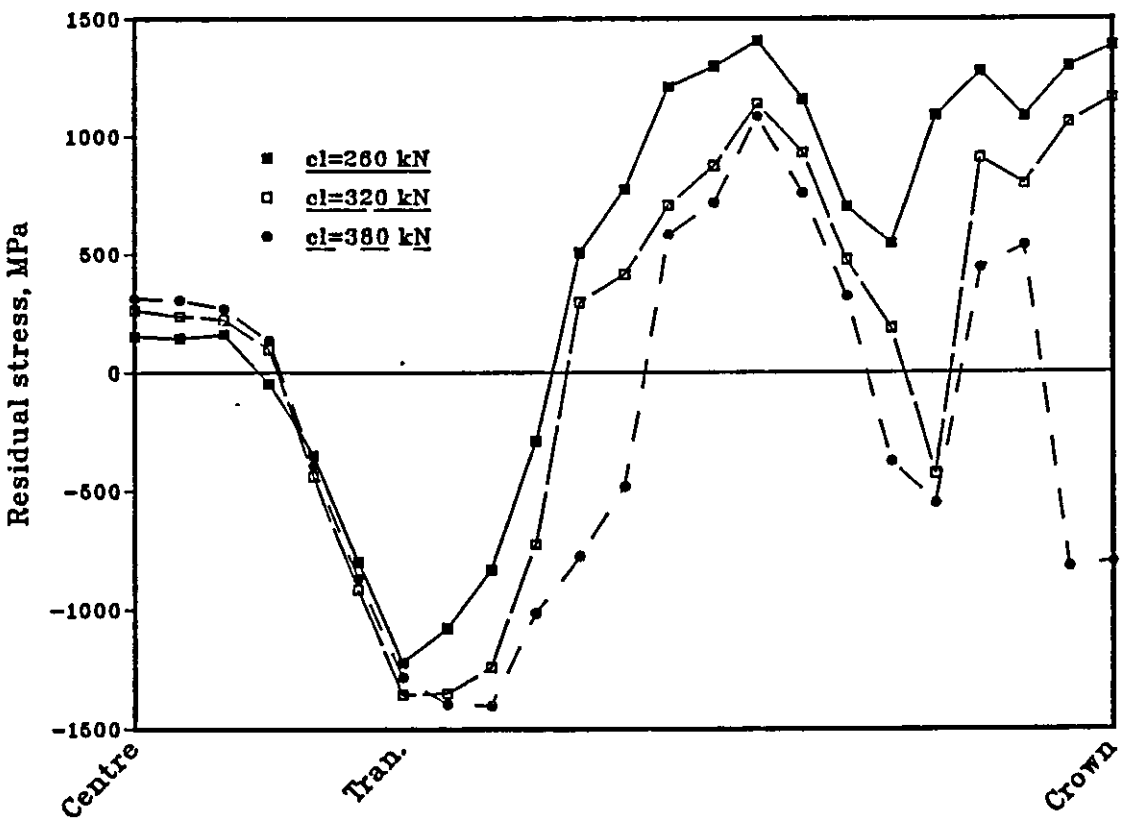

Fig. 8.17 Effect of increase in calibration load on the residual stresses at the inside of the 19 mm eight shape mining chain.

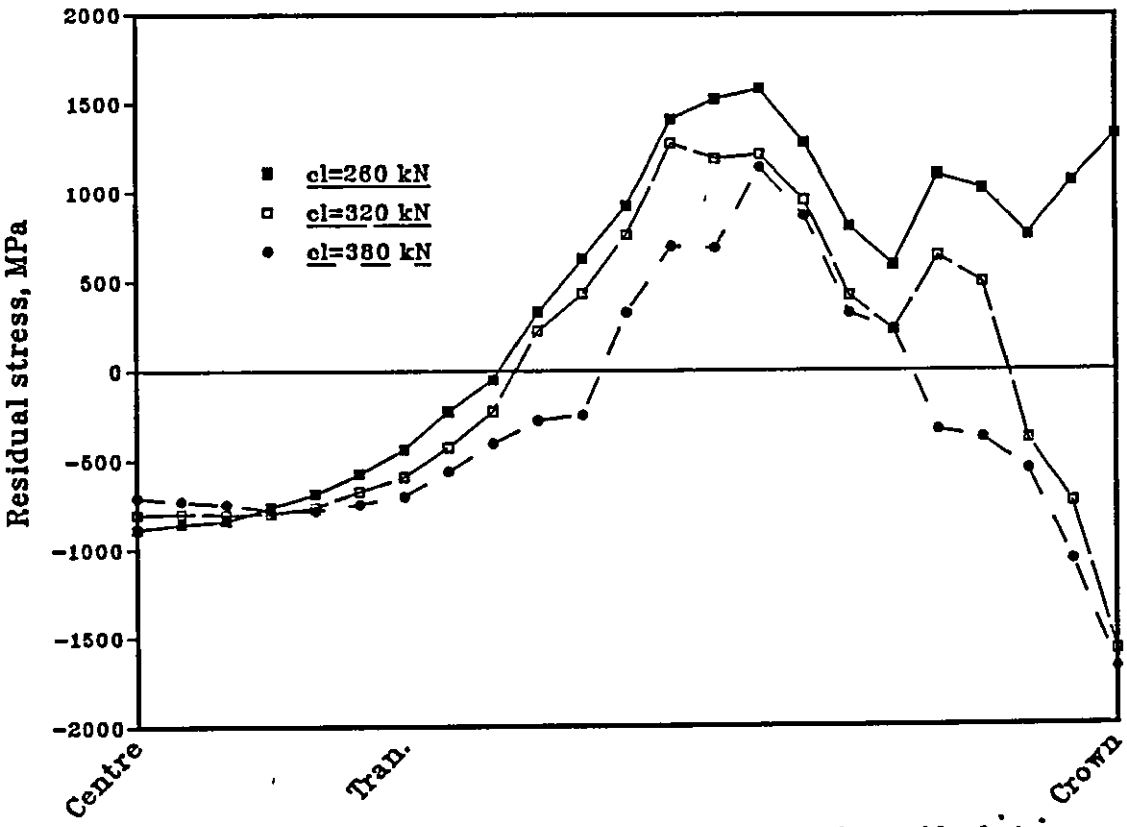

Fig. 8.18 Effect of increase in calibration load on the residual stresses at the inside of the 19 mm elliptical mining chain.

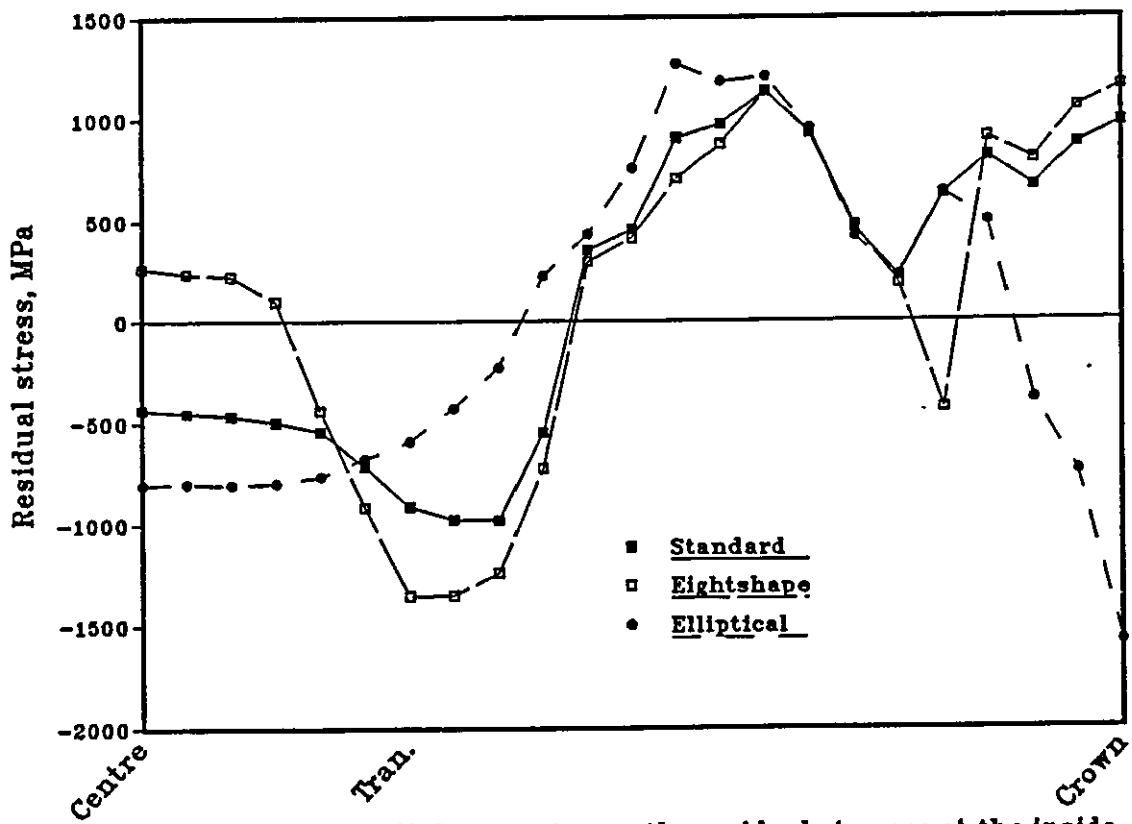

Fig. 8.19 Effect of link geometry on the residual stresses at the inside of the 19 mm mining chain under calibration load of 320 kN.

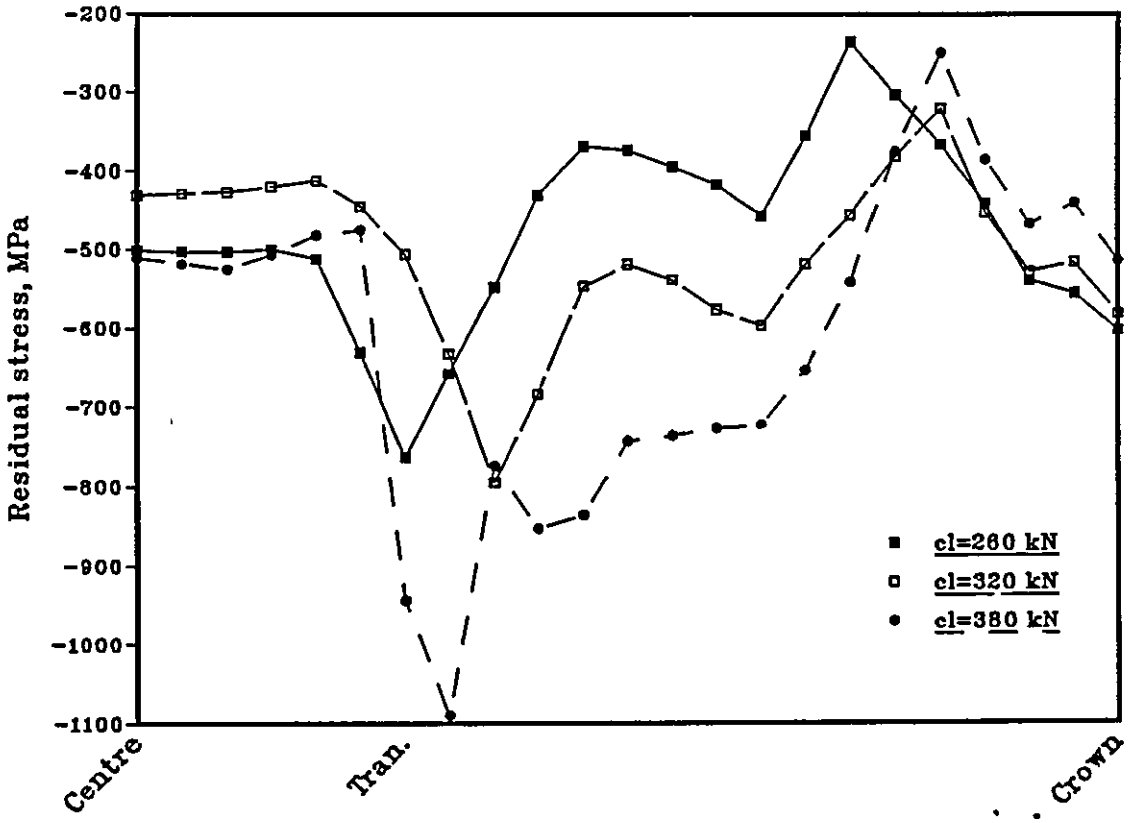

Fig. 8.20 Effect of increase in calibration load on the residual stresses at the outside of the 19 mm standard mining chain.

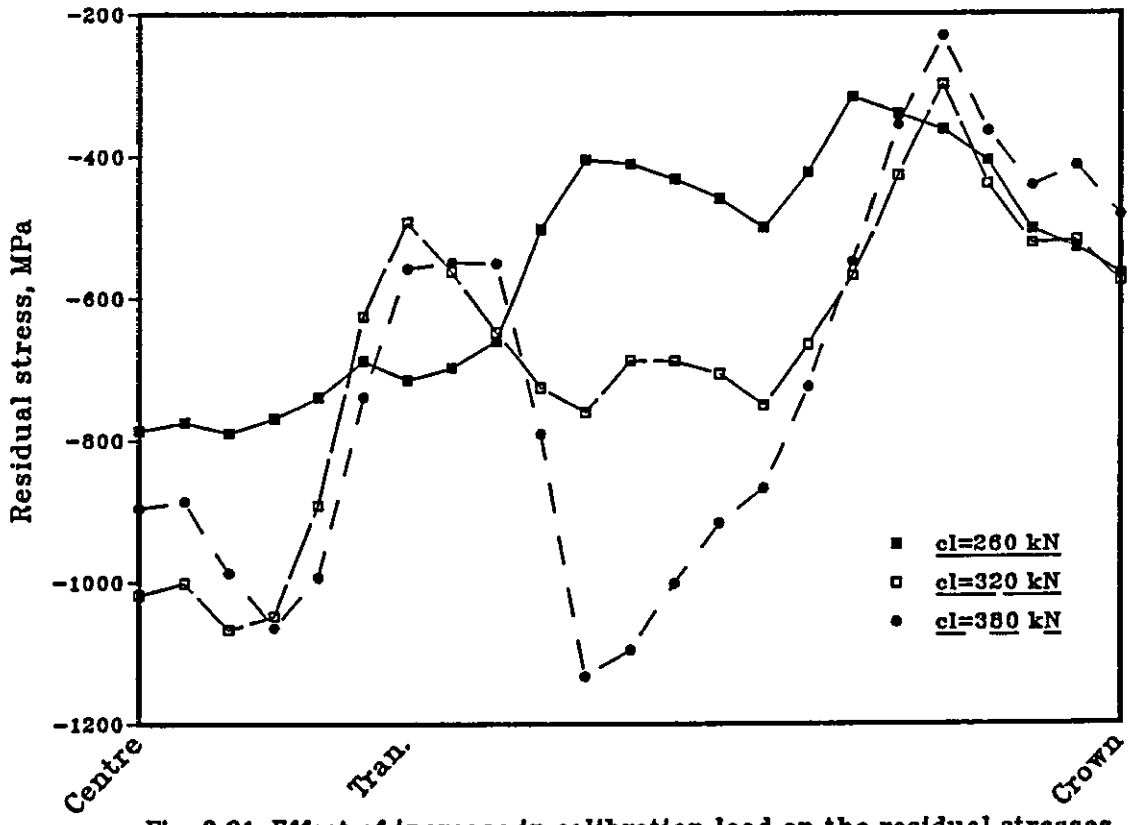

Fig. 8.21 Effect of increase in calibration load on the residual stresses at the outside of the 19 mm eight shape mining chain.

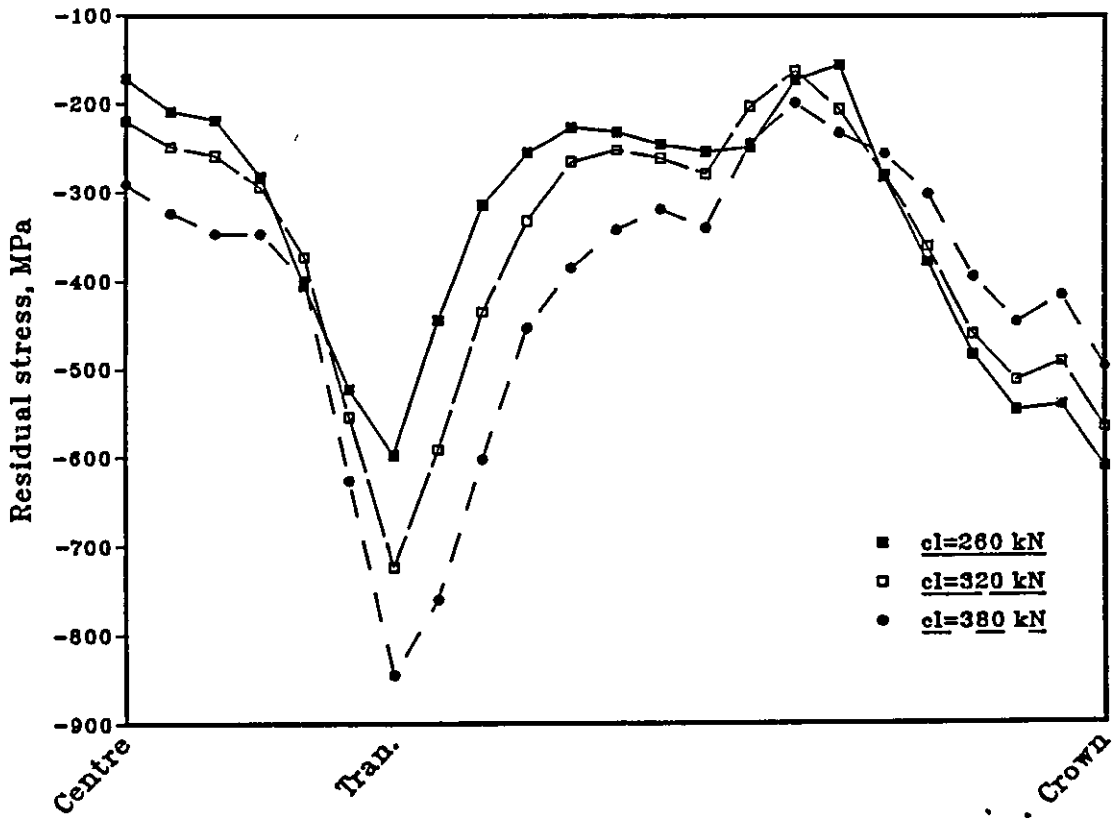

Fig. 8.22 Effect of increase in calibration load on the residual stresses at the outside of the 19 mm elliptical mining chain.

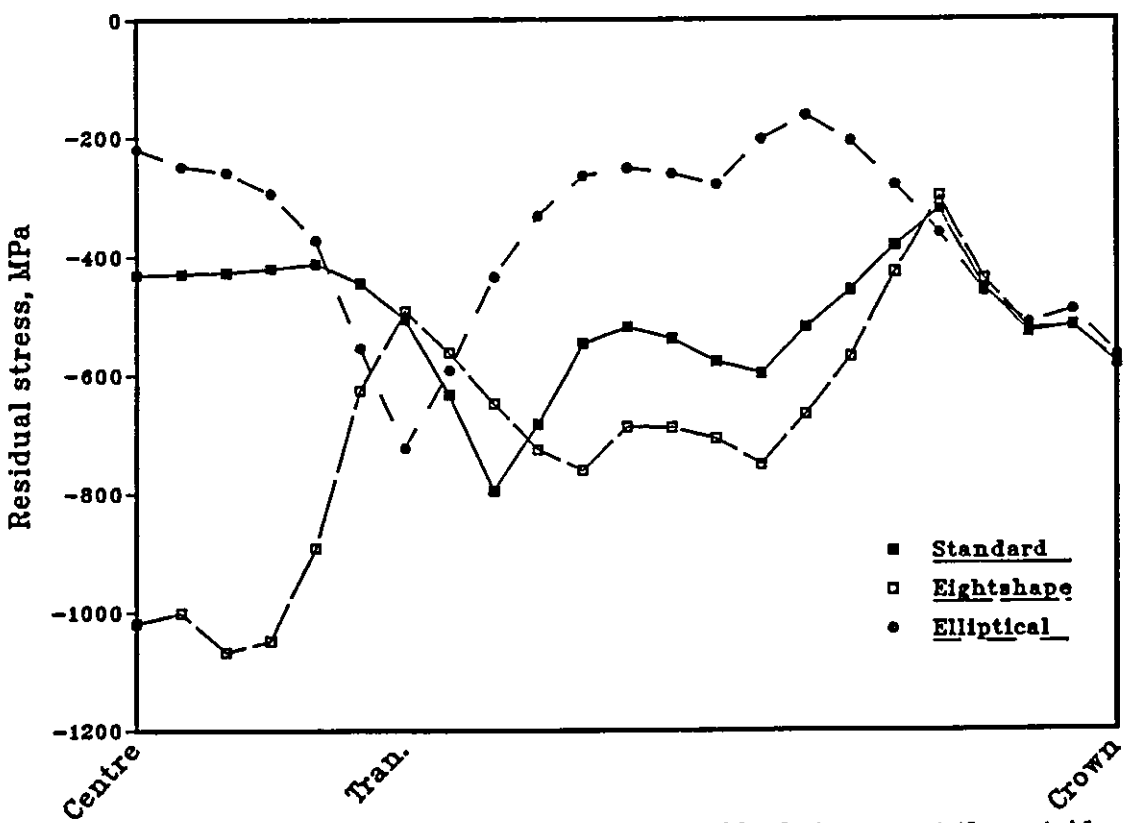

Fig 8.23 Effect of link geometry on the residual stresses at the outside of the 19 mm mining chain under calibration load of 320 kN.

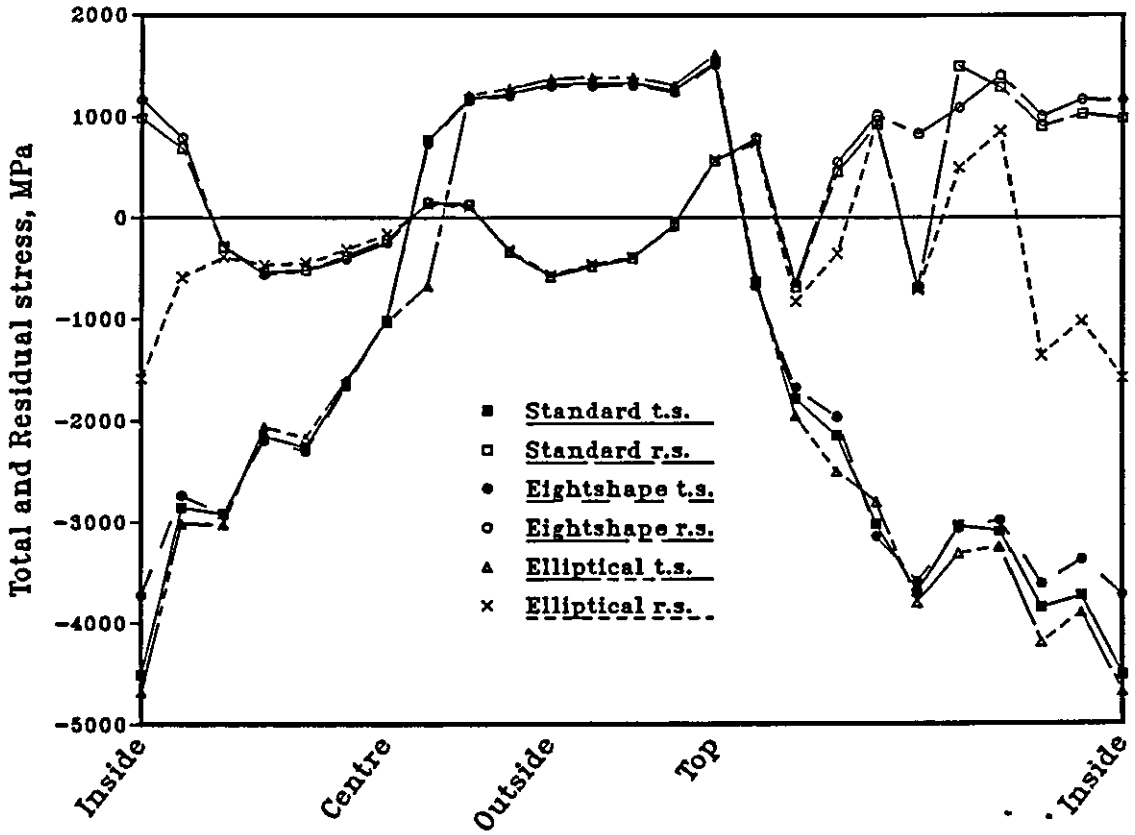

Fig. 8.24 Effect of link geometry on the stresses (total and residual) at the crown of the 19 mm mining chain under calibration load of 320 kN.

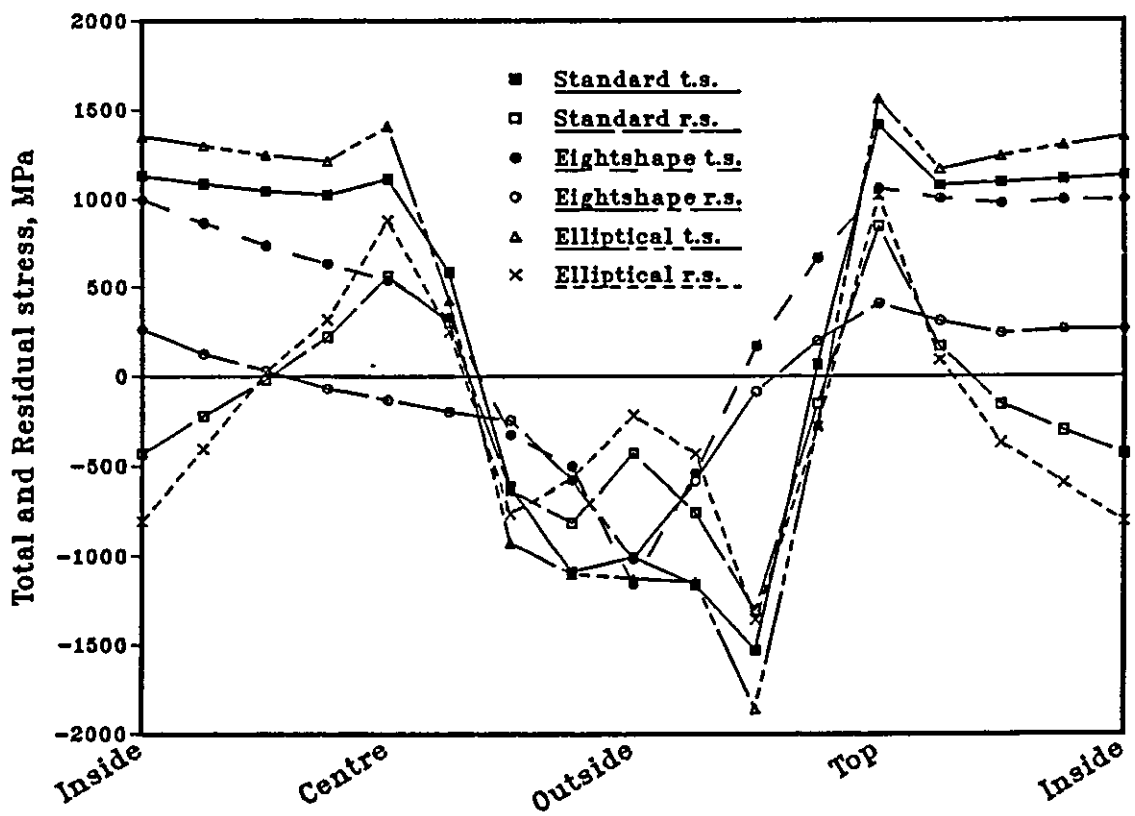

Fig. 8.25 Effect of link geometry on the stresses (total and residual) at the centre of the 19 mm mining chain under calibration load of 320 kN.

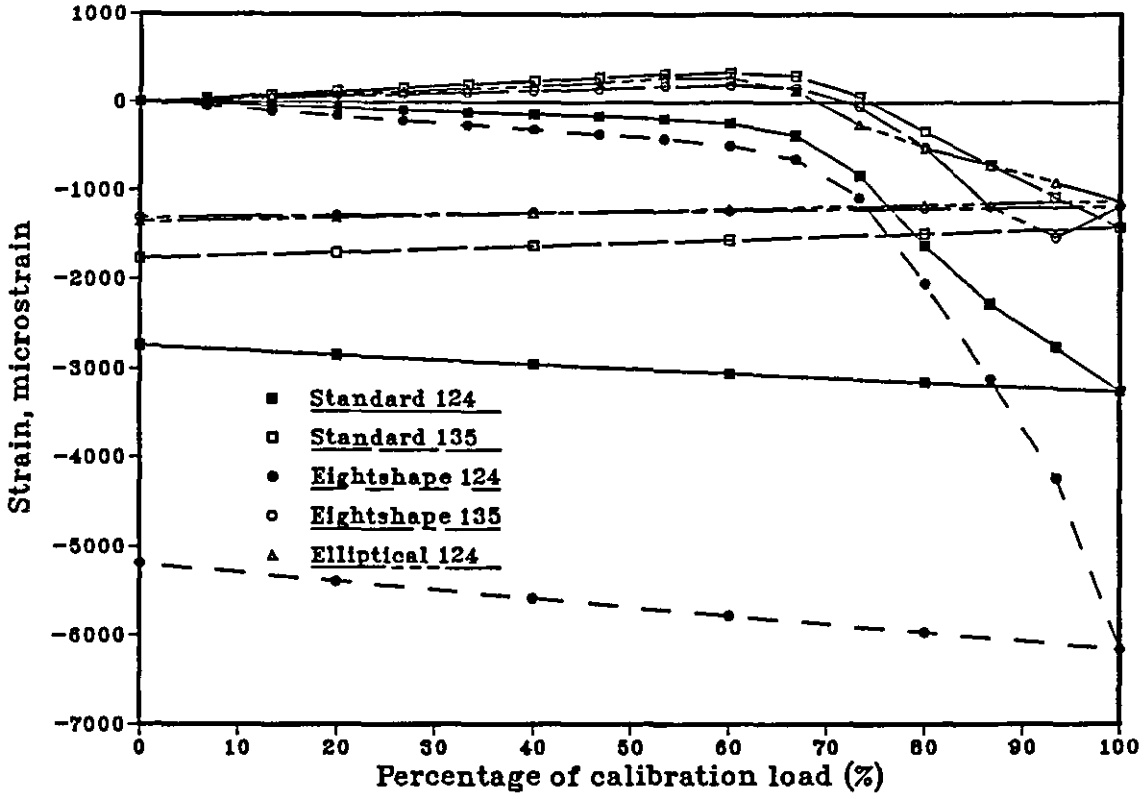

Fig. 8.26 Effect of loading–unloading cycle on the strains corresponding to the positions of the strain gauges no 3 and 10 for the 19 mm mining chain with different link geometry under calibration load of 320 kN.

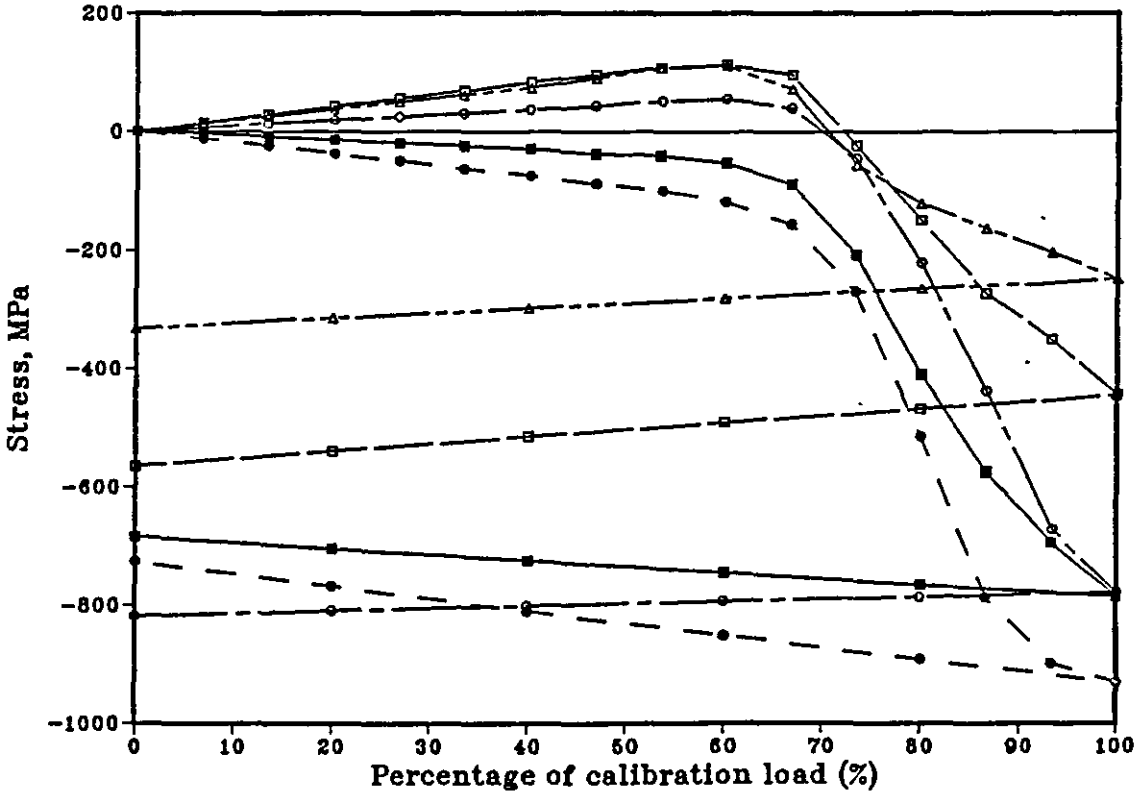

Fig. 8.27 Effect of loading–unloading cycle on the stresses corresponding to the positions of the strain gauges no 3 and 10 for the 19 mm mining chain with different link geometry under calibration load of 320 kN.

TITLE OVAL-SECTION 13.5 9.0 19.75 3.0 3 2 54.5 36.33

PAFEC

VIEW FROM X = 1.000
Y = 0.5672
Z = 1.666

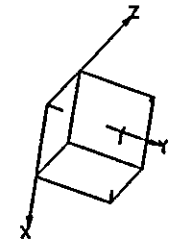

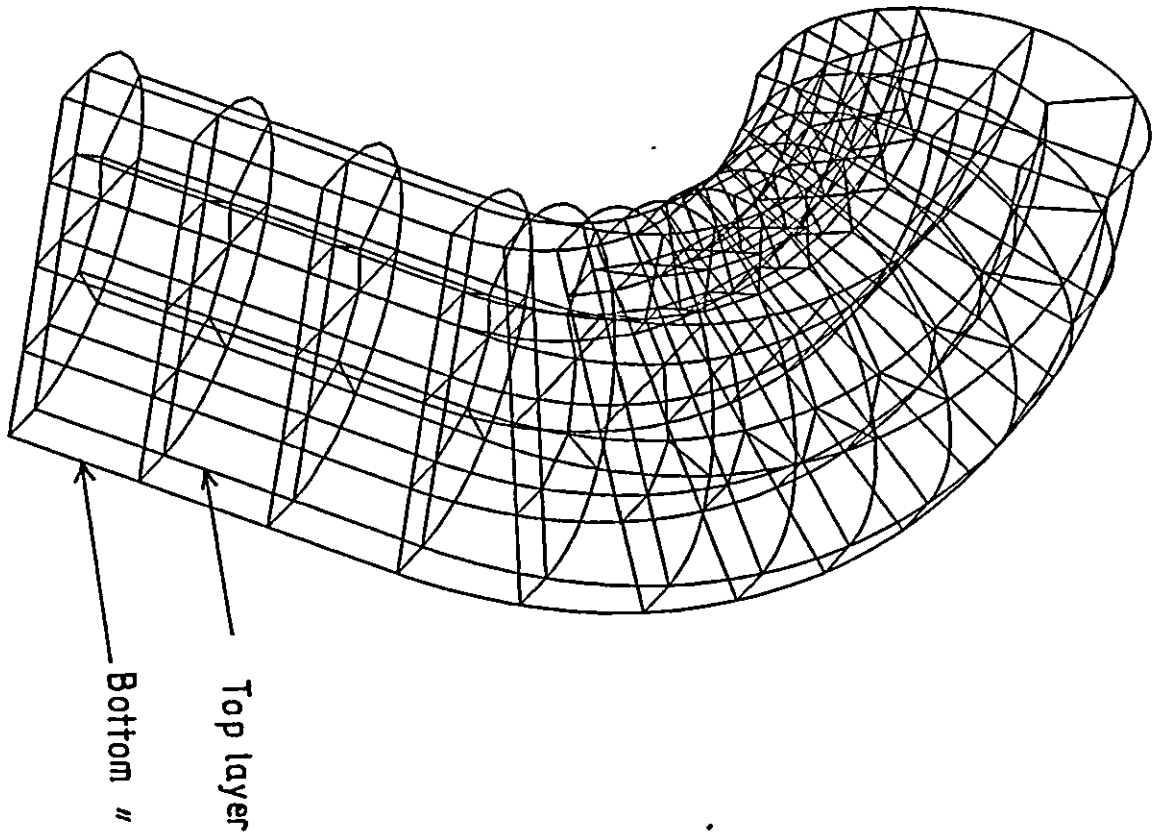

290

WHOLE STRUCTURE DRAWN

PRODUCED BY PAFWOR
ON 13/04/89 AT 2317 HOURS

Fig. 8.28 FE mesh of oval-link chain.

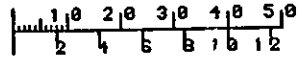

DRAWING NO. 1
SCALE = .01000 E+2 :1
DRAWING TYPE= 2

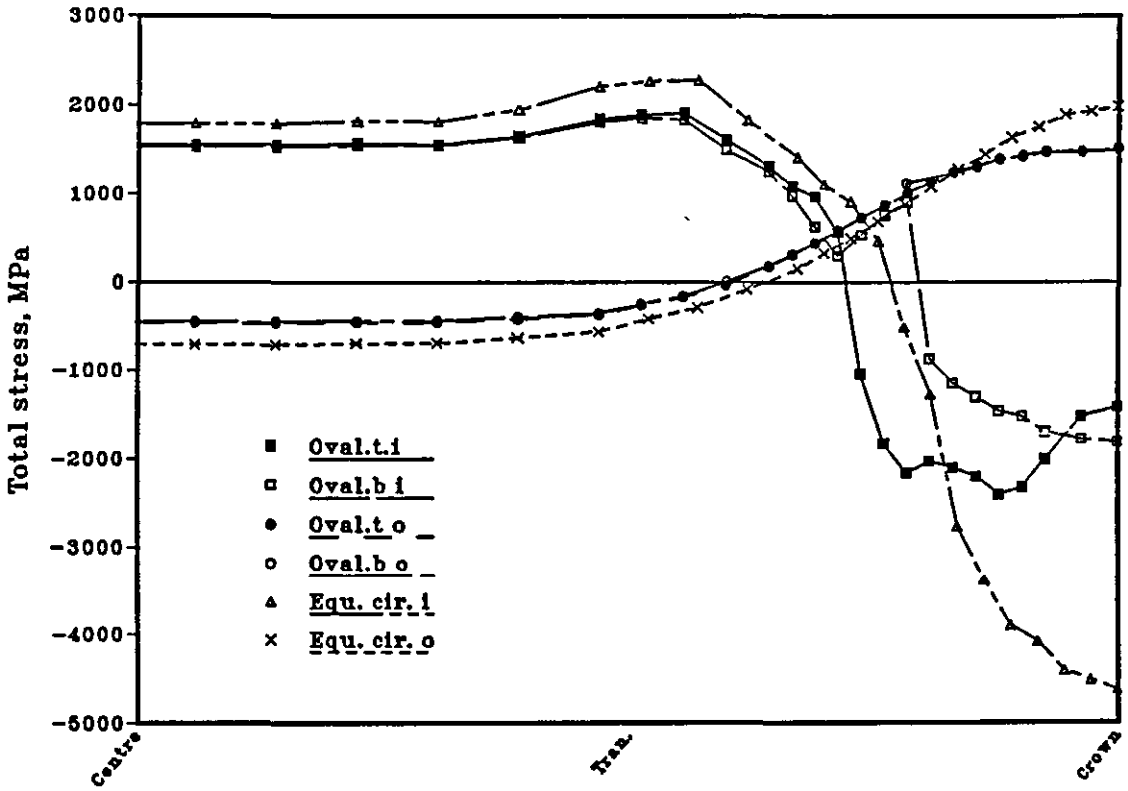

Fig. 8.29 Total stresses of the oval-link and equivalent circular cross section mining chains at the inside and outside under calibration load of 393 kN for elastic analysis (mid-plane, .b and its parallel plane, t.).

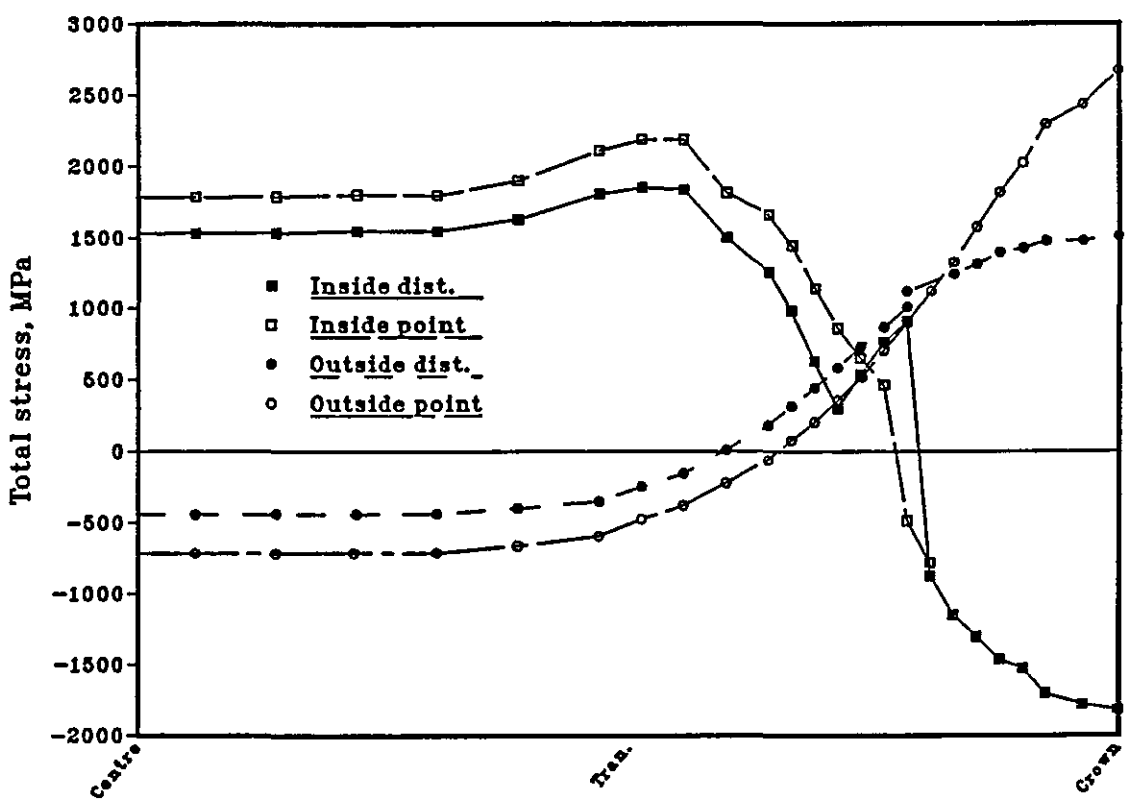

Fig 8.30 Effect of point and distributed load on the total stresses of the oval-link mining chains at the inside and outside under calibration load of 393 kN for elastic analysis.

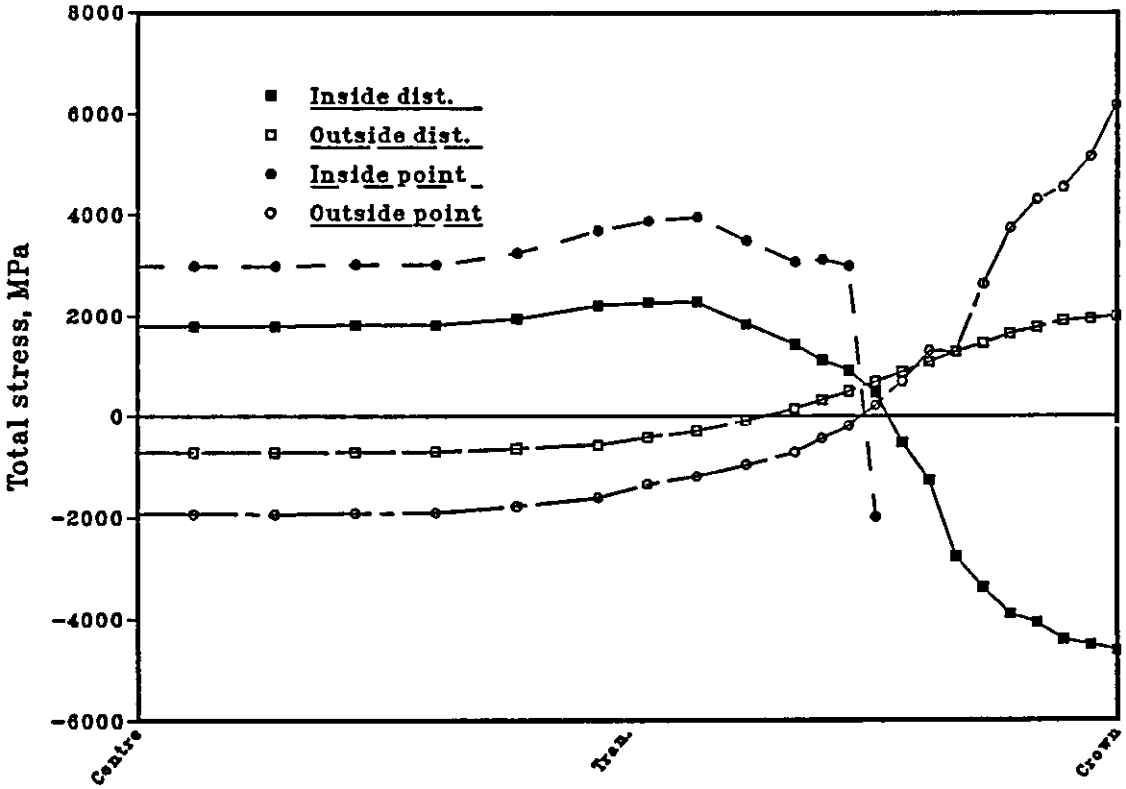

Fig 8.31 Effect of point and distributed load on the total stresses of the equivalent circular cross-section mining chain at the inside and outside under calibration load of 393 kN for elastic analysis.

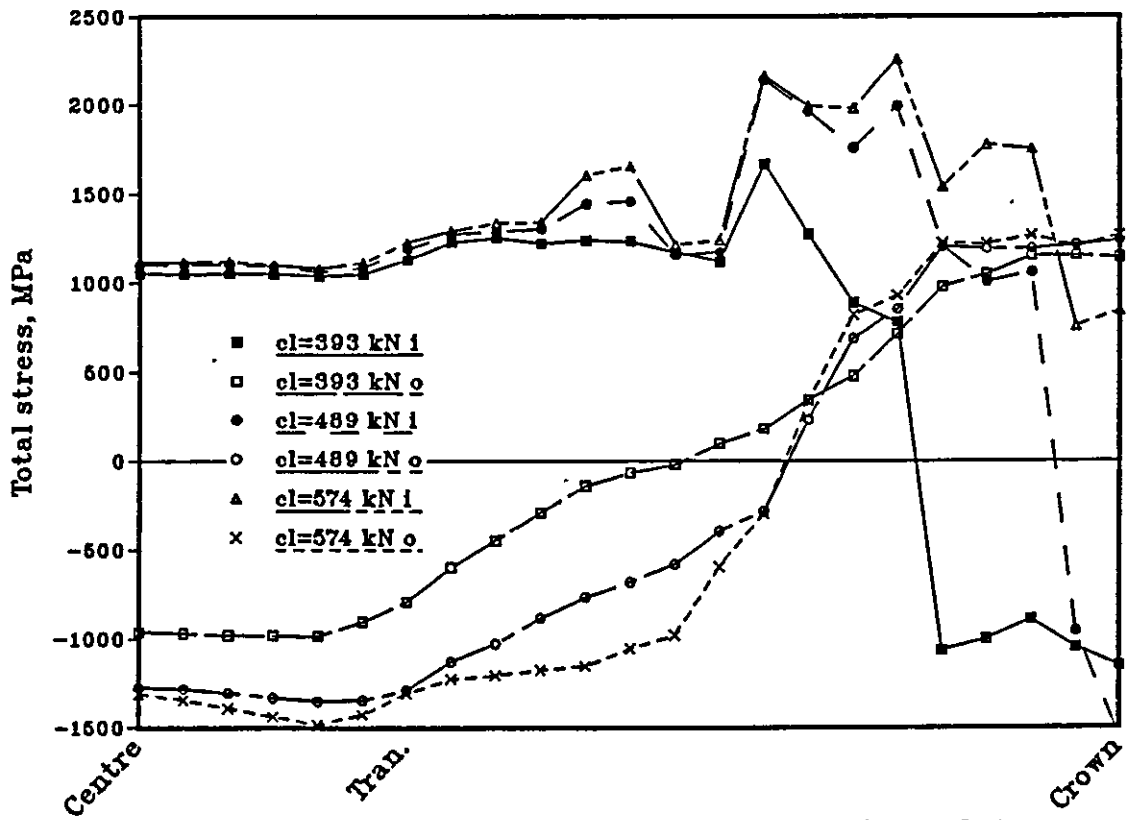

Fig. 8.32 Effect of increase in calibration load on the total stresses of the oval-link mining chain at the inside and outside.

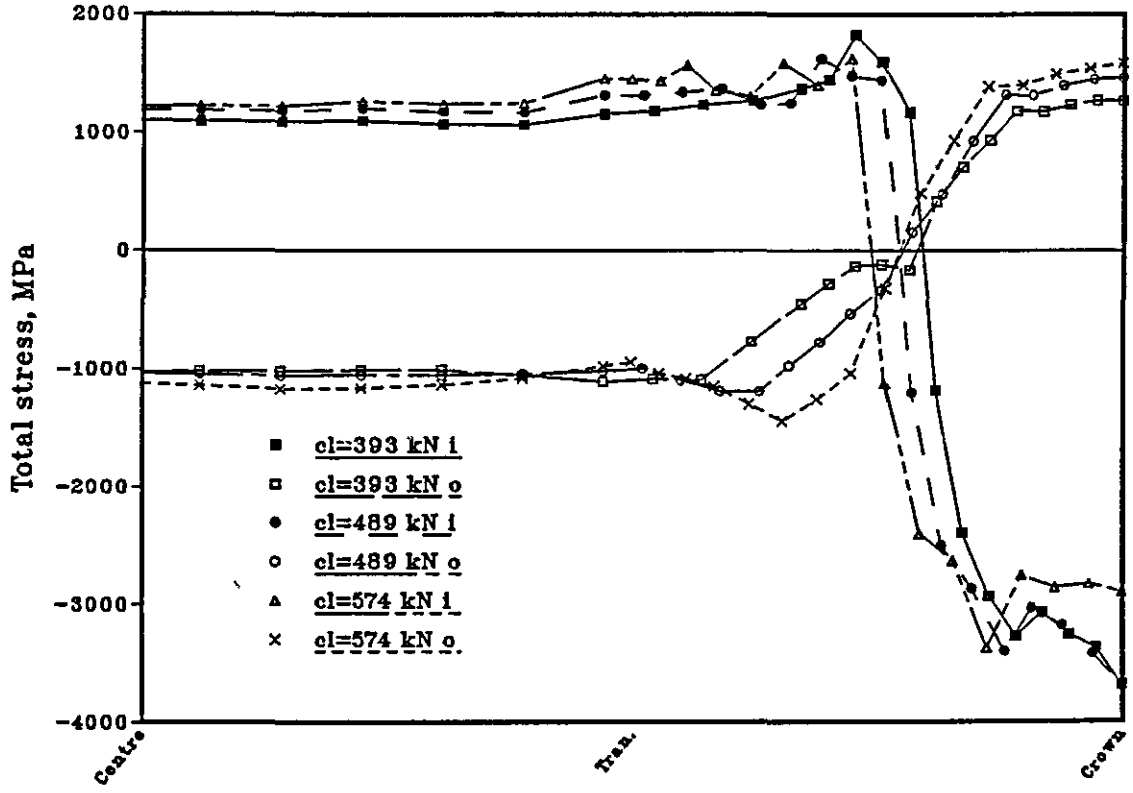

Fig. 8.33 Effect of increase in calibration load on the total stresses of the equivalent circular cross-section mining chain at the inside and outside.

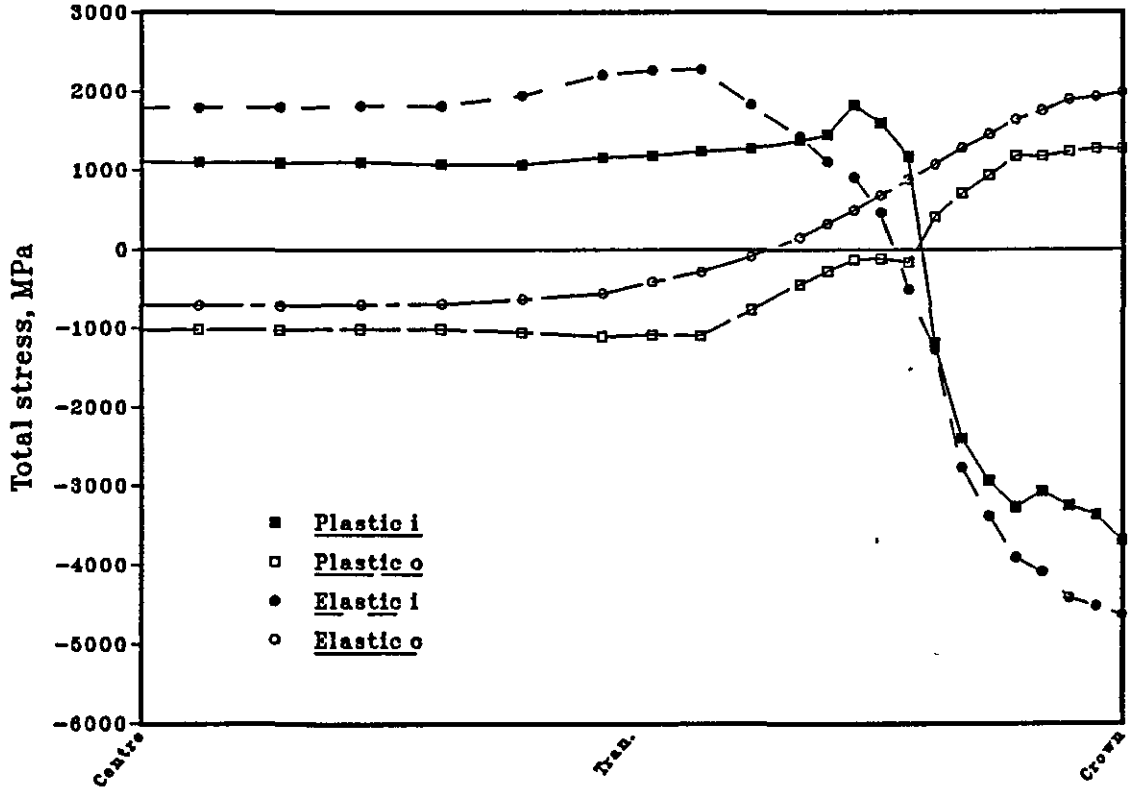

Fig. 8.34 Effect of elastic and elasto-plastic analysis on the total stresses of the equivalent circular cross-section mining chain at the inside and outside under calibration load of 489 kN.

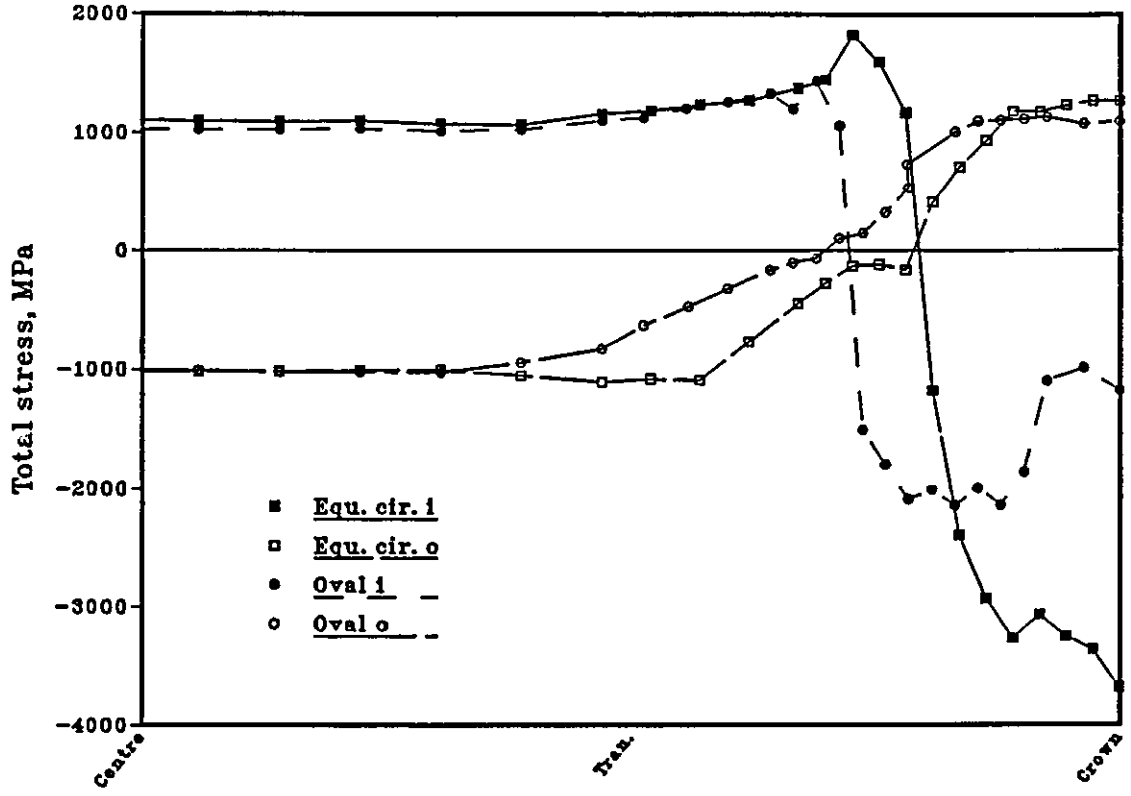

Fig. 8.35 Comparison of total stresses of the oval-link and equivalent circular cross-section mining chain at the inside and outside under calibration load of 393 kN.

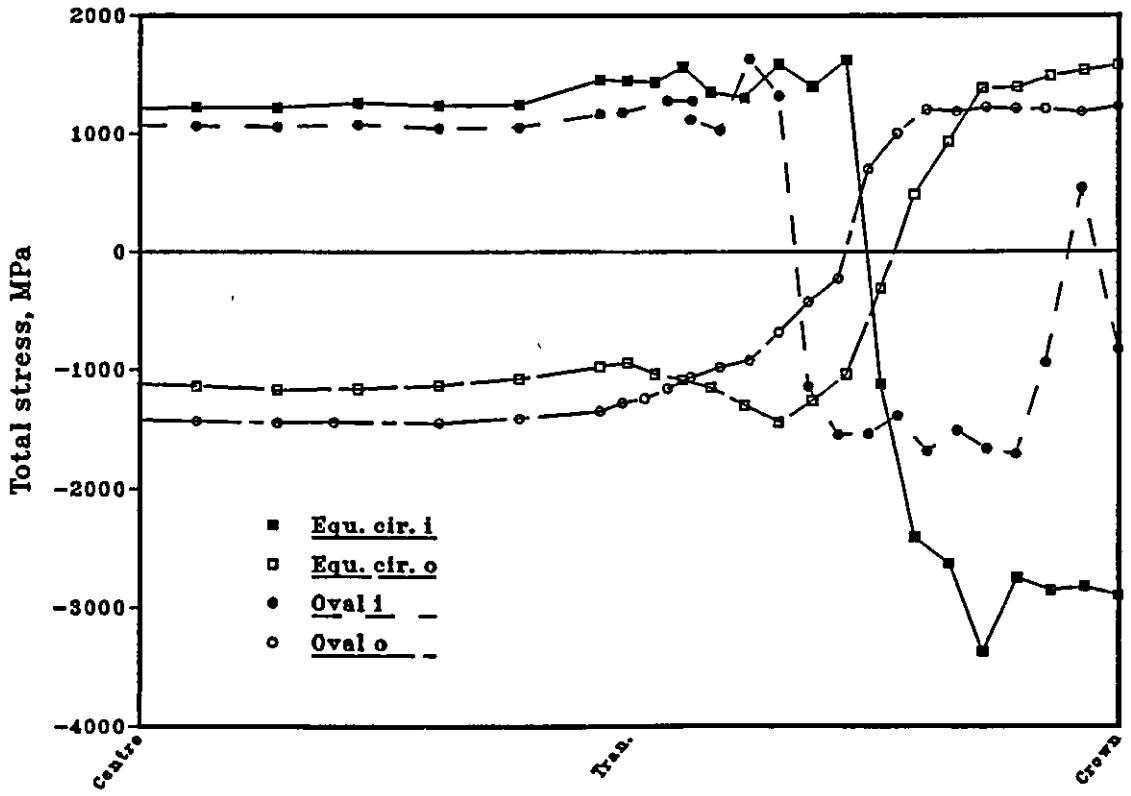

Fig. 8.36 Comparision of total stresses of the oval-link and equivalent circular cross-section mining chains at the inside and outside under the failure loads (546 and 565 kN respectively).

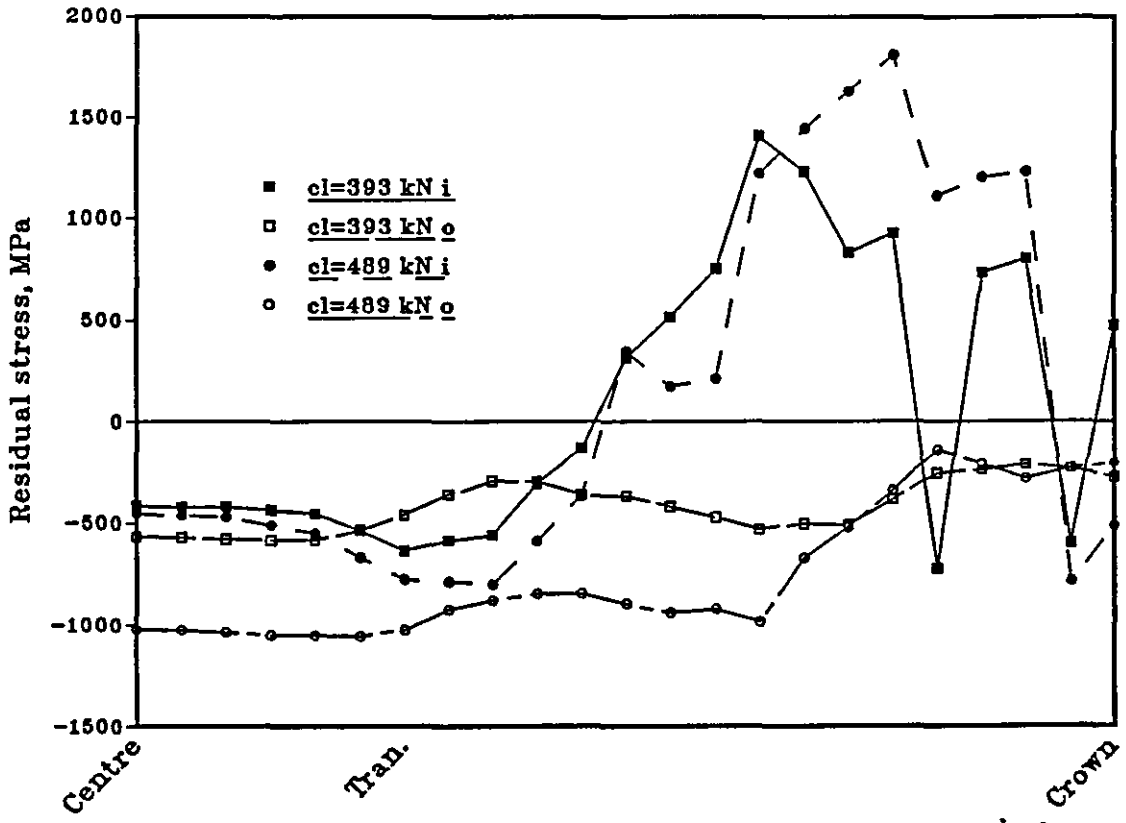

Fig. 8.37 Effect of increase in calibration load on the residual stresses of the oval-link mining chain at the inside and outside.

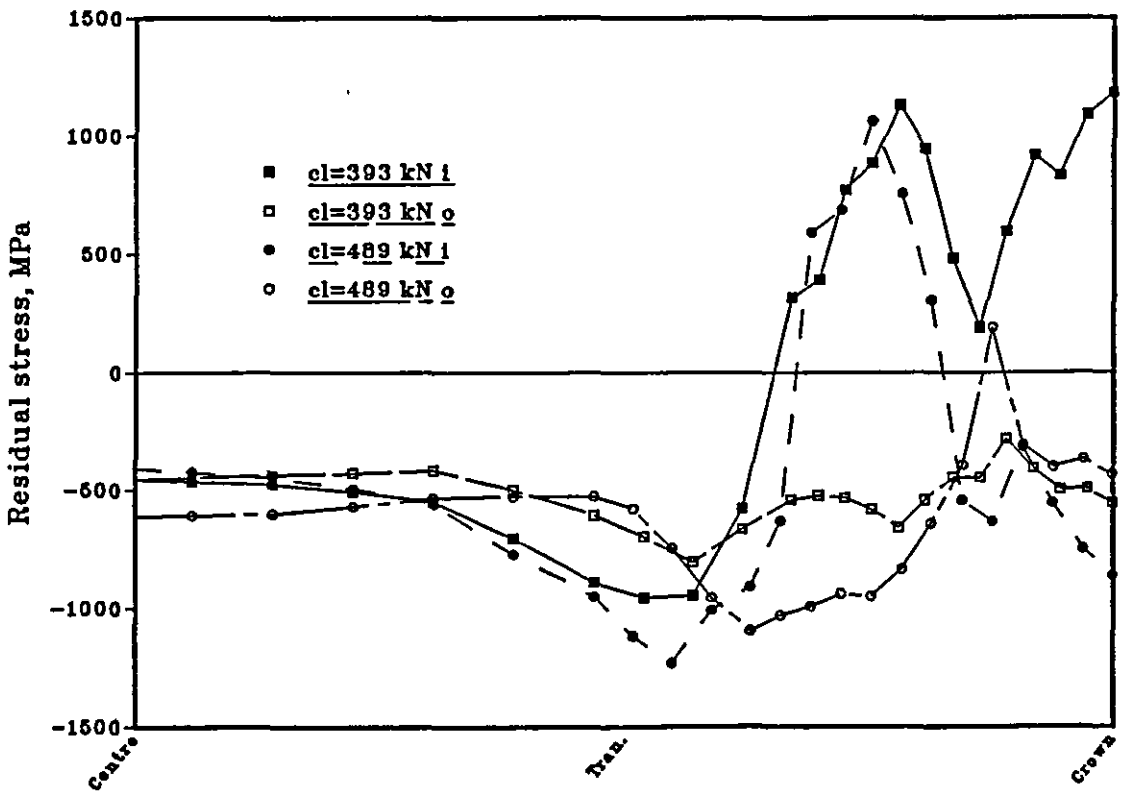

Fig 8.38 Effect of increase in calibration load on the residual stresses of the equivalent circular cross-section mining chain at the inside and outside.

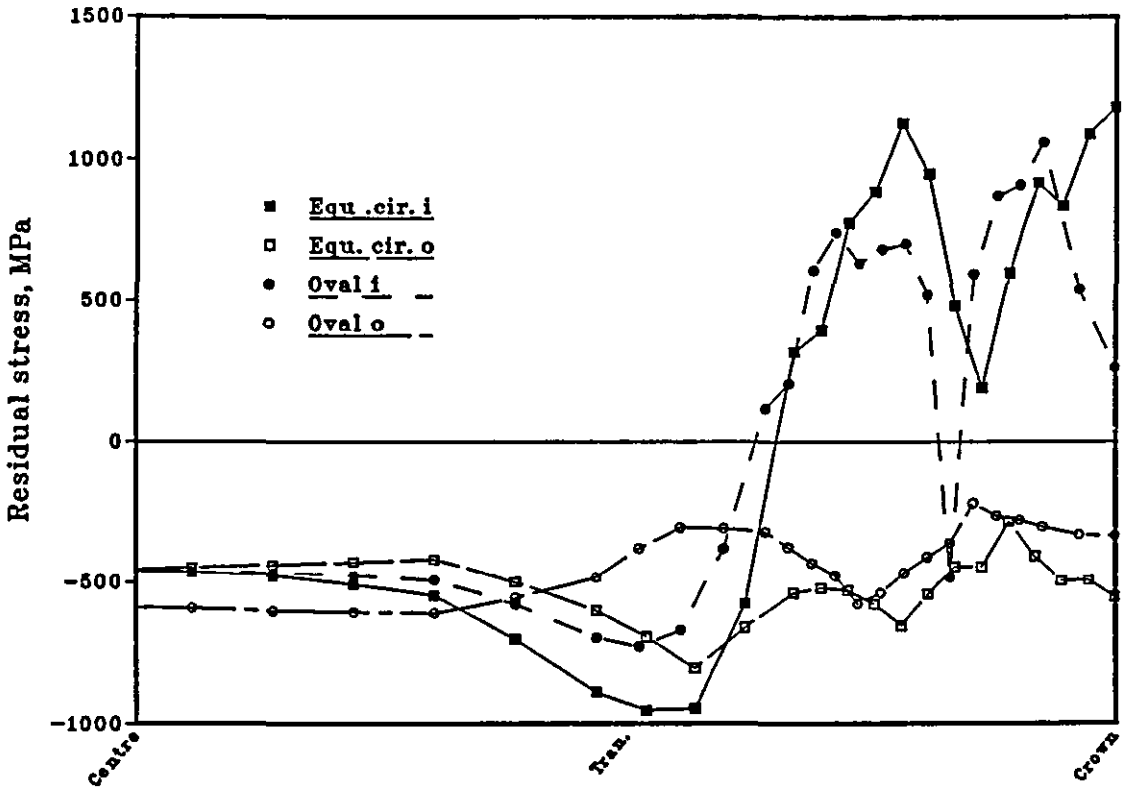

Fig. 8.39 Residual stresses of the oval-link and equivalent circular cross-section mining chains at the inside and outside for the calibration load of 393 kN.

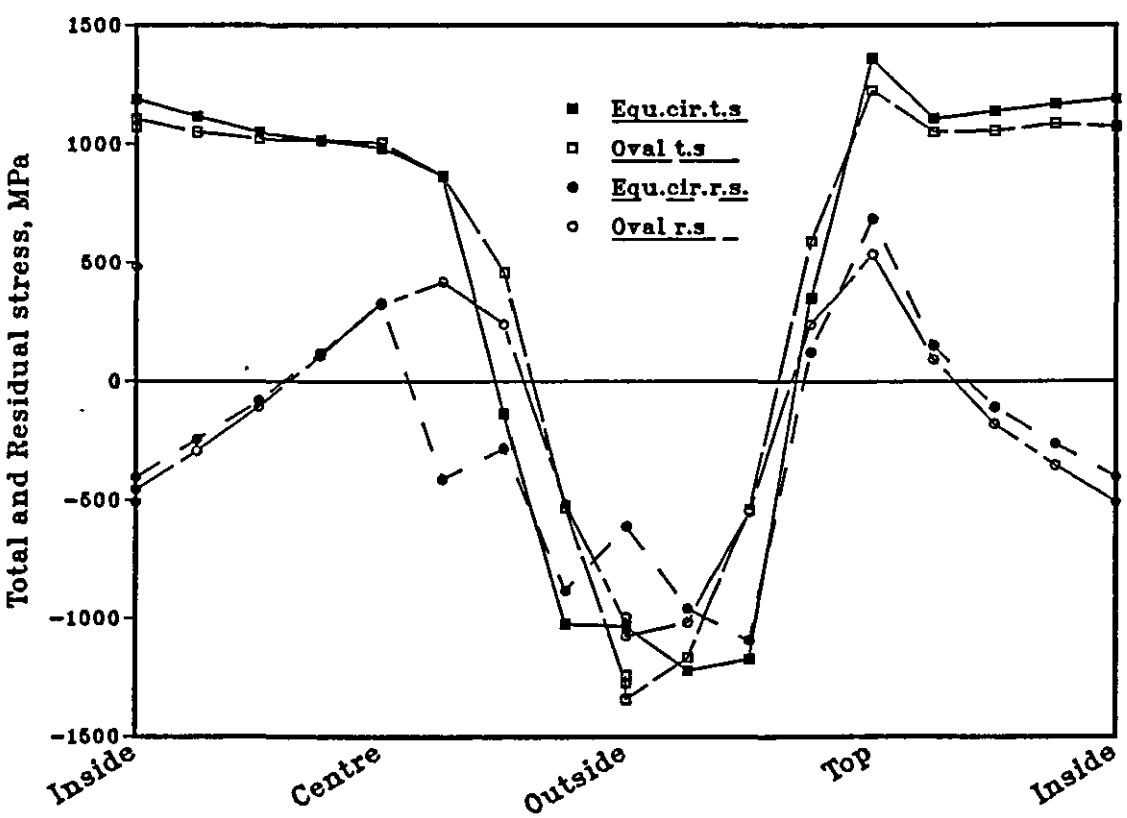

Fig. 8.40 Total and residual stresses of the oval-link and equivalent circular cross-section mining chain at the cross-section through the centre under calibration load of 489 kN.

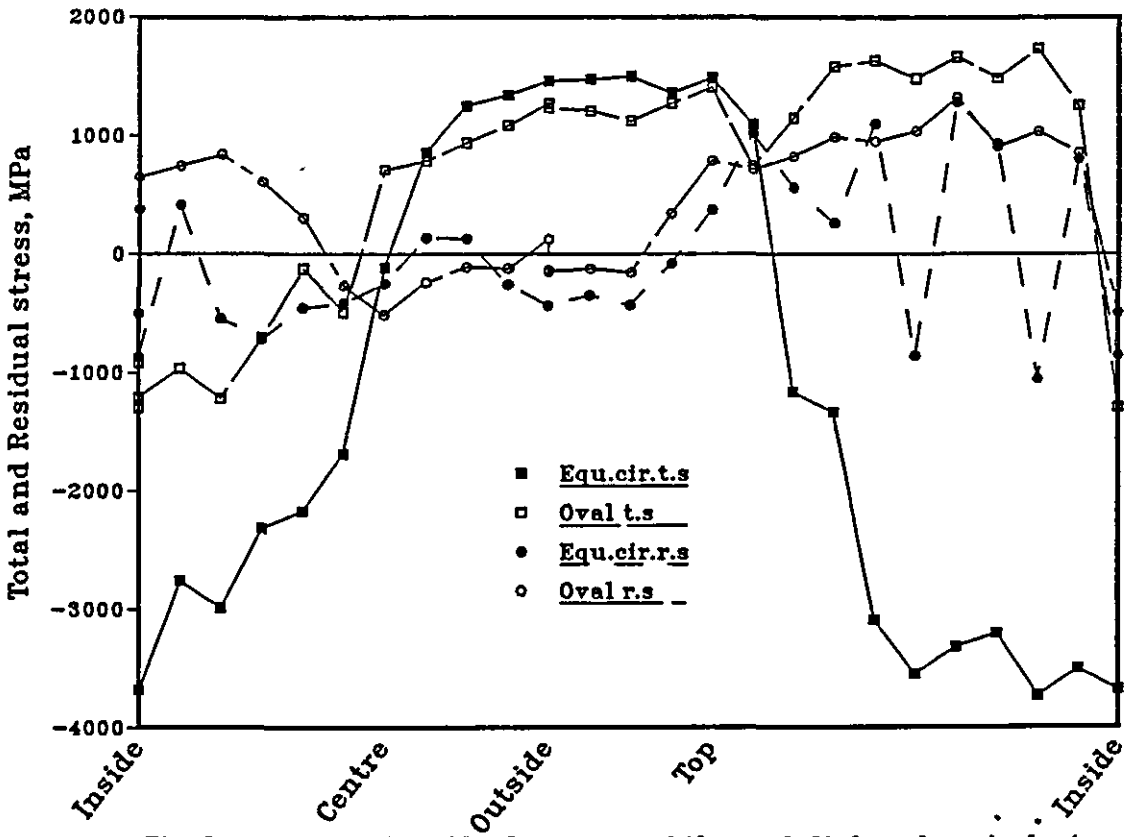

Fig. 8.41 Total and residual stresses of the oval-link and equivalent circular cross-section mining chain at the cross-section through the crown under calibration load of 489 kN.

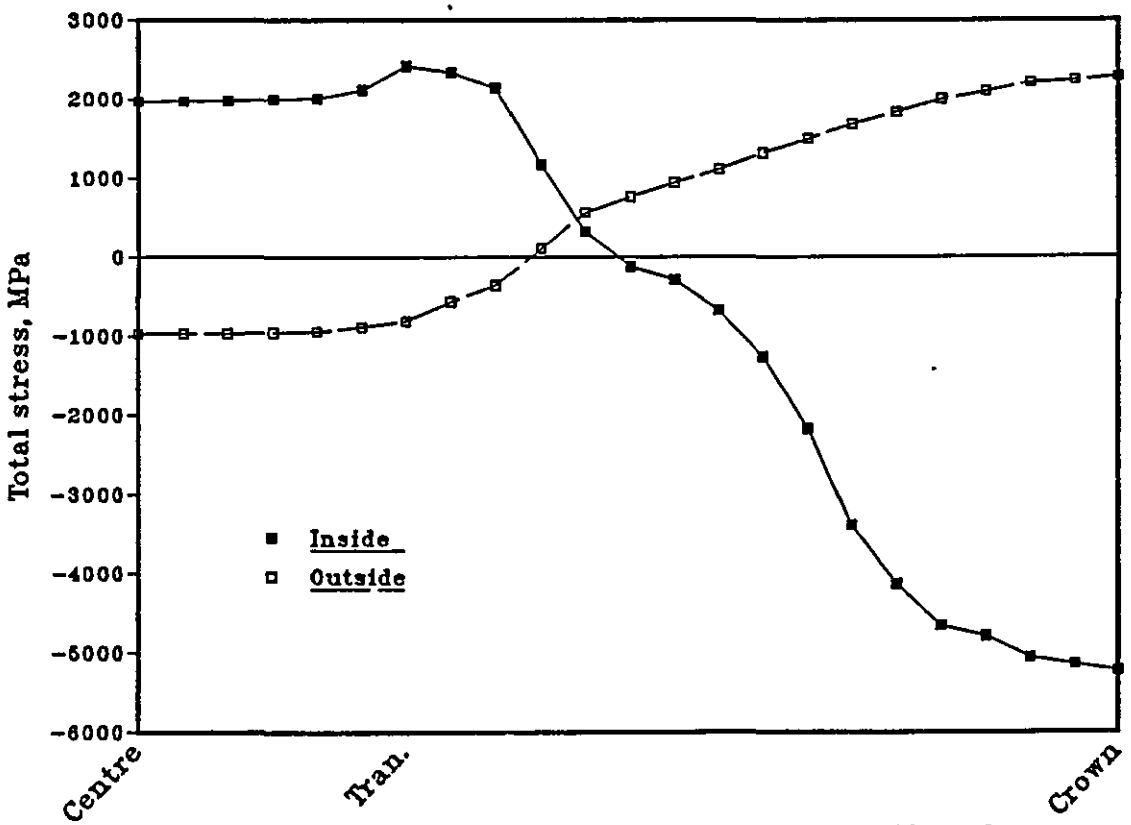

Fig. 8.42 Total stresses of the lifting chain at the inside and outside under calibration load of 38.5 kN for elastic analysis.

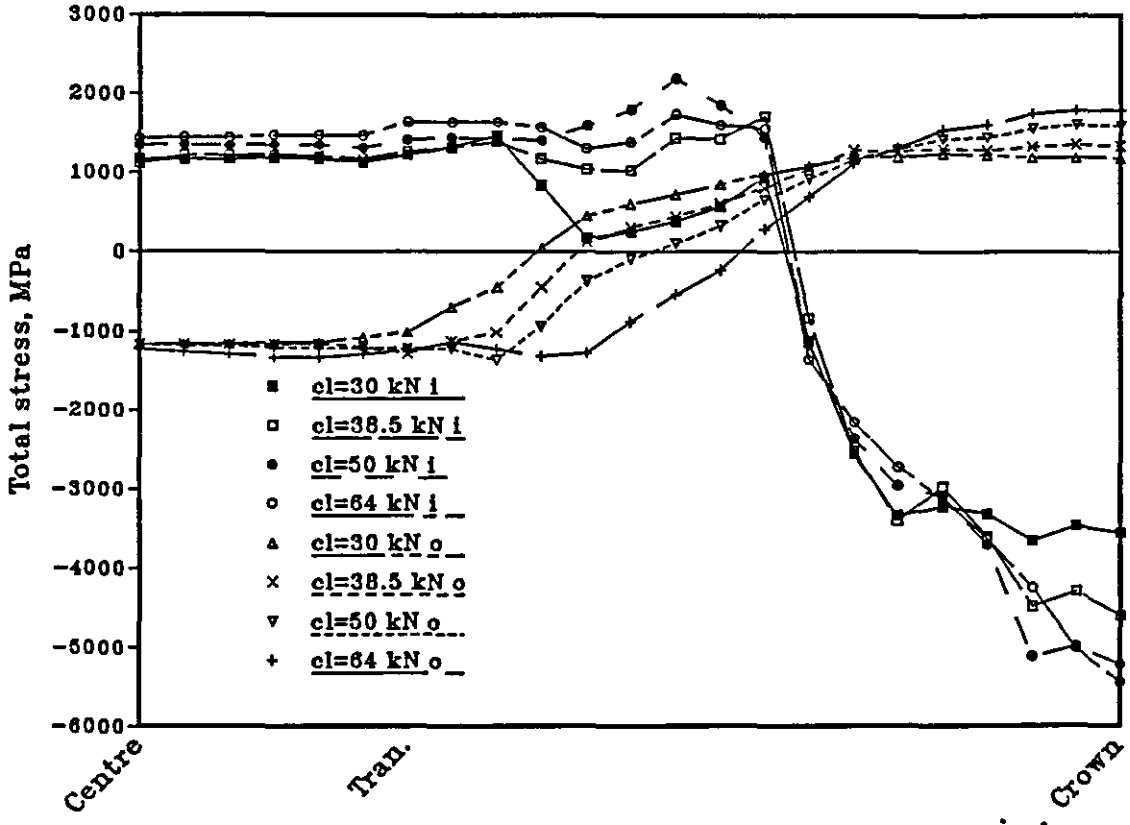

Fig. 8.43 Total stresses of the lifting chain at the inside and outside under increasing calibation load.

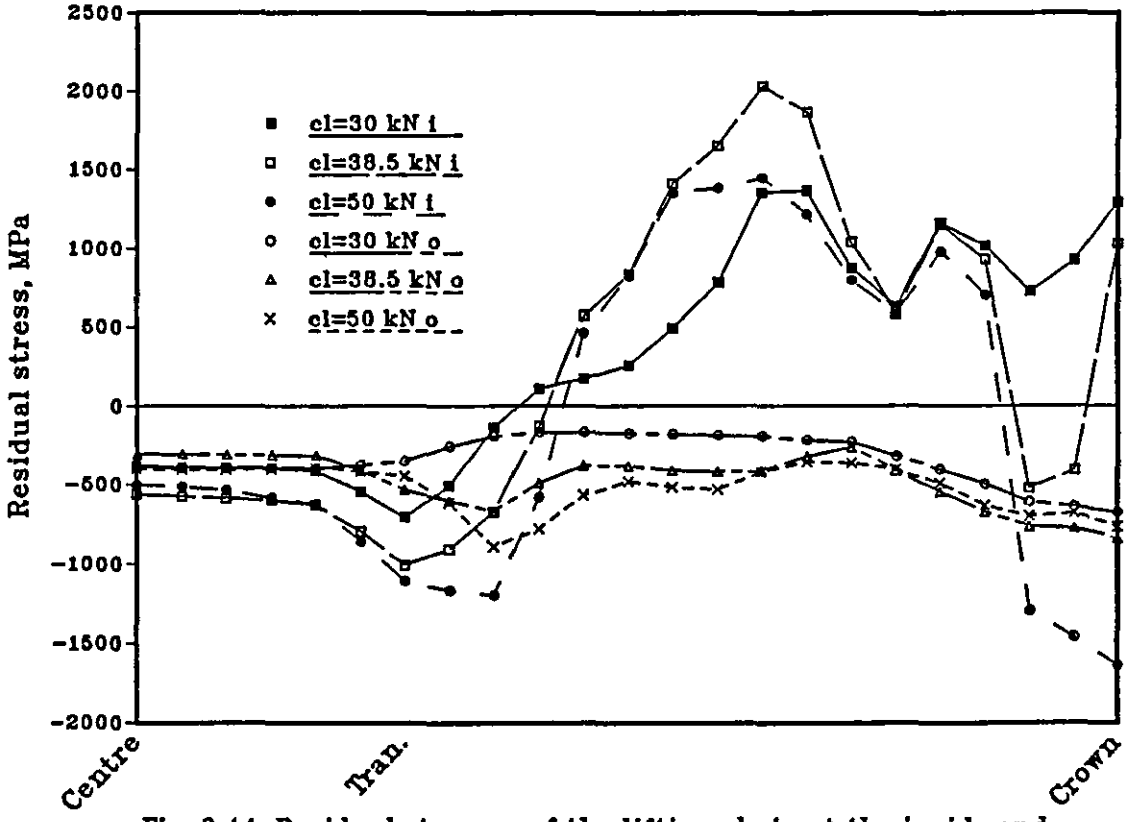

Fig. 8.44 Residual stresses of the lifting chain at the inside and outside under increasing calibation load.

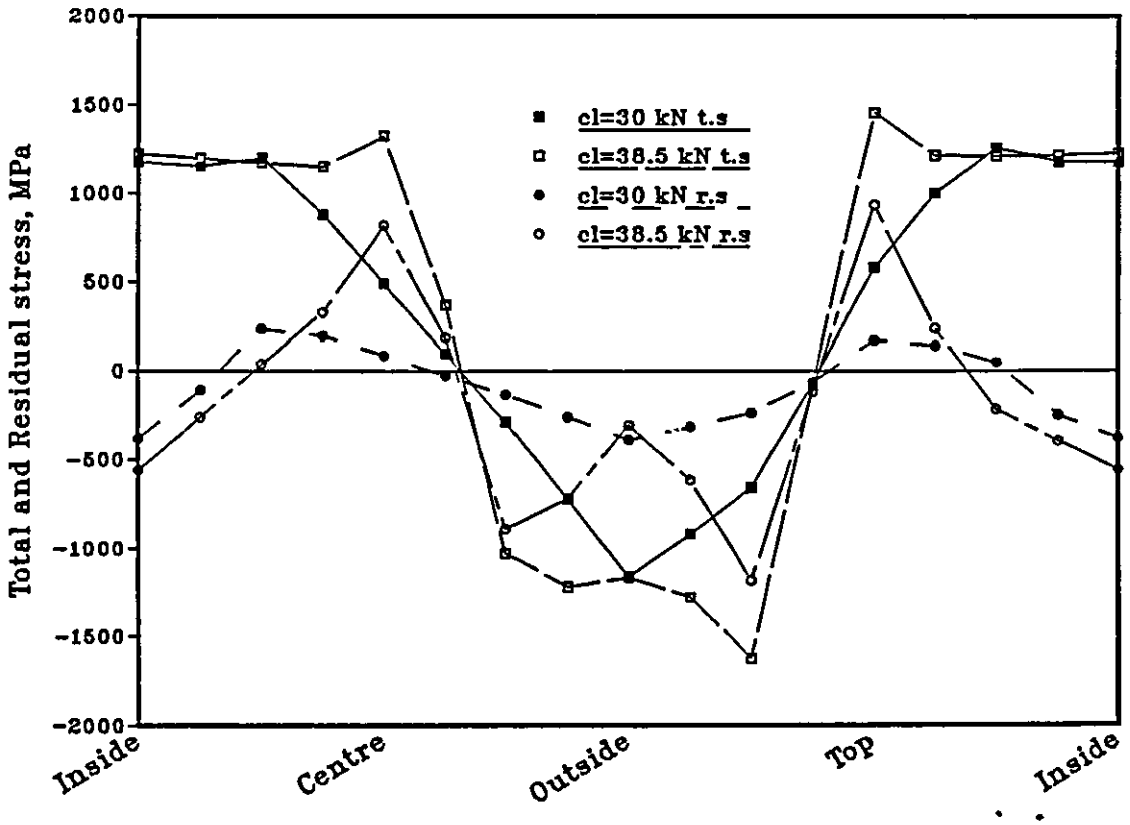

Fig. 8.45 Total and residual stresses of the lifting chain at the section through the centre under increasing calibration load.

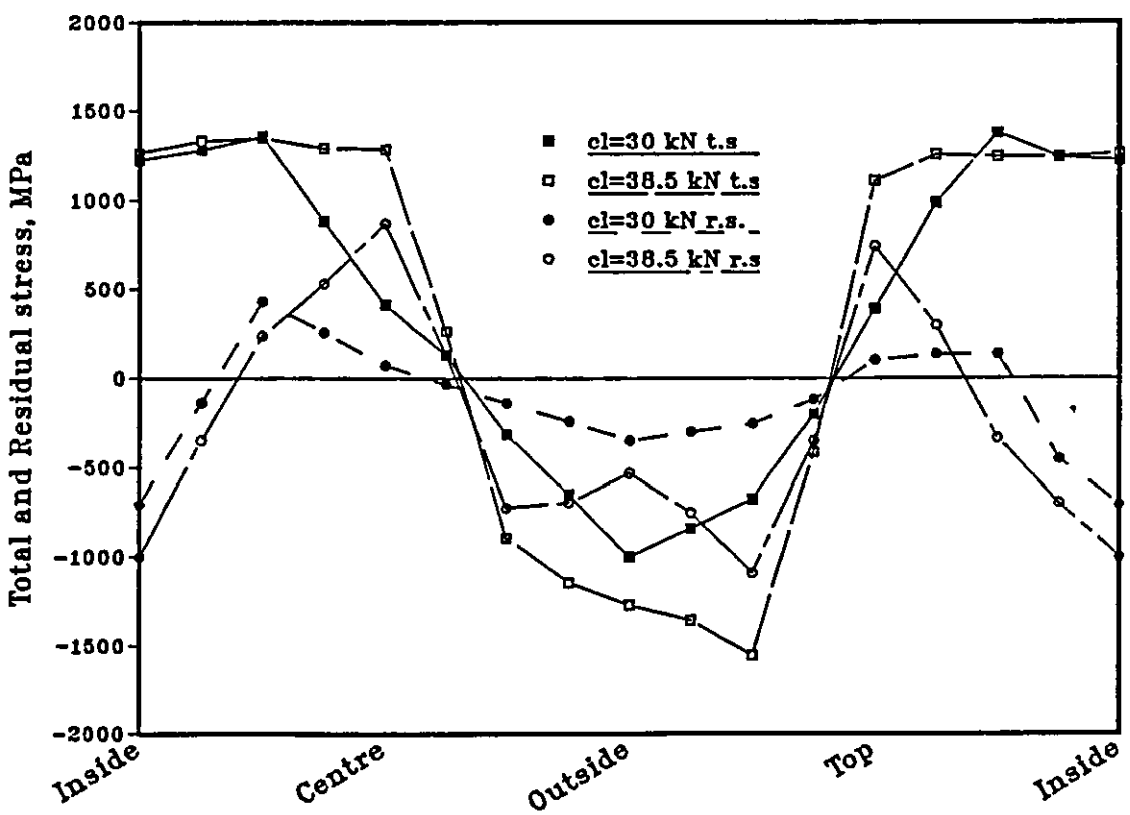

Fig. 8.46 Total and residual stresses of the lifting chain at the section through the transition under increasing calibration load.

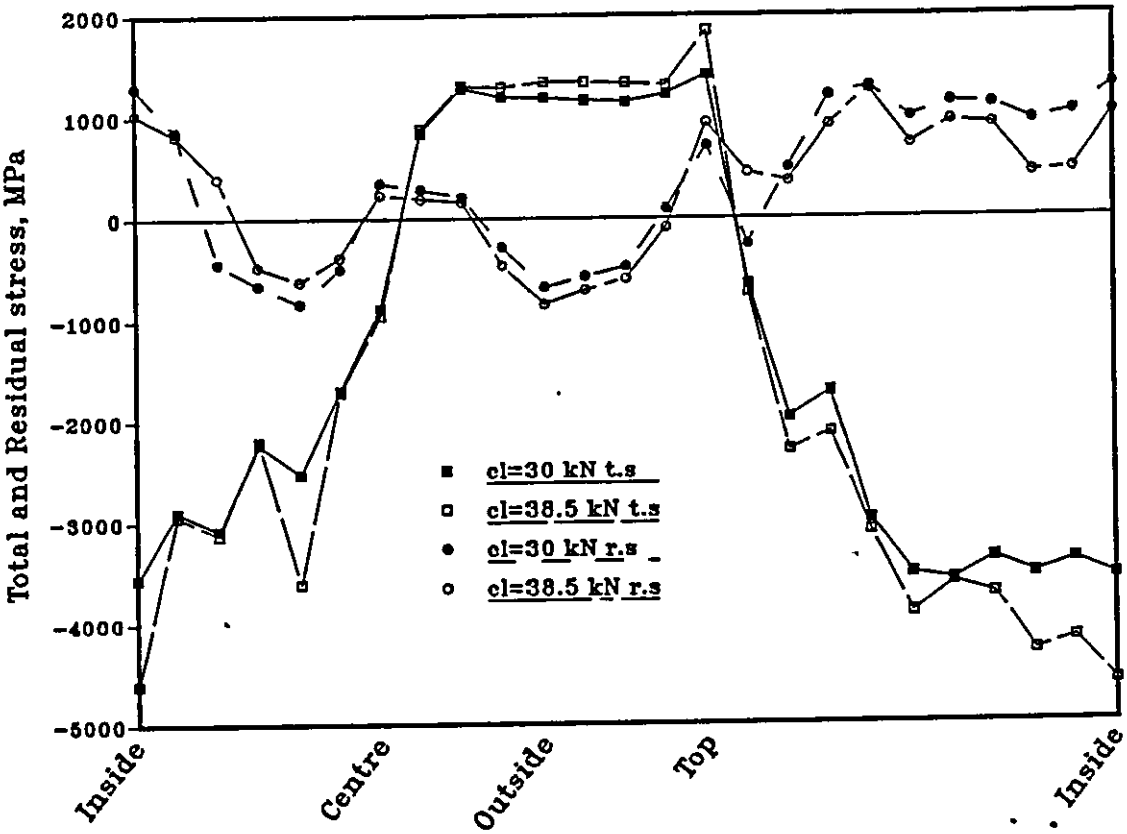

Fig. 8.47 Total and residual stresses of the lifting chain at the section through the crown under increasing calibration load.

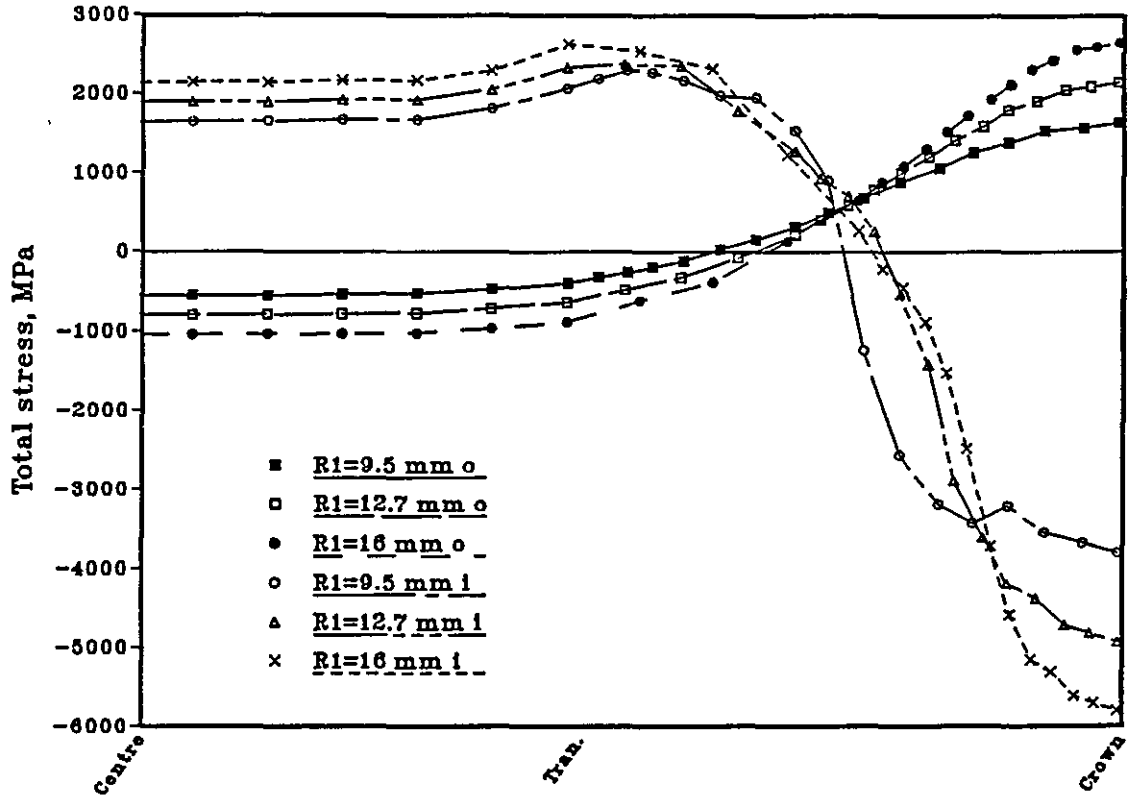

Fig. 8.48 Effect of increase in the internal radius (or inside width) of the 19 mm mining chain on the total stresses at the outside and inside under calibration load of 320 kN for elastic analysis.

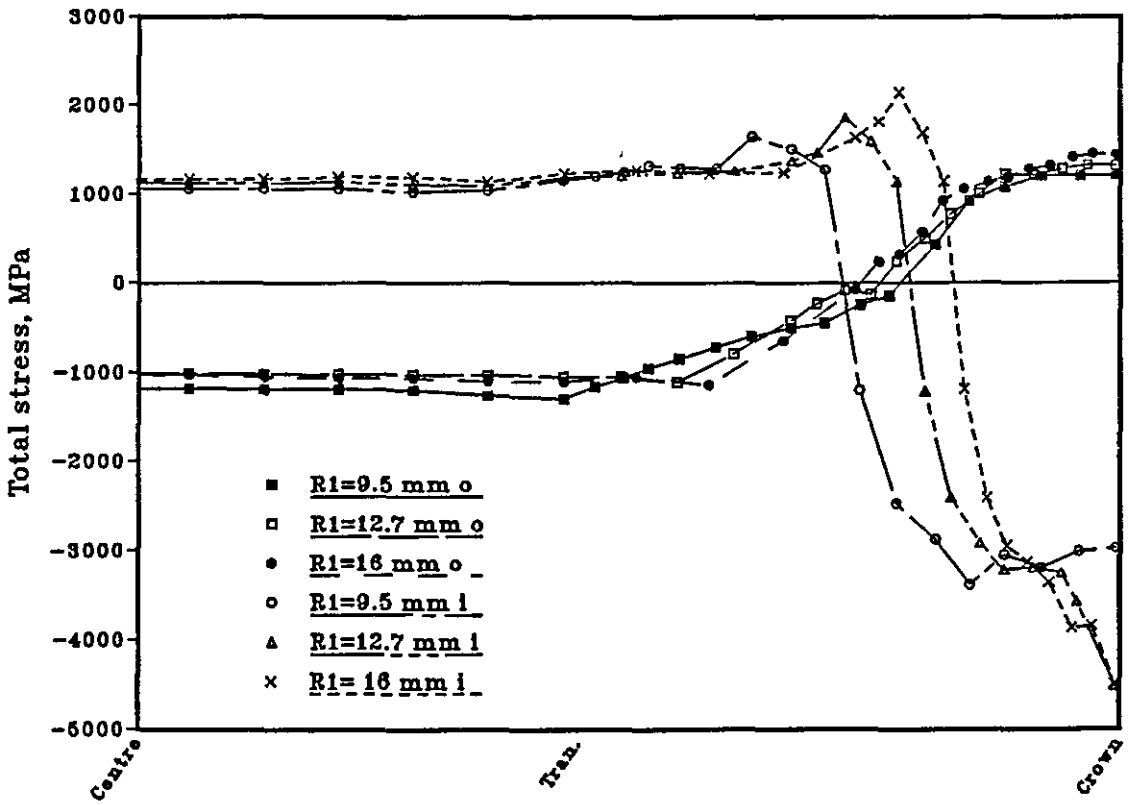

Fig. 8.49 Effect of increase in the internal radius (or inside width) of the 19 mm mining chain on the total stresses at the outside and inside under calibration load of 320 kN for elasto-plastic analysis.

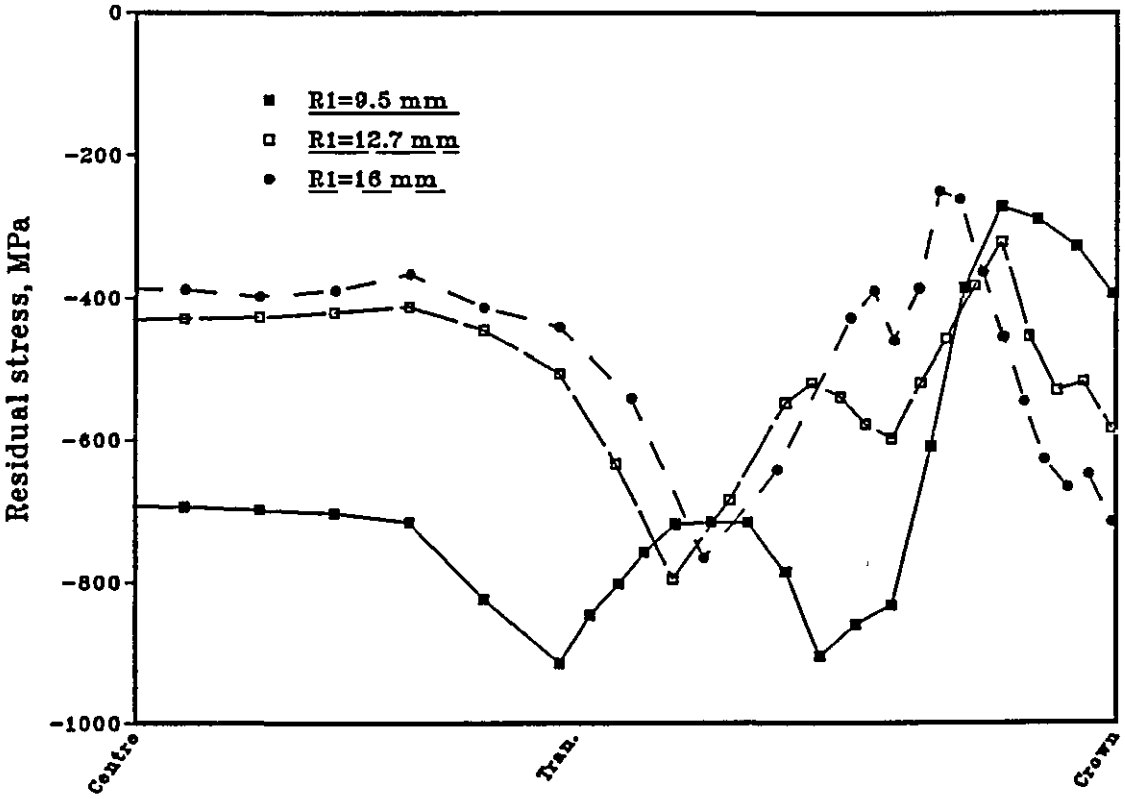

Fig. 8.50 Effect of increase in the internal radius (or inside width) of the 19 mm mining chain on the residual stresses at the outside under calibration load of 320 kN.

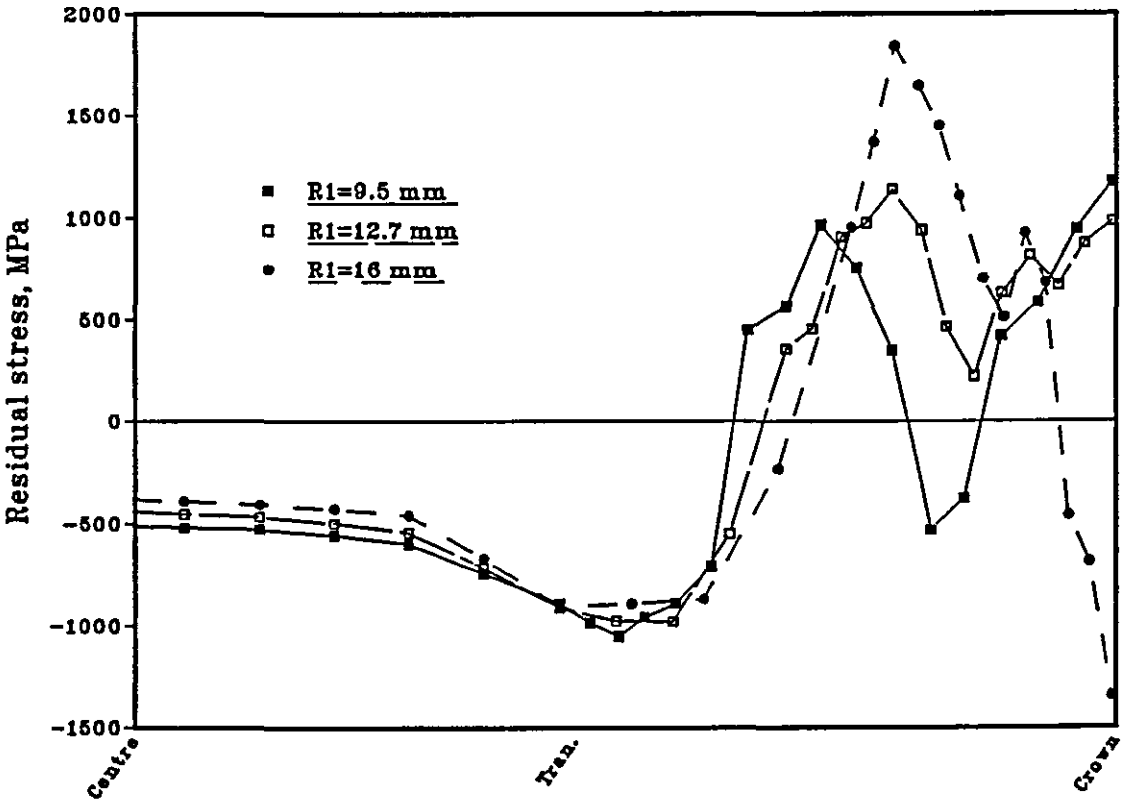

Fig. 8.51 Effect of increase in the internal radius (or inside width) of the 19 mm mining chain on the residual stresses at the inside under calibration load of 320 kN.

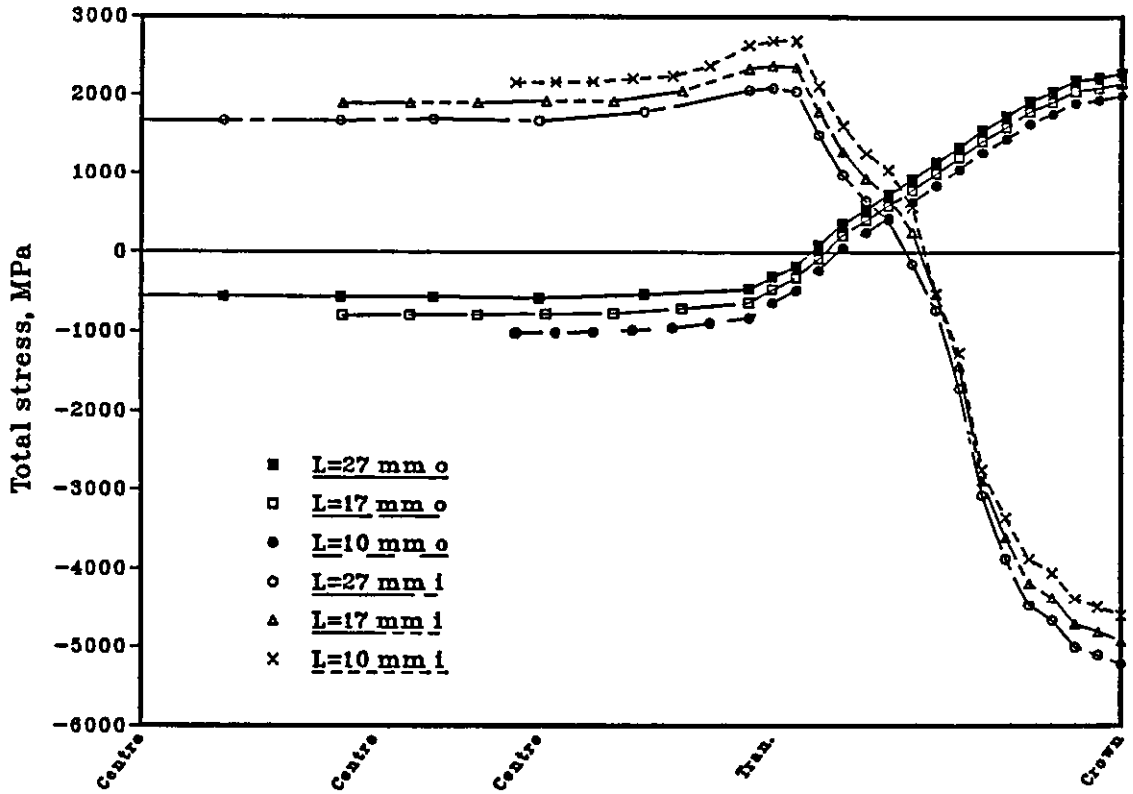

Fig. 8.52 Effect of increase in the barrel length (or pitch) of the 19 mm mining chain on the total stresses at the outside and inside under calibration load of 320 kN for elastic analysis.

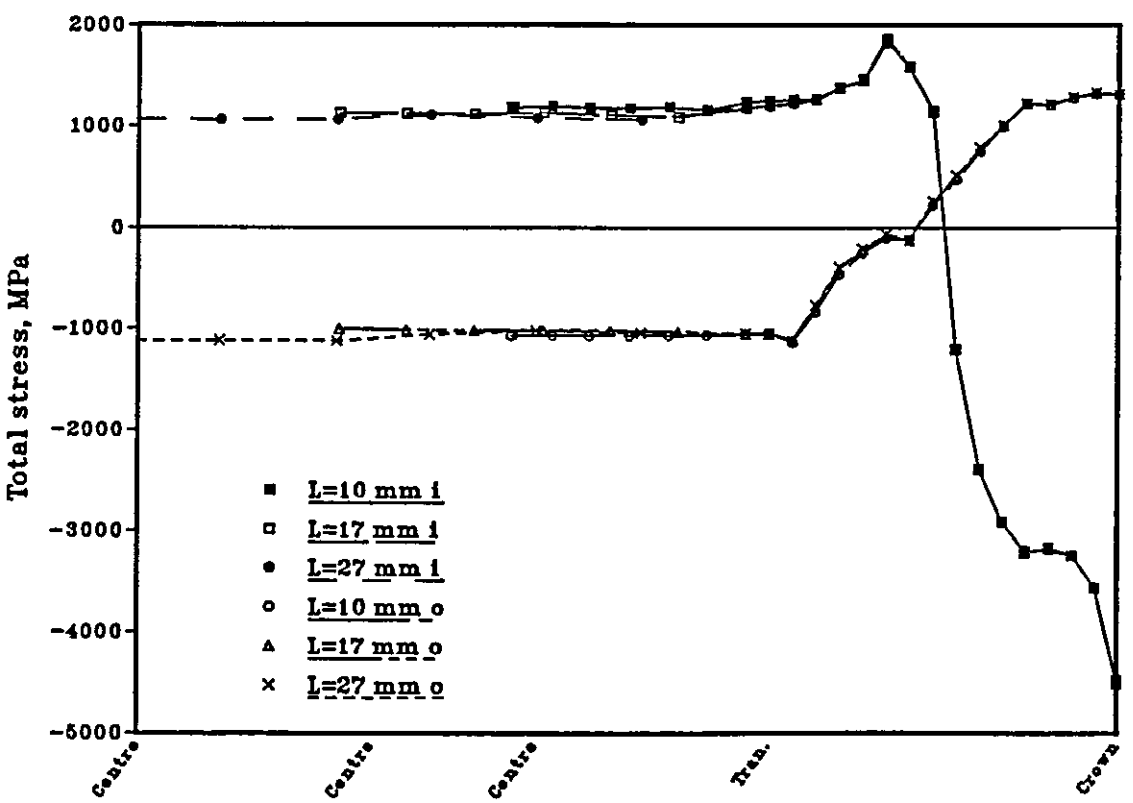

Fig. 8.53 Effect of increase in the barrel length (or pitch) of the 19 mm mining chain on the total stresses at the outside and inside under calibration load of 320 kN for elasto-plastic analysis.

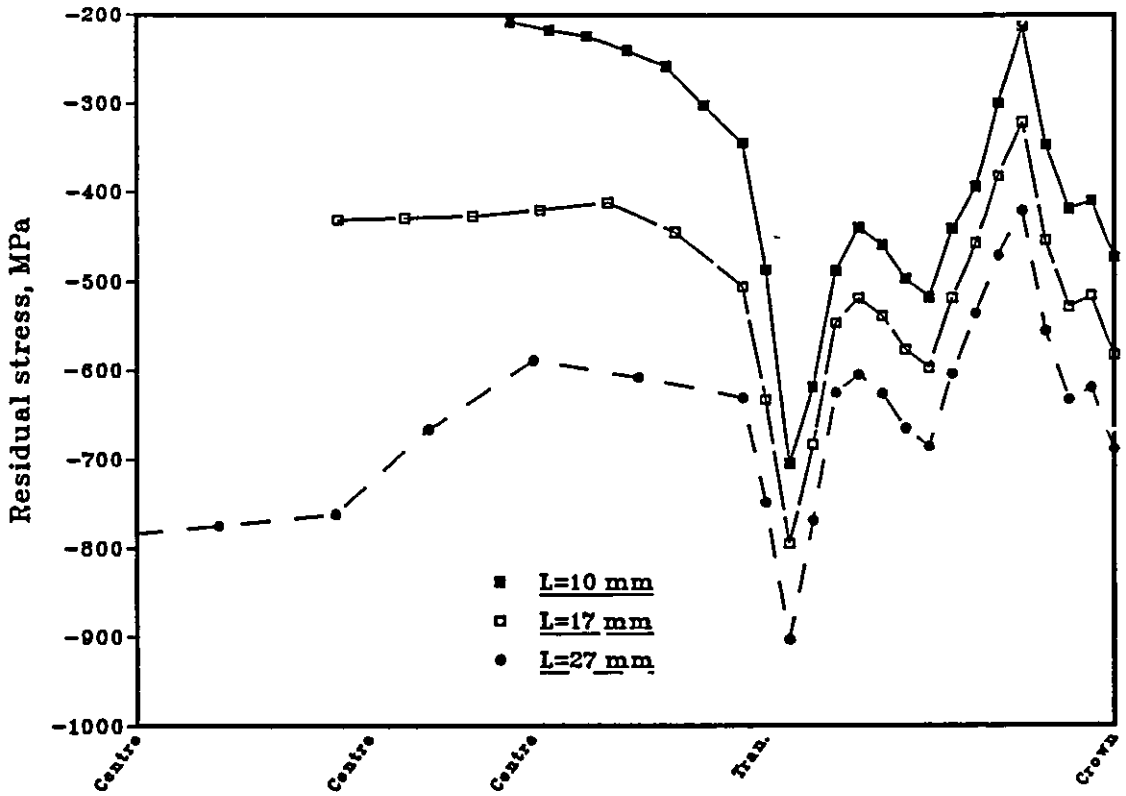

Fig. 8.54 Effect of increase in the barrel length (or pitch) of the 19 mm mining chain on the residual stresses at the outside under under calibration load of 320 kN .

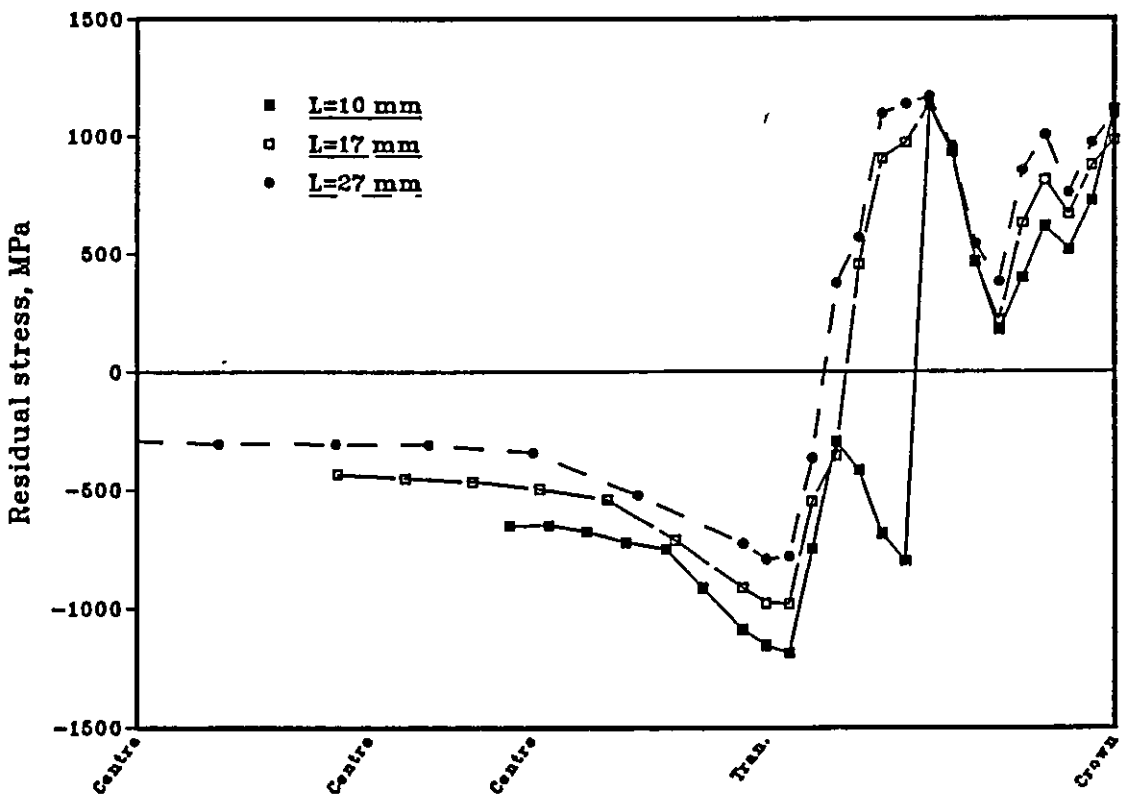

Fig. 8.55 Effect of increase in the barrel length (or pitch) of the 19 mm mining chain on the residual stresses at the inside under under calibration load of 320 kN .

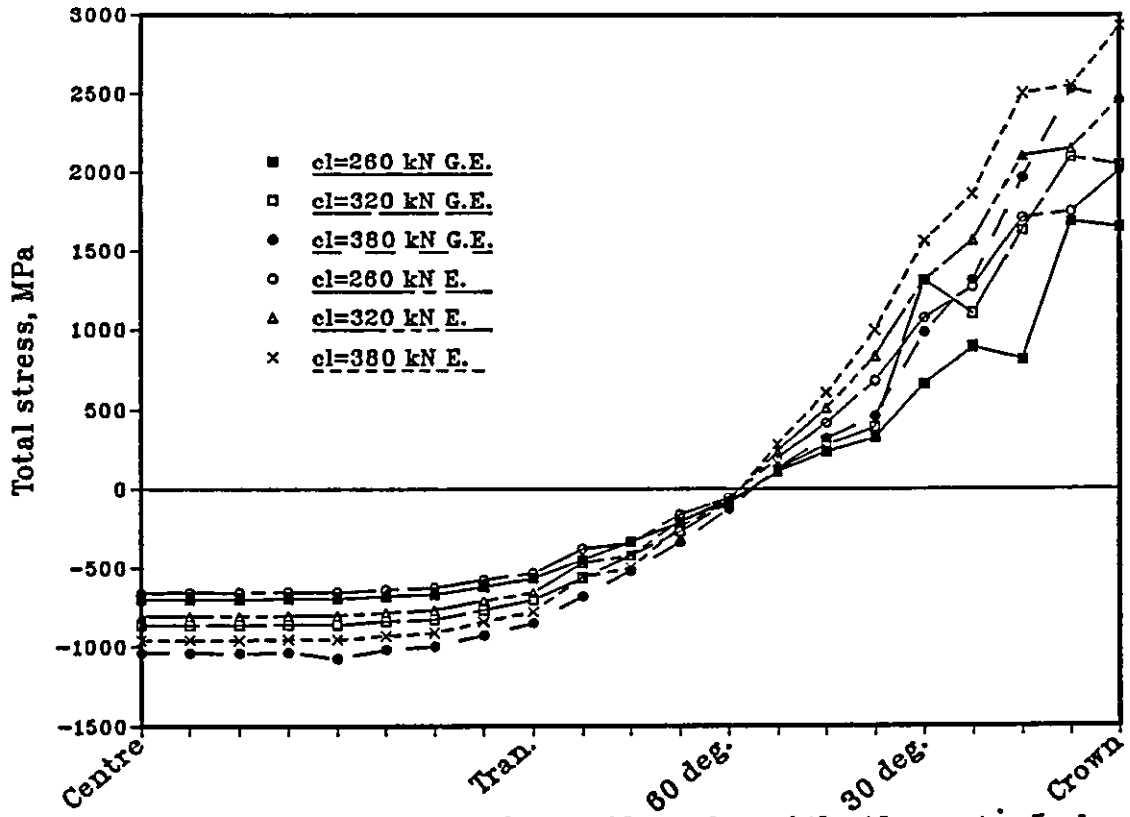

Fig. 9.1 Total stresses at the outside surface of the 19 mm standard mining chain under various calibration load for elastic (E.) and geometrically nonlinear elastic (G.E.) analysis.

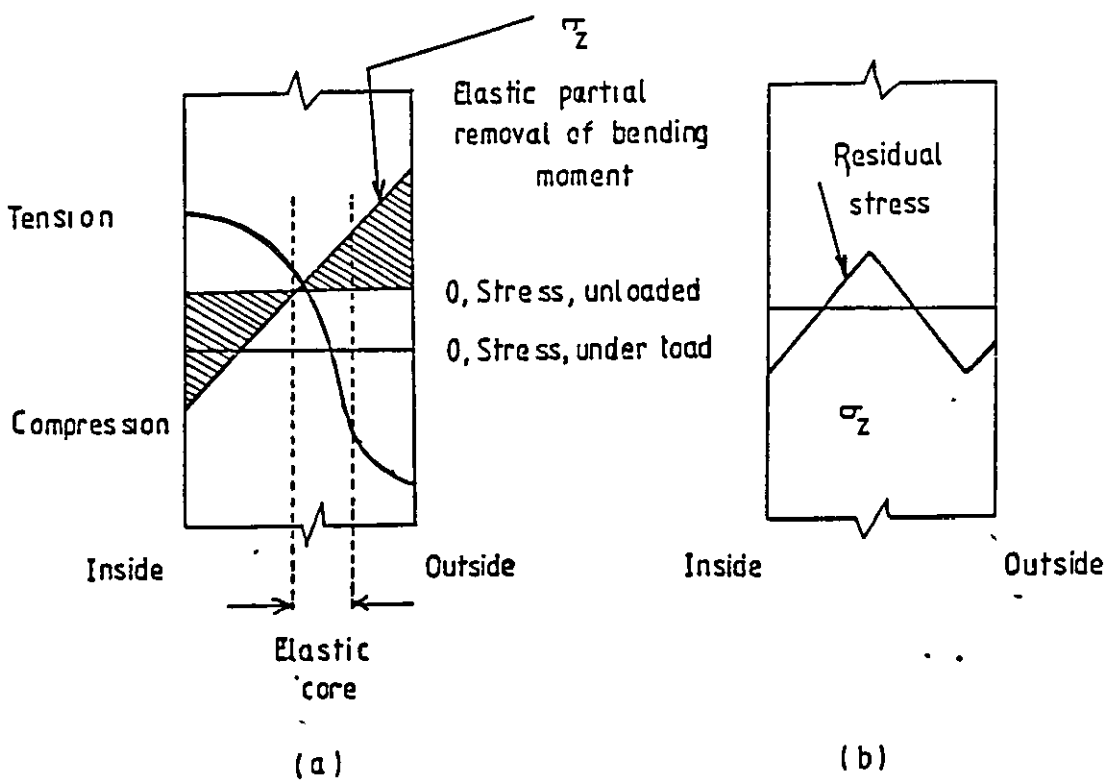

Fig. 9.2 Residual stresses induced by plastic flow in bending and direct tension in the barrel of the chains: (a) Total stresses; (b) Residual stresses.

APPENDIX A

ENERGY ABSORPTION FACTOR

ENERGY ABSORPTION FACTOR

A chain normally breaks for one of the two reasons, either the application of a static load equal to, or in excess of, the breaking load, or the sudden application of a load ('snatch' or 'shock' loading) which in the absence of shock would not have caused breakage. Static over-loading is a less frequent cause of breakage and the specifications guards against breakage due to this cause by laying down a minimum actual breaking load and the adoption of an appropriate safe working load. The ability of a link to withstand 'shock' loading is dependent on the amount of energy which a chain absorbs and is a function of the product of load and extension: any increase in either, accepted by the chains, will denote an increase in the energy which the chain is capable of absorbing. This is called energy absorption factor and expressed in the appropriate standards in terms of constant X d^2 (d being the diameter of the bar of which the chain is made), [140]. This is employed for chains made from mild steel.

For the lifting chains, the total ultimate elongation shall not be less than 17% and 10 % for non-calibrated and calibrated chains respectively [10,11,12,13,14,15]. In the case of mining chain it is 12 % [19].

For comparison purposes all the results are based on a test length of 36 inches. The equivalent extension is the extension measured, multiplied by 36 and divided by the unstretched test length in inches. The equivalent extension - irrespective of the size of the chain - shall not be less than 3.5 inches [140].

For the 7 mm lifting chain tested in Chapter 3 the following applies:

Before test length/link = 4.315/5 = .863 inches

After test length/link = 3.131/3 = 1.044 inches

Equivalent extension = 36*(1.044-.863)/.863 = 7.550 in > 3.5 in [140]

The product obtained by multiplying the equivalent extension in inches by the breaking load in tons shall be not less than that specified in BS4114, i.e. 320 d^2 tons in, where d is the size of the chain in inches (diameter of the rod used in the chain's manufacture).

The breaking load was 68.5 kN, so the energy absorption factor when uncalibrated is (1 tonf = 9964 N):

68.5*1000*7.55/9964 = 51.9 ton in > 320 d^2 = 24.3 ton in [140]

Also percentage elongation for the non-calibrated chain is

(1.044-.863)/.863 = 21 % > 17 % [10,11,12,13,14,15]

The requirements of the standard are thus met by the uncalibrated chain.

To examine whether the calibrated chain meets the requirements of the standard, let us consider calibration loads of 38.5 and 50 kN.

a) cl=38.8

From Fig. 3.27 the extension is .27 on the scale (.27*50/15 = .9 mm)

i.e. .9*100/25.4*4.315 = .82 %

b) cl=50 kN

From Fig 3.27 the extension is .175 on the scale (1.75*50/15= 5.83 mm)

i.e. 5.83*100/25.4*4.315 = 5.32 %

The remaining extension is therefore (21 - 5.32)= 15.68 % > 10 %

Hence the requirement was satisfied.

c) Calculation of the maximum calibration load

If x is the maximum calibration load and l(x) the corresponding extension then

$[5*(1.044) - l(x)]/l(x) = .1$

$l(x) = 4.745$ in

$\Delta l(x) = 4.745 - 5*.863 = .430$ in (i.e. 3.28 on the scale)

From Fig 3.27 maximum calibration load which can be applied is 56 kN. Hence, cl=50 kN used in Chapter 3 is well below the maximum calibration load.